U.PORTO
FACULDADE DE CIÊNCIAS
UNIVERSIDADE DO PORTO

U.PORTO
FEUP FACULDADE DE ENGENHARIA
UNIVERSIDADE DO PORTO

PhD

3rd CYCLE

FCUP
FEUP
2025

U.PORTO

Use of photocatalytic nanocomposites for the degradation of antibiotics in wastewater

Ricardo Sendão

FC

U.PORTO
FACULDADE DE CIÊNCIAS
UNIVERSIDADE DO PORTO

U.PORTO
FEUP FACULDADE DE ENGENHARIA
UNIVERSIDADE DO PORTO

Use of photocatalytic nanocomposites for the degradation of antibiotics in wastewater

Ricardo Miguel Sá Sendão
Doctoral Program in Chemistry
Faculty of Sciences of the University of Porto and Faculty of Engineering of the University of Porto
2025

Use of photocatalytic nanocomposites for the degradation of antibiotics in wastewater

Ricardo Miguel Sá Sendão

Thesis carried out as part of the Doctoral Program in Chemistry

Chemistry Research Unit – Institute of Molecular Sciences

2025

Supervisor
Prof. Dr. Luís Pinto da Silva, Assistant Professor, Faculty of Sciences of the University of Porto

Co-supervisor
Prof. Dr. Joaquim Esteves da Silva, Full Professor, Faculty of Sciences of the University of Porto

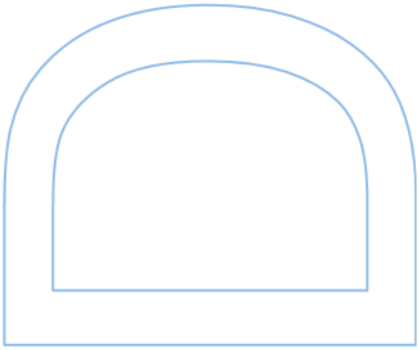
CIQUP
Centro de Investigação em Química da Universidade do Porto

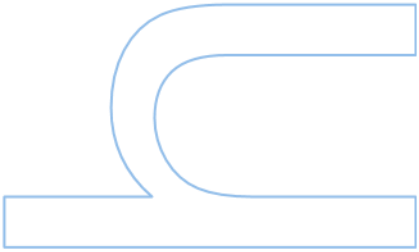
IMS
Institute of Molecular Sciences

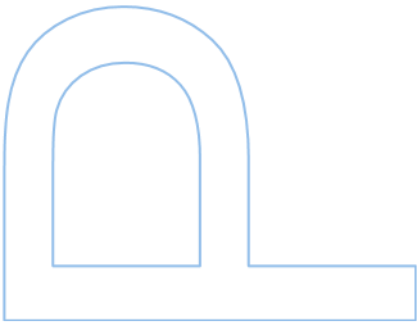
All the corrections determined by the jury, and only those, were made.

The Supervisor,

Porto, _____/_____/_____







Dedicated to Bárbara

Acknowledgements

The Portuguese Foundation for Science and Technology (FCT) is acknowledged for financing my PhD grant (Ref. 2021.06149.BD) using funding from the Ministry for Higher Education. FCT is also acknowledged for financing the R&D Units CIQUP (UIDB/00081/2020 and UIDP/00081/2020), and the Associated Laboratory IMS (LA/P/0056/2020). The research made during this dissertation was also funded by the FCT (https://ror.org/00snfqn58), under the Grants 2023.13127.PEX and PTDC/QUI-QFI/2870/2020 (https://doi.org/10.54499/PTDC/QUI-QFI/2870/2020).

First and foremost, I thank my supervisor, Prof. Dr. Luís Pinto da Silva, for his exceptional guidance, encouragement, patience, and support throughout the course of my doctoral studies, not only contributing to my growth as a professional but also as a human. To Prof. Dr. Joaquim Esteves da Silva, I thank him for his expertise, critical insight, and commitment to science, which have been instrumental in shaping both me and my development as a researcher. I thank them both for the freedom they allowed me in exploring my research interests, while always being available to provide valuable feedback and perspective when needed. Their mentorship has contributed immensely to the enrichment of this work.

I would also like to extend my heartfelt thanks to my lab colleagues Diana, Carla, Sónia, Paulo, Patrícia, and Archana (in no particular order!), who over the years have become much more than just coworkers. Working alongside such incredible people has been one of the most rewarding aspects of this journey. Whether we were working, having lunch, exchanging ideas, taking a coffee break, or simply joking with one another, your presence and personality made every day more enjoyable and something to cherish.

To Dr. Manuel Algarra and Dr. Antonio Gil for their collaboration and contribution to the work I developed over my doctoral project. Their expertise, availability, and contribution are valued immensely and were fundamental in enabling me to properly characterize and study my composites. To Prof. Dr. Nuno Vale and his research group for contributing with both knowledge and human resources to this project.

Finally, and most importantly, to Bárbara, for being an amazing human, being loving and caring, and for showering me with unwavering love, patience, and support throughout this entire journey. This thesis is as much yours as it is mine, and I am endlessly grateful to have shared this chapter of life with you by my side.

This work is licensed under a CC BY 4.0 license.



Resumo

A água é essencial para a sobrevivência da humanidade e a sua contaminação por poluentes orgânicos, como antibióticos, é um problema cada vez mais grave e que deve ser controlado. Isto é preocupante dado que a presença destes poluentes nos recursos hídricos pode representar riscos para a saúde e causar efeitos prejudiciais nos ecossistemas circundantes. Adicionalmente, os métodos convencionais de tratamento de água são ineficazes para este tipo de poluentes e, por isso, é necessário desenvolver métodos alternativos para os remover de forma eficiente de meios aquáticos.

Uma dessas alternativas é a fotocatálise, uma tecnologia limpa que utiliza irradiação para promover uma reação catalítica. É conhecida por ter impactos mais baixos que métodos convencionais, possui um elevado potencial redox e, sob as condições adequadas, pode utilizar o sol, uma fonte de energia renovável, para impulsionar o processo. O TiO_2 é um fotocatalisador particularmente importante devido ao seu baixo custo e estabilidade química. No entanto, apresenta várias limitações que impedem uma utilização eficiente sob irradiação solar. Nomeadamente, requer irradiação UV de elevada energia, que representa apenas cerca de 5% do espectro solar, sofre de uma rápida recombinação de cargas, o que reduz a sua eficiência fotónica, e, por fim, apresenta baixa afinidade para poluentes orgânicos. Embora várias estratégias de dopagem tenham sido testadas para ultrapassar estas limitações, todas elas apresentam os seus próprios problemas e limitações.

Como alternativa a essas estratégias, existe a conjugação do TiO_2 com *carbon dots* (CDs), que, devido à sua estrutura e propriedades, podem melhorar a separação de cargas no TiO_2, alargar a gama de absorção para a luz visível e aumentar a afinidade para poluentes orgânicos. Assim, a adição de CDs ao TiO_2 tem o potencial de aumentar a eficiência fotocatalítica sob luz solar ao mesmo tempo que evita os inconvenientes associados às estratégias de dopagem. Por fim, a síntese de CDs é altamente versátil, podendo estes ser produzidos a partir de uma vasta gama de precursores, incluindo resíduos orgânicos, contribuindo assim para a valorização desses resíduos, promovendo uma economia circular e reduzindo os impactos ambientais associados.

Numa primeira fase do projeto, começámos por desenvolver nanocompósitos que fossem ativos sob luz visível para a fotodegradação de azul de metileno (MB), um poluente modelo. O nanocompósito inicial foi preparado a partir de TiO_2 e de CDs produzidos através do tratamento hidrotermal de ácido cítrico e etilenodiamina, sendo

este doravante designado como NC_{100}. A adição de CDs ao semicondutor teve um efeito significativo na eficiência fotocatalítica da degradação do MB sob luz visível. Nomeadamente, o NC_{100} teve aumento de 367% no desempenho catalítico quando comparado com o TiO_2. Quando caraterizado, observou-se que houve um aumento da absorção no visível e um aumento da eficiência fotónica com a adição dos CDs. Estudos com *scavengers* revelaram ainda que a fotodegradação era mediada por radicais superóxido, diferindo do TiO_2 e indicando que a adição de CDs pode também influenciar as espécies reativas envolvidas no processo de fotodegradação. Por fim, estudos de Avaliação do Ciclo de Vida (ACV) demonstraram que o NC_{100} é a melhor alternativa quando se considera o desempenho do catalisador, já que os seus impactos ambientais são amplamente compensados pela sua eficiência. Em suma, estes resultados iniciais demonstram que os CDs são uma forma eficaz de colmatar as limitações do TiO_2.

Seguiu-se o desenvolvimento de uma versão alterada do NC_{100}, na qual ajustamos a síntese para incorporar palha de milho como co-precursor de carbono na produção dos CDs, resultando no $NC_{50:50}$. Ao incorporar palha de milho, reaproveitámos um resíduo orgânico normalmente descartado, promovendo uma economia circular. Além disso, o uso desta biomassa permite evitar a parte dos impactos associados à produção do ácido cítrico, que de outro modo seria utilizado. Em termos de propriedades, o $NC_{50:50}$, quando comparado com o NC_{100}, apresentou uma ligeiramente melhor absorção na gama do visível, melhor eficiência fotónica e um ligeiro aumento da eficiência catalítica face ao TiO_2 (374% contra 367% para o NC_{100}). Em termos de impactos ambientais, estudos de ACV confirmaram que o $NC_{50:50}$ apresentou impactos ambientais inferiores aos do NC_{100} e TiO_2, tanto em termos absolutos como quando se considera a funcionalidade. Assim, este trabalho estabelece uma base sobre como desenvolver nanocompósitos sustentáveis de TiO_2/CDs, reduzindo os impactos associados à produção das matérias-primas sem comprometer o desempenho.

O principal objetivo deste projeto de doutoramento era desenvolver um fotocatalisador para a degradação de ciprofloxacina (CIP) sob irradiação solar. Após testar o $NC_{50:50}$ para a fotodegradação de MB e outros corantes orgânicos sob luz visível, empregámo-lo agora para remover CIP de amostras aquosas. Usando um simulador solar, o $NC_{50:50}$ conseguiu completamente remover 20 ppm de CIP em menos 20 minutos de irradiação, atingindo uma constante de reação de 0,2372 min^{-1}, a qual é superior a qualquer outro sistema baseado em TiO_2 descrito na literatura para este composto, e que corresponde a um aumento de 217% na eficiência catalítica face ao TiO_2. Embora alguns subprodutos tenham sido detetados, estes desapareceram subsequentemente

durante o processo de fotodegradação. Além disso, o $NC_{50:50}$ mostrou boa estabilidade e manteve a sua atividade catalítica durante pelo menos três ciclos. Por fim, testes usando radiação solar natural e efetuados em diversos estados atmosféricos demonstraram que o $NC_{50:50}$ é eficiente mesmo nestas condições. Concretamente, sob luz solar direta, o $NC_{50:50}$ foi capaz de degradar completamente a CIP em menos 30 minutos de irradiação, independentemente do dia, das condições do céu e da temperatura, com apenas o fator UV a ser capaz de afetar o processo. Em suma, este trabalho traça um caminho para alcançar uma maior eficiência fotocatalítica sob luz solar ao mesmo tempo que valoriza um resíduo orgânico e promove uma economia circular.

A parte final da tese consiste num estudo de ACV sobre os impactos ambientais de três nanocompósitos de TiO_2/CDs diferentes e desenvolvidos para a fotodegradação de MB sob luz visível. Dado que este tipo de material fotocatalítico ainda se encontra numa fase inicial em termos de desenvolvimento, é importante obter dados concretos relativos aos impactos associados com o fabrico deste tipo de nanomaterial. A partir dos dados obtidos, verificámos que, para além de os nanocompósitos com maior atividade fotocatalítica apresentarem os menores impactos (quando se utiliza uma unidade funcional baseada no desempenho), o parâmetro que mais afeta os impactos resultantes foi a origem do TiO_2 utilizado e a identidade dos precursores dos CDs, demonstrando assim que a substituição dos precursores dos CDs por fontes de biomassa (tal como a palha de milho) reduz ativamente os impactos ambientais associados ao nanocompósito e melhora a sua sustentabilidade.

Em suma, este projeto demonstrou que a conjugação de TiO_2 com CDs é uma abordagem válida para alcançar um método mais eficiente e sustentável para a degradação antibióticos, tais como a CIP, aproveitado para isso a radiação solar. Isto foi conseguido utilizando palha de milho como co-precursor de carbono, valorizando assim um resíduo orgânico sem comprometer a eficiência catalítica. Isto indica que a utilização de CDs à base de biomassa para superar as limitações do TiO_2 é viável e pode ser feita tendo em consideração os impactos ambientais resultantes e a promover uma economia circular. Assim, este estudo estabelece uma base para o desenvolvimento sustentável de novos nanocompósitos para o tratamento fotocatalítico de águas residuais sob luz solar.

Palavras-chave: fotocatálise, nanocompósitos, TiO_2, carbon dots, poluentes orgânicos, corantes, azul de metileno, antibióticos, ciprofloxacina, ACV.

Abstract

Water is essential for the survival of humanity, and its contamination by organic pollutants such as antibiotics is an increasingly larger problem and must be controlled. This is troublesome given that the presence of these pollutants in water supplies may cause health hazards and have damaging effects on the surrounding ecosystems. Worryingly, conventional water treatment methods are ineffective for these types of pollutants and so, alternative methods must be developed to efficiently remove these pollutants from wastewaters.

One such alternative is photocatalysis, a clean technology that uses irradiation to drive a catalytic reaction. It is frequently less impactful than conventional alternatives, has a high redox potential, and, under the right conditions, may employ the sun, a clean and renewable energy source, to drive the process. TiO_2 is a particularly important and studied photocatalyst because of its widespread application, low cost, and chemical stability. However, it has several limitations that prevent its efficient use under solar irradiation. Namely, it has a wide band gap and, consequently, requires high energy UV irradiation, which accounts for only around 5% of the whole solar spectrum, it suffers from a rapid recombination of photogenerated charge carriers, thus reducing its photonic efficiency, and finally, it presents a poor affinity for organic pollutants. While several doping strategies have been tried to bridge these limitations, they all have their own problems and different challenges.

As an alternative to those strategies, we have the conjugation of TiO_2 with carbon dots (CDs), which, due to their unique structure and properties, may improve TiO_2's separation of photogenerated charge carriers, extend the absorption range into the visible, and provide a functionalized surface with affinity toward organic pollutants. Thus, adding CDs to TiO_2 has the potential to enhance the sunlight-driven photocatalytic efficiency of TiO_2 while avoiding the drawbacks associated with doping strategies. Moreover, the synthesis of CDs is highly versatile, and they may be produced from a wide array of carbon precursors, including organic waste. This may help in upcycling these residues, thus contributing to a circular economy while decreasing the environmental impacts associated with the synthesis of the photocatalyst.

In the first stage of the project, we started by developing visible-light active nanocomposites for the visible-light-driven photodegradation of Methylene Blue (MB), a model pollutant that we selected for our starting studies. The first successful nanocomposite we developed was the foundation for our future work. It was prepared

from TiO_2 nanoparticles and CDs prepared via hydrothermal treatment from citric acid and ethylenediamine, hereby termed as NC_{100}. With this nanocomposite, we observed that adding CDs to the semiconductor had a significant effect on the photocatalytic efficiency toward the visible-light-driven degradation of MB. Namely, NC_{100} displayed a 367% enhancement of the catalytic performance when compared to bare TiO_2. When characterizing NC_{100}, we observed an increase in absorption in the visible range and evidence of a better photonic efficiency upon the addition of the CDs, thus providing two potential causes for the increased catalytic efficiency. Scavenger studies revealed that the photocatalytic mechanism was based mostly on superoxide radicals, differing from TiO_2, indicating that adding CDs may also affect the species involved in the photodegradation process. Finally, Life Cycle Assessment (LCA) studies demonstrated that NC_{100} is a better alternative when considering a function-based functional unit, as its environmental impacts are greatly offset by a higher photocatalytic performance. Altogether, these initial findings affirm that CDs are an effective, low-toxicity, and scalable additive to transform TiO_2 into a highly active and sustainable photocatalyst for sunlight-driven processes for the removal of organic pollutants.

This was followed by the development of another iteration of NC_{100} in which we altered the synthesis in order to incorporate corn stover as a co-carbon precursor for the synthesis of CDs, resulting in $NC_{50:50}$. By incorporating corn stover, we are adding value to an otherwise discarded organic residue and thus promoting a circular economy. Moreover, the use of this biomass also allows us to avoid some of the impacts associated with the production of citric acid that would otherwise be employed as the sole carbon source. $NC_{50:50}$, when compared to NC_{100}, had a slightly better absorption in the visible range, better photonic efficiency, and a slightly larger enhancement of the catalytic performance over TiO_2 (374% versus 367% for NC_{100}). In terms of environmental impacts, LCA studies confirmed that $NC_{50:50}$ had lower environmental impacts than NC_{100} and TiO_2, both when considering a weight or a function-based functional unit. By demonstrating that waste materials can be upcycled into high-performance nanocomposites, this work provides a basis for developing sustainable TiO_2/CDs nanocomposites by reducing the impacts associated with the production of the raw materials without compromising the performance.

The main objective of the doctoral project was to develop a highly efficient sunlight-driven photocatalyst for the photodegradation of ciprofloxacin (CIP). After testing $NC_{50:50}$ toward the visible-light-driven photodegradation of MB and other organic dyes, we employed it to remove CIP from aqueous samples. Under a solar simulator,

$NC_{50:50}$ achieved a virtually complete removal of 20 ppm of CIP within 20 minutes of irradiation and a rate constant of 0.2372 min^{-1}, which was higher than any other TiO_2-based system available in the literature for this compounds, and corresponds to a 217% enhancement of the catalytic efficiency over TiO_2 and, even though some by-products were detected, they subsequently disappear during the photodegradation. Furthermore, $NC_{50:50}$ displayed good stability and retained its catalytic activity during at least three cycles. Finally, tests under natural sunlight and varying atmospheric conditions revealed that $NC_{50:50}$ is efficient even under these conditions. Namely, under direct sunlight, it was capable of fully degrading CP within 30 minutes of irradiation, irrespective of the day, sky conditions, and temperature, with only the UV factor being able to affect the degradation process. In summary, this work lays a pathway to achieve enhanced photocatalytic efficiency under natural sunlight while upcycling an otherwise discarded organic waste and promoting a circular economy.

The final part of the thesis consists of a comprehensive LCA study of the environmental impacts of three different TiO_2/CDs nanocomposites developed towards the visible-light-driven photodegradation of MB. Given that this type of photocatalytic material is still at an early stage of development, it is important to obtain concrete and verified data regarding the sustainable development and fabrication of this type of nanomaterial. From the data we obtained, we found that, aside from the nanocomposites with the highest photocatalytic activity having the lowest impacts when using a function-based functional unit, the most critical parameter affecting the overall impacts was the source of the TiO_2 used in the nanocomposites and the identity of the CDs' precursors, demonstrating that changing the CDs' precursors to biomass sources (i.e. corn stover) actively decreases the environmental impacts associated with the nanocomposite.

In summary, this project confirmed that the conjugation of TiO_2 and CDs is a valid approach to achieve a more sustainable yet efficient degradation of a relevant antibiotic, such as CIP, under both simulated and natural solar irradiation. Moreover, this was achieved while employing corn stover as a co-carbon precursor, thus upcycling an organic waste while maintaining the catalytic efficiency. This indicates that using biomass-incorporating CDs to bridge the limitations of TiO_2 is feasible and can be achieved while taking into consideration the resulting impacts and promoting a circular economy, thus providing a basis on which to further develop novel sustainable nanocomposites toward the sunlight-driven photocatalytic treatment of wastewater.

Keywords: photocatalysis, nanocomposites, TiO_2, carbon dots, wastewater treatment, organic pollutants, dyes, methylene blue, antibiotics, ciprofloxacin, LCA.

Publications and Presentations of the Author Containing Work Related to this Thesis

The following list comprises the publications and presentations of the author regarding the work developed within the doctoral project:

A. Book chapter

1. Sendão, Ricardo M. S.; Silva, José P.; Freitas, Martinho; Carneiro, Beatriz; Esteves da Silva, Joaquim C. G.; Pinto da Silva, Luís. “Citric Acid as a Precursor for Carbon Dots: Synthesis, Properties, Applications and Sustainability” (Chapter 2). In: Advances in Chemistry Research, Volume 79 (Ed.: James C. Taylor). Nova Science Publishers, **2023**. ISBN: 979-8-88697-947-3.

B. Scientific Papers

1. Sendão, Ricardo M. S.; Brandão, Ana; Pereira, Carlos, Esteves da Silva, Joaquim C. G.; Pinto da Silva, Luís. “Enhanced Photocatalytic Degradation of Ciprofloxacin Under Natural Sunlight Using a Waste-Derived Carbon Dots–TiO_2 Nanocomposite”. *Catalysts* 16(2) (**2026**): 142. http:// doi.org/10.3390/catal16020142;

2. Sendão, Ricardo M. S.; Esteves da Silva, Joaquim C. G.; Pinto da Silva, Luís. "Comparative life cycle assessment of the fabrication of visible-light-driven photocatalytic TiO_2 – Carbon dots nanocomposites for wastewater treatment". *NanoImpact* 38(22) (**2025**): 100556. https://doi.org/10.1016/j.impact.2025.100556;

3. Sendão, Ricardo M. S.; Algarra, Manuel; Martínez, Juan; Brandão, Ana; Gil, Antonio; Pereira, Carlos; Esteves da Silva, Joaquim C. G.; Pinto da Silva, Luís. “Visible-light-driven photocatalytic degradation of organic dyes using a TiO_2 and waste-based Carbon Dots nanocomposite”. *Colloids and Surfaces A: Physicochemical and Engineering Aspects* 713 (**2025**): 136475. https://doi.org/10.1016/j.colsurfa.2025.136475;

4. Sendão, Ricardo M. S.; Esteves da Silva, Joaquim C. G.; Pinto da Silva, Luís. "Polyfluoroalkyl Substances (PFASs) Detection Via Carbon Dots: A Review". *Sustainable Chemistry* 4(4) (**2023**): 339-362. http://doi.org/10.3390/suschem4040024;

5. Sendão, Ricardo M. S.; Algarra, Manuel; Ribeiro, Eduarda; Pereira, Mariana; Gil, Antonio; Vale, Nuno; Esteves da Silva, Joaquim C. G.; Pinto da Silva, Luís. "Carbon Dots–TiO_2 Nanocomposites for the Enhanced Visible-Light Driven Photodegradation of

Methylene Blue". *Advanced Sustainable Systems* 8(1) (**2023**): 2300317. http://doi.org/10.1002/adsu.202300317;

6. Sendão, Ricardo M. S.; Esteves da Silva, Joaquim C. G.; Pinto da Silva, Luís. "Applications of Fluorescent Carbon Dots as Photocatalysts: A Review". *Catalysts* 13(1) (**2023**): 179-179. http://doi.org/10.3390/catal13010179;

7. Sendão, Ricardo M. S.; Esteves da Silva, Joaquim C. G.; Pinto da Silva, Luís. "Photocatalytic removal of pharmaceutical water pollutants by TiO_2 – Carbon dots nanocomposites: A review". *Chemosphere* 301 (**2022**): 134731 https://doi.org/10.1016/j.chemosphere.2022.134731.

C. Oral communications

1. Sendão, Ricardo M. S.; Esteves da Silva, Joaquim C. G.; Pinto da Silva, Luís. “Waste-based carbon dots – TiO_2 nanocomposites for the sunlight-driven photodegradation of ciprofloxacin” at IMS/CIQUP-RG4 Meeting – Chemistry Unveiled – Pushing Boundaries in Research (**2024**) Matosinhos, Portugal;

2. Sendão, Ricardo M. S.; Esteves da Silva, Joaquim C. G.; Pinto da Silva, Luís. “Titanium Dioxide – Carbon Dots Nanocomposites for the visible-light and sunlight–driven photodegradation of organic pollutants” at 24th European Meeting on Environmental Chemistry (**2024**) Alicante, Spain;

3. Sendão, Ricardo M. S.; Esteves da Silva, Joaquim C. G.; Pinto da Silva, Luís.; “Titanium Dioxide – Carbon Dots Nanocomposites for the Sunlight – Driven Photodegradation of Organic Pollutants” at Advances in Luminescent Materials (**2024**) Online;

4. Sendão, Ricardo M. S.; Esteves da Silva, Joaquim C. G.; Pinto da Silva, Luís. “Carbon dots-TiO_2 nanocomposites for the photodegradation of methylene blue under visible light” at IMS/CIQUP-RG4 Meeting – Chemistry Unveiled – Pushing Boundaries in Research (**2023**) Matosinhos, Portugal;

5. Sendão, Ricardo M. S.; Esteves da Silva, Joaquim C. G.; Pinto da Silva, Luís. “Carbon dots-TiO2 nanocomposites for the visible-light driven photodegradation of methylene blue” at XXVII Encontro Luso-Galego de Química (**2023**) Porto, Portugal;

6. Sendão, Ricardo M. S.; Esteves da Silva, Joaquim C. G.; Pinto da Silva, Luís. “Insight into the interaction between fluorescent Carbon Dots and molecular by-products of their synthesis” at PhotOnline’2023 (**2023**) by SP2P, Paris, France.

Structure of the thesis

The work developed within the scope and presented in this thesis was divided into three major sections: the introduction, the presentation and discussion of the results, and a conclusion with a future perspective section.

The introduction consists of two publications related to the topics discussed in the thesis. First, we present a book chapter that provides a comprehensive review concerning carbon dots, including their synthesis, purification, sustainability, reactivity, applications, potential use in emerging technologies, and potential mitigation of environmental impacts. This is followed by a publication consisting of a comprehensive review of the reports concerning the photodegradation of antibiotics by TiO_2/CDs nanocomposites available at the start of the doctoral project. Finally, a brief description of the project's main objectives is included.

The second section, concerning the results obtained during the project, consists of four scientific articles depicting the continuous development of a photocatalytic system steered towards the sunlight-driven photodegradation of antibiotics and an evaluation of the environmental impacts that can be ascribed to such systems. First, an article is presented reporting an improved visible-light-driven photodegradation of MB, which, at this point, was chosen as a model pollutant for our starting studies. This was followed by a second article concerning MB in which we managed to make a more sustainable nanocomposite by including biomass in its constitution. A further development led to the publication of the third article of this section, in which we achieved a virtually complete degradation of an antibiotic, CIP, within thirty minutes of solar-light irradiation, both using a solar simulator and real sunlight, which consisted of the main objective of the doctoral project. Finally, a fourth article concerning the environmental impacts associated with the synthesis of TiO_2/CDs nanocomposites for the photodegradation of MB is also presented.

Finally, the third section of this thesis presents the main conclusions of the work performed and the future perspectives of this research.

Table of Contents

List of Abbreviations xiv

1. Introduction 1

1.1 Carbon dots: synthesis, properties, applications, and sustainability 2

1.1.1. Introduction and contributions to this work 2

1.2. Photocatalytic degradation of organic pollutants using TiO_2 and CDs nanocomposites 53

1.2.1. Introduction and contributions to this work 53

1.3. Aim and objectives 69

2. Results and discussion 70

2.1. Development of visible-light active photocatalytic nanocomposites 71

2.1.1. Preparation of first catalytic nanocomposite from commercial reagents 71

2.1.1.1. Introduction and contributions to this work 71

2.1.1.2. Supplementary information 88

2.1.1.3. Conclusion 95

2.1.2. Incorporation of corn stover as a carbon source in visible-light active photocatalytic TiO_2-CDs nanocomposites 96

2.1.2.1. Introduction and contributions to this work 96

2.1.2.2. Supplementary information 113

2.1.2.3. Conclusion 117

2.2. Sunlight-driven photodegradation of ciprofloxacin 118

2.2.1. Introduction and contributions to this work 118

2.2.2. Supplementary information 142

2.2.3. Conclusion 146

2.3. Life Cycle Assessment studies of photocatalytic TiO_2/CDs nanocomposites 147

2.3.1. Introduction and contributions to this work 147

2.3.2. Supplementary information 158

2.3.3. Conclusion 162

3. Conclusion and future perspectives 163
3.1. Development of visible-light-active photocatalytic nanocomposites 164
3.2. Sunlight-driven photodegradation of ciprofloxacin 165
3.3. Life Cycle Assessment studies of photocatalytic TiO_2/CDs nanocomposites .. 166
3.4. Future works 167

List of Abbreviations

AOP	ADVANCED OXIDATION PROCESS
BH	BERBERIDE CHLORIDE HYDRATE
CA	CITRIC ACID
CB	CONDUCTION BAND
CDS	CARBON DOTS
CIE	INTERNATIONAL COMMISSION ON ILLUMINATION
CIEEL	CHEMICALLY INITIATED ELECTRON EXCHANGE LUMINESCENCE
CIP	CIPROFLOXACIN
COD	CHEMICAL OXYGEN DEMAND
CV	CRYSTAL VIOLET
DPA	DIPHENYLAMINE
EB	ETHIDIUM BROMIDE
ECL	ELECTROCHEMILUMINESCENCE
EDA	ETHYLENEDIAMINE
EIS	ELECTROCHEMICAL IMPEDANCE SPECTROSCOPY
EFSA	EUROPEAN FOOD SAFETY AUTHORITY
FE	FRESHWATER EUTROPHICATION
FET	FRESHWATER ECOTOXICITY
FPM	FINE PARTICULATE MATTER FORMATION
FR	FOSSIL RESOURCE SCARCITY
FU	FUNCTIONAL UNIT
GW	GLOBAL WARMING
HER	HYDROGEN EVOLUTION REACTION
HPPT	4-HYDROXY-1H-PYRROLO-[3,4-C]-PYRIDINE-1,3,6,-TRIONE
HOMO	HIGHEST OCCUPIED MOLECULAR ORBITAL
LCA	LIFE CYCLE ASSESSMENT
LOD	LIMIT OF DETECTION
LU	LAND USE
LUMO	LOWEST UNOCCUPIED MOLECULAR ORBITAL
HC	HUMAN CARCINOGENIC
HNC	HUMAN NON-CARCINOGENIC
HT	HYDROTHERMAL TREATMENT

IC	INDIGO CARMINE
IR	IONIZATION RADIATION
PET	PHOTOINDUCED ELECTRON TRANSFER
PFAS	PER- AND POLYFLUOROALKYL SUBSTANCES
PFOA	PERFLUOROOCTANOIC ACID
PFOS	PERFLUOROOCTANE SULFONATE
PL	PHOTOLUMINESCENCE
MB	METHYLENE BLUE
ME	MARINE EUTROPHICATION
MET	MARINE ECOTOXICITY
MG	MALACHITE GREEN
MO	METHYL ORANGE
MR	MINERAL RESOURCE SCARCITY
MY	METANIL YELLOW
NC_{100}	NANOCOMPOSITE PREPARED WITH CDS MADE FULLY FROM COMMERCIAL REAGENTS
$NC_{50:50}$	NANOCOMPOSITE PREPARED WITH CDS CONTAINING CORN STOVER
NM	NITROMETHANE
QDS	QUANTUM DOTS
QY_{PL}	PHOTOLUMINESCENCE QUANTUM YIELD
OER	OXYGEN EVOLUTION REACTION
OF	OZONE FORMATION – HUMAN HEALTH
OF-TE	OZONE FORMATION – TERRESTRIAL ECOTOXICITY
PEC	PHOTOELECTROCHEMICAL
PET	PHOTOINDUCED ELECTRON TRANSFER
RHB	RHODAMINE B
ROS	REACTIVE OXYGEN SPECIES
RT	RETENTION TIME
SO	STRATOSPHERIC OZONE DEPLETION
SPE	SOLID PHASE EXTRACTION
SPR	SURFACE PLASMON RESONANCE
TA	TERRESTRIAL ACIDIFICATION
TET	TERRESTRIAL ECOTOXICITY
TIO_2	TITANIUM DIOXIDE
TMB	3,3’,5,5’-TETRAMETHYLBENZIDINE

TTBO	TITANIUM (IV) BUTOXIDE
TTIP	TITANIUM (IV) ISOPROPOXIDE
UCPL	UPCONVERSION PHOTOLUMINESCENCE
USEPA	U. S. ENVIRONMENTAL PROTECTION AGENCY
VB	VALENCE BAND
WC	WATER CONSUMPTION

1. Introduction

1.1 Carbon dots: synthesis, properties, applications, and sustainability

Book Chapter

Citric Acid as a Precursor for Carbon Dots: Synthesis, Properties, Applications and Sustainability

Sendão, Ricardo M. S.; Silva, José P.; Freitas, Martinho; Carneiro, Beatriz; Esteves da Silva, Joaquim C. G.; Pinto da Silva, Luís. "Citric Acid as a Precursor for Carbon Dots: Synthesis, Properties, Applications and Sustainability" (Chapter 2). In: Advances in Chemistry Research, Volume 79 (Ed.: James C. Taylor). Nova Science Publishers, **2023**. ISBN: 979-8-88697-947-3.

1.1.1. Introduction and contributions to this work

Carbon dots (CDs) are carbon-based nanoparticles that present several interesting properties, chief among which are a high photoluminescence, good water solubility, biocompatibility, and an extended absorption range. Because of this, research teams have focused on the development of CDs toward several different applications, such as sensing and biosensing, photodynamic therapy, photovoltaics, light-emitting devices, nanothermometry, and photocatalysis. CDs can be prepared either via top-down or bottom-up strategies, with citric acid (CA) being perhaps the most widely employed carbon precursor in the synthesis of CDs due to presenting the desired characteristics for the synthesis while being inexpensive and readily available. Herein we performed an in-depth review of CA-based CDs, a common study case, in terms of it using during the synthesis (either solo or with dopants), the properties and reactivity of the resulting nanoparticles, their applications and a study of their sustainability and potential environmental impacts, including the outcome of substituting commercially available CA by biomass as the carbon source.

In this work, I was responsible for the bibliographic research, the writing of the first draft, with assistance from other co-authors, with the revision of the final draft being made the supervision of Professor Dr. Luís Pinto da Silva and Professor Dr. Joaquim Esteves da Silva.

Chapter 2

Citric Acid as a Precursor for Carbon Dots: Synthesis, Properties, Applications and Sustainability

Ricardo M. S. Sendão
José Pedro Silva
Martinho Freitas
Beatriz Azevedo Carneiro
Joaquim C. G. Esteves da Silva
and Luís Pinto da Silva*

Chemistry Research Unit (CIQUP), Institute of Molecular Sciences (IMS),
Department of Geosciences, Environment and Territorial Planning,
Faculty of Sciences, University of Porto (FCUP), Porto, Portugal

Abstract

Citric acid is a versatile weak acid compound that is best known for its role in the citric acid cycle, a process that occurs in the metabolism of all aerobic organisms. Citric acid is also employed in several other applications, including the synthesis of carbon dots (CDs). These carbonaceous nanoparticles present several interesting properties, such as a high photoluminescence, broadband absorption of light, biocompatibility, and low toxicity, making them good candidates for a wide range of applications.

CDs are produced following either top-down or bottom-up methodologies, with citric acid being commonly used as a carbon source

* Corresponding Author's Email: luis.silva@fc.up.pt.

In: Advances in Chemistry Research. Volume 79
Editor: James C. Taylor
ISBN: 979-8-88697-947-3
© 2023 Nova Science Publishers, Inc.

in the synthesis. Due to being inexpensive, readily available, and presenting the desirable characteristics for the synthesis, citric acid can easily be employed solo or in conjugation with heteroatom or metallic dopants to yield finely tuned CDs with the desired properties.

Herein, we will discuss the use of citric acid (both solo and in conjugation with dopants) for the synthesis of CDs, the particles resulting thereof, their applications and potential development of novel technologies. Furthermore, the effect role of the synthesis by-products on the citric acid-based CDs' properties and reactivity is also reviewed.

Finally, considering the importance of environmental sustainability of a process in today's world, the efficient substitution of commercial grade citric acid by biomass and waste products as carbon source for the synthesis is also reviewed, including the different environmental impacts that result thereof. The potential of carbon dots as catalysts for energy-efficient reactions, such as marine chemiluminescence, will also be reported.

Keywords: citric acid, carbon dots, sustainability, engineered nanomaterials, sensing, bioimaging, catalysis, fluorescence, chemiluminescence

Introduction

Citric acid (CA), also denominated as 2-Hydroxypropane-1,2,3-tricarboxylic acid is a colorless weak organic acid presenting the chemical formula $HOC(CO_2H)(CH_2CO_2H)_2$ (Figure 1). CA is naturally present in several fruits and vegetables, most important of which are citrus fruits (such as limes and lemons), from which its name is derived. In fruits with a high concentration of CA, it can constitute as high as 8% of the fruits' dry weight, with the concentration in the citrus fruits ranging anywhere between 0.005 M and 0.3 M for oranges and grapefruits, respectively [1]. The best-known application of CA is its role as an intermediate in the CA cycle, which is a part of the metabolism of aerobic organisms.

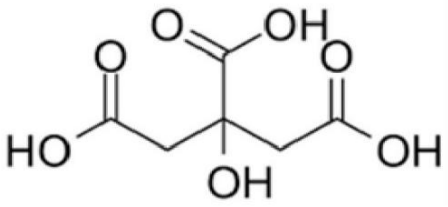


Figure 1. CA structure.

Regarding its general properties, CA is available in both as an anhydrous (MW = 192.123 g mol^{-1}) or as a monohydrate (MW = 210.140 g mol^{-1}), having the appearance of small-sized white or colorless crystalline structures. It is highly soluble in water (up to 64.3% w/w at 30ºC) and ethanol. CA solutions can be employed as buffer solutions between pH 2 and pH 8, whereas a 1 mM solution of the compound presents a pH of 3.2, explaining the acidity of citrus fruits, who tend to have a higher concentration of CA, and thus a lower pH.

Albeit naturally occurring, CA was not isolated until 1784, when it was crystallized from lemon juice. It took another century (1890) for it to be industrially produced, a process based in the citrus juice being mixed with calcium hydroxide to precipitate calcium citrate, which was then converted into CA via interaction with sulfuric acid. Three years later, another process, based on the microbial production of CA from sugar, was reported. The microbial pathway became the predominant CA production method, with the pharmaceutical companies Pfizer and Citrique Belge employing the mold *Aspergillus niger* in the large-scale production of CA. Thus, the major production route for CA was discovered and is still used to this day.

Cultures of *A. niger* are inserted into a sucrose or glucose-rich medium, feed on the sugars, and are then filtered [2]. After this, similar to the process first used in 1784, calcium hydroxide is added to precipitate citrate, which is turned into CA by reacting with sulfuric acid. In our age, it is estimated that over two million tons of CA are produced every year, with over half of the total production originating in China. The large amount is justified by the wide range of everyday applications. More than 50% of the total production is used in the beer industry as an acidity regulator, whereas an additional 20% is used in other food applications and other 20% in detergent applications. The remaining 10% of the production is for all the remaining applications, including its use in cosmetics, pharmaceuticals and in the chemical industry [3].

CA is required for many applications and processes, most important of which, the cyclic acid cycle, or Krebs cycle. This is of paramount important for aerobic organisms, the chains of reactions involved are responsible for around two-thirds of all food-derived energy obtained by complex organisms. However, CA is also important in processes outside the realm of biochemistry. Its major industrial application is in the food and beverage industry. Due to being one of the stronger, but edible, acids, it is commonly used as a flavoring and preservative in food and beverages, especially soft drinks and sugar-rich candies [3]. Due to CA being an excellent chelating agent, citrate salts of diverse metals are chosen as carriers to facilitate the uptake of these minerals

by the organism. Moreover, CA is also used as an emulsifying agent in ice cream and caramel and is even employed as a substitute of lemon juice and vinegar in some recipes.

Outside the food and beverage industry, it is used for purposed as varied as the making of bath salts and bombs, shampoos, a degreasing agent, removal of limescale from boilers, water treatment via metal removal, rust removal, stainless steel passivation, soldering flux and production of antiviral facial tissues. Finally, being a versatile precursor to several organic molecules, it is also employed in the chemical industry. This chapter concerns a particular application of CA, its use as a carbon source in the fabrication of carbon-based nanoparticles, also known as carbon dots (CDs).

Carbon Dots: What Are They?

Over the past few years, nanostructured materials have been extensively studied as potential substitutes to traditionally used materials. Due to the properties enabled by their nanosized structure, these materials present superior properties for a whole range of applications. Regarding a particular nanomaterial class, carbon-based nanomaterials, several subtypes of nanomaterials have been added to the family over the years, each presenting their own unique properties and advantages. Carbon is a black material that, when in bulk, is not soluble in water and is not able to present photoluminescence. However, when in a nanosized form, it displays properties that are largely different from those of the bulk material. These nanosized materials, suitable for a diverse range of applications, include both single [4] and multi-walled [5] carbon nanotubes, nanodiamonds [6], nanofibers [7], graphene [8], buckminsterfullerene [9], and CDs [10-15].

CDs were first discovered in 2004 by Xu et al., who, during the synthesis of single-walled carbon nanotubes, managed to isolate carbon nanoparticles as a by-product [16]. This novel class of carbon-based nanomaterials were named as CDs in 2006 by Sun et al., [17] becoming a topic of interest for the scientific community ever since. CDs are usually sized between 1 and 10 nm and display a spherical or near-spherical shape [18]. They may have a sp^2-conjugated amorphous or nanocrystalline core (depending on the synthetic methodology) with oxygenated functional groups on the surface, such as -OH, -COOH and -CHO [18, 19].

The CDs core is mostly made of sp^2-carbon or graphene/graphene oxide sheets interconnected by sp^3 carbon atoms located in-between the layers,

forming a diamond-like array [20, 21]. On the surface level, several functional groups may be found (e.g., alcohols, amines, and carboxylic acids). These groups contribute to the CDs superior water solubility and allow the CDs to undergo additional functionalization and passivation steps (to enhance the CDs properties), as they provide binding sites for other molecules [20]. All this leads to a highly complex internal and external nanoparticle structure, whose constitution depends on the precursors and conditions used during the synthesis, both of which can be controlled and tuned to obtain the desired outcome.

From their structure results that CDs possess several desirable properties and characteristics, including its production being inexpensive, presenting a high photoluminescence quantum yield (QY_{PL}) [12, 13, 19, 22], broadband absorption range [20], good water solubility [12, 18], high photo- and chemical stability [18, 23], biocompatibility [9, 24, 25], and low toxicity [25, 26]. Moreover, when compared to their most direct competitors, metal-based quantum dots, CDs are considerably less toxic (due to not using heavy metals that are prone to cause bioaccumulation) and present a larger Stokes shift, meaning that the fluorescence wavelength maximum of the CDs can vary greatly depending on the excitation wavelength, which is contrary to what happens with quantum dots [23]. From this results that, for CDs, a variation of the excitation wavelength causes a shift of the emission spectrum and that if the nanoparticles' synthesis and post-synthetic treatment are performed properly, it is possible to obtain emissions in the near infrared region upon absorption of ultraviolet radiation [24].

Finally, there is also the possibility of fabricating CDs with up-conversion photoluminescence, something which allows the CDs to convert lower-energy higher-wavelength radiation into higher-energy lower-wavelength radiation, widening the potential uses of CDs and increasing their effectiveness in applications such as photocatalysis [27]. Considering the diverse properties displayed by CDs and the interest they might create for diverse applications, CDs usually need to be thoroughly characterized via techniques such as TEM/SEM, UV-Vis and photoluminescence spectroscopy, FTIR and XPS, among others.

CDs: Synthesis and Purification

Regarding their production, CDs can be prepared via an array of methodologies that can be separated into two main groups: top-down and

bottom-up methodologies (Figure 2). Top-down methodologies are based on the CDs being prepared by breaking down bigger, macroscopic, bulk carbon materials, such as activated carbon, graphite, and carbon nanotubes. Usually, this requires expensive equipment and work-intensive techniques. This group includes the preparation of CDs via techniques such as arc-discharge [16], laser ablation [17], chemical exfoliation [28], ultrasonic treatment [29] and electrochemical shocking [30].

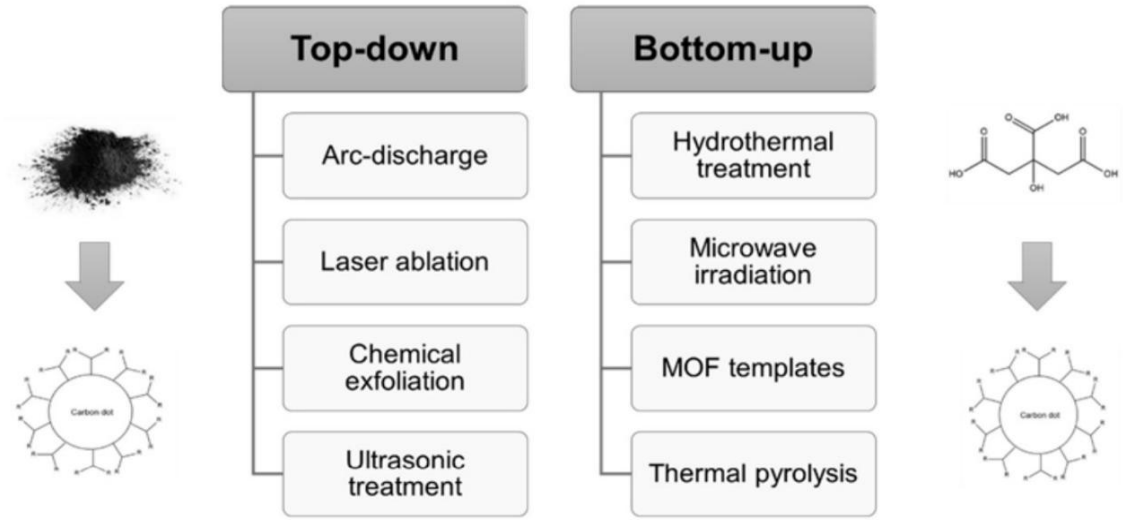


Figure 2. Top-down and bottom-up synthetic pathways to produce CDs.

Opposite to this we have bottom-up methodologies, which are based in the association of smaller, molecular-sized, carbon-based compounds (e.g., glucose and CA) into bigger structures, the CDs. Bottom-up methodologies include hydrothermal treatment [31-33], microwave irradiation [22, 31, 34, 35], metal-organic framework templates [36], plasma treatment [37] and thermal pyrolysis [38]. While each methodology has its merits and demerits, bottom-up routes are typically simpler, less expensive and faster than top-down routes. Because of this, typically bottom-up strategies are preferred in detriment of top-down routes. Across the variety of possible synthetic pathways, the most commonly employed routes for the synthesis of CDs are based in the microwave irradiation or hydrothermal treatment of a solution containing a molecular carbon-source, and, if doping the CDs is intended, heteroatom-containing compounds (typically nitrogen and Sulphur-sources) can be added to the precursor solution [22, 24, 27, 31-35, 39-42].

The first report concerning CDs produced via microwave irradiation came from Zhu et al., who in 2009 produced the carbon nanoparticles from a

solution of poly(ethylene glycol) (PEG-200) and glucose/fructose [35]. A microwave oven was employed to irradiate to solution for 2 to 10 minutes (potency of 500W), after which resulted CDs ranging from 2.57 ± 0.45 to 3.65 ± 0.60 nm in diameter [35]. The CDs presented a high QY_{PL}, a broad absorption range (from the UV into the infrared), a high oxygen content and hydrophilic groups that permitted a superior water solubility, a characteristic trait of this kind of synthesis [35, 43, 44].

As for the hydrothermally synthesized CDs, the first ones were reported by Yang et al. in 2011 [45]. A mixture of glucose and potassium phosphate was prepared, dissolved, and transferred into a Teflon-lined autoclave. It was then subjected to a temperature of 200ºC for 12 h, after which a centrifugation and salt removal steps ensued [45]. By managing the molar ratios between the species in the precursor mixture, the authors obtained CDs with tunable emission and particle sizes, allowing for the making of tailor-made CDs for specific applications. The possibilities were nearly endless, as CDs with emissions across the whole visible range were produced [45].

Due to the easiness and low-cost of bottom-up strategies, in particular when compared to top-down methods, and due to the tunable emission properties of CDs, strategies such as hydrothermal treatment and microwave-assisted synthesis are regarded as the most commonly used ways of fabricating tailor-made CDs. Furthermore, with bottom-up strategies, when employing natural bioresources, it is possible to avoid the need of passivating the CDs surface, as -OH groups are already oxidized during the process, thus permitting a one-step synthesis of ready to use CDs while also reducing the cost in terms of time and resources [46, 47].

Finally, to obtain the CDs' carbogenic core, a carbon-source must always be used to provide the required components. Whereas CDs can derive from a variety of different precursors, both commercially available chemical reagents and natural resources (e. g. corn stover, bee wax, fish scales, among others), the most commonly employed carbon-source in CDs synthesis is CA. This reagent, which is inexpensive and easy to obtain, has been used in a multitude of CDs synthesis since they were discovered, as it possesses both carbon and oxygen atoms, is easily soluble and is known to produce highly photoluminescent CDs via both top-down and bottom-up synthetic methodologies.

Moreover, to further enhance the optical properties of the resulting nanoparticles, researchers frequently resort to heteroatom doping, a process in which a heteroatom containing molecule (e.g., urea or ethylenediamine for N-doping or thiourea for N,S-doping) is added to the reaction mixture [43, 48].

This requires a good interaction between the carbon source and the heteroatom containing molecules. CA, due to its chemical structure, can easily interact with heteroatom-containing groups such as amines, promoting the formation of citrazinic acid and its respective derivatives, which are strongly emissive blue fluorophores [49-51].

CA-Based CDs: Applications

Since their discovery, CDs have been used in several applications (Figure 3), even some for which quantum dots are unsuitable because of their toxicity. Thus far, the use of CDs has been reported for bioimaging [24, 52], sensing and biosensing [12, 32, 53], drug delivery systems [26, 54], photodynamic therapy [55, 56], nanothermometry [15], light emitting devices [57, 58], photocatalysis [10, 11, 59], and photovoltaic devices [60, 61], just to name a few. It is unsurprising that CA, being such a common carbon-source for CDs, was already used in nearly all of these applications. A brief paragraph on each main application is given below.

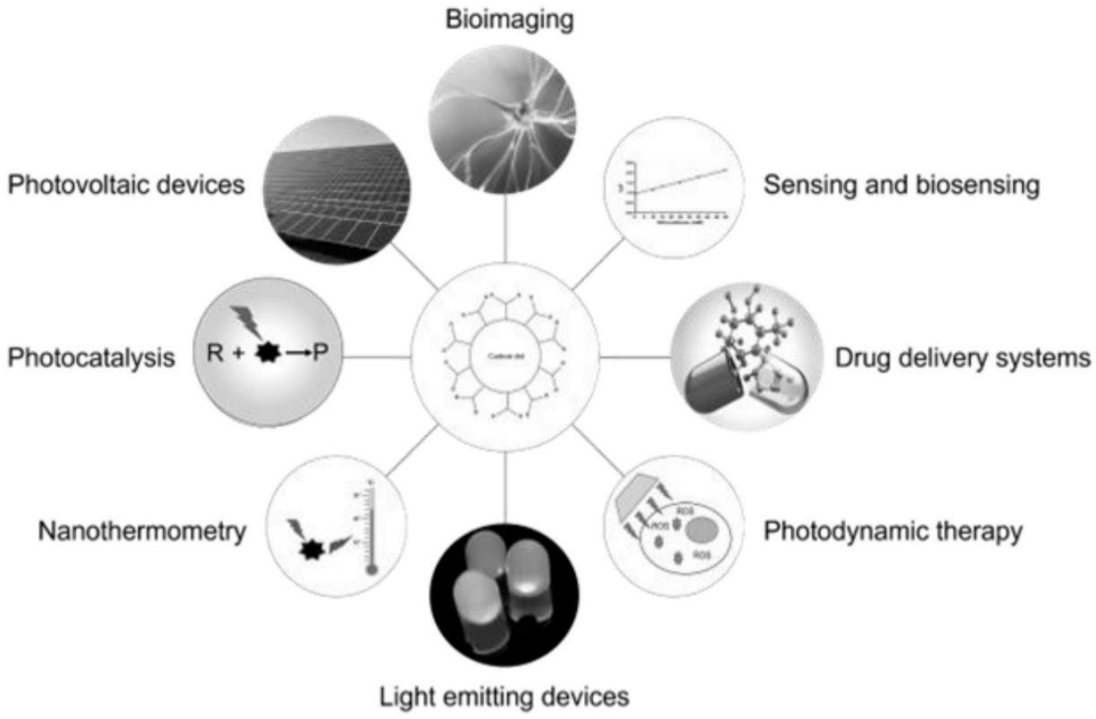


Figure 3. General representation of several applications for CDs.

Bioimaging

The low toxicity and high biocompatibility of CDs makes them good candidates for bioimaging, as their high photoluminescence permits an easier detection of the particles inside the study object. Fiori et al., using a hydrothermal route, prepared CDs from a combination of CA and either tris (hydroxymethyl)-aminomethane (tris) or arginine methyl ester dihydrochloride [62]. When characterized, the CDs made from CA and tris presented an average size of 2 nm, a high photostability and a QY_{PL} of 37%. Furthermore, the CDs proved to be biocompatible, allowing for a 100% cell survivability rate after 24 h of incubation [62]. Cell imaging tests confirmed the uptake of the CDs by the tested cells, with the CDs being mainly localized in the cytoplasm and occasionally in the nucleus.

Overall, the low cytotoxicity, high photoluminescence and easy uptake by the cells make these CDs potential candidates for application in bioimaging without risking damaging the targeted cells [62]. The previous work being just one example, more study cases can be found regarding successful CA-based CDs in bioimaging with other precursors: CA and ethylenediamine by Ding et al. [63], CA and tetraoctyalammonium bromide by Bhaisare et al. [64], CA and metformin by Wan et al. [65], CA and 8-aminiquinol by Li et al. [66], and CA and polyethylene imine by Wang et al. [67], just to name a few.

Sensing and Biosensing

Several cases have been reported on the successful use of CA-based CDs for both sensing and biosensing. Shan et al. [68] developed CA and benzoylurea-based CDs for the selective sensing of Fe(III). The CDs were prepared via calcination and presented an average size of 5.2 nm and a high, excitation-dependent, photoluminescence. In the presence of Fe(III), the CDs photoluminescence suffered quenching, allowing for a quantitative sensing of species with a detection limit as low as 1.1 μM. Furthermore, of 20 tested metal ions, only Fe(III) could quench the CDs' photoluminescence, indicating a high selectivity, which is important for sensing applications [68].

In another study, Wang et al. prepared CA and 3,5-diaminobenzoic acid-based CDs for the sensing of NO_2^- and pH on living cells [69]. The hydrothermal synthesis resulted in CDs with an average size of 2.16 nm, broad absorption, a high QY_{PL} of 41%, and more importantly, a low toxicity which enabled their use in biological samples. NO_2^- and pH sensing were achieved

in HeLa cells using the CDs. Increasing NO_2^- concentrations and pH led to a quenching of the CDs' photoluminescence [69]. Other cases were reported for the sensing of both metals [70-72] and organic compounds [73-75] using CA-based CDs.

Drug Delivery Systems

The biocompatibility and molecular binding spots of CDs enable them to become potential drug delivery systems capable of transporting a coupled pharmaceutical into the target site (e.g., by easing their passage through the blood brain barrier).

Kong et al. reported the preparation of CA and ethylenediamine-based CDs via hydrothermal treatment towards the delivery of doxorubicin to the target site in breast cancer cells [54]. The prepared CDs were biocompatible and presented a quasi-spherical morphology with an average size of 0.5 nm. A quenching of the CDs' photoluminescence intensity confirmed the successful electrostatic-driven loading of doxorubicin onto the nanoparticles. A doxorubicin capacity of 28.75 mg g^{-1} was achieved with the CDs, with a release rate of 71% after 72 h at pH 7.4 (physiological levels) [54].

In terms of anti-tumoral efficiency, due to a higher degree of drug uptaking by the cell, doxorubicin-loaded CDs showed more cytotoxicity towards MCF-7 breast cancer cells than free doxorubicin. This was due to more doxorubicin being delivered to the drug target site with the complex, in this case, the cell nucleus [54]. Other examples of CA-based CDs for drug delivery systems can be found on [76-79].

Photodynamic Therapy

Good biocompatibility and low toxicity towards healthy human cells are known properties of CDs. However, in specific cases under suitable light irradiation, CDs are capable of a localized toxic effect by producing ROS when photoexcited, hence presenting potential for photodynamic therapy. In 2022 Suner et al. reported producing CA, ethylenediamine and arginine-based CDs via microwave-assisted synthesis [80]. The CDs presented an average size of 2.3 nm, a graphitic structure and high photoluminescence.

Their biocompatibility was confirmed via cytotoxicity analysis and blood compatibility tests. When excited under UV-light (315-400 nm, 300 W lamp),

a 5 mg mL^{-1} concentration of CDs inhibited circa 49 ± 7% of the tested bacteria (*E. coli*) within 5 minutes of irradiation [80]. Other studies regarding the use of CDs for photodynamic therapy were reported for both microorganisms [81, 82] and tumor cells [83, 84].

Light Emitting Devices

Due to their high photoluminescence, tunable emission and photostability, it is no surprise that CDs have been studied for applications in light emitting devices. Wang et al. reported the microwave-assisted fabrication of CA and cyclen-based CDs for white light-emitting diodes [85]. The synthesized CDs, sized between 1 and 4 nm, presented an intense yellow solid-state fluorescence under UV-light and a QY_{PL} of 48%. However, when the excitation wavelength is changed to 450 nm, the CDs' emission peak is located at 546 nm (CIE coordinates 0.43, 0.55). This enables them to, when combined with a blue-emitting chip, to fabricate low-cost, non-toxic, and environmentally friendly white light-emitting diodes [85].

This is quite significant, as the current alternative for white light-emitting diodes is based on the use of semiconductor quantum dots, which use toxic heavy metals, and rare earth-based phosphors, which are both expensive and non-renewable. Other examples regarding the use of CDs for light-emitting applications can be found on [86-88].

Nanothermometry

One of the many possible operating principles behind nanothermometry is that of non-contact luminescent thermometry, which exploits temperature-dependent emissive behaviors as a base for temperature determination, a characteristic which CDs may present.

Kalytchuk et al. fabricated a nanothermometer out of CA and cysteine-based CDs prepared via hydrothermal treatment [15]. The particles displayed an average size of 4.5 nm, a stable photoluminescence, low toxicity, and good biocompatibility. Their photoluminescence lifetime is stable across different concentrations, ionic strengths, and pH values. Their photoluminescence lifetime was stable over 40 h, and sensible to temperature changes between 15 and 45 ºC.

Furthermore, this was reversible for at least 7 cycles, confirming its reusability and they presented a sensitivity of 1.79% K^{-1}. Due to their low cytotoxicity, high stability at biological pH and temperature ranges, high sensitivity to relevant temperatures, the CDs have potential for use in applications related to temperature measurements in biological samples [15]. Other examples of CA-based CDs exist for this application [89-91].

Photocatalysis

CDs are potential candidates for applications in photocatalysis due to their broad absorption range, photostability and capacity of generating charge carriers (e^- and h^+) upon suitable light absorption. In fact, they have been used for varied photocatalytic applications such as hydrogen generation via water splitting, photodegradation of organic pollutants and photoreduction (Figure 4) [92].

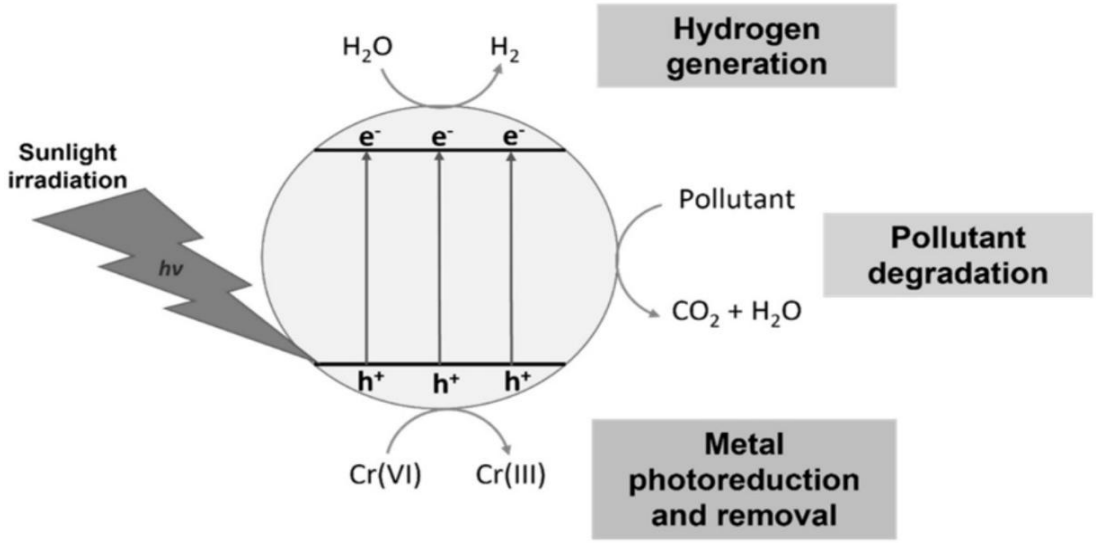


Figure 4. Possible application of CDs in photocatalysis. Reproduced with authorization from [92].

Jana et al. achieved efficient hydrogen generation using CA and urea-based CDs [93]. The CDs were prepared using a microwave-assisted method and presented sizes between 2.5 and 3.5 nm and potential for photoinduced electron transfer (PET). Under Xe lamp irradiation the best performing CDs achieved a maximum turnover frequency (TOF) of 15.15 mmol (H_2) g(CD2)$^{-1}$ h^{-1} after 1 h, which is comparable to that of most semiconductors [93].

Regarding pollutant degradation, Zhou et al. prepared gel-like CDs from CA and ethylenediamine towards the sunlight-driven degradation of common organic dyes [94]. The CDs managed to fully degrade the pollutants methylene blue, methyl orange and rhodamine B in 20, 40 and 60 minutes, respectively [94]. The use of CA-based CDs has been studied for hydrogen generation [95, 96], photodegradation [41, 97] and photoreduction [98, 99].

Photovoltaic Devices

Due to their properties, CDs are interesting study cases for application in photovoltaic devices. Lim et al. prepared CA and ethylenediamine-based CDs to be employed as an interlayer on photovoltaic devices [100]. The microwave-assisted synthesis yielded CDs with an average size of 10 nm. After synthesis and purification, they were then dispersed by spin coating on an ethoxylated polyethylenimine to act as an electron extraction layer on the polymer nanocomposite-based photovoltaic device [100]. The addition of the CDs to the interfacial layer led to a 12.2% increase of the photovoltaic performance when compared to the control devices. Furthermore, the power conversion efficiency was enhanced by 8.34% while the external quantum efficiency was enhanced by over 30% (around the 440 nm range) [100]. Other examples of CA-based CDs for photovoltaic devices can be found on [101, 102].

CDs: Heteroatom and Metal Doping

Over the course of the years, several strategies have been developed to enhance the photoluminescence intensity of CDs. The best-known example of this is that of modifying the nanoparticles' surface with heteroatoms in a process dubbed heteroatom doping. Doping is a useful process commonly used to increase the QY_{PL} of CDs. This is due to it prompting the formation of n- and p-type carriers (extra e^- and h^+), changing the CDs' electronic structure [103]. Thus far, heteroatom doping has been reported for elements such as nitrogen [68, 104], boron [12, 40], sulphur [96, 105] and phosphor [106, 107].

Among heteroatom doping, nitrogen-doped CDs are the most commonly used systems, as nitrogen atoms are known to affect the edge states, energy levels, catalytic activities and even physicochemical properties [108-110]. In

2021, Lee et al. published a study regarding the effect of N-doping on the optical properties and enzymatic activity of CDs [111]. Several CA and ethylenediamine-based CDs were prepared via a hydrothermal method, yielding CDs with a ratio of CA to ethylenediamine of 1:1.5 (N-CD1), 1:1 (N-CD2), 1:0.5 (N-CD3), 1:0.3 (N-CD4) and 1:0.25 (N-CD5). The CDs average sizes ranged between 5.9 and 13.7 nm, with the smallest particle being observed on N-CD3. FTIR analysis confirmed the presence of the same surface functional groups on all CDs (Table 1).

Table 1. Summary of data from high resolution analysis representing both band energies and corresponding groups

C *1s*	N *1s*	O *1s*
C-C / C=C – 284.0 eV	N-pyrrole – 399.5 eV	C=O – 531.1 eV
C-N – 288.5 eV	N-graphite – 401 eV (except N-CD1)	C-O = 532.6 eV
C=O – 288.2 eV		

The XPS profile of the CDs exhibits defined C_{1s}, N_{1s} and O_{1s} signals, as was expected. Interestingly, it also showed that N-CD2 displayed the highest N_{1s} peak, even though it was not made using the highest ratio of nitrogen-source. Further high-resolution analysis was performed. For C_{1s}, all CDs' display a peak at 284 eV ascribed C-C and C=C bonds (from carbon atoms in the carbogenic core of the nanoparticles), a peak at 285.5 eV attributed to C-N bonds (thus confirming the success of N-doping) and a peak at 288.2 eV derived from C=O bonds. Both C-N and C=O are peaks of carbon-heteroatom bonds, suggesting the presence of functional groups on the CDs' surface [111]. Furthermore, it was demonstrated that N-CD2, N-CD3 and N-CD4 present a high ratio of carbon-heteroatom bonds and that the N_{1s} spectra of all CDs shows a peak attributed to N-pyrrole (399.5 eV) at the edge sites of the carbogenic domain and a peak of N-graphite (401 eV) on the sp^2 carbon domain (except on N-CD1) [111].

Finally, the O_{1s} spectra shows two peaks at 532.6 and 531.1 eV, corresponding to C-O and C=O bonds, with the latter being predominant due to the polymerization of the material via amide bond formation [111]. This demonstrates that while the same dopant was employed on all synthesis, it led to different outcomes depending on the carbon:nitrogen ratio.

Lee's team then proceeded to investigate the optical properties of the N-doped CDs. First, they observed that a new absorption band at 340 nm (C=O, assigned to n-π* edge transition) and a shoulder at 240 nm (-C=C-, ascribed to π-π* on sp^2 carbogenic core) appeared when compared to non-doped CDs [111]. Secondly, each N-doped CD presented a different photoluminescence spectrum when excited at 350 nm. When excited, N-CD1 and N-CD2 emission presented two bands (450/517 nm and 450/500 nm, respectively), whereas N-CDs 3, 4 and 5 exhibited only one emission band (450, 450 and 464 nm, respectively) [111].

It is considered that graphitic domains may induce red-shifts on the particles emission, whereas pyrrolic domains do not affect the band gap of the carbogenic domains [112]. However, N-CDs 1,2 and 5 all show red-shifted emissions, despite containing mostly pyrrole functional groups. Given that a higher number of edge functional groups leads to a decrease in the size of p-conjugated carbogenic domains, it can be considered that N-CDs 3 and 4, which present a relatively low carbon content, emit lower-wavelength, higher-energy, radiation due to the small size of the p-conjugated carbogenic domains, which are, on the other hand, of expanded size in N-CDs 1,2 and 5 [111].

The QY_{PL} of the CDs was also measured. By order (N-CD1 to 5), the QY_{PL} were estimated to be 6.6, 15.1, 22.6, 14.9 and 9.3%, respectively, which is higher than the 3% calculated for non-doped CDs. The optimal carbon:nitrogen ratio for QY_{PL} was 1:0.5 (N-CD3), with lower N contents decreasing the QY_{PL}. N-CDs 1 and 2 presented also lower QY_{PL} despite their higher N content, something that can be attributed to the generation of long-lived defect states on the nanoparticles' surface by the large quantities of N dopant [111, 113]. Finally, the photoluminescence lifetimes of N-doped CDs are longer than that of non-doped CDs due to the surface passivation of the CDs decreasing the non-radiative recombination and self-trapping of excitons [111]. All being said, the content of N-dopant included during the CDs synthesis is a crucial factor affecting their optical properties, which are of paramount importance for most CD-related applications.

Furthermore, Lee's team explored the use of the N-doped CDs as a nanozyme platform, which is a material that can catalyze enzymatic reaction and presents similar kinetics and mechanisms to those of naturally occurring enzymes [111]. Considering previous reports, the team decided to assess the peroxidase-like activity of the nanoparticles (Figure 5). This was achieved by monitoring the oxidation of 3,3',5,5'-tetramethylbenzidine (TMB) with hydrogen peroxide at pH2. By introducing N-doped CDs in the solution, the

color changes from pale green to blue, an indicative of the oxidation of TMB. The amount of oxidized TMB, as quantified by the absorbance value at 652 nm, gradually increases due to the enzymatic reaction in the presence of both non-doped and N-doped CDs. However, N-doped CDs promoted a faster rate of TMB oxidation than non-doped CDs, which is shown by the higher initial velocity of the reaction presented by all the N-doped CDs when compared to the non-doped variant [111]. This may be a result of the high amount of C=O groups present in N-doped CDs, which are reported to act as catalytic sites [114]. Additionally, graphitic N atoms promote the adsorption of molecular oxygen to generate ROS. In conjugation, abundant C=O groups and graphitic N atoms promote a relatively high peroxidase-like activity [111].

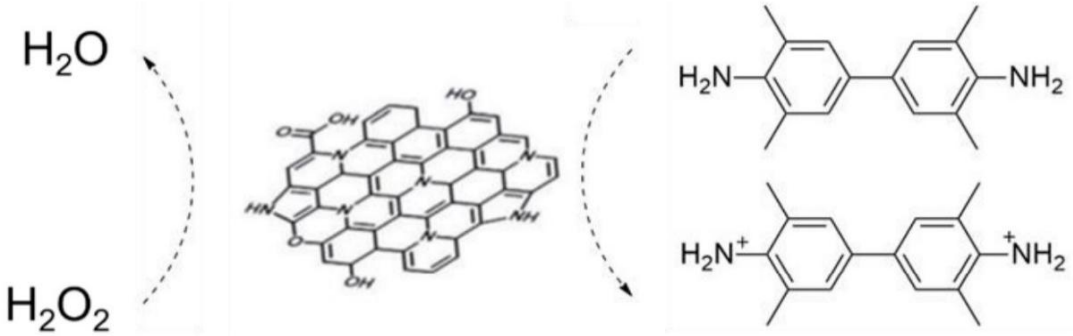


Figure 5. Schematic representation of the suggested peroxidase-like activity of N-doped CDs.

The number of possible heteroatom dopants and their combinations might result in a variety of properties which are not possible with undoped CDs. To study this, and considering the different types of heteroatom dopants and properties resulting thereof, Wibrianto et al. compared the effects of the synthesis of B, N, S or P-doped CA-based CDs, prepared by either furnace-assisted or microwave-assisted carbonization [115]. The CDs were fabricated by combining CA with either boric (B-CDs), nitric (N-CDs), sulfuric (S-CDs) or phosphoric acid (P-CDs), or no dopant at all (CDs).

In the furnace-assisted synthesis (x-CDs1, x = dopant), the mixtures were calcinated at 300 ºC for 2 h, whereas the microwave-assisted synthesis (x-CDs2) consisted of subjecting the mixtures to a microwave system with 600 W and high heat for 2 h. In either case, after the reaction the samples were dissolved in NaOH and the pH was set to neutral.

Finally, the solution was dialyzed using a dialysis bag with a MWCO of 1 kDa to exclude by-products and specify the CDs' size distribution [115]. After the synthesis, FTIR analysis confirmed the presence of common

functional groups (O-H, C-H, C-O, C=O and C=C) in all the prepared CDs. However, specific dopant-derived groups are also to be found, such as B-O, S=C, C-N and P-O-C, confirming the success of the doping process by both pyrolysis and microwave-assisted synthesis [115].

It is commonly accepted that besides size confinement and solvent effects, the photoluminescence of CDs may result from a synergy between sp^2-conjugated atoms on the CDs' core with functional groups present on the nanoparticles' surface [116, 117]. As the use of different dopants inherently results in a different surface composition, it is expected to affect both the resulting CDs' band gap and the absorption-emission profile of the nanoparticle.

Optical analysis revealed that while maximum absorption and absorption peaks are quite similar using both furnace- and microwave-assisted methods, this is not true for the energy band gaps presented by the nanoparticles [115]. Band gap values between 4.52 and 5.37 eV were found for the CDs and their order (in terms of dopants) changes depending on whether the CDs were prepared via furnace- or microwave-assisted synthesis. The band gap sequence when using the furnace method is B-CDs1 < S-CDs1 < CDs1 < N-CDs1 < P-CDs1, whereas when using microwave irradiation we have P-CDs2 < S-CDs2 < CDs2 < N-CDs2 < B-CDs2. Both P-CDs and B-CDs presented both the lowest or the highest energy band gaps, depending on the method [115]. While the differences could be due to the difficulty of controlling the precise structure of the CDs, additional studies using another CD system suggest that the thermal induction from microwave irradiation can set carbonization. In this case, the position of doped atoms matches with the proposed structure. Using a microwave rather than the furnace allows a fast, efficient, heating of material through direct energy transfer, thus reducing the energy dissipation responsible for damage to the CDs' structure and allowing a more effective carbonization [118].

Moreover, the band gaps are also affected by the doping type of the used elements. Whereas B, N and P are mostly n-type dopants, S acts as a p-type dopant on CDs, which may result in a constriction of the original band gap [119]. When it comes to photoluminescence, all CDs demonstrated a strong blue emission (peaks between 410-445 nm) when excited at 360 nm [115]. Most CDs (except for B-CDs2 and N-CDs2) demonstrated an excitation-dependent photoluminescence, a common characteristic of CDs that happens due to the defect state caused by the oxygenated groups on CDs [38]. All CDs were similar in terms of photoluminescence quantum yields with a slight

enhancement of the emission intensity being obtained through doping, with the values ranging between 31.17% (CDs2) and 32.96% (B-CDs2) [115].

Aside from heteroatom doping, CDs can also be doped using metals such as zinc [120, 121], manganese [122], copper [123, 124], gold [125] and silver [125], among others. Metallic ions can be used as electron donors in CDs, enhance the electron transfer capacity and ultimately confer new applications to the CDs. However, contrary to heteroatom-doped CDs, the majority of metal-doped CDs present a low QY_{PL} and an unclear mechanism for their photoluminescence.

Gencer et al. studied Zn(II)-incorporated CDs prepared from citric acid and zinc chloride via a microwave-assisted synthesis [121]. Two different molar ratios of CA:Zn were chosen, 1:1 (Zn(1)-CDs) and 1:10 (Zn(10)-CDs). After synthesis, the authors characterized the CDs. Differences were also observed using FTIR. In Zn(1)-CDs and Zn(10)-Cds, peaks attributed to C-O and C=O stretching partially of fully disappear, giving place to a new peak corresponding to the asymmetric stretching of COO^- groups present in zinc carboxylate [121]. These results imply that carboxylic groups on the CDs' surface are passivated as Zn(II) is added. A complete XPS survey also confirmed the presence of Zn in the CDs. Importantly, as the Zn quantity is increased, a peak attributed to CO^- gradually decreases as Zn passivate these groups, increasing the stability of the CDs.

Regarding photoluminescence, the team found that Zn(1)-CDs' photoluminescence was largely diminished when using a 1:1 ratio of CA:Zn. However, the emission intensity increased considerably in the Zn(10)-CDs compared to the non-doped CDs, with the CDs presenting QY_{PL} of 20 and 51%, respectively [121]. Furthermore, Zn(10)-CDs presented a narrower, red-shifted emission peak when compared to normal CDs, suggesting that incorporating Zn(II) in the CDs leads to an increase of non-radiative transitions, possibly due to causing heterogeneity in the CDs' structure. Whereas this would normally result in a decreased QY_{PL}, as the amount of zinc is increased the CDs' structure start to become homogeneous, resulting in a QY_{PL} higher than that of the normal CDs [121].

The photoluminescence excitation spectrum of the CDs also changed upon incorporation of Zn(II). Whereas the CDs presented two excitation peaks (288 and 343 nm) before the addition of Zn, Zn(1)-CDs nor presents three excitation peaks at 264, 325 and 400 nm (λ_{em} = 440 nm). When the Zn ratio was further increased and Zn(10)-CDs again presented 2 different peaks (281 and 372 nm), presenting an excitation spectrum closer to that of the conventional CDs, albeit with slightly different peak positions. These changes

in the excitation and emission profiles of the CDs indicate that adding Zn(II) first results in defects in the CDs' structure (increasing heterogeneity), but later starts contributing to the homogeneity of the nanoparticles as the Zn amount increases [121]. This explains the decrease and then increase in QY_{PL} of the CDs as Zn is added and also the similarity between the excitation spectra of CDs and Zn(10)-CDs and the difference between those and that of Zn(1)-CDs.

Finally, a nearly excitation-independent emission occurs in Zn(10)-CDs, which may derive from the high degree of passivation of the CDs' surface with Zn(II) [121]. The summary of these results illustrates the major differences that one can obtain when doping CDs with a metal dopant in terms of photophysical properties and how it can be used to tailor CDs to specific applications.

CDs: Impurities and Respective Consequences

Although the number of studies concerning CDs has been growing year after years, the origin of their main point of interest, their photoluminescence, is still a matter of debate. Thus far several models and possible explanations have been presented by the scientific study, including the quantum confinement effect and band gap emission [126], surface states emission [127], self-trapped excitons [128], surface dipole emissive centers [129], H-type aggregates excitonic states formation [130], among others. More recently, the role of molecular fluorophores formed during the CD synthesis on the nanoparticles' photoluminescence has also been under focus.

It has been previously reported in several studies that during the bottom-up synthesis of CDs, which is arguably the majority of the cases, leads to the production of several molecular by-products alongside the CDs during their synthesis [49, 131, 132]. This is of considerable importance when we take into account that these by-products possess an intense fluorescence that is significantly higher than that of the nanoparticles themselves. Thus, unless the synthesis products are thoroughly purified via methods such as dialysis or chromatography, the fluorescence associated to a CD solution could result instead of these molecular by-products, constituting a significant setback of our knowledge database regarding theses nanomaterials.

To study this, Sendão et al. studied the photoluminescence displayed by CDs and the molecular by-products resulting of their synthesis, as well as how these molecular fluorophores might affect the CDs' photochemical properties

and reactivity [22]. To this end, CA and urea-based CDs were synthesized via a microwave-assisted methodology and purified via centrifugation and dialysis, yielding different fractions (Figure 6): $CD_{centrifuged}$, containing both the CDs and the molecular by-products (which are low-weight and soluble) and obtained after a simple centrifugation to remove insoluble particles after the synthesis; $CD_{dialyzed}$, containing only the CD and obtained by dialyzing the synthesis products over 72 h with a MWCO of 1 kDa; and $Water_{FI}$, containing the smaller molecular by-products (whose relatively small size compared to CDs allows them to cross the dialysis bad membrane while CDs are retained) and obtained by collecting the dialysis wash water resulting from the CDs' dialysis [22, 131].

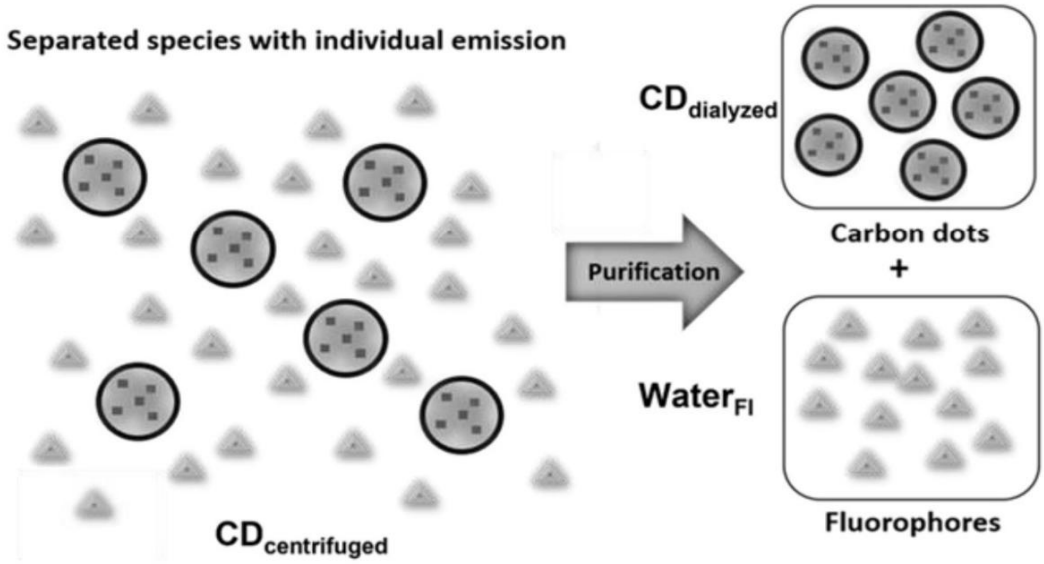


Figure 6. Schematic representation of the different fractions obtained before and after dialysis of an unpurified CDs solution.

The authors started by analyzing the CDs' structure both with and without the presence of the by-products. A full XPS survey followed by detailed scans for the C_{1s}, O_{1s} and N_{1s} levels was made. Both in the presence and absence of the by-products ($CD_{centrifuged}$ and $CD_{dialyzed}$, respectively) the CDs' fractions results are quite similar, except for a very slight increase of the C content and subsequent decrease of N and O content. Thus, the CDs' surface composition is identical between the fractions and dialysis has a limited effect on the nanoparticles [22]. This is further supported by FTIR analysis, which revealed similar spectra for both fractions.

However, this similarity is not corroborated by optical analysis. The UV-Vis absorption spectrum (Figure 7a) of $CD_{dialyzed}$ displays a band at 340 nm and a shoulder at 245 nm, which can be ascribed to n-π and π-π* transitions (C=C and C-N bonds), respectively, and an additional less discernible small band at 410 nm [22]. By its turn, the $CD_{centrifuged}$ sample presents two shoulders (245 and 275 nm), and a well-resolved band at 410 nm that is now higher than the one at 340 nm. Furthermore, the two CD-containing fractions present a major difference in terms of photoluminescence (Figure 7b), despite both presenting an excitation-dependent emission. Whereas the $CD_{centrifuged}$ samples presents an emission peak at 550 nm, the $CD_{dialyzed}$ peak is considerably blue-shifted to 475 nm.

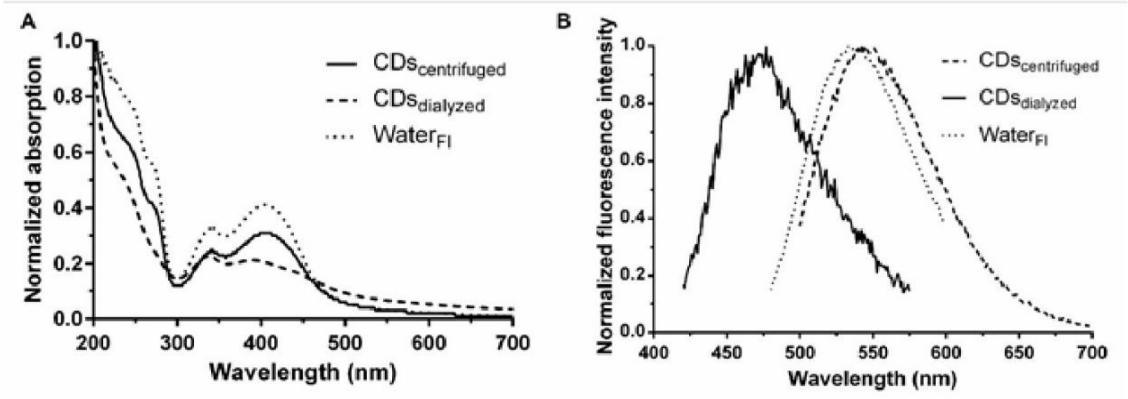


Figure 7. a) Normalized UV-Vis absorption spectra, and b) Normalized emission spectra for $CD_{centrifuged}$ (λ_{exc} = 410 nm), $CD_{dialyzed}$ (λ_{exc} = 380 nm) and $Water_{FI}$ (λ_{exc} = 410 nm). Reproduced with authorization from [22].

Additionally, the excitation wavelength maxima also change from 410 nm to 380 nm after the dialysis. Thus, purification by dialysis significantly affects the photoluminescence of the CDs and the differences between the optical properties of two fractions can be ascribed to the presence (or absence) of the molecular by-products. This is further confirmed by the fact that the $Water_{FI}$ fraction, containing only the synthesis by-products, reveals an emission profile almost identical to that of $CD_{centrifuged}$. Specifically, $Water_{FI}$ maximum excitation and emission wavelengths are 410 and 540 nm, respectively, and its absorption spectrum displays the same bands and shoulders as $CD_{centrifuged}$.

Furthermore, the $CD_{centrifuged}$ and $Water_{FI}$ samples present emission intensities of the same magnitude that are 6-8 times higher than those of $CD_{dialyzed}$ samples (the CDs by themselves). In summary, the optical properties observed on the $CD_{centrifuged}$ sample are not a result of the CDs themselves, but

rather a result of the properties of the low-weight highly fluorescent by-products which mask the emission of the carbon nanoparticles [22].

Knowing this, the authors employed mass spectroscopic analysis via ESI-MS to evaluate the samples. While not being enough to fully determine the molecular species behind the $CD_{centrifuged}$ fluorescence, it confirmed that the bottom-up synthesis of CDs results in a mixture of CDs and fluorescent by-products that require further purification steps to separate the fractions [22, 131]. Nevertheless, despite not being able to positively identify the by-products, the authors point that in the ESI-MS analysis a predominant peak, common both to $CD_{centrifuged}$ and $Water_{FI}$, but absent in the $CD_{dialyzed}$ fraction, is identified and can be attributed to 4-hydroxy-1H-pyrrolo[3,4-c]pyridine 1,3,6(2H,5H)-trione (HPPT, M.W. of 180 g mol^{-1}) [22].

HPPT was already reported by Kasprzyk et al. as being a photoluminescence by-product that resulted from the microwave-assisted synthesis of CDs [132]. Furthermore, HPPT is known to have a green emission with an absorption peak at 410, which is quite in line with the properties of both $CD_{centrifuged}$ and $Water_{FI}$. Thus, HPPT seems to be the main responsible for the CDs' photoluminescence in the $CD_{centrifuged}$ sample but, as it is removed during dialysis, it is no longer present in the $CD_{dialyzed}$ samples, explaining the difference in the properties [22].

Besides affecting the optical properties of the CDs, the presence of molecular by-products also affected the way in which the nanoparticles responded to other parameters [22]. By measuring the fractions' photoluminescence in water, HCl (0.1 M) and NaOH (0.1 M), the team confirmed that the impurities conferred pH sensitivity. Both $CD_{centrifuged}$ and $Water_{FI}$ suffered a blue-shift at basic pH while $CD_{dialyzed}$ presents no change whatsoever with the different pH. A similar study was performed by analyzing the photoluminescence spectra of the fractions in different solves, namely methanol (MeOH), acetonitrile (CAN), dimethylformamide (DMF) and dimethyl sulfoxide (DMSO).

Again, despite the range of properties of the different solvents, they had a negligible effect on $CD_{dialyzed}$, possible suggesting that the emissive moieties of the CDs are inside the nanoparticle, and so, not exposed to surrounding microenvironment [133]. By its turn, the emission spectra of $Water_{FI}$ suffers a blue-shift when compared to the 540 nm peak in water. This indicates that the fluorescent moieties are exposed to the external medium, and thus affected by it.

Interestingly, $CD_{centrifuged}$ shows an intermediate effect, in which there is also a blue-shift, but of a lesser extent of that of $Water_{FI}$. This would indicate

that like in $Water_{FI}$ the fluorescent moieties are exposed to the solvent, however, they are also somewhat more shielded of the solvents effect. Thus, in the same way that the CDs' photoluminescence is affected by the by-products, the CDs' by their turn also affect the fluorescent properties of the molecular by-products [22].

Alongside altering the optical properties of CDs, the molecular by-products of their bottom-up synthesis also seem to alter the excited state reactivity of the nanoparticles. The photoluminescent response of the three fractions was analyzed in the presence of both electron-donor and electron-acceptor molecules, diphenylamine (DPA) and nitromethane (NM), respectively [22]. The comparison of the responses of the individual parts ($CD_{dialyzed}$ and $Water_{FI}$, Figures 8b and 8c, respectively) with that of the whole ($CD_{centrifuged}$, Figure 8a) permitted to verify the existence of a synergistic effect which was more than just the sum of the effects of the individual parts.

Starting with the fractions' response to the electron-donating molecule, DPA, it was observed that the three different fractions presented a different response to increasingly higher concentrations of DPA. The photo-luminescence of $CD_{centrifuged}$ was quenched ($K_{SV} = 0.0054\ \mu M^{-1}$), whereas in $CD_{dialyzed}$ the opposite effect was observed, with the fluorescence intensity increasing with rising concentrations of DPA. Interestingly, DPA seemed to have no effect whatsoever on $Water_{FI}$. These results suggest that the DPA-induced quenching observed on $CD_{centrifuged}$ could not be a result neither from the CDs themselves nor the by-products resulting of their synthesis, both of which presented different responses to DPA than $CD_{centrifuged}$. Thus, we are left with the conclusion that, when combined in solution, the CDs and the by-products may interact and generate a synergistic effect resulting in a different response to DPA than that of either individual species [22].

When evaluating the fractions response to the electron-withdrawing molecule, it was observed that NM induced quenching in all samples (Figure 8d), suggesting that all fractions are capable of PET reactions by acting as an electron-donor. However, when irradiated at their maximum excitation, the photoluminescence $CD_{dialyzed}$ is considerably more quenched (Stern-Volmer constant, $K_{SV} = 23.7 \pm 0.1\ \mu M^{-1}$) than $CD_{centrifuged}$ and $Water_{FI}$ ($K_{SV} = 5.4 \pm 0.2\ \mu M^{-1}$ and $K_{SV} = 6.1 \pm 0.4\ \mu M^{-1}$, respectively), which present a similar response to NM.

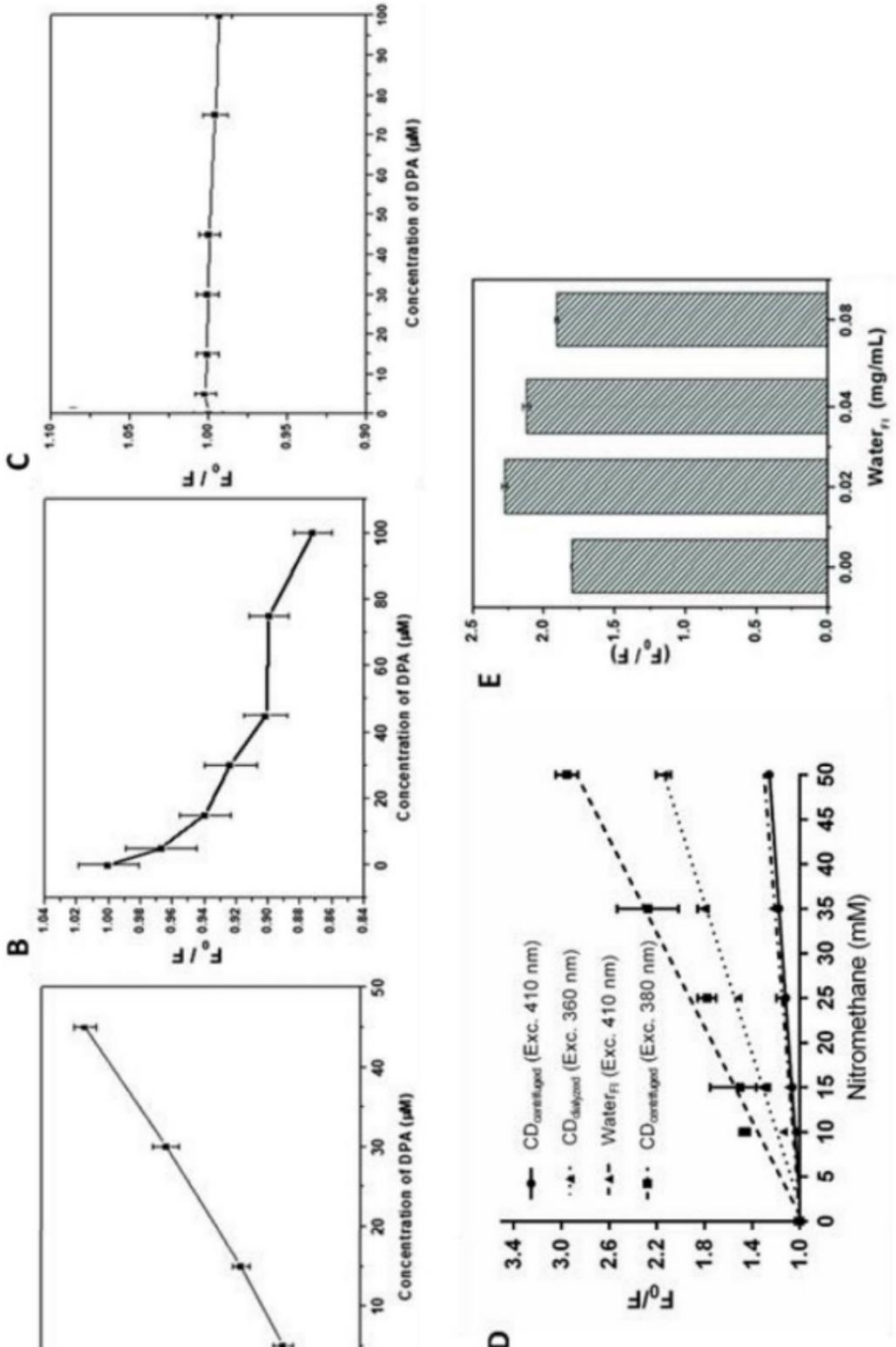


Figure 8. F_0/F correlation for A) $CD_{centrifuged}$, B) $CD_{dialyzed}$ and C) $Water_{FI}$ with increasing concentrations of DPA. D) F_0/F correlation for all fractions with increasing concentrations of NM. E) Variation of F_0/F of a constant amount of $CD_{dialyzed}$ and NM, but varying concentrations of $Water_{FI}$. In all cases, positive F_0/F values indicate quenching, whereas a negative value indicates an enhancement of the photoluminescence. F_0 – Photoluminescence intensity in the absence of DPA or NM; F – photoluminescence intensity with a given amount of DPA or NM. Reproduced with authorization from [22].

Furthermore, considering the synergistic effect previously observed with DPA, the team analyzed $CD_{centrifuged}$ response to NM, but changed the excitation wavelength to that used for $CD_{dialyzed}$. This yielded interesting results, as using a 380 nm excitation resulted in a new shoulder in the emission spectrum (at around 460 nm), which can be attributed to the emission of the nanoparticle itself, as it lines neatly with the emission peak observed with $CD_{dialyzed}$. Monitoring the new peak allowed the team to evaluate the response of the CDs themselves, but still in the presence of the fluorescent by-products. In this case, the photoluminescence of the CDs again presented quenching in the presence of NM, but in a much larger scale than before (K_{SV} = 38.0 ± 2.5 μM^{-1} *versus* 23.7 ± 0.1 μM^{-1} obtained for $CD_{dialyzed}$). The presence of the by-products enhanced the NM-induced quenching of the nanoparticles themselves, and, considering that $Water_{FI}$ do not suffer significant quenching by themselves (K_{SV} = 6.1 ± 0.4 μM^{-1}), the larger extent of the quenching must be a result of the synergistic effect previously observed between the CDs and the fluorescent by-products [22].

Finally, to confirm if the by-products can in fact modulate the photochemical reactivity of the nanoparticles, the photoluminescent response of a constant amount of $CD_{dialyzed}$ towards NM was evaluated in the presence increasing concentrations of $Water_{FI}$ (Figure 8e). The addition of the by-products did indeed increase the NM-derived quenching at the start. However, this effect decreases as the amounts of $Water_{FI}$ added increase. The proposed reason for this is that the by-products interact with the CDs and prompt the formation of a hybrid material presenting synergistic properties. However, increasing the amount of by-products added beyond a certain threshold may mask the surface of the CDs, preventing its interaction with the quencher and thus limiting the effect observed resulting from the synergy [22].

In summary, the work of Sendão et al. provides an example of why the by-products that may result from a CD bottom-up synthesis must be taken into consideration [22]. They successfully demonstrated that these by-products may mask the photoluminescence of the CDs and, more importantly, they may react with the CDs in solution and give rise to a synergistic effect that may affect not only the optoelectronic properties of the nanoparticles, but also their photochemical reactivity to other compounds, such as DPA and NM [22]. If required, these by-products may be removed from the CDs' solution via purification through dialysis or chromatography. However, the potential of discovering new applications based on the hybrid photoluminescence and reactivity resulting from the synergistic effect between CDs and molecular by-products may justify a deeper study of these hybrid materials.

Environmental Impact of CA and Natural Alternatives to Its Use

The last part of this chapter concerns itself with the sustainability of CA-based CDs. It is known that engineered nanomaterials have different properties than their respective bulk materials, and this led to an increased exploration of their potential. However, the environmental impacts resulting from their synthesis and use is still quite unclear [134]. This led to studies aiming to understand the impact of the nanomaterials during their life cycle. Studies based on a life cycle assessment (LCA) of the products were employed, as it permitted to quantify the environmental impacts of system during its life cycle based on information inventories [135, 136].

Regarding CDs, studies regarding the potential environmental impacts of different synthetic conditions are available [31, 34, 137]. This is of particular importance, as the production stage of engineered nanomaterials was already identified of consisting of an important environmental concern, as it can be orders of magnitude more material and energy-consuming than pharmaceuticals and fine chemicals [138]. In particular, the electricity and chemicals used during the synthesis are major contributors to the resulting environmental impact of a product during its life cycle [131].

One of the first studies considering the environmental impacts resulting from the synthesis of CDs was the work of Sendão et al. who, via LCA, compared the relative environmental impacts of bottom-up synthetic routes for the production of CA,urea-based CDs [31]. Six representative bottom-up strategies were analyzed via a cradle-to-gate LCA. The routes consisted of the hydrothermal of microwave-assisted synthesis of CA or CA,urea-based CDs. The results were presented regarding the three endpoint categories of environmental impacts (human health, ecosystems and resources). In general, hydrothermal treatments presents more environmental impacts than microwave-assisted synthesis due to the high energy usage. However, whereas electricity is the main contributor towards the impact of hydrothermal synthetic routes, the carbon source (in this case CA) is the major responsible behind the impacts associated to microwave-assisted synthesis, meaning that it is also an important factor for the environmental impact of the resulting particles [31].

Finally, a sensitivity analysis based on the change of the carbon precursors conditions was performed. In hydrothermal-based procedures, changing the amount of carbon precursor by ±30% leads only to a moderate effect (impact

variation of around 6%), whereas changing the carbon precursors from CA to glucose led to a 15% decrease of the impact in all three main categories. By its turn, in microwave-assisted synthesis, varying the amount of CA caused a more significant variation of the environmental impacts (between 10 and 16%), in part due to the low contribution of electricity in this strategy. Furthermore, replacing CA with glucose led to a drastic decrease in the environmental impacts in all categories: 44% in human health, 33% in ecosystems and 27% in categories, further confirming the influence of the carbon precursor in the sustainability of a synthetic strategy [31].

Another study, by Christé et al., studied the environmental impact of different N-doping strategies in the synthesis of the nanoparticles [34]. N-doped CDs were prepared via a bottom-up strategy from CA with either small organic molecules (urea and ethylenediamine) or N-containing organic solves (such as *N*,*N*-dimethylformamide, acetonitrile and pyridine). For CA,urea- and CA,ethylenediamine-based CDs, the highest contributor towards environmental impacts was the carbon source (CA) in almost every category [34]. The contribution of electricity was small due to the small irradiation times inherent to microwave-assisted synthesis. Regarding the CDs prepared with CA and N-containing solvents, generally, the main source of impact was from the solvents themselves. However, the carbon source is still the main factor of impact for categories such as land use and water consumption, being still a factor that needs to be accounted for [34].

Also using LCA, Fernandes et al. compared different high-yield synthetic routes for the production of CDs [137]. The routes included the production of hydrochar via hydrothermal treatment of carbon precursors and alkaline-peroxide treatment, and the thermal treatment of carbon sources mixed in a eutectic mixture of salts. In accordance with previous studies [31], Fernandes et al. found that the most crucial parameter affecting the environmental impacts is the identity of the carbon precursors, of which glucose yielded the lower impact when compared to CA and *para*-phenylenediamine [137].

Taking into consideration the abovementioned works [31, 34, 137], the role of the carbon precursor must be seriously considered when attempting the sustainable synthesis of CDs. Whereas the carbon precursor quantity might be of relative relevance, in particular when concerning less energy-intensive synthesis, the identity of the carbon precursor is always of major importance and must be considered. Even between commonly used commercial grade chemical reagents, such as CA and glucose, differences in terms of environmental impacts are observed. Choosing a more sustainable, if possible renewable, carbon precursor is an important step towards achieving

environmental sustainability in the process. The alternative is the use of biomass, and some reports have already been published regarding the valorization of a waste or renewable material into the making of CDs [33, 47, 59, 139-143], thus promoting reusability, sustainability and a circular economy.

Crista et al. investigated the use of spent coffee grounds as a precursor for the sustainable making of CDs and compared them to CA and urea-based CDs in terms of environmental sustainability [141]. The use of spent coffee grounds takes advantage of the significant increase in the worldwide consumption of coffee seen in the past few years. As spent coffee grounds are known to possess organic compounds, such as carbohydrates, lipids and proteins, they are a good candidate for valorization and to be used in the making of CDs [144]. The CDs, obtained via a one-pot solvent-free carbonization of solid coffee grounds samples, generated CDs sized between 2.1 and 3.9 nm presenting an excitation-dependent blue photoluminescence and moderate QY_{PL} (2.9 – 5.8%), which are typical characteristics of CDs.

Furthermore, the CDs proved to be usable as photoluminescent probes for Fe(III) in water with a limit of detection as low as 3.51 μM (*versus* 3.07 μM for CA,urea-based CDs), confirming their potential applicability for sensing [141]. Finally, when the team analyzed the environmental impacts associated to the CDs via a LCA using a QY_{PL}-based functional unit they found that the coffee grounds-based CDs had a considerably lower environmental impact than the traditional CA,urea-based CDs in all categories. Thus, despite a lower synthesis yield and QY_{PL}, the coffee-based CDs are still an environmentally better option than the typical CA and urea precursors, even when considering a function based QY_{PL} functional unit [141].

Another example on the valorization of biomass is the work of Aggarwal et al., who prepared cellulose-based CDs for the photocatalytic removal of toxic Cr(VI) [59]. The cellulose was transformed into CDs via an acid-assisted one-step thermal carbonization (90ºC for 30 minutes). Within 120 minutes of sunlight irradiation the CDs were able to completely remove Cr(VI) ions (20 ppm) from wastewater. Thus, cellulose, a low cost, green, alternative carbon source, was used to prepare photoactive CDs for photocatalysis, making the overall process sustainable and economical [59].

Campalani et al. prepared CDs from fish scales, a carbon and nitrogen-rich waste material consisting mostly of chitin and collagen [33]. The hydrothermally prepared CDs were compared to CA and diethylenetriamine-based CDs, presenting a similar morphology and a higher initial methyl viologen photoreduction rate than the conventional alternative (despite

presenting lower QY_{PL} and excited state lifetime) [33]. Wang and Zhou reported the synthesis of milk-based CDs for imaging applications [47]. The hydrothermal treatment of milk yielded highly photoluminescent CDs that were used for high resolution imaging of human brain glioma cells. The synthesis was simple and environmentally friendly, originating CDs from a widely available renewable source [47].

Thakur et al. reported the making of CDs from Citrus limetta waste pulp via a one-step pyrolysis procedure [143]. The CDs exhibited a high QY_{PL} (63.3%), which is above most conventional CDs. When tested, the CDs revealed potential for several applications, such as hydrogen production via water splitting, photocatalytic degradation of organic dyes, Fe(III) sensing, bactericidal activity versus *E. coli* and *S. aureus* and bioimaging [143]. The immense versatility of the CDs is an indicator of the wealth of potential of CDs prepared from waste products such as this. Furthermore, these CDs have the edge on both environmental sustainability and economy, as they use an otherwise useless biological waste to generate valuable products, promoting a circular economy.

Here, we are also to report the synthesis of new CDs by using an otherwise waste product to replace CA as the chosen carbon precursor. Namely, we are going to use corn stover as an alternative carbon source. Corn stover consists of the leaves, stalk and cobs of corn plant left on the field after harvest. It constitutes a significant agricultural waste that makes about half of the corn crop's yield [145]. Despite this, ninety percent of corn stover is discarded instead of being used for other applications [145]. Given this, corn stover appears as a waste material with potential for valorization as a carbon source for CDs. To dope CDs with heteroatoms, thiosulfate was introduced as an S-dopant.

Corn stover was collected from an agricultural area in Vairão, Portugal. The collected corn stover was first washed with deionized area and left to dry at 50ºC. Subsequently, the corn stover was shredded by employing a LAARMANN Power Cutting Mill CM 500, with a sieve of 0.5 mm. The resulting material was collected and stored at -80ºC. The CDs were then synthesized via thermal heating. Briefly, 0.25 g of processed corn stover and 0.25 g of sodium thiosulphate pentahydrate were weighted and mixed before being transferred into a *Teflon*-lined reactor with steel outer plating. The reactor was then transferred to an oven (VWR DL 112 Prime oven (2500 W power consumption) and subjected to a temperature of 225ºC for 4 hours. The resulting product was suspended in 10 mL of deionized water, which was

followed by centrifugation (10000 rpm for 10 minutes) and dialysis (24 hours, MWCO of 1 kDa), after which a solution of purified CDs was obtained.

The particle size presented by individual CDs was estimated to be 1.28 ± 0.50 nm, as calculated from data obtained from AFM measurements (collected from 80 individual measurements). While individual CDs can be discerned and present a spherical shape, there can be observed some agglomerates in the AFM image (Figure 9). This can be attributed to the known tendency of CDs to aggregate [146, 147].

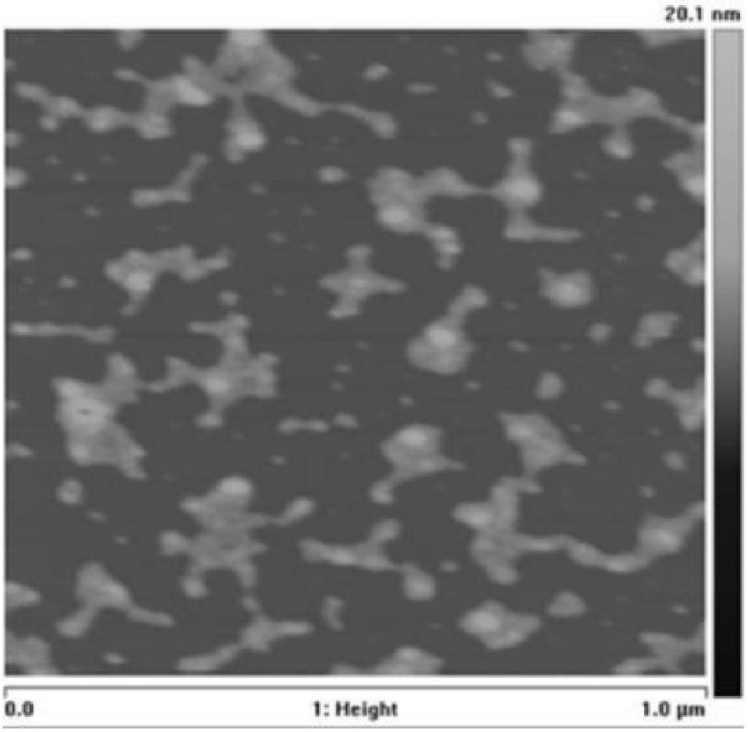


Figure 9. AFM image of the CD in a silica plate support. AFM was carried out using a Veeco Metrology Multimode/Nanoscope IVA by tapping. A silica plate was used to deposit the sample for analysis and an AFM TESP-SS cantilever (curvature radius of 2 nm) was used. The software used for the AFM data analysis was NanoScope.

The absorption spectrum of the CD displays a broad absorption ranging from the UV region and extending into the visible region. The spectrum is typical for the absorption displayed by CDs [22, 148, 149]. Furthermore, when the absorption and excitation spectra (obtained for the maximum emission wavelength of 470 nm) are overlapped (Figure 10) it is possible to observe that the maximum excitation wavelength (370 nm) falls outside the region in which the CDs absorb the most radiation.

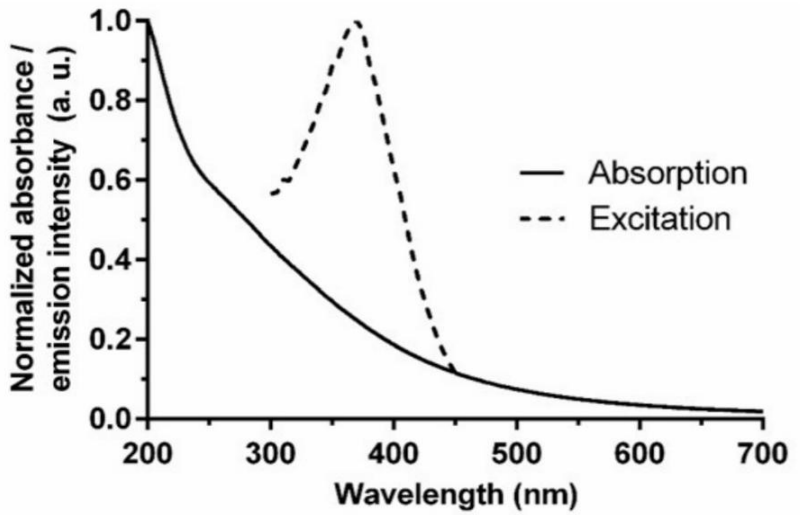


Figure 10. Absorption and excitation spectra of the CD in water. The absorption profile was recorded using a VWR® UV3100PC spectrophotometer. The excitation spectrum was obtained using a Horiba Jovin Yvon Fluoromax-4 spectrofluorimeter.

Regarding its photoluminescence (Figure 11a), the CD is capable of emitting light with an emission wavelength maximum of 470 nm, when excited both at 270 and 370 nm (two excitation maxima). Furthermore, it displays an excitation-dependent emission (Figure 11b), with the emission wavelength ranging between 470 and 550 nm for excitation wavelengths between 300 and 500 nm.

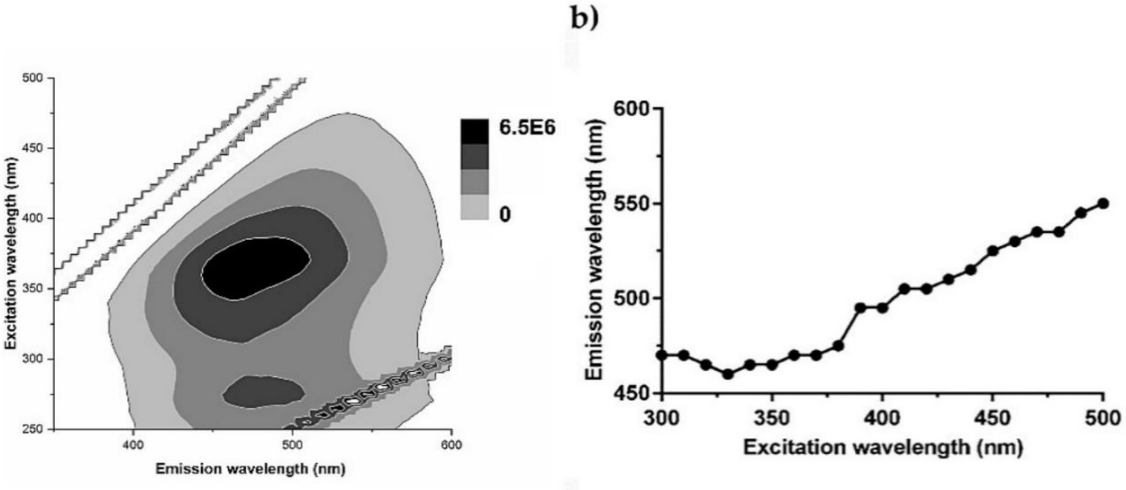


Figure 11. a) 2D excitation-emission matrix, EEM, contour surface;
b) Emission wavelength variation in function of the excitation wavelength. The photoluminescence profile of the CDs was analyzed, in aqueous solution, using a Horiba Jovin Yvon Fluoromax-4 spectrofluorimeter. Standard fluorescence quartz cells were used.

To better understand the surface composition and electronic states of the elements present in the CDs, an XPS analysis was performed. It revealed that the surface of the CDs is composed mainly of C, O, N and S, with a content (in %) of 65.6, 20.9, 1.3 and 4.1%, respectively. These elements are to be expected from the composition of corn stover and sodium thiosulfate [150], which were used as precursors for these CDs.

A scan for the C_{1s}, O_{1s}, N_{1s} and S_{2p} internal levels for deconvolution and chemical state was subsequently performed (Figure 12). Regarding the C_{1s} core level spectrum, after deconvolution it splits into five peaks. Binding energies of 285.0 eV (70.32%), 286.4 eV (16.22%), 287.0 eV (3.99%), 288.3 eV (7.81%) and 289.5 eV (1.66%) were detected. The observed C_{1s} peaks are attributed to C-C/C-H/adventitious carbon (285.0 eV), C-N/C-S/C-O (286.4-287.0 eV), C=O/O-C=O carbonyl/carboxylic groups (288.3 eV) and C-O-C ether groups (289.5 eV). Regarding the O_{1s} core level spectrum, when deconvoluted, a major peak at 531.9 eV (92.38%) and a smaller one at 539.3 eV (7.62%), ascribed to carbonyl (C=O) linkage and C-O/O-C-O groups, respectively. By its turn, the deconvolution of the N_{1s} core level spectrum yielded a major peak at 400.0 eV (96.09%) and a shoulder at around 401.8 eV (3.91%), attributed to groups of amines/amides and protonated amines, respectively. Finally, the deconvolution of the S_{2p} core level spectrum results in two similar peaks at 164.5 eV (50.22%) and 168.9 eV (49.78%).

Having characterized the obtained CDs, we have then investigated the potential effect of these CDs on a marine chemiluminescent reaction. Chemiluminescence consists in the emission of light due to a chemical reaction, with a sub-type of chemiluminescence being bioluminescence, in which light is emitted due to a biochemical reaction. Both chemi- and bioluminescent reactions present a diminished probability for autofluorescence arising from the background signal, thereby increasing the signal-to-noise ratio. So, these systems can generate luminescent signals with high sensitivity and almost no background noise. This is a very important feature, which explains why chemi- and bioluminescence have been gaining practical applications in fields such as sensing and bioimaging [151-153]. One of the most well-known chemi- and bioluminescent systems is that of Coelenterazine, a substrate widely found in marine species [154, 155]. More specifically, it is capable of both bioluminescence (in the presence of either photoproteins or luciferase enzymes) or chemiluminescence (in polar aprotic solvents, such as DMF or DMSO) [156, 157].

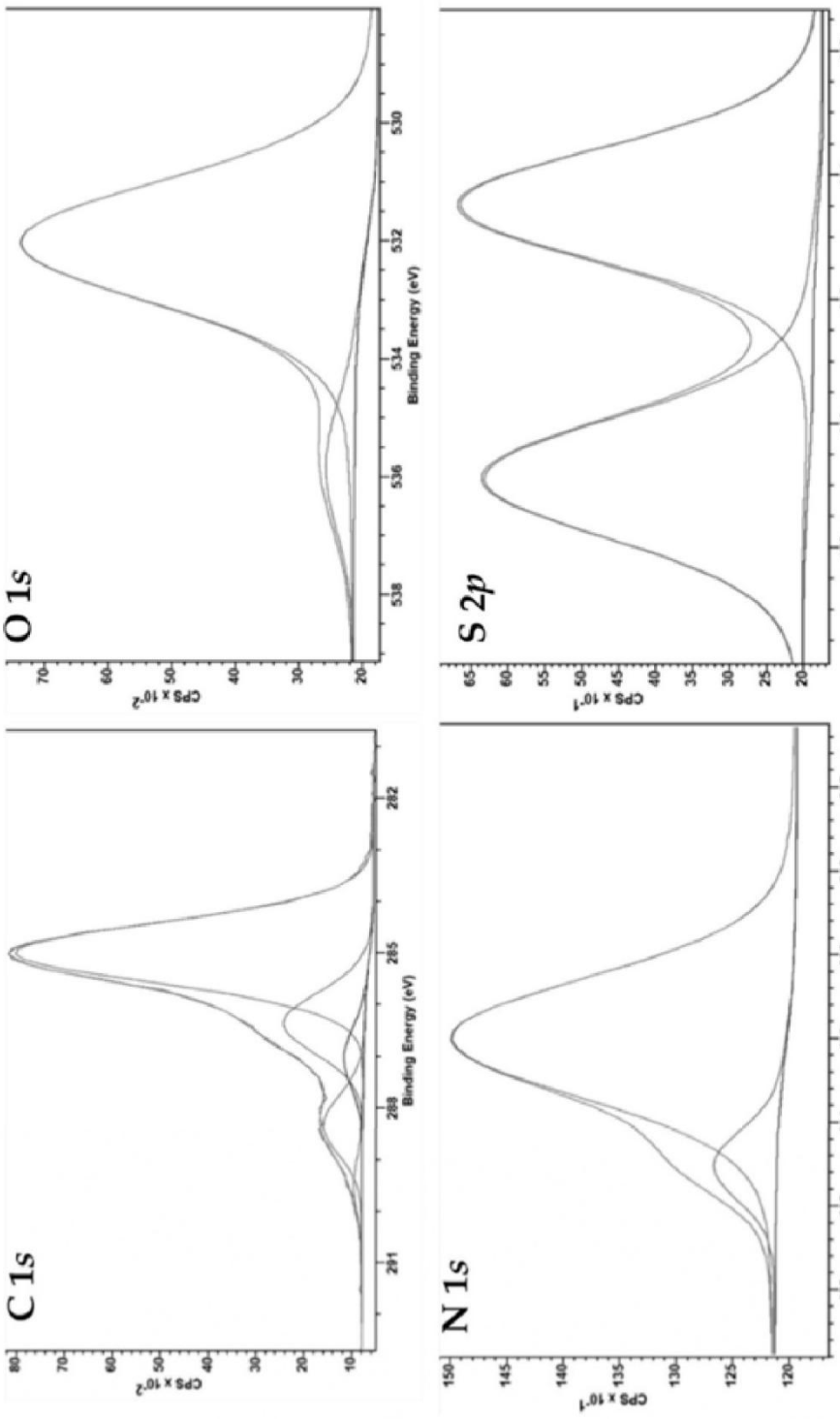


Figure 12. XPS core level spectra of the CD: a) C 1s b) O 1s, c) N 1s and d) S 2p. X-Ray Photoelectron Spectroscopy (XPS) was carried out using a Kratos Axis Ultra HSA spectrometer utilizing Al monochromatic radiation with a hemispherical multichannel detector (90 W and 15 kV). The was deposited upon a silicon wafer. CasaXPS software was used to analyze the results and the carbon C 1s signal, 285.0 eV, was used as a reference to obtain the binding energy values, using Gauss-Lorentz curves and Shirley-type background.

The energy necessary to promote a chemical species to an electronically excited state can be obtained from a chemical reaction involving high-energy intermediates. This type of process is essential for chemi- and bioluminescence, and involves high-energy peroxide intermediates, such as dioxetanes and dioxetanones [158, 159]. In the case of Coelenterazine, the high-energy intermediate is a dioxetanone-based compound [160]. It should be noted that despite decades of research, the mechanism behind efficient chemiexcitation is still not fully understood.

The Chemically Induced Electron-Exchange Luminescence (CIEEL) was the first to be employed in attempts to rationalize these processes and consists in electron transfer from an electron-rich group to the peroxide, followed by back electron transfer. This latter step leads to chemiexcitation due to charge annihilation [161]. Interestingly, within this context, it was found that oxidizable fluorophores can activate the decomposition of some high-energy peroxide intermediates, leading to ground state carbonyl compounds and to the excitation to the fluorophore in its first singlet excited state [159].

To our knowledge, there is no information regarding either if CDs can be used as fluorophores and activators, or if the chemiluminescence of Coelenterazine could be catalyzed in such a way. Thus, we have tested the CDs referred to above, produced from corn stover and sodium thiosulfate, as possible activator/catalyst for the chemiluminescent reaction of marine Coelenterazine.

The chemiluminescent kinetic curves, in the presence or absence of the CDs, can be found on Figure 13. Qualitatively, the resulting kinetic profiles are quite similar. However, and more interestingly, the chemiluminescence reaction, which occurred in the presence of CDs, showed an increase of the light-emission maxima when comparing with the reaction that occurred in the absence of the CDs (1.24 ± 0.14). When reducing the concentrations of both Coelenterazine and CDs to half, but maintaining the same relationship between them, the results are similar (1.36 ± 0.16). Thus, the CDs showed an ability to enhance, at least moderately, the chemiluminescence emission of Coelenterazine.

To our knowledge, this is the first report of CDs being able to enhance the light-emission of a chemiluminescent reaction, with focus on the coelenterazine system.

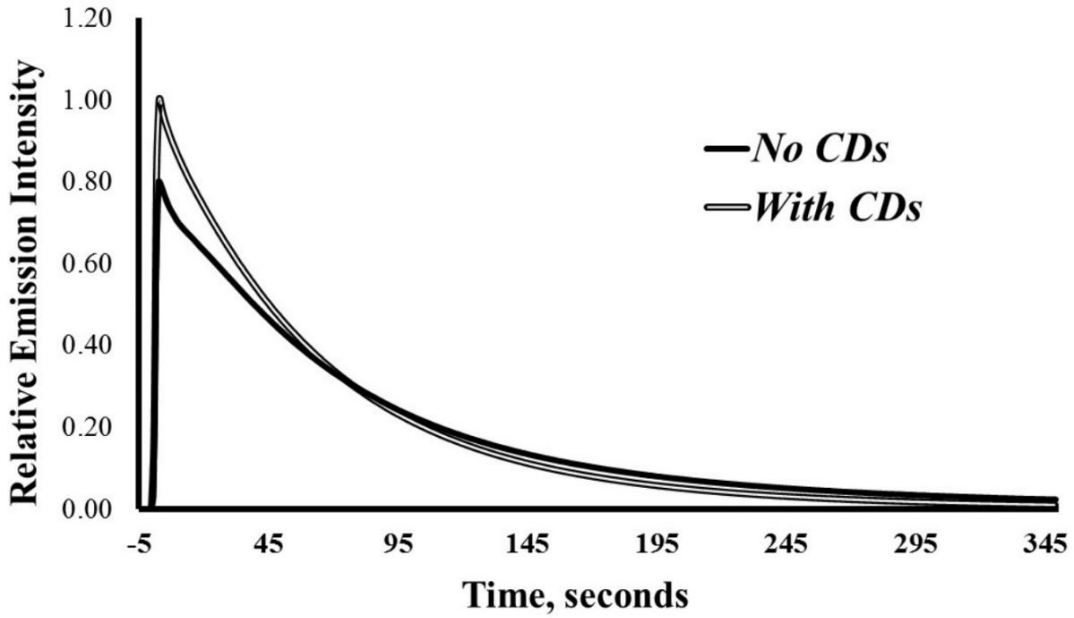


Figure 13. Relative emission intensity, as a function of time, of the chemi-luminescent reaction of marine Coelenterazine in DMSO, in the presence and absence of CDs. The chemiluminescence kinetics were measured in a homemade luminometer, in which a Hamamatsu HC135-01 photomultiplier tube is found. The light was integrated and recorded in 1 second intervals. Measurements were performed in DMSO with a final volume of 500 μL. The concentration of Coelenterazine was of eight μM and the CDs of 0.002 g/l. Assays were made at least in quintuplicate.

Having made this discovery, the next step was to try to find if this enhancement was due to a CIEEL-like mechanism, in which the CDs act as activators and as the light-emitters. To that end, we have measured the chemiluminescent spectra of Coelenterazine reaction, in DMSO and in both the presence and absence of CDs (Figure 14).

Quite interestingly, there is an essentially total overlap between the spectra obtained in the presence and absence of CDs, which indicates that there is no contribution to light-emission from the CDs directly. In fact, the obtained chemiluminescent spectra are consistent with that of just Coelenterazine [154]. More importantly, the fluorescence quantum yield of the CDs was determined by using quinine sulfate [31, 141, 162]. The obtained value was quite low, and of just ~0.7% (also meaning that there is the need for further optimization of synthesis reactions involving corn stover as a precursor, if the aim is the production of highly luminescent CDs). Thus, if the chemiluminescent reaction led to the excitation of CDs, we would probably see a relevant decrease in light-emission, and not an increase. So, these results indicate that

the CDs are acting as catalysts of the chemiluminescent reaction, which results in the enhancement of light-emission from Coelenterazine itself. Thus, these results show the potential for the enhancement of chemiluminescent reactions by using CDs as catalysts. Future work would be needed to investigate the mechanism through which the CDs catalyze this type of reaction.

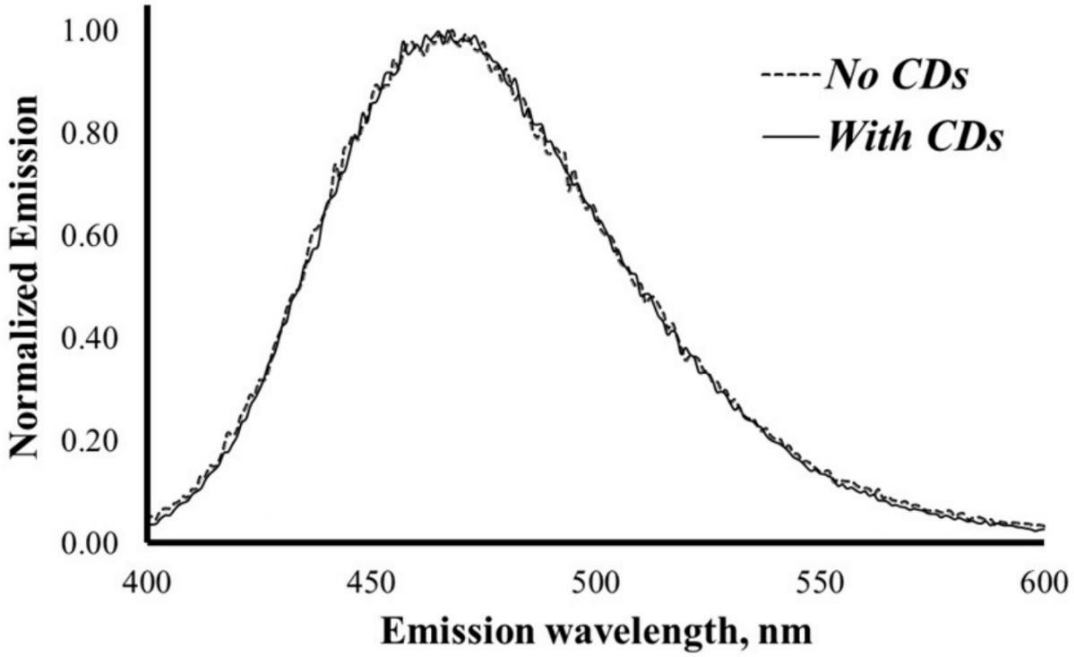


Figure 14. Normalized chemiluminescence spectra for Coelenterazine in DMSO, in the presence or absence of CDs. Spectra obtained with a Horiba Jovin Fluoromax 4 spectrofluorimeter, with a slit width of 29 nm for the emission monochromator.

Conclusion

This chapter focused on the use of CA for the making of CDs, with references to their synthetic procedures, properties, applications, doping mechanisms and results thereof, possible by-products, sustainability, and respective environmentally friendlier carbon source alternatives. CA is a versatile molecule naturally present in several fruits and vegetables, most important of which are citrus fruits. While it is used in many processes and applications, is CA is mostly known for its role in the Krebs cycle, which is of paramount importance for all aerobic organisms and a crucial part of obtaining food-derived energy in complex organisms. Regarding industrial applications, CA is used mostly in the food and beverage industry, and for a variety of other

applications such as making bath salts, shampoos, degreasing agents, metal removal from water, rust removal, among others.

The low cost and characteristics of CA meant that it was a suitable carbon source for the synthesis of CDs, so much so that it is arguably the most commonly used precursor used to fabricate these nanoparticles. CDs are carbon-based nanoparticles that have been under the scope of the scientific community since their discovery in 2004. CDs can be synthesized via either top-down or bottom-up strategies, with the latter being more frequently employed due to its relative easiness and inexpensiveness. From the synthesis results a nanoparticle commonly presenting a carbogenic sp^2-hybridized core with a surface covered in functional groups (such as -OH). Among other properties, CDs are known to present a high photoluminescence, good water solubility, broadband absorption, and biocompatibility. From this results that CDs are suitable for a variety of applications in different fields, including bioimaging, photocatalysis, photodynamic therapy, sensing and light-emitting devices.

Additionally, the optoelectronic properties of CDs can be further enhanced by doping them with either heteroatoms or metallic dopants. Doping is a process that increases the particles' QY_{PL}, by prompting the formation of n- and p-type carriers (extra e^- and h^+), changing the CDs' electronic structure. The most commonly used dopant heteroatom in the synthesis of CDs is nitrogen, with combinations of CA with either urea or ethylenediamine (nitrogen-containing molecules) being extremely common for all kinds of CDs' applications. Other heteroatom dopants and combinations of dopants are also commonly used. Although metallic ions can also act as electron donors in CDs and enhance their electron transfer capacity (and ultimately extend the range of their applications), metallic doping is less common than its heteroatom counterpart. This may be attributed to the fact that metal-doped CDs present a relatively lower QY_{PL} and that their photoluminescence mechanism is still very unclear.

Among the properties of CDs, their photoluminescence is arguably the most important. However, the origins behind it are still a matter of debate, with several explanations and theories being presented by the scientific community over the years. The role of molecular by-products formed alongside the CDs during their synthesis has been under focus, as it was seen that these by-products are intensely photoluminescent, even more so than the nanoparticles themselves. In fact, the by-products might mask the nanoparticles' emission and, more importantly, they may even react with the CDs and alter their optical properties and photochemical reactivity. When co-

existing in solution a synergistic effect may occur between CDs and by-products. Whereas this causes a need of a proper purification of the CDs after their synthesis, it also brings potential in terms of discovering new applications based on the hybrid photoluminescence and synergy between CDs and photoluminescent by-products.

Finally, the sustainability of using carbon sources such as CA for the synthesis of CDs was also reviewed. We found that the carbon source plays an important in the environmental impacts of the synthesis. Several LCA-based studies point that the carbon precursor quantity and, more importantly, the identity of the carbon precursor play a major role in determining the sustainability of the CDs' synthesis. Choosing a more sustainable and renewable alternative carbon precursor is an important step towards sustainability that is already being studied by several teams across the world. Several waste and biomass-based CDs have been reported over the last years, using precursors as varied as corn stover, spent coffee grounds, fish scales and milk, presenting properties in line with those of conventional CDs and capable of being employed in the same applications, all while also being much more sustainable, less expensive and promoting a circular economy. It was here also demonstrated a potential application of waste-based CDs in the catalysis of chemiluminescent reactions.

Acknowledgments

The Portuguese "*Fundação para a Ciência e Tecnologia* [Foundation for Science and Technology]" (FCT, Lisbon) is acknowledged for funding of project PTDC/QUI-QFI/2870/2020, R&D Unit CIQUP (UIDB/00081/2020), and Associated Laboratory IMS (LA/P/0056/ 2020). Luís Pinto da Silva acknowledges funding from FCT under the Scientific Employment Stimulus (CEECINST/00069/2021). The Materials Center of the University of Porto (CEMUP) is acknowledged. Ricardo Sendão acknowledges FCT for his Ph.D. grant (2021.06149.BD).

References

[1] Penniston, K. L., S. Y. Nakada, R. P. Holmes, and D. G. Assimos, Quantitative assessment of citric acid in lemon juice, lime juice, and commercially-available fruit juice products. *J. Endourol.*, 2008. 22(3): p. 567-70.

[2] Lotfy, W. A., K. M. Ghanem, and E. R. El-Helow, Citric acid production by a novel Aspergillus niger isolate: II. Optimization of process parameters through statistical experimental designs. *Bioresour. Technol.*, 2007. 98(18): p. 3470-7.

[3] Verhoff, F. H. and H. Bauweleers, *Ullmann's Encyclopedia of Industrial Chemistry*. 2014, Weinheim: Wiley-VCH.

[4] Amir, D., A. Hendler-Neumark, V. Wulf, R. Ehrlich, and G. Bisker, Oncometabolite Fingerprinting Using Fluorescent Single-Walled Carbon Nanotubes. *Adv. Mater. Interfaces*, 2021. 9(4).

[5] Abdullah, T. A., T. Juzsakova, S. A. Hafad, R. T. Rasheed, N. Al-Jammal, M. A. Mallah, A. D. Salman, P. C. Le, E. Domokos, and M. Aldulaimi, Functionalized multi-walled carbon nanotubes for oil spill cleanup from water. *Clean Technol. Environ. Policy*, 2021. 24(2): p. 519-541.

[6] Norouzi, A., E. Nemati Lay, A. Arabloo nareh, A. Hosseinkhani, and M. Chapalaghi, Functionalized nanodiamonds in polyurethane mixed matrix membranes for carbon dioxide separation. *Results in Materials*, 2022. 13.

[7] Chhetri, K., T. Kim, D. Acharya, A. Muthurasu, B. Dahal, R. M. Bhattarai, P. C. Lohani, I. Pathak, S. Ji, T. H. Ko, and H. Y. Kim, Hollow Carbon Nanofibers with Inside-outside Decoration of Bi-metallic MOF Derived Ni-Fe Phosphides as Electrode Materials for Asymmetric Supercapacitors. *Chem. Eng. J.*, 2022. 450.

[8] Lu, D., X. Shi, H. S. Wong, Z. Jiang, and J. Zhong, Graphene coated sand for smart cement composites. *Const. Build. Mater.*, 2022. 346.

[9] Jayanand, K., S. Chugh, N. Adhikari, M. Min, L. Echegoyen, and A. B. Kaul, Sc3N@C80 and La@C82 doped graphene for a new class of optoelectronic devices. *J. Mater. Chem. C*, 2020. 8: p. 3970.

[10] Zhu, Z., X. Li, M. Luo, M. Chen, W. Chen, P. Yang, and X. Zhou, Synthesis of carbon dots with high photocatalytic reactivity by tailoring heteroatom doping. *J. Colloid. Interface Sci.*, 2022. 605: p. 330-341.

[11] Smrithi, S. P., N. Kottam, and B. R. Vergis, Heteroatom Modified Hybrid Carbon Quantum Dots Derived from Cucurbita pepo for the Visible Light Driven Photocatalytic Dye Degradation. *Top. Catal.,* 2022.

[12] Simoes, E. F. C., L. P. da Silva, J. da Silva, and J. M. M. Leitao, Hypochlorite fluorescence sensing by phenylboronic acid-alizarin adduct based carbon dots. *Talanta*, 2020. 208: p. 120447.

[13] Ladomenou, K., G. Landrou, G. Charalambidis, E. Nikoloudakis, and A. G. Coutsolelos, Carbon dots for photocatalytic H2 production in aqueous media with molecular Co catalysts. *Sustain. Energy Fuels*, 2021. 5(2): p. 449-458.

[14] Li, L.-S. and L. Xu, Highly fluorescent N,S,P tri-doped carbon dots for Cl− detection and their assistance of TiO_2 as the catalyst in the degradation of methylene blue. *J. Photochem. Photobiol. A*, 2020. 401.

[15] Kalytchuk, S., K. Polakova, Y. Wang, J. P. Froning, K. Cepe, A. L. Rogach, and R. Zboril, Carbon Dot Nanothermometry: Intracellular Photoluminescence Lifetime Thermal Sensing. *ACS Nano*, 2017. 11(2): p. 1432-1442.

[16] Xu, X., R. Ray, Y. Gu, H. J. Ploehn, L. Gearheart, K. Raker, and W. A. Scrivens, Electrophoretic analysis and purification of fluorescent single-walled carbon nanotube fragments. *J. Am. Chem. Soc.*, 2004. 126(40): p. 12736-7.

[17] Sun, Y. P., B. Zhou, Y. Lin, W. Wang, K. A. Fernando, P. Pathak, M. J. Meziani, B. A. Harruff, X. Wang, H. Wang, P. G. Luo, H. Yang, M. E. Kose, B. Chen, L. M. Veca, and S. Y. Xie, Quantum-sized carbon dots for bright and colorful photoluminescence. *J. Am. Chem. Soc.*, 2006. 128(24): p. 7756-7.

[18] Esteves da Silva, J. C. G. and H. M. R. Gonçalves, Analytical and bioanalytical applications of carbon dots. *Trends Analyt. Chem.*, 2011. 30(8): p. 1327-1336.

[19] Hola, K., Y. Zhang, Y. Wang, E. P. Giannelis, R. Zboril, and A. L. Rogach, Carbon dots—Emerging light emitters for bioimaging, cancer therapy and optoelectronics. *Nano Today*, 2014. 9(5): p. 590-603.

[20] Baker, S. N. and G. A. Baker, Luminescent carbon nanodots: emergent nanolights. *Angew. Chem. Int. Ed. Engl.*, 2010. 49(38): p. 6726-44.

[21] Demchenko, A. P. and M. O. Dekaliuk, Novel fluorescent carbonic nanomaterials for sensing and imaging. *Methods Appl. Fluoresc.*, 2013. 1(4): p. 042001.

[22] Sendão, R. M. S., D. M. A. Crista, A. C. P. Afonso, M. D. V. Martinez de Yuso, M. Algarra, J. C. G. Esteves da Silva, and L. Pinto da Silva, Insight into the hybrid luminescence showed by carbon dots and molecular fluorophores in solution. *Phys. Chem. Chem. Phys.*, 2019. 21(37): p. 20919-20926.

[23] Wang, J., S. Sahu, S. K. Sonkar, K. N. Tackett Ii, K. W. Sun, Y. Liu, H. Maimaiti, P. Anilkumar, and Y.-P. Sun, Versatility with carbon dots – from overcooked BBQ to brightly fluorescent agents and photocatalysts. *RSC Adv.*, 2013. 3(36).

[24] Saini, D., J. Kaushik, A. K. Garg, C. Dalal, and S. K. Sonkar, N, S-codoped Carbon Dots for Nontoxic Cell Imaging and As a Sunlight-Active Photocatalytic Material for the Removal of Chromium. *ACS Appl. Bio. Mater.*, 2020. 3(6): p. 3656-3663.

[25] Vale, N., S. Silva, D. Duarte, D. M. A. Crista, L. Pinto da Silva, and J. C. G. Esteves da Silva, Normal breast epithelial MCF-10A cells to evaluate the safety of carbon dots. *RSC Med. Chem.*, 2021. 12(2): p. 245-253.

[26] Hettiarachchi, S. D., R. M. Graham, K. J. Mintz, Y. Zhou, S. Vanni, Z. Peng, and R. M. Leblanc, Triple conjugated carbon dots as a nano-drug delivery model for glioblastoma brain tumors. *Nanoscale*, 2019. 11(13): p. 6192-6205.

[27] Deng, Y., M. Chen, G. Chen, W. Zou, Y. Zhao, H. Zhang, and Q. Zhao, Visible-Ultraviolet Upconversion Carbon Quantum Dots for Enhancement of the Photocatalytic Activity of Titanium Dioxide. *ACS Omega*, 2021. 6(6): p. 4247-4254.

[28] Gu, S., C.-T. Hsieh, Y.-M. Chiang, D.-Y. Tzou, Y.-F. Chen, and Y. A. Gandomi, Optimization of graphene quantum dots by chemical exfoliation from graphite powders and carbon nanotubes. *Mater. Chem. Phys.*, 2018. 215: p. 104-111.

[29] Zhuo, S., M. Shao, and S. T. Lee, Upconversion and downconversion fluorescent graphene quantum dots: ultrasonic preparation and photocatalysis. *ACS Nano*, 2012. 6(2): p. 1059-64.

[30] Zhou, J., C. Booker, R. Li, X. Zhou, T. K. Sham, X. Sun, and Z. Ding, An electrochemical avenue to blue luminescent nanocrystals from multiwalled carbon nanotubes (MWCNTs). *J. Am. Chem. Soc.*, 2007. 129(4): p. 744-5.

[31] Sendão, R., M. d. V. M. d. Yuso, M. Algarra, J. C. G. Esteves da Silva, and L. Pinto da Silva, Comparative life cycle assessment of bottom-up synthesis routes for carbon dots derived from citric acid and urea. *J. Clean. Prod.*, 2020. 254.

[32] Crista, D. M. A., G. P. C. Mello, O. Shevchuk, R. M. S. Sendao, E. F. C. Simoes, J. M. M. Leitao, L. P. da Silva, and J. C. G. Esteves da Silva, 3-Hydroxy-phenylboronic Acid-Based Carbon Dot Sensors for Fructose Sensing. *J. Fluoresc.*, 2019. 29(1): p. 265-270.

[33] Campalani, C., E. Cattaruzza, S. Zorzi, A. Vomiero, S. You, L. Matthews, M. Capron, C. Mondelli, M. Selva, and A. Perosa, Biobased Carbon Dots: From Fish Scales to Photocatalysis. *Nanomaterials*, 2021. 11(2).

[34] Christe, S., J. C. G. Esteves da Silva, and L. Pinto da Silva, Evaluation of the Environmental Impact and Efficiency of N-Doping Strategies in the Synthesis of Carbon Dots. *Materials*, 2020. 13(3).

[35] Zhu, H., X. Wang, Y. Li, Z. Wang, F. Yang, and X. Yang, Microwave synthesis of fluorescent carbon nanoparticles with electrochemiluminescence properties. *Chem. Commun.*, 2009(34): p. 5118-20.

[36] Gu, Z. G., D. J. Li, C. Zheng, Y. Kang, C. Woll, and J. Zhang, MOF-Templated Synthesis of Ultrasmall Photoluminescent Carbon-Nanodot Arrays for Optical Applications. *Angew. Chem. Int. Ed. Engl.*, 2017. 56(24): p. 6853-6858.

[37] Jiang, H., F. Chen, M. G. Lagally, and F. S. Denes, New strategy for synthesis and functionalization of carbon nanoparticles. *Langmuir*, 2010. 26(3): p. 1991-5.

[38] Krysmann, M. J., A. Kelarakis, P. Dallas, and E. P. Giannelis, Formation mechanism of carbogenic nanoparticles with dual photoluminescence emission. *J. Am. Chem. Soc.*, 2012. 134(2): p. 747-50.

[39] Crista, D. M. A., J. C. G. Esteves da Silva, and L. Pinto da Silva, Evaluation of Different Bottom-up Routes for the Fabrication of Carbon Dots. *Nanomaterials*, 2020. 10(7).

[40] Peng, Z., Y. Zhou, C. Ji, J. Pardo, K. J. Mintz, R. R. Pandey, C. C. Chusuei, R. M. Graham, G. Yan, and R. M. Leblanc, Facile Synthesis of "Boron-Doped" Carbon Dots and Their Application in Visible-Light-Driven Photocatalytic Degradation of Organic Dyes. *Nanomaterials*, 2020. 10(8).

[41] Zhou, Y., E. M. Zahran, B. A. Quiroga, J. Perez, K. J. Mintz, Z. Peng, P. Y. Liyanage, R. R. Pandey, C. C. Chusuei, and R. M. Leblanc, Size-Dependent Photocatalytic Activity of Carbon Dots with Surface-State Determined Photoluminescence. *Appl. Catal. B*, 2019. 248: p. 157-166.

[42] Tan, J., R. Zou, J. Zhang, W. Li, L. Zhang, and D. Yue, Large-scale synthesis of N-doped carbon quantum dots and their phosphorescence properties in a polyurethane matrix. *Nanoscale*, 2016. 8(8): p. 4742-7.

[43] Qu, S., X. Wang, Q. Lu, X. Liu, and L. Wang, A biocompatible fluorescent ink based on water-soluble luminescent carbon nanodots. *Angew. Chem. Int. Ed. Engl.*, 2012. 51(49): p. 12215-8.

[44] Jiang, J., Y. He, S. Li, and H. Cui, Amino acids as the source for producing carbon nanodots: microwave assisted one-step synthesis, intrinsic photoluminescence property and intense chemiluminescence enhancement. *Chem. Commun.*, 2012. 48(77): p. 9634-6.

[45] Yang, Z. C., M. Wang, A. M. Yong, S. Y. Wong, X. H. Zhang, H. Tan, A. Y. Chang, X. Li, and J. Wang, Intrinsically fluorescent carbon dots with tunable

emission derived from hydrothermal treatment of glucose in the presence of monopotassium phosphate. *Chem. Commun.*, 2011. 47(42): p. 11615-7.

[46] De, B. and N. Karak, A green and facile approach for the synthesis of water soluble fluorescent carbon dots from banana juice. *RSC Adv.*, 2013. 3(22).

[47] Wang, L. and H. S. Zhou, Green synthesis of luminescent nitrogen-doped carbon dots from milk and its imaging application. *Anal. Chem.*, 2014. 86(18): p. 8902-5.

[48] Dong, Y., H. Pang, H. B. Yang, C. Guo, J. Shao, Y. Chi, C. M. Li, and T. Yu, Carbon-based dots co-doped with nitrogen and sulfur for high quantum yield and excitation-independent emission. *Angew. Chem. Int. Ed. Engl.*, 2013. 52(30): p. 7800-4.

[49] Schneider, J., C. J. Reckmeier, Y. Xiong, M. von Seckendorff, A. S. Susha, P. Kasák, and A. L. Rogach, Molecular Fluorescence in Citric Acid-Based Carbon Dots. *J. Phys. Chem. C*, 2017. 121(3): p. 2014-2022.

[50] Kasprzyk, W., S. Bednarz, P. Żmudzki, M. Galica, and D. Bogdał, Novel efficient fluorophores synthesized from citric acid. *RSC Adv.*, 2015. 5(44): p. 34795-34799.

[51] Fang, Q., Y. Dong, Y. Chen, C.-H. Lu, Y. Chi, H.-H. Yang, and T. Yu, Luminescence origin of carbon based dots obtained from citric acid and amino group-containing molecules. *Carbon*, 2017. 118: p. 319-326.

[52] Belkahla, H., R. Boudjemaa, V. Caorsi, D. Pineau, A. Curcio, J. S. Lomas, P. Decorse, A. Chevillot-Biraud, T. Azaïs, C. Wilhelm, H. Randriamahazaka, and M. Hémadi, Carbon dots, a powerful non-toxic support for bioimaging by fluorescence nanoscopy and eradication of bacteria by photothermia. *Nanoscale Adv.*, 2019. 1(7): p. 2571-2579.

[53] Li, J., K. Tang, J. Yu, H. Wang, M. Tu, and X. Wang, Nitrogen and chlorine co-doped carbon dots as probe for sensing and imaging in biological samples. *R. Soc. Open Sci.,* 2019. 6(1): p. 181557.

[54] Kong, T., L. Hao, Y. Wei, X. Cai, and B. Zhu, Doxorubicin conjugated carbon dots as a drug delivery system for human breast cancer therapy. *Cell Prolif.*, 2018. 51(5): p. e12488.

[55] Yang, K., C. Wang, C. Liu, S. Ding, F. Tian, and F. Li, Bioluminescence-initiated photodynamic therapy bridged on high-luminescent carbon dots-conjugated protoporphyrin IX. *J. Mater. Sci.*, 2019. 54(4): p. 3383-3391.

[56] Yang, K., C. Wang, X. Wei, S. Ding, C. Liu, F. Tian, and F. Li, Self-Illuminating Photodynamic Therapy with Enhanced Therapeutic Effect by Optimization of the Chemiluminescence Resonance Energy Transfer Step to the Photosensitizer. *Bioconjug. Chem.*, 2020. 31(3): p. 595-604.

[57] An, Y., C. Liu, Y. Li, M. Chen, Y. Zheng, H. Tian, R. Shi, X. He, and X. Lin, Preparation of Multicolour Solid Fluorescent Carbon Dots for Light-Emitting Diodes Using Phenylethylamine as a Co-Carbonization Agent. *Int. J. Mol. Sci.*, 2022. 23(19).

[58] Yuan, F., Y.-K. Wang, G. Sharma, Y. Dong, X. Zheng, P. Li, A. Johnston, G. Bappi, J. Z. Fan, H. Kung, B. Chen, M. I. Saidaminov, K. Singh, O. Voznyy, O. M. Bakr, Z.-H. Lu, and E. H. Sargent, Bright high-colour-purity deep-blue carbon dot light-emitting diodes via efficient edge amination. *Nat. Photon.*, 2019. 14(3): p. 171-176.

[59] Aggarwal, R., D. Saini, S. K. Sonkar, A. K. Sonker, and G. Westman, Sunlight promoted removal of toxic hexavalent chromium by cellulose derived photoactive carbon dots. *Chemosphere*, 2022. 287(Pt 3): p. 132287.

[60] Huang, P., S. Xu, M. Zhang, W. Zhong, Z. Xiao, and Y. Luo, Green carbon dots based ultraviolet photovoltaic window with high transparence to visible light. *Int. J. Energy Res.*, 2021. 45(12): p. 17709-17720.

[61] Ansón-Casaos, A., J. Hernández-Ferrer, L. Vallan, H. Xie, M. Lira-Cantú, A. M. Benito, and W. K. Maser, Functionalized carbon dots on TiO_2 for perovskite photovoltaics and stable photoanodes for water splitting. *Int. J. Hydrog. Energy*, 2021. 46(22): p. 12180-12191.

[62] Fiori, F., H. Moukham, F. Olia, D. Piras, S. Ledda, A. Salis, L. Stagi, L. Malfatti, and P. Innocenzi, Highly Photostable Carbon Dots from Citric Acid for Bioimaging. *Materials*, 2022. 15(7).

[63] Ding, H., J. S. Wei, N. Zhong, Q. Y. Gao, and H. M. Xiong, Highly Efficient Red-Emitting Carbon Dots with Gram-Scale Yield for Bioimaging. *Langmuir*, 2017. 33(44): p. 12635-12642.

[64] Bhaisare, M. L., A. Talib, M. S. Khan, S. Pandey, and H.-F. Wu, Synthesis of fluorescent carbon dots via microwave carbonization of citric acid in presence of tetraoctylammonium ion, and their application to cellular bioimaging. *Microchim. Acta*, 2015. 182(13-14): p. 2173-2181.

[65] Wan, J., S. Xu, J. Li, M. Yu, K. Zhang, G. Wei, and Z. Su, Facile synthesis of multifunctional pharmaceutical carbon dots for targeted bioimaging and chemotherapy of tumors. *Nanoscale*, 2022. 14(31): p. 11359-11368.

[66] Li, S., X. Song, Z. Hu, and G. Feng, A carbon dots-based ratiometric fluorescence probe for monitoring intracellular pH and bioimaging. *J. Photochem. Photobiol. A*, 2021. 409.

[67] Wang, L., B. Wang, E. Liu, Y. Zhao, B. He, C. Wang, G. Xing, Z. Tang, Y. Zhou, and S. Qu, Polyetherimide functionalized carbon dots with enhanced red emission in aqueous solution for bioimaging. *Chin. Chem. Lett.*, 2022. 33(8): p. 4111-4115.

[68] Shan, F., H. Xia, X. Xie, L. Fu, H. Yang, Q. Zhou, Y. Zhang, Z. Wang, and X. Yu, Novel N-doped carbon dots prepared via citric acid and benzoylurea by green synthesis for high selectivity Fe(III) sensing and imaging in living cells. *Microchem. J.*, 2021. 167.

[69] Wang, Q., L. Shi, J. Zhao, and S. Shuang, Fluorescent carbon dots with real-time nucleolus-monitoring capability for gene delivery and biosensing of NO2– and pH. *Appl. Surf. Sci.*, 2022. 599.

[70] Singaravelu, C. M., X. Deschanels, C. Rey, and J. Causse, Solid-State Fluorescent Carbon Dots for Fluorimetric Sensing of Hg2+. *ACS Appl. Nano Mater.*, 2021. 4(6): p. 6386-6397.

[71] Bogireddy, N. K. R., S. E. Sotelo Rios, and V. Agarwal, Simple one step synthesis of dual-emissive heteroatom doped carbon dots for acetone sensing in commercial products and Cr (VI) reduction. *Chem. Eng. J.,* 2021. 414.

[72] Zhou, Y., S. Zhang, S. Li, L. Wei, and L. Zhang, Multifunctional N doped carbon dots for cellular sensing, light-emitting-diode, and additive manufacturing. *Mater. Lett.*, 2022. 325.

[73] Lin, Z., Q. Zeng, Q. Deng, W. Yao, H. Deng, X. Lin, and W. Chen, Citric acid-derived carbon dots as excellent cysteine oxidase mimics for cysteine sensing. *Sens. Actuators B Chem.*, 2022. 359.

[74] Hu, Q., W. Wang, Z. Q. Yang, L. Xiao, X. Gong, L. Liu, and J. Han, An ultrasensitive sensing platform based on fluorescence carbon dots for chlorogenic acid determination in food samples. *Food Chem.*, 2023. 404(Pt A): p. 134395.

[75] Zou, G.-Y., L. Guo, S. Chen, N.-Z. Liu, and Y.-L. Yu, Multifunctional ratiometric fluorescent sensing platform constructed by grafting various response groups on carbon dots with bromine active site for biosensing and bioimaging. *Sens. Actuators B Chem.*, 2022. 357.

[76] Zeng, Q., D. Shao, X. He, Z. Ren, W. Ji, C. Shan, S. Qu, J. Li, L. Chen, and Q. Li, Carbon dots as a trackable drug delivery carrier for localized cancer therapy in vivo. *J. Mater. Chem. B*, 2016. 4(30): p. 5119-5126.

[77] Peng, Z., E. H. Miyanji, Y. Zhou, J. Pardo, S. D. Hettiarachchi, S. Li, P. L. Blackwelder, I. Skromne, and R. M. Leblanc, Carbon dots: promising biomaterials for bone-specific imaging and drug delivery. *Nanoscale*, 2017. 9(44): p. 17533-17543.

[78] Pandey, A., A. Devkota, A. Sigdel, Z. Yadegari, K. Dumenyo, and A. Taheri, Citric acid/beta-alanine carbon dots as a novel tool for delivery of plasmid DNA into E. coli cells. *Sci. Rep.*, 2021. 11(1): p. 23964.

[79] Zhou, Y., P. Y. Liyanage, D. Devadoss, L. R. Rios Guevara, L. Cheng, R. M. Graham, H. S. Chand, A. O. Al-Youbi, A. S. Bashammakh, M. S. El-Shahawi, and R. M. Leblanc, Nontoxic amphiphilic carbon dots as promising drug nanocarriers across the blood-brain barrier and inhibitors of beta-amyloid. *Nanoscale*, 2019. 11(46): p. 22387-22397.

[80] Suner, S. S., M. Sahiner, A. S. Yilmaz, R. S. Ayyala, and N. Sahiner, Light-Activated Modified Arginine Carbon Dots as Antibacterial Particles. *Catalysts*, 2022. 12(11).

[81] Lv, Y., P. Li, R. Su, J. Cai, H. Zhong, F. Wen, and W. Su, Methylene Blue/Carbon Dots Composite with Photothermal and Photodynamic Properties: Synthesis, Characterization, and Antibacterial Application. *Photochem. Photobiol.*, 2022.

[82] Romero, M. P., F. Alves, M. D. Stringasci, H. H. Buzza, H. Ciol, N. M. Inada, and V. S. Bagnato, One-Pot Microwave-Assisted Synthesis of Carbon Dots and in vivo and in vitro Antimicrobial Photodynamic Applications. *Front. Microbiol.*, 2021. 12: p. 662149.

[83] Kong, T., T. Liu, Y. Zhang, and M. Wang, Carbon dots with intrinsic theranostic properties for photodynamic therapy of oral squamous cell carcinoma. *J. Biomater. Appl.*, 2022. 37(5): p. 850-858.

[84] Yang, Y., H. Ding, Z. Li, A. C. Tedesco, and H. Bi, Carbon Dots Derived from Tea Polyphenols as Photosensitizers for Photodynamic Therapy. *Molecules*, 2022. 27(23).

[85] Wang, H. J., W. Y. Hou, Y. W. Hao, W. S. Jiang, H. L. Chen, and Q. Q. Zhang, Novel yellow solid-state fluorescent-emitting carbon dots with high quantum yield for white light-emitting diodes. *Spectrochim. Acta A Mol. Biomol. Spectrosc.*, 2021. 250: p. 119340.

[86] Qiu, H., F. Yuan, Y. Wang, Z. Zhang, J. Li, and Y. Li, Green-light-emitting carbon dots via eco-friendly route and their potential in ferric-ion detection and WLEDs. *Mater. Adv.*, 2022. 3(19): p. 7339-7347.

[87] Yang, X., L. Sui, B. Wang, Y. Zhang, Z. Tang, B. Yang, and S. Lu, Red-emitting, self-oxidizing carbon dots for the preparation of white LEDs with super-high color rendering index. *Sci. China Chem.*, 2021. 64(9): p. 1547-1553.

[88] Zhang, C., T. Lin, X. Yin, X. Wu, and X. Wei, Preparation of transparent wood containing carbon dots for application in the field of white-LED. *J. Wood Chem. Technol.*, 2022. 42(5): p. 331-341.

[89] Zhang, J., D. Nan, S. Pan, H. Liu, H. Yang, and X. Hu, N,S co-doped carbon dots as a dual-functional fluorescent sensor for sensitive detection of baicalein and temperature. *Spectrochim. Acta A Mol. Biomol. Spectrosc.*, 2019. 221: p. 117161.

[90] Zuo, P., J. Liu, H. Guo, C. Wang, H. Liu, Z. Zhang, and Q. Liu, Multifunctional N,S co-doped carbon dots for sensitive probing of temperature, ferric ion, and methotrexate. *Anal. Bioanal. Chem.*, 2019. 411(8): p. 1647-1657.

[91] Zhang, H., J. You, J. Wang, X. Dong, R. Guan, and D. Cao, Highly luminescent carbon dots as temperature sensors and "off-on" sensing of Hg^{2+} and biothiols. *Dyes Pigm.*, 2020. 173.

[92] Sendão, R. M. S., J. C. G. Esteves da Silva, and L. Pinto da Silva, Applications of Fluorescent Carbon Dots as Photocatalysts: A Review. *Catalysts*, 2023. 13(1).

[93] Jana, B., Y. Reva, T. Scharl, V. Strauss, A. Cadranel, and D. M. Guldi, Carbon Nanodots for All-in-One Photocatalytic Hydrogen Generation. *J. Am. Chem. Soc.*, 2021. 143(48): p. 20122-20132.

[94] Zhou, Y., A. E. ElMetwally, J. Chen, W. Shi, E. K. Cilingir, B. Walters, K. J. Mintz, C. Martin, B. Ferreira, W. Zhang, S. D. Hettiarachchi, L. F. Serafim, P. L. Blackwelder, A. H. Wikramanayake, Z. Peng, and R. M. Leblanc, Gel-like carbon dots: A high-performance future photocatalyst. *J. Colloid Interface Sci.*, 2021. 599: p. 519-532.

[95] Nabid, M. R., Y. Bide, and N. Fereidouni, Boron and nitrogen co-doped carbon dots as a metal-free catalyst for hydrogen generation from sodium borohydride. *New J. Chem.*, 2016. 40(10): p. 8823-8828.

[96] Al-Azmi, A. and S. Keshipour, New bidental sulfur-doped graphene quantum dots modified with gold as a catalyst for hydrogen generation. *J. Colloid Interface Sci.*, 2022. 612: p. 701-709.

[97] Aghamali, A., M. Khosravi, H. Hamishehkar, N. Modirshahla, and M. A. Behnajady, Synthesis and characterization of high efficient photoluminescent sunlight driven photocatalyst of N-Carbon Quantum Dots. *J. Lumin.*, 2018. 201: p. 265-274.

[98] Amadio, E., S. Cailotto, C. Campalani, L. Branzi, C. Raviola, D. Ravelli, E. Cattaruzza, E. Trave, A. Benedetti, M. Selva, and A. Perosa, Precursor-Dependent Photocatalytic Activity of Carbon Dots. *Molecules*, 2019. 25(1).

[99] Kaushal, N., A. L. Sharma, and A. Saha, Visible LED-based photo-redox properties of sulfur and nitrogen-doped carbon dots designed by solid-state synthesis. *Mater. Adv.*, 2022. 3(1): p. 355-361.

[100] Lim, H., Y. Liu, H. Y. Kim, and D. I. Son, Facile synthesis and characterization of carbon quantum dots and photovoltaic applications. *Thin Solid Films*, 2018. 660: p. 672-677.

[101] Bora, A., K. Mohan, and S. K. Dolui, Carbon Dots as Cosensitizers in Dye-Sensitized Solar Cells and Fluorescence Chemosensors for 2,4,6-Trinitrophenol Detection. *Ind. Eng. Chem. Res.*, 2019. 58(51): p. 22771-22778.

[102] Efa, M. T. and T. Imae, Effects of carbon dots on ZnO nanoparticle-based dye-sensitized solar cells. *Electrochim. Acta*, 2019. 303: p. 204-210.

[103] Zhang, X., J. Lu, X. Zhou, C. Guo, and C. Wang, Rapid microwave synthesis of N-doped carbon nanodots with high fluorescence brightness for cell imaging and sensitive detection of iron (III). *Opt. Mater.*, 2017. 64: p. 1-8.

[104] Zhang, Z., G. Yi, P. Li, X. Zhang, H. Fan, X. Wang, C. Zhang, Y. Zhang, and Q. Sun, Construction of N-Doped Carbon Dots/Macroporous TiO_2 Composites (N-CDs/m-TiO_2) with Dramatically Enhanced Photocatalytic Activity. *Ind. Eng. Chem. Res.,* 2021. 60(32): p. 11954-11963.

[105] Huang, B., J. He, S. Bian, C. Zhou, Z. Li, F. Xi, J. Liu, and X. Dong, S-doped graphene quantum dots as nanophotocatalyst for visible light degradation. *Chin. Chem. Lett.*, 2018. 29(11): p. 1698-1701.

[106] Bhati, A., S. R. Anand, D. Saini, Gunture, and S. K. Sonkar, Sunlight-induced photoreduction of Cr(VI) to Cr(III) in wastewater by nitrogen-phosphorus-doped carbon dots. *NPJ Clean Water*, 2019. 2(1).

[107] Guo, Z., H. Wu, M. Li, T. Tang, J. Wen, and X. Li, Phosphorus-doped graphene quantum dots loaded on TiO_2 for enhanced photodegradation. *Appl. Surf. Sci.*, 2020. 526.

[108] Li, L. and T. Dong, Photoluminescence tuning in carbon dots: surface passivation or/and functionalization, heteroatom doping. *J. Mater. Chem. C*, 2018. 6(30): p. 7944-7970.

[109] Mombrú, D., M. Romero, R. Faccio, and Á. W. Mombrú, Electronic and optical properties of sulfur and nitrogen doped graphene quantum dots: A theoretical study. *Physica E Low dimens. Syst. Nanostruct.*, 2019. 113: p. 130-136.

[110] Lou, Z., S. Zhao, Q. Wang, and H. Wei, N-Doped Carbon As Peroxidase-Like Nanozymes for Total Antioxidant Capacity Assay. *Anal. Chem.*, 2019. 91(23): p. 15267-15274.

[111] Lee, A., S. Yun, E. S. Kang, J. W. Kim, J. H. Park, and J. S. Choi, Effect of heteroatoms on the optical properties and enzymatic activity of N-doped carbon dots. *RSC Adv.*, 2021. 11(31): p. 18776-18782.

[112] Miao, X., D. Qu, D. Yang, B. Nie, Y. Zhao, H. Fan, and Z. Sun, Synthesis of Carbon Dots with Multiple Color Emission by Controlled Graphitization and Surface Functionalization. *Adv. Mater.*, 2018. 30(1).

[113] Hien, N. T., T. T. K. Chi, N. D. Vinh, H. T. Van, L. D. Thanh, P. V. Do, V. P. Tuyen, and N. X. Ca, Synthesis, characterization and the photoinduced electron-transfer energetics of CdTe/CdSe type-II core/shell quantum dots. *J. Lumin.*, 2020. 217.

[114] Sun, H., A. Zhao, N. Gao, K. Li, J. Ren, and X. Qu, Deciphering a nanocarbon-based artificial peroxidase: chemical identification of the catalytically active and

substrate-binding sites on graphene quantum dots. *Angew. Chem. Int. Ed. Engl.*, 2015. 54(24): p. 7176-80.

[115] Wibrianto, A., S. Q. Khairunisa, S. C. W. Sakti, Y. L. Ni'mah, B. Purwanto, and M. Z. Fahmi, Comparison of the effects of synthesis methods of B, N, S, and P-doped carbon dots with high photoluminescence properties on HeLa tumor cells. *RSC Adv.*, 2020. 11(2): p. 1098-1108.

[116] Zhu, S., Y. Song, X. Zhao, J. Shao, J. Zhang, and B. Yang, The photoluminescence mechanism in carbon dots (graphene quantum dots, carbon nanodots, and polymer dots): current state and future perspective. *Nano Res.*, 2015. 8(2): p. 355-381.

[117] Xia, C., S. Zhu, T. Feng, M. Yang, and B. Yang, Evolution and Synthesis of Carbon Dots: From Carbon Dots to Carbonized Polymer Dots. *Adv. Sci.*, 2019. 6(23): p. 1901316.

[118] Kim, T., J. Lee, and K.-H. Lee, Microwave heating of carbon-based solid materials. *Carbon Lett.,* 2014. 15(1): p. 15-24.

[119] Liang, C., Y. Wang, and T. Li, Synthesis of sulfur-doped p-type graphene by annealing with hydrogen sulfide. *Carbon*, 2015. 82: p. 506-512.

[120] Xu, Q., W. Cai, M. Zhang, R. Su, Y. Ye, Y. Li, L. Zhang, Y. Guo, Z. Yu, S. Li, X. Lin, Y. Chen, Y. Luo, J. Street, and M. Xu, Photoluminescence mechanism and applications of Zn-doped carbon dots. *RSC Adv.*, 2018. 8(31): p. 17254-17262.

[121] Gencer, O., Ö. F. Çeven, and C. Ünlü, Triggering excitation independent fluorescence in zinc(II) incorporated carbon dots: Surface passivation of carbon dots with zinc(II) ions by microwave assisted synthesis methods. *Diam. Relat. Mater.*, 2022. 123.

[122] Zhuo, S., J. Fang, M. Li, J. Wang, C. Zhu, and J. Du, Manganese(II)-doped carbon dots as effective oxidase mimics for sensitive colorimetric determination of ascorbic acid. *Mikrochim. Acta*, 2019. 186(12): p. 745.

[123] Ma, Y., Y. Cen, M. Sohail, G. Xu, F. Wei, M. Shi, X. Xu, Y. Song, Y. Ma, and Q. Hu, A Ratiometric Fluorescence Universal Platform Based on N, Cu Codoped Carbon Dots to Detect Metabolites Participating in H(2)O(2)-Generation Reactions. *ACS Appl. Mater. Interfaces*, 2017. 9(38): p. 33011-33019.

[124] Liu, J., Q. Chen, Z. Zhang, Z. Wang, and Z. Gong, Nitrogen and copper (II) co-doped carbon dots as multi-functional fluorescent probes for Fe3+ ions and tetracycline. *Microchem. J.*, 2022. 181.

[125] Kumar, V. B., R. Kumar, A. Gedanken, and O. Shefi, Fluorescent metal-doped carbon dots for neuronal manipulations. *Ultrason. Sonochem.*, 2019. 52: p. 205-213.

[126] Jiang, K., S. Sun, L. Zhang, Y. Lu, A. Wu, C. Cai, and H. Lin, Red, green, and blue luminescence by carbon dots: full-color emission tuning and multicolor cellular imaging. *Angew. Chem. Int. Ed. Engl.*, 2015. 54(18): p. 5360-3.

[127] Tang, L., R. Ji, X. Cao, J. Lin, H. Jiang, X. Li, K. S. Teng, C. M. Luk, S. Zeng, J. Hao, and S. P. Lau, Deep ultraviolet photoluminescence of water-soluble self-passivated graphene quantum dots. *ACS Nano*, 2012. 6(6): p. 5102-10.

[128] Xiao, L., Y. Wang, Y. Huang, T. Wong, and H. Sun, Self-trapped exciton emission from carbon dots investigated by polarization anisotropy of photoluminescence and photoexcitation. *Nanoscale*, 2017. 9(34): p. 12637-12646.

[129] Ghosh, S., A. M. Chizhik, N. Karedla, M. O. Dekaliuk, I. Gregor, H. Schuhmann, M. Seibt, K. Bodensiek, I. A. Schaap, O. Schulz, A. P. Demchenko, J. Enderlein, and A. I. Chizhik, Photoluminescence of carbon nanodots: dipole emission centers and electron-phonon coupling. *Nano Lett.*, 2014. 14(10): p. 5656-61.

[130] Demchenko, A. P. and M. O. Dekaliuk, The origin of emissive states of carbon nanoparticles derived from ensemble-averaged and single-molecular studies. *Nanoscale*, 2016. 8(29): p. 14057-69.

[131] Essner, J. B., J. A. Kist, L. Polo-Parada, and G. A. Baker, Artifacts and Errors Associated with the Ubiquitous Presence of Fluorescent Impurities in Carbon Nanodots. *Chem. Mater.,* 2018. 30(6): p. 1878-1887.

[132] Kasprzyk, W., T. Swiergosz, S. Bednarz, K. Walas, N. V. Bashmakova, and D. Bogdal, Luminescence phenomena of carbon dots derived from citric acid and urea - a molecular insight. *Nanoscale*, 2018. 10(29): p. 13889-13894.

[133] Ren, J., F. Weber, F. Weigert, Y. Wang, S. Choudhury, J. Xiao, I. Lauermann, U. Resch-Genger, A. Bande, and T. Petit, Influence of surface chemistry on optical, chemical and electronic properties of blue luminescent carbon dots. *Nanoscale*, 2019. 11(4): p. 2056-2064.

[134] Fadeel, B., C. Bussy, S. Merino, E. Vazquez, E. Flahaut, F. Mouchet, L. Evariste, L. Gauthier, A. J. Koivisto, U. Vogel, C. Martin, L. G. Delogu, T. Buerki-Thurnherr, P. Wick, D. Beloin-Saint-Pierre, R. Hischier, M. Pelin, F. Candotto Carniel, M. Tretiach, F. Cesca, F. Benfenati, D. Scaini, L. Ballerini, K. Kostarelos, M. Prato, and A. Bianco, Safety Assessment of Graphene-Based Materials: Focus on Human Health and the Environment. *ACS Nano*, 2018. 12(11): p. 10582-10620.

[135] Hischier, R. and T. Walser, Life cycle assessment of engineered nanomaterials: state of the art and strategies to overcome existing gaps. *Sci. Total Environ.*, 2012. 425: p. 271-82.

[136] Ramos, A., C. A. Teixeira, and A. Rouboa, Assessment study of an advanced gasification strategy at low temperature for syngas generation. *Int. J. Hydrog. Energy*, 2018. 43(21): p. 10155-10166.

[137] Fernandes, S., J. C. G. Esteves da Silva, and L. Pinto da Silva, Comparative life cycle assessment of high-yield synthesis routes for carbon dots. *NanoImpact*, 2021. 23.

[138] Pourzahedi, L. and M. J. Eckelman, Comparative life cycle assessment of silver nanoparticle synthesis routes. *Environ. Sci. Nano*, 2015. 2(4): p. 361-369.

[139] Algarra, M., L. d. Orfãos, C. S. Alves, R. Moreno-Tost, M. S. Pino-González, J. Jiménez-Jiménez, E. Rodríguez-Castellón, D. Eliche-Quesada, E. Castro, and R. Luque, Sustainable Production of Carbon Nanoparticles from Olive Pit Biomass: Understanding Proton Transfer in the Excited State on Carbon Dots. *ACS Sustain. Chem. Eng.*, 2019. 7(12): p. 10493-10500.

[140] Jing, S., Y. Zhao, R.-C. Sun, L. Zhong, and X. Peng, Facile and High-Yield Synthesis of Carbon Quantum Dots from Biomass-Derived Carbons at Mild Condition. *ACS Sustain. Chem. Eng.*, 2019. 7(8): p. 7833-7843.

[141] Crista, D. M. A., A. El Mragui, M. Algarra, J. C. G. Esteves da Silva, R. Luque, and L. Pinto da Silva, Turning Spent Coffee Grounds into Sustainable Precursors for the Fabrication of Carbon Dots. *Nanomaterials*, 2020. 10(6).

[142] Dager, A., T. Uchida, T. Maekawa, and M. Tachibana, Synthesis and characterization of Mono-disperse Carbon Quantum Dots from Fennel Seeds: Photoluminescence analysis using Machine Learning. *Sci. Rep.*, 2019. 9(1): p. 14004.

[143] Thakur, A., P. Devi, S. Saini, R. Jain, R. K. Sinha, and P. Kumar, Citrus limetta Organic Waste Recycled Carbon Nanolights: Photoelectro Catalytic, Sensing, and Biomedical Applications. *ACS Sustain. Chem. Eng.*, 2018. 7(1): p. 502-512.

[144] Campos-Vega, R., G. Loarca-Piña, H. A. Vergara-Castañeda, and B. D. Oomah, Spent coffee grounds: A review on current research and future prospects. *Trends Food Sci. Technol.*, 2015. 45(1): p. 24-36.

[145] Zhao, W., Y. Cui, X. Sun, H. Wang, and X. Teng, Corn stover biochar increased edible safety of spinach by reducing the migration of mercury from soil to spinach. *Sci. Total Environ.*, 2021. 758: p. 143883.

[146] Langer, M., M. Paloncýová, M. Medveď, M. Pykal, D. Nachtigallová, B. Shi, A. J. A. Aquino, H. Lischka, and M. Otyepka, Progress and challenges in understanding of photoluminescence properties of carbon dots based on theoretical computations. *Appl. Mater. Today*, 2021. 22.

[147] Ru, Y., G. I. N. Waterhouse, and S. Lu, Aggregation in carbon dots. *Aggregate*, 2022. 3(6).

[148] Ding, H., L.-W. Cheng, Y.-Y. Ma, J.-L. Kong, and H.-M. Xiong, Luminescent carbon quantum dots and their application in cell imaging. *New J. Chem.*, 2013. 37(8).

[149] Lu, S., Z. Li, X. Fu, Z. Xie, and M. Zheng, Carbon dots-based fluorescence and UV–vis absorption dual-modal sensors for Ag^{+} and l-cysteine detection. *Dyes Pigm.*, 2021. 187.

[150] Wu, M., Y. Demissie, and E. Yan, Simulated impact of future biofuel production on water quality and water cycle dynamics in the Upper Mississippi river basin. *Biomass Bioenergy*, 2012. 41: p. 44-56.

[151] Grinstead, K. M., L. Rowe, C. M. Ensor, S. Joel, P. Daftarian, E. Dikici, J. M. Zingg, and S. Daunert, Red-Shifted Aequorin Variants Incorporating Non-Canonical Amino Acids: Applications in In Vivo Imaging. *PLoS One*, 2016. 11(7): p. e0158579.

[152] Zhang, Y., L. Pang, C. Ma, Q. Tu, R. Zhang, E. Saeed, A. E. Mahmoud, and J. Wang, Small molecule-initiated light-activated semiconducting polymer dots: an integrated nanoplatform for targeted photodynamic therapy and imaging of cancer cells. *Anal. Chem.*, 2014. 86(6): p. 3092-9.

[153] Ievtukhov, V., B. Zadykowicz, M. Y. Blazheyevskiy, and K. Krzyminski, New luminometric method for quantification of biological sulfur nucleophiles with the participation of 9-cyano-10-methylacridinium salt. *Lumin.*, 2022. 37(2): p. 208-219.

[154] Magalhães, C. M., J. C. G. Esteves da Silva, and L. Pinto da Silva, Study of coelenterazine luminescence: Electrostatic interactions as the controlling factor for efficient chemiexcitation. *J. Lumin.*, 2018. 199: p. 339-347.

[155] Haddock, S. H., M. A. Moline, and J. F. Case, Bioluminescence in the sea. *Ann. Rev. Mar. Sci.*, 2010. 2: p. 443-93.

[156].Magalhaes, C. M., J. C. G. Esteves da Silva, and L. Pinto da Silva, Comparative study of the chemiluminescence of coelenterazine, coelenterazine-e and Cypridina luciferin with an experimental and theoretical approach. *J. Photochem. Photobiol. B*, 2019. 190: p. 21-31.

[157] Magalhaes, C. M., J. C. Esteves da Silva, and L. Pinto da Silva, Chemiluminescence and Bioluminescence as an Excitation Source in the Photodynamic Therapy of Cancer: A Critical Review. *Chemphyschem*, 2016. 17(15): p. 2286-94.

[158] Magalhaes, C. M., J. C. G. Esteves da Silva, and L. Pinto da Silva, Tuning the Intramolecular Chemiexcitation of Neutral Dioxetanones by Interaction with Ionic Species. *Molecules*, 2022. 27(12).

[159] Pinto da Silva, L. and J. C. Esteves da Silva, Firefly chemiluminescence and bioluminescence: efficient generation of excited states. *Chemphyschem*, 2012. 13(9): p. 2257-62.

[160] Pinto da Silva, L., C. M. Magalhaes, D. M. A. Crista, and J. C. G. Esteves da Silva, Theoretical modulation of singlet/triplet chemiexcitation of chemiluminescent imidazopyrazinone dioxetanone via C(8)-substitution. *Photochem. Photobiol. Sci.*, 2017. 16(6): p. 897-907.

[161] Koo, J.-Y. and G. B. Schuster, Chemically initiated electron exchange luminescence. A new chemiluminescent reaction path for organic peroxides. *J. Am. Chem. Soc.*, 1977. 99(18): p. 6107-6109.

[162] Melhuish, W. H., Quantum Efficiencies of Fluorescence of Organic Substances: Effect of Solvent and Concentration of the Fluorescent Solute1. *J. Phys. Chem.*, 1961. 65(2): p. 229-235.

1.2. Photocatalytic degradation of organic pollutants using TiO_2 and CDs nanocomposites

Article

Photocatalytic removal of pharmaceutical water pollutants by TiO_2 – Carbon dots nanocomposites: A review

Sendão, Ricardo M. S.; Esteves da Silva, Joaquim C. G.; Pinto da Silva, Luís. "Photocatalytic removal of pharmaceutical water pollutants by TiO_2 – Carbon dots nanocomposites: A review". *Chemosphere* 301 (**2022**): 134731. https://doi.org/10.1016/j.chemosphere.2022.134731.

1.2.1. Introduction and contributions to this work

The use of pharmaceuticals by humanity is increasing on a year-on-year basis, and this specific class of organic pollutants is becoming an increasingly more relevant water contaminant. The problem is aggravated by the fact that conventional water treatment technologies are inefficient when it comes to this type of pollutant, and thus, alternatives must be developed. This objective is directly related to the doctoral project, which concerns the development of sunlight-active catalytic nanocomposites for the photodegradation of antibiotics. As the main base for our work, we used the study presented below, which focuses on and reviews the available reports concerning the development of TiO_2/CDs nanocomposites for the photocatalytic removal of pharmaceutical water contaminants. It highlights the potential of CDs to bridge the limitations of TiO_2 that prevent an efficient application under solar irradiation, explaining how the carbon-based nanoparticles can improve the uptake of visible irradiation, improve the photonic efficiency, and contribute toward a better adsorption of organic pollutants. Some aspects that need to be addressed before these nanocomposites are widely used are also pointed out.

In this work, I was responsible for the bibliographic research and the writing of the draft, under the supervision of Professor Dr. Luís Pinto da Silva and Professor Dr. Joaquim Esteves da Silva.

Chemosphere 301 (2022) 134731

Contents lists available at ScienceDirect

Chemosphere

journal homepage: www.elsevier.com/locate/chemosphere

Photocatalytic removal of pharmaceutical water pollutants by TiO_2 – Carbon dots nanocomposites: A review

Ricardo M.S. Sendão [a], Joaquim C.G. Esteves da Silva [a, b], Luís Pinto da Silva [a, b, *]

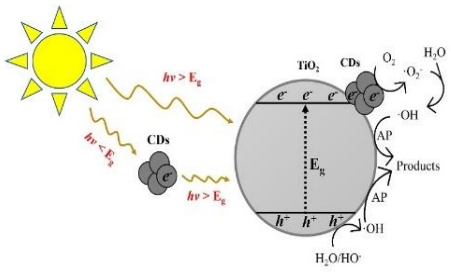
[a] Chemistry Research Unit (CIQUP), Institute of Molecular Sciences (IMS), Faculty of Sciences of University of Porto (FCUP), Rua do Campo Alegre 687, 4169-007, Porto, Portugal

[b] LACOMEPHI, GreenUPorto, Department of Geosciences, Environment and Territorial Planning, Faculty of Sciences of University of Porto (FCUP), Rua do Campo Alegre 687, 4169-007, Porto, Portugal

HIGHLIGHTS

- Pharmaceuticals are contaminating Earth's drinking water.
- Photocatalysts, such as TiO_2, may be used to photodegrade pharmaceuticals.
- TiO_2 is limited in terms of photonic efficiency and pollutant adsorption.
- Carbon dots bridge those limitations and led to a lower TiO_2's energy band gap.
- TiO_2/CDs nanocomposites efficiently remove pharmaceuticals from water.

GRAPHICAL ABSTRACT



ARTICLE INFO

Handling Editor: Jun Huang

Keywords:
TiO_2
Carbon dots
Photocatalysis
Aquatic pharmaceutics products
Pharmaceuticals
Nanocomposites

ABSTRACT

Pharmaceuticals are becoming increasingly more relevant water contaminants, with photocatalysts (such as TiO_2) being a promising approach to remove these compounds from water. However, TiO_2 has poor sunlight-harvesting capacity, low photonic efficiency, and poor adsorption towards organic pollutants. One of the emerging strategies to enhance the photocatalytic performance of TiO_2 is by conjugating it with fluorescent carbon dots. Herein, we performed a critical review of the development of TiO_2 – carbon dots nanocomposites for the photocatalytic removal of pharmaceuticals. We found that carbon dots can improve the photocatalytic efficiency of the resulting nanocomposites, mostly due to increasing the adsorption of organic pollutants and enhancing the absorption in the visible range. However, while this approach shows significant promise, we also identified and discussed several aspects that need to be addressed before this strategy could be more widely used. We hope that this review can guide future studies aiming to the development of enhanced photocatalytic TiO_2 – carbon dots nanocomposites.

* Corresponding author. Chemistry Research Unit (CIQUP), Faculty of Sciences of University of Porto (FCUP), Rua do Campo Alegre 687, 4169-007, Porto, Portugal.
E-mail address: luis.silva@fc.up.pt (L. Pinto da Silva).

https://doi.org/10.1016/j.chemosphere.2022.134731
Received 22 December 2021; Received in revised form 6 April 2022; Accepted 22 April 2022
Available online 27 April 2022
0045-6535/© 2022 Elsevier Ltd. All rights reserved.

1. Introduction

Water is one of the most crucial resources on Earth. While it is valuable and in very high demand, the contamination of the drinkable water necessary for human survival is an increasingly worrying problem as it may cause a scarcity of water fit for human consumption (Rodell et al., 2009; Tollefson, 2011; Mekonnen and Hoekstra, 2016). Common causes of water pollution are industrial effluents, heavy metals, and organic pollutants. The extended exposition to pharmaceuticals is a major health hazard as it may trigger the unintended development of resistance against the pharmaceutic effect of a given compound, thus endangering human health (Webb et al., 2003; Bu et al., 2013; Malchi et al., 2015). As an example, in the case of antibiotics, after ingestion, while a part of the compound is metabolized by the human body, most is excreted through urine and faeces (Zhang et al., 2013a; Kafaei et al., 2018), flowing mostly unchanged into domestic sewage systems (Yuan et al., 2019). Antibiotics, due to commonly being highly soluble in water (Kümmerer, 2008) and the low level of regulation, are now near ubiquitous in aquatic environments. This is considered one of the main routes for the propagation of antibiotic resistance in European wastewater treatment plants (Klevens et al., 2007; Berendonk et al., 2015).

Current water treatment technology includes coagulation/precipitation techniques and Fenton oxidation treatment, which are incapable of efficiently removing organic pollutants (Centi et al., 2000; Ghosh et al., 2011; Hanay and Hasar, 2011; Ferreira et al., 2013). The treatment of aquatic pollutants through advanced photocatalytic oxidation processes (AOPs) has been the focus of several studies over the past decades. Photocatalysis focus on the conversion of solar energy into chemical energy. The use of photocatalytic technologies has several advantages: it is a more environmentally friendly approach when compared to traditional chemical oxidation, it achieves near complete degradation of the targeted pollutants, and there are no by-products originating from the photocatalyst during the reaction (Malato et al., 2009; Zhang et al., 2019a).

Semiconductors are an example of heterogeneous photocatalysts. A semiconductor has an energy band structure comprised of a low energy valence band (VB) and a high energy conduction band (CV) with a void energy region in-between. In this region there are no energy levels available to promote recombination between the photogenerated charge carriers (electron and electron hole). This region, located between the top of the filled VB and the bottom of the empty CB, is called the band gap (Linsebigler et al., 2002). Fig. 1 represents the basic mechanism for a general photocatalytic degradation, in which a photon with enough energy to overcome the band gap is absorbed. After excitation, the process will either culminate in the generation of reactive species that decompose the pollutant or in the recombination of charge carriers and subsequent release of energy as heat (Kapinus et al., 2003; Lee and Park, 2013; Ahmari et al., 2018; Awfa et al., 2018, 2019; Chinnaiyan et al., 2018; Farner Budarz et al., 2019; Loeb et al., 2019; Lyu et al., 2019; Si et al., 2019). However, the latter is undesirable as it leads to an inefficient photocatalysis (Karvinen et al., 2003). Summarizing, a photocatalyst aims to facilitate reactions between excited electrons and oxidant/reductant substrates to produce reduced or oxidized products, respectively. In both cases the outcome is generally the generation of hydroxyl radicals, which are very oxidative in nature and capable of easily decomposing most organic pollutants (Lee and Park, 2013; Ahmari et al., 2018; Awfa et al., 2018, 2019; Chinnaiyan et al., 2018; Farner Budarz et al., 2019; Loeb et al., 2019; Lyu et al., 2019).

One of the best known photocatalysts is titanium dioxide (TiO_2), capable of degrading several types of water pollutants, including heavy metals (Kyung et al., 2005; Poursani et al., 2016), dyes (Zulfiqar et al., 2018; Fernandes et al., 2020), pesticides (Ahmari et al., 2018; Farner Budarz et al., 2019), hormones (Sornalingam et al., 2018; Toth et al., 2019), microbes (Bilek et al., 2019; Cheng et al., 2019), and pharmaceuticals (Awfa et al., 2018, 2019; Chinnaiyan et al., 2018; El Mragui et al., 2019; Loeb et al., 2019; Lyu et al., 2019) This review aims to provide information regarding the conjugation of TiO_2 with carbon dots (CDs), focusing on the photocatalytic degradation of pharmaceuticals and the advantages resulting thereof. We aim to provide a base on which researchers may find useful information when developing new technologies in the field.

2. Titanium dioxide as a basis for photocatalytic water treatment

TiO_2 is the naturally occurring oxide of titanium. It is a relatively inexpensive photocatalyst that is highly active under UV radiation (Gaya and Abdullah, 2008; Han et al., 2009; Hu et al., 2010). Among its several forms, Degussa P25 (made of 75% anatase and 25% rutile), is the most frequently used form., while other common forms include nanotubes, with intricate pathways allowing the transfer of radiation and an enhanced ionic diffusion (Bauer et al., 2011), and nanosheets, which present very powerful adhesive properties (Yang et al., 2008).

TiO_2 presents a fast and efficient photocatalytic response and does not suffer decomposition when going through a change in its oxidation state (Malato et al., 2002; Kabra et al., 2004; Meng et al., 2010). This means that TiO_2 can be an efficient, greener, alternative to the more energy-intensive and polluting chemical oxidation (Oller et al., 2011).

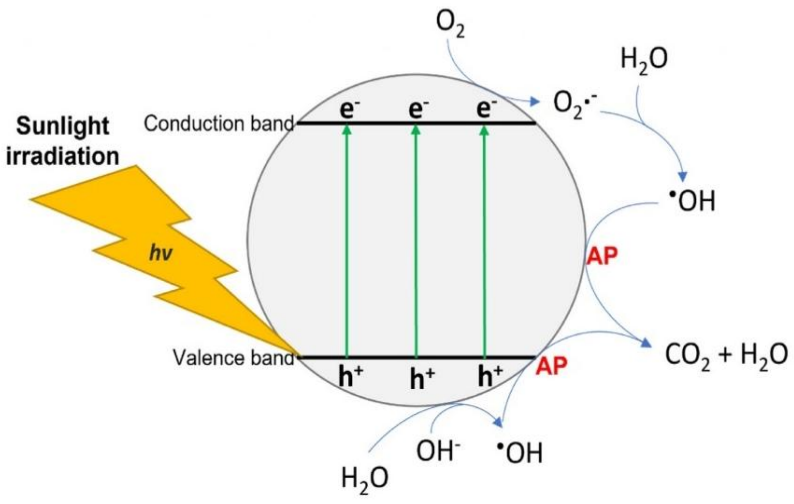


Fig. 1. General photocatalytic reaction mechanism for a semiconductor. AP - adsorbed pollutant.

Furthermore, using nanostructured TiO_2 is advantageous for photocatalysis due to the increased surface areas, low toxicity, biocompatibility, easy preparation of the nanostructures and faster rates of reaction (Guan et al., 2016; Wang et al., 2017a). TiO_2's surface can be easily modified and the morphology can be changed to include nanostructures (Zhang et al., 2006), presenting greater mass transfer rates, better adsorption of non-biodegradable organic compounds, and mesoporous surfaces (Seo and Park, 2009). When TiO_2 is used as a spherical nanoparticle, the rate at which the photocatalytic degradation of the organic components happens is quite high and independent of the occupation of the active sites by other molecules (such as water) (Liu et al., 2010, 2011; Wang et al., 2017a). TiO_2 nanoparticles have a high surface area, a highly crystalline structure, a larger number of active sites and increased mass transfer rates (Liu et al., 2010, 2011; Zheng et al., 2010). The photocatalytic mechanism of TiO_2 is an AOP, which are based on the decomposition of pollutants by hydroxyl radicals and other reactive oxygen species (ROS) produced *in situ* in a spontaneous and thermodynamically favourable process (Fig. 2). (Keen et al., 2014)

A prime example of the use of TiO_2 as an alternative to remove common pharmaceuticals from water is that of Degussa P25, which was successfully employed towards the removal of acetaminophen, diclofenac, ibuprofen, and sulfamethoxazole (Murgolo et al., 2015). By using lower-wavelength light, Degussa P25 nanoparticles were very effective in photodegrading these pharmaceuticals and were easily recovered by a simple centrifugation afterwards. However, the efficiency of the photocatalyst suffers severely when using solar light (Murgolo et al., 2015).

Despite many successful cases, TiO_2 presents some limitations that might prevent its commercial use. Chief among which is its narrow photocatalytic region ($\lambda < 400$ nm), harvesting only around 5% of sunlight, which limits its large-scale application due to requiring high-energy irradiation (energy band gap of 2.8–3.2 eV) (Yin et al., 2003; Ren et al., 2007). Moreover, TiO_2 suffers from rapid charge recombination, which reduces its photonic efficiency (Daghrir et al., 2012). A possible solution to extend the absorption edge toward the visible region is doping the photocatalyst (Pan et al., 2015; Zhou et al., 2018). The incorporation of dopants (*e. g.* platinum, nitrogen, sulphur, among others both metals and non-metals) enables the use of TiO_2 under visible-light by originating new energy levels and an improved, more stable, nanocrystalline structure (Pan et al., 2015; Zhou et al., 2018). However, doping, beside using mostly costly and toxic metal elements (Pan et al., 2015), also tends to accelerate the recombination of photogenerated charge carriers (Pan et al., 2015; Chen et al., 2016).

TiO_2's adsorption capabilities also limit its photocatalytic efficiency when dealing with organic pollutants (Dong et al., 2015). Considering that TiO_2's surface has poor affinity toward organic pollutants and that the photocatalytic degradation mainly takes place on said surface, the photocatalytic degradation rate is limited because the pollutants do not reach the active site easily (Dong et al., 2015). The limited adsorption capacity can be improved by employing dopants and/or co-catalytic systems to promote the accessibility to active sites on the photocatalysts' surface (Tu et al., 2013; Yu et al., 2014a). Finally, TiO_2 nanoparticles are prone to agglomerate due to the instability of the nanosized structures. This originates large aggregates with a reduced surface area and number of active sites, that also exhibits a high level of scattering and hampers the light incidence on the active sites, thus decreasing the photocatalytic efficiency due to two different factors (Gao et al., 2011; Mallakpour and Nikkhoo, 2014).

AOPs using TiO_2 have been extensively used for the removal of organic pollutants from water. Nevertheless, there are some limitations, some of which responsible for considerably impeding a more prolific use of such technologies. The conjugation of TiO_2 with other nanostructured materials, such as carbon nanomaterials, is now becoming a topic of interest for several research groups around the world that are now realizing it to be a better alternative than the costlier and more toxic traditional doping.

3. Carbon dots and TiO_2/CDs nanocomposites for the photocatalytic removal of pharmaceutical pollutants from water sources

3.1. Carbon dots – what are they and properties

Discovered in 2004 by Xu et al. during the production of single-wall carbon nanotubes (Xu et al., 2004), the fluorescent carbon-based nanoparticles present a spherical or quasi-spherical shape, usually sized between 1 and 10 nm, with a core that might be amorphous or nanocrystalline (Esteves da Silva and Gonçalves, 2011; Wang et al., 2017b). On the surface, CDs present several functional groups (such as

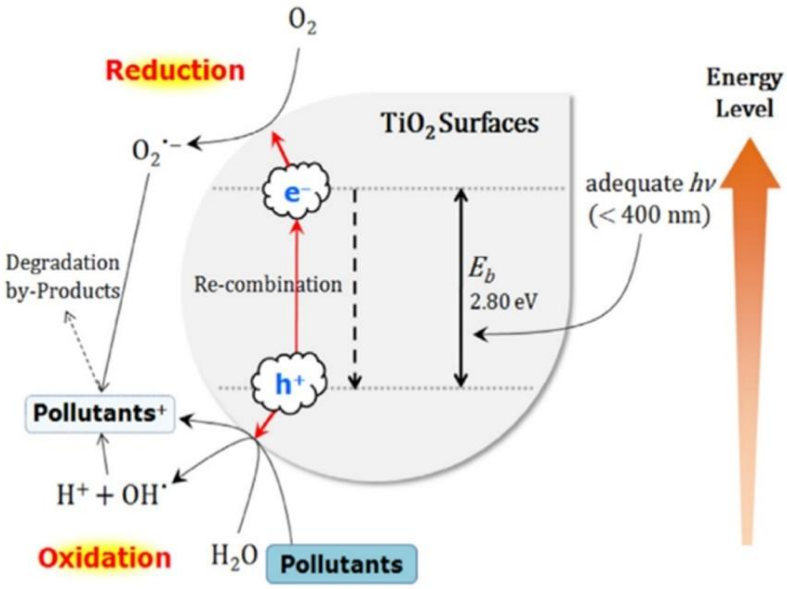


Fig. 2. Schematic representation of the photocatalytic removal of pollutants by TiO_2 through photogenerated charge carriers (electrons and electron holes). Reproduced here with authorization from Lee and Park (2013).

amines, alcohols or carboxylic acids) (Baker and Baker, 2010; Lim et al., 2015; Crista et al., 2020b) that contribute towards an exceptional water solubility and provide a chemical base for the binding of other molecules. CDs present several highly desirable properties for nanomaterials, such as high photoluminescence (PL) (Esteves da Silva and Gonçalves, 2011; Wang et al., 2017b), broad optical absorption range (Peng et al., 2017), biocompatibility (Sun et al., 2006; Baker and Baker, 2010; Vale et al., 2021), low toxicity (Wang et al., 2013), high photostability and chemical stability (Lim et al., 2015), good water solubility (Esteves da Silva and Gonçalves, 2011; Lim et al., 2015) and a high degree of tunability in terms of their physical and optoelectronic properties (Hola et al., 2017; Tian et al., 2019). Due to their high PL, CDs have been the focus of several studies aiming to replace traditional fluorescent materials with a superior nanomaterial. Furthermore, CDs may display upconversion PL, which consists of the emission of higher-energy lower-wavelength radiation upon excitation with lower-energy higher-wavelength light, effectively causing an anti-Stokes shift (Aghamali et al., 2018; Deng et al., 2021). While the origins behind CDs' upconversion photoluminescence is still a matter of debate, the most commonly proposed mechanism is that of the two-photon absorption. In this mechanism, electrons in the π orbital are excited by multiple low-energy photons and move into a higher energy state, and then fall back into the σ orbital *via* radiative relaxation (Yang et al., 2009; Li et al., 2010). Because of upconversion PL, some CDs can convert light in the visible and near infrared (NIR) region into shorter-wavelength higher-energy radiation that can be used for the photocatalytic activity of TiO_2 (Deng et al., 2021). Practical applications for CDs include bioimaging (Belkahla et al., 2019; Li et al., 2019), sensing and biosensing (Li et al., 2019; Simoes et al., 2020; Afonso et al., 2021), drug delivery systems (Hettiarachchi et al., 2019), photodynamic therapy (He et al., 2018), light-emitting devices (Joseph and Anappara, 2017), nanothermometry (Kalytchuk et al., 2017), photovoltaic devices (Zhang et al., 2013b) and photocatalysis (including several cases of TiO_2/CDs nanocomposites) (Li et al., 2010; Zhang et al., 2013b; Sabri et al., 2019).

CDs may be used to bridge TiO_2's limitations, thus promoting its photocatalytic activity. CDs present a core consisting mostly of sp^2 carbon connected by sp^3 carbon atoms with a surface that may be covered by different functional groups (Baker and Baker, 2010; Lim et al., 2015). The high electron storage capacity resulting thereof implies that the photoexcited electrons in TiO_2's CB can be accepted by the carbon nanostructure. This results not only in the extension of the photocatalytic reaction into the visible-light range, but also in a better separation of photogenerated charge carriers and an improved photonic efficiency. In addition, upconversion PL might also enhance the visible-light-harvesting capacity of TiO_2/CDs nanocomposites by transforming lower-energy radiation into higher-energy lower-wavelength radiation more suitable to being absorbed by TiO_2 (Fig. 3). (Pan et al., 2015; Rahbar et al., 2019) Finally, the functionalized surface presented by CDs provides a higher pollutant adsorption capacity for the photocatalyst, increasing the amount of pollutants reaching the active site (Chen et al., 2017).

3.2. TiO_2/CDs nanocomposites for the photocatalytic degradation of pharmaceutical pollutants from water sources – case studies

The work of Sharma et al. is a prime example of the use of TiO_2/CDs nanocomposites to photodegrade a pharmaceutical compound, in this case levofloxacin (Sharma et al., 2018). CDs were fabricated from L-ascorbic acid via a hydrothermal method (150 °C for 4 h) and used without further purification. While the reason for the precursor and synthetic conditions is not specified, it could be related to a previous work, in which the authors used similar conditions for the preparation of CDs for a ZnO/CDs photocatalyst for the degradation of malachite green dye (Sharma et al., 2017). To prepare the nanocomposites, TiO_2 nanoparticles were simply dispersed in a CD solution, and the resulting mixture was stirred, filtered, and dried. A change of colour from clear white to pale white indicated the successful preparation of TiO_2/CDs nanocomposites (Sharma et al., 2018).

Through a detailed characterization, the team confirmed that the CDs were uniformly distributed over the surface of TiO_2 nanoparticles (Sharma et al., 2018). Optical studies demonstrated that the CDs possessed upconversion PL and could emit light between 350 and 650 nm when excited with light ranging from 500 to 850 nm (Sharma et al., 2018). When the PL of the nanocomposites was assessed, it was found that it was lower than that of bare TiO_2, suggesting some hindrance of the recombination of photogenerated charge carriers, possibly due to some electrons transferring from TiO_2 into CDs (Zhang et al., 2017a; Sharma et al., 2018). Furthermore, when compared to bare TiO_2, the nanocomposite presents a slight absorption shift towards the visible region and a lower energy band gap (2.87 eV *versus* 3.04 eV for TiO_2), a higher absorption intensity, and a greater specific surface area when compared to bare TiO_2 (Sharma et al., 2018).

The photocatalytic activity of TiO_2 and TiO_2/CDs nanocomposites was evaluated by monitoring the photodegradation of levofloxacin. Under visible-light irradiation, interaction with the photocatalyst induces a gradual degradation of levofloxacin. Within 90 min of sunlight irradiation, nearly all of the initial compound (around 99%) had suffered photodegradation, whereas only 28% was degraded in the dark (Sharma et al., 2018). In order to optimize the process, the team carried out several catalyst dose-dependent, pH-dependent, and initial drug

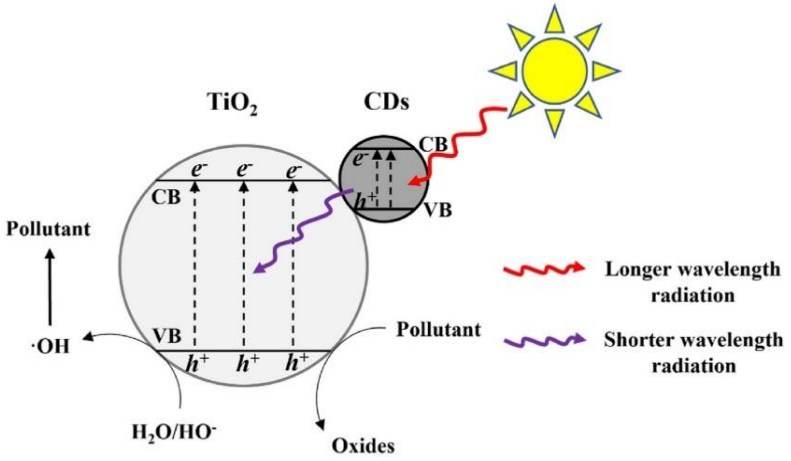


Fig. 3. Representation of a mechanism in which upconversion PL by CDs contribute towards a better photocatalytic efficiency under visible-light by TiO_2.

concentration-dependent experiments, finding that under optimal conditions (catalyst loading of 0.25 g L^{-1}, pH 6 and initial levofloxacin loading of 5 mg L^{-1}), the nanocomposites could achieve nearly complete degradation of the pharmaceutical within 90 min of sunlight irradiation, whereas bare TiO_2 could only manage a removal rate of 66.5%. Furthermore, when compared to the commercial benchmarks TiO_2PC-50 and TiO_2PC-500, the efficiency of the prepared nanocomposite was considerably higher (99% *versus* 36% and 50%, respectively) (Sharma et al., 2018). The stability of the prepared TiO_2/CDs nanocomposite was studied by performing recyclability experiments up to five cycles. A removal rate of 78% was obtained after the last cycle, indicating considerable recoverability, stability and reusability (Sharma et al., 2018). Finally, a possible degradation pathway and some intermediates were proposed by the team. Based on the identification of molecular ion peaks $[M+H]^+$, the team found that the degradation of the parent levofloxacin molecule yielded eight different by-products. However, no indication of their toxicity relatively to levofloxacin was provided (Sharma et al., 2018).

In a more recent work by the same group, also regarding the photodegradation of levofloxacin, Sharma et al. reported a highly effective novel Z-scheme Bi_2WO_6/CDs/TiO_2 photocatalyst (Sharma et al., 2020). A Z-scheme heterojunction was chosen by the authors as it presents an improved light-harvesting ability and strong redox capacity. Following a method similar to before, L-ascorbic acid was dissolved, stirred and subjected to hydrothermal treatment (180 °C for 4 h). The resulting precipitates were separated by centrifugation, washed, and dried. A change of colour indicated the successfully preparation of TiO_2/CDs nanocomposites. Bi_2WO_6/CDs/TiO_2 was prepared by dispersing bismuth tungstate and TiO_2/CDs in ethanol. The mixture was kept under stirring overnight and the precipitates were collected, washed, filtered, and dried (Sharma et al., 2020). The optical characteristics of the compounds were studied, demonstrating that Bi_2WO_6/CDs/TiO_2's maximum absorption edge (495 nm) was deeper into the visible range than TiO_2's (419 nm) (Sharma et al., 2020). Accordingly so, Bi_2WO_6/CDs/TiO_2 presented an estimated energy band gap of 2.50 eV compared to 2.95 eV for TiO_2 (Sharma et al., 2020). Finally, the specific surface area and pore volumes of Bi_2WO_6/CDs/TiO_2 also increased when compared to Bi_2WO_6 (48.80 *versus* 18.36 m^2 g^{-1} and 0.102 *versus* 0.0309 cm^3 g^{-1}, respectively), promoting an increased access to the photocatalysts' active sites (Sharma et al., 2020).

To optimize the process, the team carried out several catalyst dose-dependent and pH-dependent experiments, finding that the optimal conditions were a catalyst loading of 0.075 g L^{-1} and pH 7 (Sharma et al., 2020). Similar to their previous work (Sharma et al., 2018), under optimal conditions, near complete degradation of levofloxacin was achieved within 90 min of sunlight irradiation, whereas no degradation was observed without the catalyst and a 28% degradation occurred in the dark (Sharma et al., 2020). Bi_2WO_6/CDs/TiO_2's removal efficiency (99%) is higher than that of TiO_2 (removal rate of 66% in the same conditions), confirming the superiority of the studied nanocomposite (Sharma et al., 2020). The stability of the Z-scheme Bi_2WO_6/CDs/TiO_2 photocatalyst was studied by performing recyclability experiments up to three cycles. The study revealed consecutive photocatalytic degradations efficiencies of 99%, 95% and 92%. The minor loss of photocatalytic activity suggests a considerable stability and reusability (Sharma et al., 2020). Finally, like in their previous work (Sharma et al., 2018), a degradation pathway and respective intermediates were proposed by the team with several degradation species with varying *m/z* values being suggested to derive from levofloxacin's degradation. However, the relative toxicity of these compounds when compared to levofloxacin is not indicated (Sharma et al., 2020).

It is worth noting that in two different studies, Sharma et al. achieved a levofloxacin degradation rate of 99% under 90 min of sunlight irradiation with either TiO_2/CDs (Sharma et al., 2018) or Bi_2WO_6/CDs/TiO_2 nanocomposites (Sharma et al., 2020), both of which using L-ascorbic acid-based CDs. While TiO_2/CDs nanocomposite has an estimated absorption edge around 435 nm, Bi_2WO_6/CDs/TiO_2 nanocomposites' absorption edge is located deeper in the visible region, at 495 nm (Sharma et al., 2018, 2020).

Wongso et al. reported the degradation of acetaminophen by using silica-carbon quantum dots (Si-CQDs) in a TiO_2 base (Wongso et al., 2020). Rice husk was chosen as the Si-CQDs precursor due to adhering to the principles of green chemistry and having silica elements in its composition. Following a previously described method (Wang et al., 2017c), a hydrothermal method (700 °C for 2 h under N_2 atmosphere) was employed to obtain rice husk ash. This was followed by the addition of deionized water and sulphuric acid and immersion in nitric acid, after which purification of the resulting ash was done by vacuum-assisted filtration and the precipitate was dispersed and heated in an oven at 200 °C for 10 h. Purification of the resulting Si-CQDs was done by using membrane filtering and dialysis. Si-CQDs/TiO_2 nanocomposites were prepared by mixing T100 TiO_2 (hydrothermally treated at 100 °C) with different amounts of Si-CQDs solution (1, 2 and 3 wt%). The mixture was then stirred and dried in an oven until Si-CQDs/TiO_2 nanocomposites in powder form were collected (Wongso et al., 2020). The authors justified the use of CDs to enhance the photocatalytic activity of TiO_2 by mentioning that CDs extended some semiconductors' light absorption into the visible range and delayed photogenerated charge recombination rates (Wongso et al., 2020).

Characterization of the nanocomposites demonstrated that the Si-CQDs were successfully decorating TiO_2's surface (Wongso et al., 2020). Among the different loadings of Si-CQDs, the 1% Si-CQDs/TiO_2 composite was the best performer in terms of acetaminophen degradation. The addition of Si-CQDs extends TiO_2's light absorption into the visible range and promotes charge separation, with the 1% Si-CQDs/TiO_2 nanocomposite presenting an energy band gap of 3.12 eV, compared to the 3.20 eV of bare T100 TiO_2 (Wongso et al., 2020). Finally, the 1% Si-CQDs/TiO_2 composite presents a surface area of 148 m^2 g^{-1} *versus* 126 m^2 g^{-1} for bare T100 TiO_2. However, larger Si-CQDs loadings may block the active sites (Wongso et al., 2020).

After 120 min of sunlight irradiation, the best performing composite (1 wt% CD loading) achieved a photodegradation rate of 53% (Wongso et al., 2020). Under equal conditions (360 min of irradiation), the 1% Si-CQDs/TiO_2 composite removed 68% of acetaminophen while bare T100 TiO_2 only achieved a 48% removal. T100 TiO_2 removal of acetaminophen was around 30% slower than that of the 1% Si-CQDs/TiO_2 composite, indicating the superiority of the latter (Wongso et al., 2020). Furthermore, increasing the concentration of acetominophen above a certain threshold could impair the photodegradation, possibly because the larger amount of acetaminophen input was not accompanied by a larger amount of hydroxyl radicals being produced, as the nanocomposites' concentration was maintained (Shaban and Fallata, 2019; Wongso et al., 2020). The nanocomposites' stability was assessed by recycling the photocatalyst. After three cycles the 1% Si-CQDs/TiO_2 nanocomposite displayed only a 2% loss photocatalytic efficiency, confirming its stability and reusability (Wongso et al., 2020).

In another work, Chen et al. synthesized an environmentally friendly sunlight-driven TiO_2/CDs photocatalyst for the degradation of gemfibrozil (Chen et al., 2017). They chose CDs because of their upconversion PL and the fact that they were used to enhance the photocatalytic degradation of other organic pollutants such as methylene blue (MB) and rhodamine B (RhB) (Chen et al., 2017). The authors followed a previously described hydrothermal method (Qu et al., 2012) to prepare CDs from citric acid and urea, two commonly used CDs precursors (Chen et al., 2017). The precursors were subjected to hydrothermal treatment (180 °C for 5 h). The resulting solution was centrifuged and dried to obtain dry CDs powder. TiO_2/CDs nanocomposites were prepared by a facile hydrothermal-calcination method. TiO_2 and CDs were mixed and put into a furnace at 300 °C for 3 h. The resulting products were washed and dried under vacuum, resulting in powder TiO_2/CDs composite (Chen et al., 2017). Chen et al. managed to obtain CDs with upconversion PL capable of converting visible/NIR radiation into

shorter-wavelength radiation (350–650 nm) directly useable by TiO_2, promoting the photocatalytic activity under sunlight irradiation (Chen et al., 2017). The introduction of CDs shifted TiO_2's absorption peak from 395 nm to 445 nm, extending the absorption edge into the visible region. The reaction kinetics followed a pseudo-first order reaction model. TiO_2/CDs nanocomposites presented degradation rate constants as high as 0.101 min^{-1}, whereas bare TiO_2 presented a degradation rate constant of only 0.0436 min^{-1}, meaning that the best performing composite mediated a photocatalytic degradation 2.3 times faster than that of bare TiO_2. The superior performance of the nanocomposites clearly indicate the positive enhancement of the photocatalytic efficiency obtained by adding CDs (Chen et al., 2017).

The photocatalytic efficiency concerning the degradation of gemfibrozil was evaluated under different irradiation conditions for 8 min: full spectrum light, sunlight, and visible light irradiation (Chen et al., 2017). The nanocomposites displayed an improved photocatalytic activity under all the three kinds of irradiation when compared to TiO_2. With full wavelength irradiation the composite achieved a removal rate of 89% *versus* 61.8% for the prepared TiO_2. For sunlight irradiation, the removal rates were 58% *versus* 28%. Finally, under visible-light radiation, a 40% removal rate was achieved with the nanocomposite, whereas bare TiO_2 did not photodegrade any gemfibrozil whatsoever under these conditions. The nanocomposite outperforms TiO_2 even under full wavelength light irradiation, which induced the best response out of bare TiO_2 (Chen et al., 2017). Finally, the nanocomposites do not present any obvious loss of performance after five degradation cycles, and so it can be concluded that they are both stable and reusable (Chen et al., 2017).

Regarding the degradation pathway of gemfibrozil, Chen et al. found 13 peaks corresponding to degradation by-products, as detected by HPLC/MS/MS (Chen et al., 2017). By surveying the toxicity of the photocatalytic degradation procedure in two test aquatic systems, the team found that the toxicity first peaks in the start of the degradation, after which it proceeds to decrease with the increasing mineralization rate (Chen et al., 2017). Furthermore, by using the ECOSAR software, only one of gemfibrozil degradation by-products has an occasionally equal or slightly higher predicted toxicity than the initial compound (Chen et al., 2017). Finally, by comparing gemfibrozil's photocatalytic degradation by the TiO_2/CDs nanocomposites to other degradation techniques (such as chlorination and microbial degradation), the team found that while a considerable number of the degradation products resulting from these techniques present more toxicity toward aquatic organisms than gemfibrozil itself, most by-products from photocatalytic degradation present toxic levels one or two orders of magnitude lower than those of gemfibrozil (Chen et al., 2017).

In another work by the same team, Zeng et al. described the photocatalytic ozonation degradation of ciprofloxacin by a TiO_2/CDs photocatalyst prepared by the hydrothermal-calcination method coupled to an ozonation process (Zeng et al., 2019). Ozone-based degradation of organic pollutants has been extensively applied as an alternative way of water treatment capable of decomposing multiple persistent organic pollutants, either by direct ozonation or indirect generation of highly reactive hydroxyl radicals (Lee et al., 2017). However, the process requires either high-energy UV radiation or large amounts of oxidative chemicals, thus increasing its cost and limiting its application. In order to improve the oxidizing ability of ozone and expand the absorption edge, the authors have combined the method with TiO_2/CDs nanocomposites (Zeng et al., 2019). CDs were prepared following a hydrothermal methodology based on urea and citric acid (Chen et al., 2017). The precursors were dissolved and stirred before being subjected to hydrothermal treatment at 180 °C for 5 h. The product was centrifuged and dried (Zeng et al., 2019). TiO_2/CDs nanocomposites were prepared by a facile hydrothermal-calcination method. TiO_2 was mixed with CDs, and the solution was heated in a furnace (300 °C for 3 h, heating rate of 5 °C min^{-1}), resulting in the TiO_2/CDs photocatalyst (Zeng et al., 2019). Regarding the use of CDs, the authors refer the already mentioned properties that enable CDs to increase TiO_2's photocatalytic efficiencies, which they had observed first hand (Zeng et al., 2019; Chen et al., 2017).

To explain the hybrid system they created, Zeng et al. proposed a probable mechanism for the photocatalytic ozonation of ciprofloxacin (Fig. 4) which differed slightly from the mechanism generally proposed for TiO_2/CDs nanocomposites (Zeng et al., 2019). Under solar light irradiation, radiation with a wavelength over 550 nm would be converted into higher-energy lower-wavelength light (325–425 nm) due to the upconversion PL of the CDs. The higher-energy radiation is absorbed by TiO_2, resulting in the generation of electron-hole pairs and the transfer of photoexcited electrons from TiO_2 into the CDs, where they would be retained and interact with both ozone and oxygen. This prompts both the direct production of hydroxyl radicals from H_2O/HO^- and the generation of $O_3{\cdot}^-$ and $O_2{\cdot}^-$, which in turn react with other reactive species to generate hydroxyl radicals. The production and presence of reactive species leads to the decomposition of ciprofloxacin (Zeng et al., 2019). The photocatalytic ozonation degradation of ciprofloxacin fitted a pseudo-first-order kinetic model, revealing an optimal degradation rate of 0.32 min^{-1} for the 6 wt% composite when the photodegradation is conjugated with ozonation. This degradation rate is considerably higher than the rates obtained for both ozonation alone and the photodegradation without ozonation ($k = 0.083\ min^{-1}$ and $k = 0.129\ min^{-1}$, respectively) (Zeng et al., 2019)

The process efficiency was evaluated by monitoring the degradation of ciprofloxacin under sunlight irradiation. The photocatalytic efficiency using only bare TiO_2 or the TiO_2/CDs photocatalyst (1.0 wt% of CDs) was 64.0% and 91.1%, respectively, for an irradiation time of 30 min (Zeng et al., 2019). The introduction of ozonation to the process, which by itself is capable of partially decomposing ciprofloxacin, led to an increase of the degradation efficiency to 99.7% within 16 min of irradiation with the 6 wt% composite (Zeng et al., 2019). The pH value was also an important parameter, as hydroxide ions could start a chain reaction of ozone decomposition and result in higher amounts of hydroxyl radicals, with single ozone processes being more efficient at higher pH values (Levanov et al., 2018). Finally, the degradation pathway of ciprofloxacin was studied using HRAM LC-MS/MS and twelve intermediates were identified. While there is no information regarding the relative toxicity of the intermediates, the authors state that both ciprofloxacin and its intermediates are fully decomposed to inorganic matter if allowed enough time (Zeng et al., 2019).

In 2020 Koe et al. fabricated a novel photocatalytic membrane for the photodegradation of diclofenac by incorporating TiO_2/CDs nanocomposites (with N,S-doped CDs) on a polysulfone (PSF) membrane (Koe et al., 2020). Egg yolk was used as a natural precursor for the hydrothermal synthesis of CDs due to its intrinsic high number of heteroatoms suitable for doping (Koe et al., 2020). Before the synthesis, the egg was boiled and the yolk separated, dried and mashed. Afterwards, it was placed in a tube furnace with temperatures up to 300 °C under N_2 atmosphere for 3 h (heating rate of 5 °C per minute). The resulting black N-doped CDs powder was allowed to cool and mixed with H_2SO_4 and HNO_3 at a temperature of 120 °C for 6 h, resulting in a yellowish-brown solution. Later, different loadings of non-purified CDs (1, 1.5 and 2 g) were mixed with TiO_2. The resulting solution was heated at 120 °C for 12 h to form the TiO_2/CDs nanocomposite. Incorporation of the nanocomposites in the PSF membrane was achieved via an *in situ* phase inversion method (Koe et al., 2020). The evenly dispersed incorporation in a membrane makes it easier to recover the photocatalyst after using it, avoiding its release into the environment and the environmental damages resulting thereof (Geng et al., 2017; Yu et al., 2018). The authors justified the use of N,S-doped CDs by mentioning its upconversion PL, the enhanced photogenerated charges separation, the improved electron concentration due to doping, and the increased adsorption surface due to the functional groups on the CDs' surface (Koe et al., 2020).

Characterization of the prepared nanocomposites revealed that the addition of CDs shifts the nanocomposites' absorption edge towards the visible region (Koe et al., 2020). A 1.5 g loading of CDs shifts the

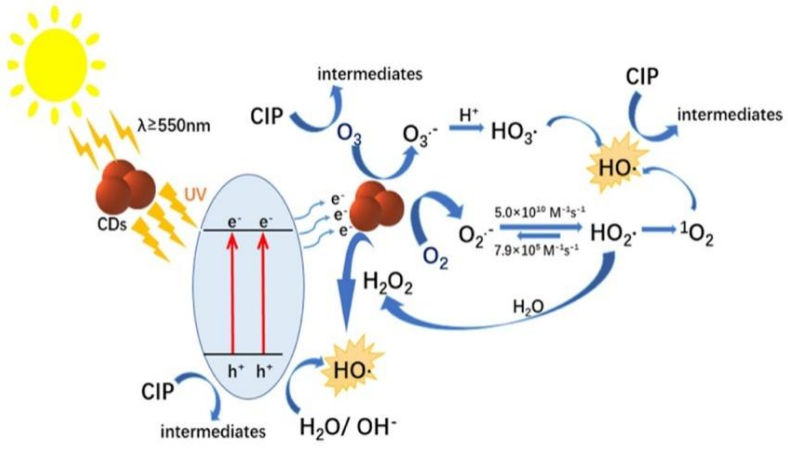


Fig. 4. Proposed degradation mechanism of ciprofloxacin by TiO_2/CDs and ozone under simulated sunlight irradiation by the authors. CIP – ciprofloxacin. Reproduced here with authorization from Zeng et al. (2019).

absorption peak from 369 nm to 412 nm. The 1.5 g loading also resulted in a narrower energy band gap, presenting a value of 3.012 eV *versus* 3.363 eV for bare TiO_2. This suggests a superior photocatalytic efficiency under visible-light when using a 1.5 g CD loading when compared to bare TiO_2, and that the presence of N,S-doped CDs clearly enhance the photocatalytic efficiency (Koe et al., 2020).

When subjected to visible-light irradiation (150 min), the photocatalytic membrane achieved a diclofenac removal efficiency of 62.3% *versus* 3.33% for TiO_2. Bare TiO_2 was outperformed by the nanocomposite even under UV-radiation, a light more readily useable by the semiconductor than visible light (Koe et al., 2020). It is worth noting that during the first 30 min of the test, under dark conditions, diclofenac was significantly degraded in the presence of the TiO_2/CDs composite, suggesting that the adsorption of diclofenac by the nanocomposites is promoted by the presence of oxygenated functional groups in the N, S-doped CDs' surface (Koe et al., 2020). Adding CDs successfully shifted, and broadened, the absorption profile of the nanocomposites into the visible region, increasing the photocatalytic region (Koe et al., 2020). However, excessive loadings of CDs lowered the photocatalytic efficiency as they supressed substance migration, buried the active sites on TiO_2's surface and filtered the light intended to reach the active sites (Koe et al., 2020). The photocatalytic nanocomposite membranes displayed improved hydrophilicity, porosity and permeating flux when compared to bare TiO_2 membranes, mostly due to the presence of hydrophilic oxygen functional groups on the CDs. The developed TiO_2/CDs membrane displayed great potential for water purification as it allowed an easy recovering of the photocatalyst after the purification (Koe et al., 2020).

In another work targeting the photodegradation of diclofenac, Wang et al. reported the development of a TiO_2/CDs nanosheet with improved broad-spectrum photocatalytic activity under UV/Visible/NIR irradiation (Wang et al., 2019). Considering that photocatalytic reactions occur mainly at the surfaces of catalysts, the morphological modelling of TiO_2 crystal facets may be used as a method to improve its photocatalytic efficiency (Wang et al., 2016). Previous reports demonstrated that TiO_2 exposing higher surface energy {001} facets (0.90 J m^{-2}) presented a higher photocatalytic efficiency than lower energy {101} facets (0.44 J m^{-2}) (Roy et al., 2013). However, despite the relatively higher efficiency of the {001} facets, the performance is still hampered by the poor utilization of radiation in the visible/NIR regions by the photocatalyst. The use of CDs to address these limitations has been already described (Yu et al., 2014b, 2016), serving as a base for the authors' work. For instance, Zhang et al. described how CDs could improve the broad-spectrum solar light response and hinder the recombination of charge carriers of WO_3 through the fabrication of direct Z-scheme heterostructures (Zhang et al., 2017b). Based on that, Wang and his team developed a nanosheet photocatalyst from N-doped CDs and {001} TiO_2 nanosheets (TNS-001), the TNS-001/CDs composite, for the degradation of diclofenac under a broad-light spectrum (Wang et al., 2019).

N-doped CDs from citric acid and ethylenediamine were fabricated via a hydrothermal method (Wang et al., 2019). The precursors were dispersed and subjected to temperatures of 200 °C for 5 h. To remove larger particles and deposits the CDs were centrifuged, after which they were dried at 80 °C. To prepare the nanocomposite, CDs were mixed with hydrothermally prepared TiO_2 nanosheets. The TNS-001/CDs nanocomposites were synthesized via a simple low temperature process (Wang et al., 2019). TNS-001 was mixed with CDs and the mixture stirred at 60 °C for 24 h while the solvent slowly vaporized, originating a composite powder which was then dried (Wang et al., 2019).

Characterization of the prepared TNS-001/CDs nanocomposites demonstrated the N-doped CDs to be evenly dispersed on the nanosheets' surface (Wang et al., 2019). The addition of CDs slightly decreased the specific surface area of TNS-001/CDs (81.04 $m^2\ g^{-1}$ to 71.20 $m^2\ g^{-1}$), possibly due to CDs occupying a part of the spots in the nanosheet (Wang et al., 2019). After coupling with CDs, the absorption edge of the nanosheet shifted from 400 nm to 458 nm. A wide absorption across both the UV and visible range was observed, confirming that CDs increased the absorption intensity of the TiO_2 nanosheets (Wang et al., 2019). In addition, CDs were able to upconvert longer-wavelength radiation (450–850 nm) into shorter-wavelength radiation (365–650 nm), thus increasing the amount of radiation directly useable by TNS-001. Accordingly, TNS-001/CDs nanocomposites presented an estimated energy band gap of 2.7 eV *versus* 3.1 eV for TNS-001 (Tian et al., 2017). Finally, the CDs were also shown to delay the recombination of photogenerated charge carriers, extending their lifetime by promoting electron transfer. Time-resolved fluorescence decay spectra proved that the addition of CDs increased the lifetime of TNS-001/CDs' photogenerated charge carriers (1.6080 ns *versus* 1.3275 ns) (Wang et al., 2019).

The photocatalytic efficiency under visible-light irradiation was evaluated. After 60 min of irradiation, the TNS-001/CDs composite was significantly more efficient than TNS-001 (91.5% *versus* 15.4%, respectively) (Wang et al., 2019). When compared to another similarly prepared nanocomposites, with {101} facets, or having Degussa P25 TiO_2 instead of nanosheets, TNS-001/CDs presented an improved photocatalytic activity, indicating the high oxidation activity of the exposed {001} facets (Wang et al., 2019). Under broad-spectrum irradiation TNS-001 nanosheets displayed poor photocatalytic performance under UV/Visible/NIR radiation, whereas TNS-001/CDs nanocomposites

exhibited considerable activity in each case and also under simulated sunlight irradiation, confirming its potential as a broad-spectrum photocatalyst (Wang et al., 2019). The stability of the TNS-001/CDs nanocomposites was assessed. After four cycles, nearly 80% of diclofenac could still be removed (*versus* 91% in the first cycle). While there was a slight loss of performance, no significant changes were observed between fresh and recycled TNS-001/CDs nanocomposites, indicating a high degree of stability and reusability (Wang et al., 2019). Finally, the intermediates of the photocatalytic process were identified *via* UPLC-Q-TOF MS and GC-MS. In total, eight intermediates were identified, and although their relative toxicities are not indicated, all of them were fully mineralized into H_2O and CO_2 upon prolonged irradiation (Wang et al., 2019).

The works of Koe et al. (2020) and Wang et al. (2019) both target the photocatalytic degradation of diclofenac by TiO_2/CDs nanocomposites, albeit through different methods. At first sight, under visible-light irradiation, the use of TNS-001/CDs nanosheets proposed by Wang et al. team seems to be superior to the photocatalytic membrane developed by Koe and co-workers. In only two fifths of the time, the TNS-001/CDs nanosheets achieved a 91.5% degradation rate of diclofenac, whereas the photocatalytic membrane only managed to remove 62.3% (Wang et al., 2019; Koe et al., 2020). A possible explanation for this is found in the energy band gaps estimated for the composites. While TNS-001/CDs nanosheets presented a band gap of 2.7 eV, the TiO_2/CDs photocatalytic membrane displayed a band gap of 3.01 eV. This indicates a poorer utilization of visible-light irradiation by the latter, which possibly explains its lackluster performance under visible-light irradiation when compared to the nanosheets reported by Wang et al. (Wang et al., 2019; Koe et al., 2020) Despite that, the photocatalytic membrane allowed an easy recovery of the photocatalyst after the pollutants' photodegradation, which consists of a major advantage worthy of consideration (Koe et al., 2020). Finally, neither CDs used in the studies were thoroughly purified, and so some impurities might have affected the photocatalytic efficiency of the resulting TiO_2/CDs nanocomposites (Wang et al., 2019; Koe et al., 2020).

In 2021, Liu et al. reported the photocatalytic degradation of tetracycline using a combination of oxygen-rich TiO_2 nanosheets and CDs (Liu et al., 2021). TiO_2/CDs nanocomposites were synthesized from TiO_2 nanosheets and citric acid via a one-step hydrothermal method (160 °C for 4 h). The resulting nanocomposites were centrifuged and dried (Liu et al., 2021). The authors chose CDs because of their enhanced PL properties, low-cost, and the fact that CDs on TiO_2 nanosheets were already used to improve the photodegradation of Cr (IV) under sunlight irradiation (Li et al., 2018; Liu et al., 2021). The characterization of the nanocomposites revealed that CDs extended the TiO_2 nanosheets' absorption edge from 400 nm to 420 nm, improving absorption the visible range. Furthermore, by observing the PL spectra, the authors found that the composite promoted the separation of charge carriers, restraining electron-hole recombination. (Liu et al., 2021).

The authors tested the photocatalytic degradation of tetracycline under visible-light irradiation (120 min) using oxygen-rich TiO_2/CDs nanocomposites, oxygen-rich TiO_2 nanosheets and normal TiO_2 nanosheets (Liu et al., 2021). The addition of CDs enhances the photodegradation of tetracycline. Under the same conditions, TiO_2/CDs nanocomposites display a superior photocatalytic efficiency, achieving a degradation rate of 94.1% (*versus* 60.6% and 54.2% for oxygen-rich and normal TiO_2 nanosheets, respectively). These results were further corroborated by the reaction rates, 0.0335 min^{-1} for the nanocomposite *versus* 0.0101 min^{-1} for the TiO_2 nanosheet. The authors attributed the improved efficiency of the nanocomposites to the widening of the absorption edge, to better charge separation and a delayed charge recombination (Liu et al., 2021). The stability and reusability of the nanocomposites were evaluated by submitting the composite to four photocatalytic cycles. After the last cycle, the composite still achieved a tetracycline degradation rate of 90% (Liu et al., 2021). The photodegradation intermediates were studied using HPLC-MS/MS, through which eight intermediate compounds were identified. Continued irradiation causes some of them to be fully mineralized into H_2O and CO_2 (Liu et al., 2021). Antibacterial activity assays revealed that, upon photodegradation, the medium's toxicity first increases when compared to tetracycline alone, but then decreases to a point comparable to that of still water. This result suggests that while some degradation intermediates might be more toxic than the original compound, gradual mineralization of the by-products eventually leads to the toxicity of the final products being insignificant (Liu et al., 2021).

In another 2021 paper regarding the photodegradation of tetracycline, Wang et al. described the preparation of a photocatalytic TiO_2/CDs composite (Wang et al., 2021). CDs were produced from olive leaves, which were placed in a tube furnace and subjected to temperatures of up to 900 °C under argon atmosphere (Wang et al., 2021). The resulting powder was poured into a mixture of HNO_3 and H_2SO_4. The solution was heated for 5 h and subsequently cooled to room temperature. After neutralization with sodium hydroxide, purification was performed through dialysis. Different loadings of CDs (1–7 wt%) were loaded onto the surface of solvothermal-prepared TiO_2 via a hydrothermal treatment. TiO_2 was dispersed and mixed with CDs before being subjected to 140 °C for 4 h. The product was then dried, resulting in TiO_2/CDs nanocomposites (Wang et al., 2021). CDs were chosen based on previous reports stating that semiconductors, when mixed with CDs, presented an improved photocatalytic performance (Shi et al., 2017; Choi et al., 2018).

Upon characterization, the CDs exhibited considerable upconversion PL (Wang et al., 2021). In the best performing nanocomposite (5 wt% loading of CDs), the absorption edge of TiO_2 shifted from 387 nm to 448 nm, with higher loadings of CDs further widening the light-response range of the nanocomposites (Wang et al., 2021). The band gap energy was estimated to be 2.09 eV for the 5 wt% TiO_2/CDs composite, whereas bare TiO_2 has an estimated band gap of 3.15 eV, suggesting a better performance under visible-light by the nanocomposite (Wang et al., 2021). The photodegradation of tetracycline could be fitted into a first-order kinetic model. The degradation rate constant for the 5 wt% TiO_2/CDs composite was 0.1633 min^{-1}, which is around 1.8 times the rate constant obtained for TiO_2 (Wang et al., 2021).

Under visible-light irradiation (10 min), the nanocomposite displayed a tetracycline degradation efficiency of 81% *versus* 65% for bare TiO_2, confirming the superior performance of the nanocomposites (Wang et al., 2021). A 7 wt% loading of CDs, despite presenting a narrower band gap and higher degradation in the dark, underperformed a 5 wt% loading when irradiated. An excessive CD loading could cause large amounts of tetracycline to be adsorbed to the surface of the nanocomposites, resulting in a decreased contact with O_2 and H_2O/HO^-, which is an essential step for the generation of the reactive species responsible for the decomposition of the pharmaceutical (Wang et al., 2021). Finally, cyclic stability tests revealed that the nanocomposite is effective at least up to five cycles, at which point the degradation rate starts decaying, suggesting that the nanocomposites are both stable and reusable (Wang et al., 2021).

When we compare the two studies regarding for the photodegradation of tetracycline, both present a very efficient method that works under visible-light irradiation, something which is not achievable with TiO_2 by itself (Liu et al., 2021; Wang et al., 2021). Whereas under the tested conditions Liu et al. (2021) reported a very high removal rate, 94.1% within 120 min of irradiation, Wang et al. (2021) described a much faster degradation, achieving a 81% removal rate within 10 min of irradiation. This is corroborated by their reported degradation rate constants of 0.0335 min^{-1} and 0.1633 min^{-1}, respectively (Liu et al., 2021; Wang et al., 2021). The much faster photodegradation might originate from the lower energy band gap of the nanocomposite prepared by Wang et al. (2.09 eV *versus* an estimated 2.95 eV for Liu et al.'s nanocomposite), which indicates a better utilization of the visible-light used to irradiate the compounds (Liu et al., 2021; Wang et al., 2021).

In 2020, Thakur et al. decorated TiO_2 nanofibers with plasmonic

nanostructures (CDs_{Au} and CDs_{Ag}), targeting the photocatalytic degradation of erythromycin (Thakur et al., 2020). CDs were prepared via a one-step synthesis using a green carbon precursor, the waste pulp of citrus limon (Thakur et al., 2018). To synthesize CDs, citrus lemon pulp was subjected to a pyrolysis (190 °C for 20 min). CDs_{Au} were fabricated by continuously stirring $HAuCl_4$ with the prepared CDs under visible-light irradiation. A colour change from pale yellow to pinkish red indicated the formation of CDs_{Au}. Similarly, CDs_{Ag} were prepared my mixing silver nitrate with CDs in the presence of ammonia. TiO_2/CDs_{Au} and TiO_2/CDs_{Ag} nanocomposites were prepared by loading either CDs_{Au} or CDs_{Ag} atop electro-spun TiO_2 nanofibers (Thakur et al., 2020). Beside the common reasons justifying the use of CDs to enhance TiO_2's efficiency, the authors also explained the rationale behind the use of gold and silver (Thakur et al., 2020). Metals possess active sites for catalytic oxidation reactions and surface plasmon resonance absorption that results in a good photocatalytic efficiency. Recently, metal-based photocatalysts were employed in the removal of pharmaceuticals. An improved photocatalytic activity resulted from a boosted surface plasmon resonance (Elhalil et al., 2017; Deng et al., 2018; Akbarzadeh et al., 2019).

Characterization of the TiO_2/CDs_{Au} and TiO_2/CDs_{Ag} nanocomposites disclosed estimated band gap energies of 2.6 eV and 2.4 eV, respectively. Those are considerably lower than the 3.2 eV of TiO_2 and in accord with the surface plasmon resonance peaks associated to both Au and Ag nanoparticles (Thakur et al., 2020). The nanocomposites presented a broader light-absorption range due to the CDs visible-light absorption and to a well-defined surface plasmon resonance effect. The photodegradation rate of either composite proved to be higher than any of the controls. TiO_2/CDs_{Au} appear to have a higher degradation efficiency than TiO_2/CDs_{Ag}, with half-time measurements for erythromycin of 60 and 108 min, respectively (Thakur et al., 2020). Decorating the CDs with Au/Ag nanoparticles improved electron transfer and caused electron traps under the form of oxygen vacancies on the surface of TiO_2 nanofibers. Between the nanocomposites, TiO_2/CDs_{Au} presented a longer photogenerated carrier lifetime (1.0216 ns) than TiO_2/CDs_{Ag}, indicating a better photogenerated charge separation capacity (Thakur et al., 2020). In summary, Thakur et al. prepared nanocomposites that could be used for the effective photodegradation of erythromycin. The retained surface plasmon effect brought by Au and the characteristics obtained upon the CDs addition are the main reasons behind the improved photocatalytic efficiency of TiO_2/CDs_{Au} nanocomposites over both TiO_2 nanofibers and TiO_2/CDs_{Ag} nanocomposites (Thakur et al., 2020).

The data regarding the performance of all bare TiO_2 and TiO_2 – CDs nanocomposites here described, can be found summarized in Table 1. It can be concluded for all causes that the introduction of CDs enhances the photocatalytic performance, both in terms of decreasing the band gap while increasing the photodegradation efficiency. The decrease in the band gap can be attributed to electron exchange between the CB of TiO_2 and VB of CDs, which promotes the extension of the photocatalytic reaction into the visible region and a more efficient separation of photogenerated charge carriers. Also, upconversion PL (attributed to several CDs here studied) could improve the light-harvesting efficiency of the nanocomposites, by converting visible light into radiation suitable to being absorbed by TiO_2 (without needing to change its band gap *per si*). The functionalized surface presented by CDs could also improve pollutant adsorption by the nanocomposite, thereby increasing the number of pollutant molecules available for the photodegradation reaction.

Table 1
Comparison of the reported energy band gaps and photodegradation efficiency of different pharmaceuticals when using either bare TiO_2 or TiO_2/CDs nanocomposites for their removal. The data for the nanocomposites refers to the best performing nanocomposite in terms of pharmaceutical photodegradation in the respective study. Efficiency refers to the amount of the pharmaceutical removed under the same conditions for TiO_2 and TiO_2/CDs nanocomposites. * - Estimated from the reported absorption edge. ** - Removal rate of the composite itself and not considering the conjugation with ozonation, which has an efficiency of 99.7% when combined. *** - Removal rate of oxygen-rich TiO_2 nanosheets, not normal TiO_2 nanosheets. HT-hydrothermal treatment. NA – specific values not available.

Removed pharmaceutical	CD synthesis and purification conditions	TiO_2 energy band gap	TiO_2 efficiency	TiO_2/CDs energy band gap	TiO_2/CDs efficiency	Ref.
Levofloxacin	L-ascorbic acid HT – 150 °C for 4 h No purification	3.04 eV	66.5%	2.87 eV	99%	Sharma et al. (2018)
Levofloxacin (Bi_2WO_6/CDs/TiO_2)	L-ascorbic acid HT – 180 °C for 4 h CDs were centrifuged	2.95 eV	66%	2.50 eV	99%	Sharma et al. (2020)
Acetaminophen	Rice husk HT – 700 °C for 2 h under N_2 + 200 °C for 10 h CDs were filtered and dialyzed	3.20 eV	48%	3.12 eV	68%	Wongso et al. (2020)
Gemfibrozil	Citric acid + urea HT – 180 °C for 4 h CDs were centrifuged	3.14 eV*	28%	2.79 eV*	58%	Chen et al. (2017)
Ciprofloxacin	Citric acid + urea HT – 180 °C for 5 h CDs were centrifuged	NA	64.0%	NA	91.1%**	Zeng et al. (2019)
Diclofenac (by PSF membrane)	Egg yolk HT – 300 °C for 3 h under N_2 No purification	3.36 eV	3.33%	3.01 eV	62.3%	Koe et al. (2020)
Diclofenac (by TiO_2 nanosheet)	Citric acid + ethylenediamine HT – 200 °C for 5 h CDs were centrifuged	3.1 eV	15.4%	2.7 eV	91.5%	Wang et al. (2019)
Tetracycline	Citric acid HT – 160 °C for 4 h CDs were centrifuged	3.10 eV*	60.6%***	2.95 eV*	94.1%	Liu et al. (2021)
Tetracycline	Olive leaves HT – gradual heating up to 900 °C CDs were dialyzed	3.15 eV	65%	2.09 eV	81%	Wang et al. (2021)
Erythromycin	Citrus limon pulp Pyrolysis – 190 °C for 20 min No purification	3.2 eV	NA	2.6 eV	NA (but improved)	Thakur et al. (2020)

3.3. TiO_2/CDs nanocomposites for the photocatalytic degradation of pollutants from water sources – photocatalytic mechanism of TiO_2/CDs

In general, the mechanism through which the photocatalytic degradation of pollutants by TiO_2/CDs nanocomposites occurs (Fig. 5) remains mostly unchanged from a normal photocatalytic mechanism (Chen et al., 2017; Sharma et al., 2018; Wang et al., 2019, 2021; Yu et al., 2019; Zeng et al., 2019; Zhang et al., 2019b, 2020; Heng et al., 2020; Koe et al., 2020; Wongso et al., 2020; Liu et al., 2021). Upon the nanocomposites' excitation, TiO_2 directly absorbs the UV part of radiation while the CDs absorb visible radiation. The CDs might sometimes convert, through upconversion, longer-wavelength radiation into shorter-wavelength higher-energy radiation more suitable to being absorbed by TiO_2. An electron-hole separation ensues within TiO_2 and CDs. Due to the easy trapping of photogenerated electrons from TiO_2's CB in the CDs VB, the CDs act as an electron reservoir in the system, increasing the surface electron-hole pair density. The charge separation of photoinduced charge carriers is facilitated while charge recombination is delayed. Furthermore, upon irradiation, electrons generated in the CDs' CB react with oxygen on the nanocomposites' surface to generate $O_2^{\cdot-}$ (or $O_3^{\cdot-}$ when coupled to ozonation processes (Zeng et al., 2019)), which may react with adsorbed H_2O and promptly promote the formation of hydroxyl radicals, whereas the hole in the VB of the semiconductor could react directly with H_2O/OH^- and form hydroxyl radicals. The hydroxyl radicals could either combine and form hydrogen peroxide, which in turn leads to an increase in the number of hydroxyl radicals in the system or proceed to decompose the pollutant due to their very oxidative nature. In summary, ROS are generated in the process and are responsible for non-selectively decomposing the pollutant.

4. Limitations and future challenges

Until this point, this review was focused on describing studies that reported enhancements of the photocatalytic performance of TiO_2 when coupled with CDs. We specified the changes in properties/features of the nanocomposites upon the introduction of CDs, while making comparisons between bare TiO_2 and TiO_2 – CDs nanocomposites. While the benefits of adding CDs are notorious (Table 1), there is still quite a number of limitations and unanswered questions in those studies that currently limit a more large-scale application of these nanocomposites in visible-light-driven photodegradation of pharmaceuticals.

For starters, some of the reported studies did not perform any purification whatsoever for CDs (Sharma et al., 2017; Koe et al., 2020; Thakur et al., 2020), while most only performed centrifugation (Chen et al., 2017; Wang et al., 2019; Zeng et al., 2019; Sharma et al., 2020; Liu et al., 2021). This can be quite problematic as it is known that bottom-up synthetic routes (such as the hydrothermal one) typically generate molecular fluorescent impurities (generally in higher quantity) besides CDs, which can only be removed from solution by either dialysis or chromatographic purification (Essner et al., 2018; Sendao et al., 2019). Furthermore, it is known that when not removed, these impurities can mask or even modify the properties of the CDs (Essner et al., 2018; Sendao et al., 2019). Thus, this means that we cannot know for certain if the observed photocatalytic enhancement of TiO_2 in the developed nanocomposites, is indeed caused by the CDs, a possible generation of impurities or a combination thereof. Further elucidation of this issue is essential for the future rational and target-oriented synthesis of novel photocatalytic nanocomposites.

Following in the same vein, even if we consider that no molecular impurities play a role in the properties of the developed nanocomposites, we are still at a loss at what properties should a CD have to enhance the photocatalytic performance of TiO_2. Namely, while different CDs were produced and all the reported cases enhanced the photocatalytic performance, this was achieved with difference degrees. Furthermore, the reviewed papers did not characterize in sufficient detail the photochemical/photophysical properties of the obtained CDs, something which is highlighted by the information presented in Table 2. More specifically, out of the reviewed publications, never was the fluorescence quantum yield of the CDs mentioned. Also, only one study reported the absorption profile of the CDs, (Liu et al., 2021), and a mere four publications refer the excitation and emission wavelengths for the CDs PL by themselves (Chen et al., 2017; Sharma et al., 2018; Wang et al., 2019, 2021). Thus, there is not enough information to understand why these CDs enhanced the properties of TiO_2, and why different CDs led to different band gaps and photodegradation efficiencies. It is essential that future works perform a more detailed optical characterization of the obtained CDs and investigate the relationship between those properties and the performance of related nanocomposites. Only with that information is possible to proceed to the rational development and improvement of photocatalytic nanocomposites.

In fact, improvement of the photocatalytic performance of the nanocomposites is still needed. While the visible range of the spectrum is the interval of ~1.8–~3.1 eV, the band gap obtained for the different nanocomposites was just between 2.09 and 3.12 eV (Table 1). Moreover, the value of 2.09 eV is so far somewhat of an outlier, being a more representative interval that of 2.50–3.12 eV (Table 1). Thus, there is still room for improvement in terms of tuning the absorption properties of the nanocomposites, so that they can take further advantage of all the visible light range.

Following the same topic, it is not yet clear how CDs improve TiO_2's

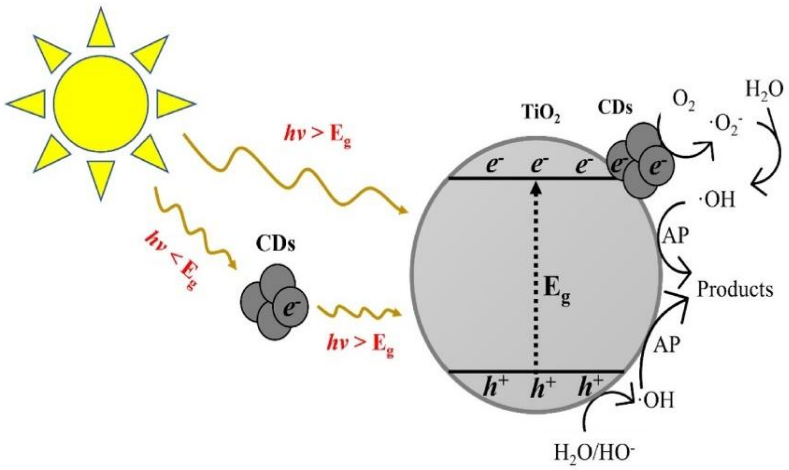


Fig. 5. General mechanism proposed for the photocatalytic degradation of organic pollutants by TiO_2/CDs nanocomposites.

Table 2
List of the reported optical properties of the CDs used in different TiO_2/CDs nanocomposites for the photocatalytic degradation of pharmaceutical pollutants. * - Data obtained from a graphic. NA – data not available.

Ref.	Absorption peak (nm)	Excitation maximum (nm)	Emission maximum (nm)	QY_{FL} %)
Sharma et al. (2018)	NA	500/850	410/500	NA
Sharma et al. (2020)	NA	NA	NA	NA
Wongso et al. (2020)	NA	NA	NA	NA
Chen et al. (2017)	NA	750*	430*	NA
Zeng et al. (2019)	NA	NA	NA	NA
Koe et al. (2020)	NA	NA	NA	NA
Wang et al. (2019)	NA	700	450	NA
Liu et al. (2021)	240*/340*	NA	NA	NA
Wang et al. (2021)	230*/340*	310*/720*	540/370*	NA
Thakur et al. (2020)	NA	NA	NA	NA

photocatalytic activity. Even though most authors consider the improvement to be an effect of the CDs' electron conduction effect, it was not verified as being the only mechanism behind the improved efficiencies. Furthermore, between all the properties conferred to the nanocomposites upon adding CDs (electron conduction effect, upconversion PL, improved light absorption and higher adsorption capacity), it is still unclear the exact way and weight in which each of these influence TiO_2's photocatalytic activity. Further studies focused on the topic should provide a more comprehensive mechanistic study regarding the way that CDs affect the photocatalytic activity in the nanocomposites.

Another limitation can be found on the fact that some pharmaceutical water pollutants consist of macromolecular organic matters which are hard to degrade using photocatalytic techniques. However, this has not yet been studied in detail and is a current limitation of the state of the art. Something else to be taken into consideration is the possibility of the photodegradation products of a given pharmaceutical being more toxic and environmentally damaging than the initial compound itself. However, not every study included a comprehensive evaluation of the intermediates involved in the photocatalytic degradation of the pharmaceutical. Little more than half the studies identified the intermediates and indicated possible pathways to their respective mineralization (Sharma et al., 2018, 2020; Chen et al., 2017; Zeng et al., 2019; Wang et al., 2019; Liu et al., 2021), while only two presented a more comprehensive understanding of the impacts of such by-products (Chen et al., 2017; Liu et al., 2021). Either by simulating using the ECOSAR software (Chen et al., 2017) or by performing antibacterial activity assays (Liu et al., 2021), both teams who did so provided a much needed information to validate the photocatalytic method they were using the clean the aquatic pollutants. If such information is not provided, it is not possible to say without doubt that the photodegradation of a given pharmaceutical ultimately leads to a less toxic environment, even if it is usually so.

It should also be noted that for actual application of these nanocomposites in "real-world" setting, their fabrication needs to be scaled-up to industrial levels. However, the current standard synthesis routes for CDs produce only low synthesis yields (below ~10%) (Tan et al., 2016; Christe et al., 2020; Fernandes et al., 2021). This is explained by those synthetic strategies (such as hydrothermal, the strategy of choice for the studies here reviewed, Table 1) generating large amounts of solid carbon material as a major by-product (Tan et al., 2016; Christe et al., 2020; Fernandes et al., 2021). It should be noted that no study here reviewed reported the synthesis yield of the produced CDs. More recent studies have been aiming to solve this problem by employing non-traditional synthetic strategies, such as including eutectic mixture of salts in the carbonization process or by subjecting the solid carbon material to posterior alkaline-peroxide treatment (Li et al., 2017; Jing et al., 2019). Thus, this type of synthesis should be preferred in the future.

Finally, most the studies here reviewed used as carbon source, for the synthesis of CDs, commercially available chemicals, such as citric acid and L-ascorbic acid. However, recent studies have revealed that one of the major parameters determining the sustainability of the synthesis of CDs is the identity of the carbon source (Christe et al., 2020; Sendão et al., 2020; Fernandes et al., 2021). Therefore, future studies should favour the use of natural waste material as carbon sources instead of commercial chemicals (Algarra et al., 2019; Crista et al., 2020a).

5. Conclusion

The effective removal of pharmaceuticals is a necessary step to ensure that our water supply will still be fit for drinking years from now. If left unchecked, the accumulation of pharmaceuticals in water sources may lead to hazardous effects towards human health. TiO_2 is a photocatalyst that has been employed in the field of water purification and been reported as an efficient tool for the photocatalytic degradation of several pharmaceutical compounds. Nevertheless, it has a narrow photocatalytic region and suffers from rapid charge recombination. Furthermore, its adsorption capacity is limited. Several strategies have been employed to bridge these limitations, chief among which is the incorporation of dopants. However, doping requires mainly expensive toxic metals and tends to accelerate the recombination of charge carriers.

The combination of TiO_2 with CDs may help to overcome these limitations. TiO_2/CDs nanocomposites have been successfully employed in the photocatalytic degradation of several pharmaceuticals. Through the analysis of a series of reports, we described how CDs can be a solution for TiO_2's limitations. The addition of CDs prompted the broadening of the nanocomposites' absorption spectrum and increased the absorption intensity, prevented the recombination of photogenerated charge carriers and improved adsorption of pollutants onto active sites. The result of this was that CDs significantly improved the photocatalytic efficiency of TiO_2 under visible-light irradiation. Further exploration of this combination may lead to the development of clean and wasteless technologies that permit the removal of other highly persistent pharmaceutical pollutants from water sources using only sunlight as the energy source.

Credit roles

Conceptualization: L.P.S.; Investigation: R.M.S.; Writing – Original Draft: R.M.S.; Writing – Review & Editing: L.P.S. and J.E.S.; Visualization: R.M.S.; Supervision: L.P.S. and J.E.S.; Funding Acquisition: L.P.S. and J.E.S.

Declaration of competing interest

The authors declare that they have no known competing financial interests or personal relationships that could have appeared to influence the work reported in this paper.

Acknowledgments

The Portuguese "Fundação para a Ciência e Tecnologia" (FCT, Lisbon) is acknowledged for funding of projects PTDC/QUI-QFI/2870/2020, UIDB/00081/2020 (CIQUP) and UIDB/05748/2020 (GreenUPorto), and the Associated Laboratory IMS (LA/P/0056/2020). Luís

Pinto da Silva acknowledges funding from FCT under the Scientific Employment Stimulus (CEECIND/01425/2017). Ricardo Sendão acknowledges FCT for his Ph.D. grant (2021.06149.BD).

References

Afonso, A.C.P., Correia, A.S., Duarte, D., Brandão, A.T.S.C., de Yuso, M.d.V.M., Jiménez-Jiménez, J., Vale, N., Pereira, C.M., Algarra, M., Pinto da Silva, L., 2021. An active surface preservation strategy for the rational development of carbon dots as pH-responsive fluorescent nanosensors. Chemosensors 9 (8), 191. https://doi.org/10.3390/chemosensors9080191.

Aghamali, A., Khosravi, M., Hamishehkar, H., Modirshahla, N., Behnajady, M.A., 2018. Preparation of novel high performance recoverable and natural sunlight driven nanocomposite photocatalyst of Fe_3O_4/C/TiO_2/N-CQDs. Mater. Sci. Semicond. Process. 87, 142–154. https://doi.org/10.1016/j.mssp.2018.07.018.

Ahmari, H., Heris, S.Z., Khayyat, M.H., 2018. The effect of titanium dioxide nanoparticles and UV irradiation on photocatalytic degradation of Imidaclopride. Environ. Technol. 39, 536–547. https://doi.org/10.1080/09593330.2017.1306115.

Akbarzadeh, R., Asadi, A., Oviroh, P.O., Jen, T.C., 2019. One-pot synthesized visible light-driven BiOCl/AgCl/$BiVO_4$ n-p heterojunction for photocatalytic degradation of pharmaceutical pollutants. Materials 12 (14), 2297. https://doi.org/10.3390/ma12142297.

Algarra, M., Orfão, L.d., Alves, C.S., Moreno-Tost, R., Pino-González, M.S., Jiménez-Jiménez, J., Rodríguez-Castellón, E., Eliche-Quesada, D., Castro, E., Luque, R., 2019. Sustainable production of carbon nanoparticles from olive pit biomass: understanding proton transfer in the excited state on carbon dots. ACS Sustain. Chem. Eng. 7, 10493–10500. https://doi.org/10.1021/acssuschemeng.9b00969.

Awfa, D., Ateia, M., Fujii, M., Johnson, M.S., Yoshimura, C., 2018. Photodegradation of pharmaceuticals and personal care products in water treatment using carbonaceous-TiO_2 composites: a critical review of recent literature. Water Res. 142, 26–45. https://doi.org/10.1016/j.watres.2018.05.036.

Awfa, D., Ateia, M., Fujii, M., Yoshimura, C., 2019. Novel magnetic carbon nanotube-TiO_2 composites for solar light photocatalytic degradation of pharmaceuticals in the presence of natural organic matter. J. Water Proc. Eng. 31, 100836. https://doi.org/10.1016/j.jwpe.2019.100836.

Baker, S.N., Baker, G.A., 2010. Luminescent carbon nanodots: emergent nanolights. Angew. Chem., Int. Ed. Engl. 49, 6726–6744. https://doi.org/10.1002/anie.200906623.

Bauer, S., Pittrof, A., Tsuchiya, H., Schmuki, P., 2011. Size-effects in TiO_2 nanotubes: diameter dependent anatase/rutile stabilization. Electrochem. Commun. 13, 538–541. https://doi.org/10.1016/j.elecom.2011.03.003.

Belkahla, H., Boudjemaa, R., Caorsi, V., Pineau, D., Curcio, A., Lomas, J.S., Decorse, P., Chevillot-Biraud, A., Azaïs, T., Wilhelm, C., Randriamahazaka, H., Hémadi, M., 2019. Carbon dots, a powerful non-toxic support for bioimaging by fluorescence nanoscopy and eradication of bacteria by photothermia. Nanoscale Adv. 1, 2571–2579. https://doi.org/10.1039/c9na00140a.

Berendonk, T.U., Manaia, C.M., Merlin, C., Fatta-Kassinos, D., Cytryn, E., Walsh, F., Burgmann, H., Sorum, H., Norstrom, M., Pons, M.N., Kreuzinger, N., Huovinen, P., Stefani, S., Schwartz, T., Kisand, V., Baquero, F., Martinez, J.L., 2015. Tackling antibiotic resistance: the environmental framework. Nat. Rev. Microbiol. 13, 310–317. https://doi.org/10.1038/nrmicro3439.

Bilek, O., Fohlerova, Z., Hubalek, J., 2019. Enhanced antibacterial and anticancer properties of Se-NPs decorated TiO_2 nanotube film. PLoS One 14, e0214066. https://doi.org/10.1371/journal.pone.0214066.

Bu, Q., Wang, B., Huang, J., Deng, S., Yu, G., 2013. Pharmaceuticals and personal care products in the aquatic environment in China: a review. J. Hazard Mater. 262, 189–211. https://doi.org/10.1016/j.jhazmat.2013.08.040.

Centi, G., Perathoner, S., Torre, T., Verduna, M.G., 2000. Catalytic wet oxidation with H_2O_2 of carboxylic acids on homogeneous and heterogeneous Fenton-type catalysts. Catal. Today 55, 61–69. https://doi.org/10.1016/s0920-5861(99)00226-6.

Chen, J., Shu, J., Anqi, Z., Juyuan, H., Yan, Z., Chen, J., 2016. Synthesis of carbon quantum dots/TiO_2 nanocomposite for photo-degradation of Rhodamine B and cefradine. Diam. Relat. Mater. 70, 137–144. https://doi.org/10.1016/j.diamond.2016.10.023.

Chen, P., Wang, F., Chen, Z.-F., Zhang, Q., Su, Y., Shen, L., Yao, K., Liu, Y., Cai, Z., Lv, W., Liu, G., 2017. Study on the photocatalytic mechanism and detoxicity of gemfibrozil by a sunlight-driven TiO_2/carbon dots photocatalyst: the significant roles of reactive oxygen species. Appl. Catal. B Environ. 204, 250–259. https://doi.org/10.1016/j.apcatb.2016.11.040.

Cheng, R., Kang, M., Shen, Z.P., Shi, L., Zheng, X., 2019. Visible-light-driven photocatalytic inactivation of bacteriophage f2 by Cu-TiO_2 nanofibers in the presence of humic acid. J. Environ. Sci. (China) 77, 383–391. https://doi.org/10.1016/j.jes.2018.09.017.

Chinnaiyan, P., Thampi, S.G., Kumar, M., Balachandran, M., 2018. Photocatalytic degradation of metformin and amoxicillin in synthetic hospital wastewater: effect of classical parameters. Int. J. Environ. Sci. 16, 5463–5474. https://doi.org/10.1007/s13762-018-1935-0.

Choi, D., Ham, S., Jang, D.-J., 2018. Visible-light photocatalytic reduction of Cr(VI) via carbon quantum dots-decorated TiO_2 nanocomposites. J. Environ. Chem. Eng. 6, 1–8. https://doi.org/10.1016/j.jece.2017.11.065.

Christe, S., Esteves da Silva, J.C.G., Pinto da Silva, L., 2020. Evaluation of the environmental impact and efficiency of N-doping strategies in the synthesis of carbon dots. Materials 13 (3), 504. https://doi.org/10.3390/ma13030504.

Crista, D.M.A., El Mragui, A., Algarra, M., Esteves da Silva, J.C.G., Luque, R., Pinto da Silva, L., 2020a. Turning spent coffee grounds into sustainable precursors for the fabrication of carbon dots. Nanomaterials 10 (6), 1209. https://doi.org/10.3390/nano10061209.

Crista, D.M.A., Esteves da Silva, J.C.G., Pinto da Silva, L., 2020b. Evaluation of different bottom-up routes for the fabrication of carbon dots. Nanomaterials 10 (7), 1316. https://doi.org/10.3390/nano10071316.

Daghrir, R., Drogui, P., Robert, D., 2012. Photoelectrocatalytic technologies for environmental applications. J. Photochem. Photobiol. Chem. 238, 41–52. https://doi.org/10.1016/j.jphotochem.2012.04.009.

Deng, F., Zhao, L., Luo, X., Luo, S., Dionysiou, D.D., 2018. Highly efficient visible-light photocatalytic performance of Ag/$AgIn_5S_8$ for degradation of tetracycline hydrochloride and treatment of real pharmaceutical industry wastewater. Chem. Eng. J. 333, 423–433. https://doi.org/10.1016/j.cej.2017.09.022.

Deng, Y., Chen, M., Chen, G., Zou, W., Zhao, Y., Zhang, H., Zhao, Q., 2021. Visible-ultraviolet upconversion carbon quantum dots for enhancement of the photocatalytic activity of titanium dioxide. ACS Omega 6, 4247–4254. https://doi.org/10.1021/acsomega.0c05182.

Dong, H., Zeng, G., Tang, L., Fan, C., Zhang, C., He, X., He, Y., 2015. An overview on limitations of TiO_2-based particles for photocatalytic degradation of organic pollutants and the corresponding countermeasures. Water Res. 79, 128–146. https://doi.org/10.1016/j.watres.2015.04.038.

El Mragui, A., Logvina, Y., Pinto da Silva, L., Zegaoui, O., Esteves da Silva, J.C.G., 2019. Synthesis of Fe- and Co-doped TiO2 with improved photocatalytic activity under visible irradiation toward carbamazepine degradation. Materials 12 (23), 3874. https://doi.org/10.3390/ma12233874.

Elhalil, A., Elmoubarki, R., Sadiq, M.h., Abdennouri, M., Kadmi, Y., Favier, L., Qourzal, S., Barka, N., 2017. Enhanced photocatalytic degradation of caffeine as a model pharmaceutical pollutant by Ag-ZnO-Al_2O_3 nanocomposite. Desalination Water Treat. 94, 254–262. https://doi.org/10.5004/dwt.2017.21587.

Essner, J.B., Kist, J.A., Polo-Parada, L., Baker, G.A., 2018. Artifacts and errors associated with the ubiquitous presence of fluorescent impurities in carbon nanodots. Chem. Mater. 30, 1878–1887. https://doi.org/10.1021/acs.chemmater.7b04446.

Esteves da Silva, J.C.G., Gonçalves, H.M.R., 2011. Analytical and bioanalytical applications of carbon dots. TrAC Trends Anal. Chem. (Reference Ed.) 30, 1327–1336. https://doi.org/10.1016/j.trac.2011.04.009.

Farner Budarz, J., Cooper, E.M., Gardner, C., Hodzic, E., Ferguson, P.L., Gunsch, C.K., Wiesner, M.R., 2019. Chlorpyrifos degradation via photoreactive TiO_2 nanoparticles: assessing the impact of a multi-component degradation scenario. J. Hazard Mater. 372, 61–68. https://doi.org/10.1016/j.jhazmat.2017.12.028.

Fernandes, S., Esteves da Silva, J.C.G., Pinto da Silva, L., 2020. Life cycle assessment of the sustainability of enhancing the photodegradation activity of TiO2 with metal-doping. Materials 13 (7), 1487. https://doi.org/10.3390/ma13071487.

Fernandes, S., Esteves da Silva, J.C.G., Pinto da Silva, L., 2021. Comparative life cycle assessment of high-yield synthesis routes for carbon dots. NanoImpact 23, 100332. https://doi.org/10.1016/j.impact.2021.100332.

Ferreira, A.D., Marchesiello, M., Thivel, P.X., 2013. Removal of copper, zinc and nickel present in natural water containing Ca^{2+} and HCO^3 ions by electrocoagulation. Separ. Purif. Technol. 107, 109–117. https://doi.org/10.1016/j.seppur.2013.01.016.

Gao, B., Yap, P.S., Lim, T.M., Lim, T.-T., 2011. Adsorption-photocatalytic degradation of Acid Red 88 by supported TiO_2: effect of activated carbon support and aqueous anions. Chem. Eng. J. 171, 1098–1107. https://doi.org/10.1016/j.cej.2011.05.006.

Gaya, U.I., Abdullah, A.H., 2008. Heterogeneous photocatalytic degradation of organic contaminants over titanium dioxide: a review of fundamentals, progress and problems. J. Photochem. Photobiol. C Photochem. Rev. 9, 1–12. https://doi.org/10.1016/j.jphotochemrev.2007.12.003.

Geng, Z., Yang, X., Boo, C., Zhu, S., Lu, Y., Fan, W., Huo, M., Elimelech, M., Yang, X., 2017. Self-cleaning anti-fouling hybrid ultrafiltration membranes via side chain grafting of poly(aryl ether sulfone) and titanium dioxide. J. Membr. Sci. 529, 1–10. https://doi.org/10.1016/j.memsci.2017.01.043.

Ghosh, P., Samanta, A.N., Ray, S., 2011. Reduction of COD and removal of Zn^{2+} from rayon industry wastewater by combined electro-Fenton treatment and chemical precipitation. Desalination 266, 213–217. https://doi.org/10.1016/j.desal.2010.08.029.

Guan, X., Chang, J., Xu, Z., Chen, Y., Fan, H., 2016. Remediation of chromium(iii)-contaminated tannery effluents by using gallic acid-conjugated magnetite nanoparticles. RSC Adv. 6, 29054–29063. https://doi.org/10.1039/c6ra02122k.

Han, F., Kambala, V.S.R., Srinivasan, M., Rajarathnam, D., Naidu, R., 2009. Tailored titanium dioxide photocatalysts for the degradation of organic dyes in wastewater treatment: a review. Appl. Catal. Gen. 359, 25–40. https://doi.org/10.1016/j.apcata.2009.02.043.

Hanay, O., Hasar, H., 2011. Effect of anions on removing Cu^{2+}, Mn^{2+} and Zn^{2+} in electrocoagulation process using aluminum electrodes. J. Hazard Mater. 189, 572–576. https://doi.org/10.1016/j.jhazmat.2011.02.073.

He, H., Zheng, X., Liu, S., Zheng, M., Xie, Z., Wang, Y., Yu, M., Shuai, X., 2018. Diketopyrrolopyrrole-based carbon dots for photodynamic therapy. Nanoscale 10, 10991–10998. https://doi.org/10.1039/c8nr02643b.

Heng, Z.W., Chong, W.C., Pang, Y.L., Sim, L.C., 2020. Photocatalytic degradation of methylene blue under visible light using carbon dot/titanium dioxide nanohybrid. IOP Conf. Ser. Mater. Sci. Eng. 991, 012092 https://doi.org/10.1088/1757-899x/991/1/012092.

Hettiarachchi, S.D., Graham, R.M., Mintz, K.J., Zhou, Y., Vanni, S., Peng, Z., Leblanc, R.M., 2019. Triple conjugated carbon dots as a nano-drug delivery model for glioblastoma brain tumors. Nanoscale 11, 6192–6205. https://doi.org/10.1039/c8nr08970a.

Hola, K., Sudolska, M., Kalytchuk, S., Nachtigallova, D., Rogach, A.L., Otyepka, M., Zboril, R., 2017. Graphitic nitrogen triggers red fluorescence in carbon dots. ACS Nano 11, 12402–12410. https://doi.org/10.1021/acsnano.7b06399.

Hu, X., Li, G., Yu, J.C., 2010. Design, fabrication, and modification of nanostructured semiconductor materials for environmental and energy applications. Langmuir 26, 3031–3039. https://doi.org/10.1021/la902142b.

Jing, S., Zhao, Y., Sun, R. C., Zhong, L., Peng, X., 2019. Facile and high-yield synthesis of carbon quantum dots from biomass-derived carbons at mild condition. ACS Sustain. Chem. Eng. 7, 7833–7843. https://doi.org/10.1021/acssuschemeng.9b00027.

Joseph, J., Anappara, A.A., 2017. White-light-emitting carbon dots prepared by the electrochemical exfoliation of graphite. ChemPhysChem 18, 292–298. https://doi.org/10.1002/cphc.201601020.

Kabra, K., Chaudhary, R., Sawhney, R.L., 2004. Treatment of hazardous organic and inorganic compounds through aqueous-phase photocatalysis: a review. Ind. Eng. Chem. Res. 43, 7683–7696. https://doi.org/10.1021/ie0498551.

Kafaei, R., Papari, F., Seyedabadi, M., Sahebi, S., Tahmasebi, R., Ahmadi, M., Sorial, G. A., Asgari, G., Ramavandi, B., 2018. Occurrence, distribution, and potential sources of antibiotics pollution in the water-sediment of the northern coastline of the Persian Gulf, Iran. Sci. Total Environ. 627, 703–712. https://doi.org/10.1016/j.scitotenv.2018.01.305.

Kalytchuk, S., Polakova, K., Wang, Y., Froning, J.P., Cepe, K., Rogach, A.L., Zboril, R., 2017. Carbon dot nanothermometry: intracellular photoluminescence lifetime thermal sensing. ACS Nano 11, 1432–1442. https://doi.org/10.1021/acsnano.6b06670.

Kapinus, E.I., Khalyavka, T.A., Shimanovskaya, V.V., Viktorova, T.I., Strelko, V.V., 2003. Photocatalytic activity of spectro-pure titanium dioxide: effects of crystalline structure, specific surface area and sorption properties. Int. J. Photoenergy 5, 159–166. https://doi.org/10.1155/s1110662x0300028x.

Karvinen, S., Hirva, P., Pakkanen, T.A., 2003. Ab initio quantum chemical studies of cluster models for doped anatase and rutile TiO_2. J. Mol. Struct. Theochem. 626, 271–277. https://doi.org/10.1016/s0166-1280(03)00108-8.

Keen, O.S., McKay, G., Mezyk, S.P., Linden, K.G., Rosario-Ortiz, F.L., 2014. Identifying the factors that influence the reactivity of effluent organic matter with hydroxyl radicals. Water Res. 50, 408–419. https://doi.org/10.1016/j.watres.2013.10.049.

Klevens, R.M., Edwards, J.R., Richards Jr., C.L., Horan, T.C., Gaynes, R.P., Pollock, D.A., Cardo, D.M., 2007. Estimating health care-associated infections and deaths in U.S. hospitals, 2002. Publ. Health Rep. 122, 160–166. https://doi.org/10.1177/003335490712200205.

Koe, W.S., Chong, W.C., Pang, Y.L., Koo, C.H., Ebrahim, M., Mohammad, A.W., 2020. Novel nitrogen and sulphur co-doped carbon quantum dots/titanium oxide photocatalytic membrane for in-situ degradation and removal of pharmaceutical compound. J. Water Proc. Eng. 33 https://doi.org/10.1016/j.jwpe.2019.101068.

Kümmerer, K., 2008. Pharmaceuticals in the Environment. Springer, Berlin, Heidelberg. https://doi.org/10.1007/978-3-540-74664-5_1.

Kyung, H., Lee, J., Choi, W., 2005. Simultaneous and synergistic conversion of dyes and heavy metal ions in aqueous TiO_2 suspensions under visible-light illumination. Environ. Sci. Technol. 39, 2376–2382. https://doi.org/10.1021/es0492788.

Lee, M., Merle, T., Rentsch, D., Canonica, S., von Gunten, U., 2017. Abatement of polychoro-1,3-butadienes in aqueous solution by ozone, UV photolysis, and advanced oxidation processes (O_3/H_2O_2 and UV/H_2O_2). Environ. Sci. Technol. 51, 497–505. https://doi.org/10.1021/acs.est.6b04506.

Lee, S.-Y., Park, S.-J., 2013. TiO_2 photocatalyst for water treatment applications. J. Ind. Eng. Chem. 19, 1761–1769. https://doi.org/10.1016/j.jiec.2013.07.012.

Levanov, A.V., Isaikina, O.Y., Gasanova, R.B., Lunin, V.V., 2018. Solubility of ozone and kinetics of its decomposition in aqueous chloride solutions. Ind. Eng. Chem. Res. 57, 14355–14364. https://doi.org/10.1021/acs.iecr.8b03371.

Li, H., He, X., Kang, Z., Huang, H., Liu, Y., Liu, J., Lian, S., Tsang, C.H., Yang, X., Lee, S. T., 2010. Water-soluble fluorescent carbon quantum dots and photocatalyst design. Angew. Chem., Int. Ed. Engl. 49, 4430–4434. https://doi.org/10.1002/anie.200906154.

Li, J., Tang, K., Yu, J., Wang, H., Tu, M., Wang, X., 2019. Nitrogen and chlorine co-doped carbon dots as probe for sensing and imaging in biological samples. R. Soc. Open Sci. 6, 181557. https://doi.org/10.1098/rsos.181557.

Li, L., Lu, C., Li, S., Liu, S., Wang, L., Cai, W., Xu, W., Yang, X., Liu, Y., Zhang, R., 2017. A high-yield and versatile method for the synthesis of carbon dots for bioimaging applications. J. Mater. Chem. B 5, 1935–1942. https://doi.org/10.1039/c6tb03003c.

Li, Y., Liu, Z.M., Wu, Y.C., Chen, J.T., Zhao, J.Y., Jin, F.M., Na, P., 2018. Carbon dots-TiO_2 nanosheets composites for photoreduction of Cr(VI) under sunlight illumination: favorable role of carbon dots. Appl. Catal. B Environ. 224, 508–517. https://doi.org/10.1016/j.apcatb.2017.10.023.

Lim, S.Y., Shen, W., Gao, Z., 2015. Carbon quantum dots and their applications. Chem. Soc. Rev. 44, 362–381. https://doi.org/10.1039/c4cs00269e.

Linsebigler, A.L., Lu, G., Yates, J.T., 2002. Photocatalysis on TiO_2 surfaces: principles, mechanisms, and selected results. Chem. Rev. 95, 735–758. https://doi.org/10.1021/cr00035a013.

Liu, B., Nakata, K., Sakai, M., Saito, H., Ochiai, T., Murakami, T., Takagi, K., Fujishima, A., 2011. Mesoporous TiO_2 core-shell spheres composed of nanocrystals with exposed high-energy facets: facile synthesis and formation mechanism. Langmuir 27, 8500–8508. https://doi.org/10.1021/la201547g.

Liu, S., Yu, J., Jaroniec, M., 2010. Tunable photocatalytic selectivity of hollow TiO_2 microspheres composed of anatase polyhedra with exposed {001} facets. J. Am. Chem. Soc. 132, 11914–11916. https://doi.org/10.1021/ja105283s.

Liu, X., Yang, Y., Li, H., Yang, Z., Fang, Y., 2021. Visible light degradation of tetracycline using oxygen-rich titanium dioxide nanosheets decorated by carbon quantum dots. Chem. Eng. J. 408, 127259. https://doi.org/10.1016/j.cej.2020.127259.

Loeb, S.K., Alvarez, P.J.J., Brame, J.A., Cates, E.L., Choi, W., Crittenden, J., Dionysiou, D. D., Li, Q., Li-Puma, G., Quan, X., Sedlak, D.L., David Waite, T., Westerhoff, P., Kim, J. H., 2019. The technology horizon for photocatalytic water treatment: sunrise or sunset? Environ. Sci. Technol. 53, 2937–2947. https://doi.org/10.1021/acs.est.8b05041.

Lyu, J., Zhou, Z., Wang, Y., Li, J., Li, Q., Zhang, Y., Ma, X., Guan, J., Wei, X., 2019. Platinum-enhanced amorphous TiO_2-filled mesoporous TiO_2 crystals for the photocatalytic mineralization of tetracycline hydrochloride. J. Hazard Mater. 373, 278–284. https://doi.org/10.1016/j.jhazmat.2019.03.096.

Malato, S., Blanco, J., Vidal, A., Richter, C., 2002. Photocatalysis with solar energy at a pilot-plant scale: an overview. Appl. Catal. B Environ. 37, 1–15. https://doi.org/10.1016/s0926-3373(01)00315-0.

Malato, S., Fernández Ibáñez, P., Maldonado, M.I., Blanco, J., Gernjak, W., 2009. Decontamination and disinfection of water by solar photocatalysis: recent overview and trends. Catal. Today 147, 1–59. https://doi.org/10.1016/j.cattod.2009.06.018.

Malchi, T., Maor, Y., Chefetz, B., 2015. Comments on "Human health risk assessment of pharmaceuticals and personal care products in plant tissue due to biosolids and manure amendments, and wastewater irrigation. Environ. Int. 82, 110–112. https://doi.org/10.1016/j.envint.2015.03.014.

Mallakpour, S., Nikkhoo, E., 2014. Surface modification of nano-TiO_2 with trimellitylimido-amino acid-based diacids for preventing aggregation of nanoparticles. Adv. Powder Technol. 25, 348–353. https://doi.org/10.1016/j.apt.2013.05.017.

Mekonnen, M.M., Hoekstra, A.Y., 2016. Four billion people facing severe water scarcity. Sci. Adv. 2, e1500323 https://doi.org/10.1126/sciadv.1500323.

Meng, F., Lu, F., Sun, Z., Lü, J., 2010. A mechanism for enhanced photocatalytic activity of nano-size silver particle modified titanium dioxide thin films. Sci. China Technol. Sci. 53, 3027–3032. https://doi.org/10.1007/s11431-010-4116-z.

Murgolo, S., Petronella, F., Ciannarella, R., Comparelli, R., Agostiano, A., Curri, M.L., Mascolo, G., 2015. UV and solar-based photocatalytic degradation of organic pollutants by nano-sized TiO_2 grown on carbon nanotubes. Catal. Today 240, 114–124. https://doi.org/10.1016/j.cattod.2014.04.021.

Oller, I., Malato, S., Sanchez-Perez, J.A., 2011. Combination of Advanced Oxidation Processes and biological treatments for wastewater decontamination–a review. Sci. Total Environ. 409, 4141–4166. https://doi.org/10.1016/j.scitotenv.2010.08.061.

Pan, D., Jiao, J., Li, Z., Guo, Y., Feng, C., Liu, Y., Wang, L., Wu, M., 2015. Efficient separation of electron–hole pairs in graphene quantum dots by TiO_2 heterojunctions for dye degradation. ACS Sustain. Chem. Eng. 3, 2405–2413. https://doi.org/10.1021/acssuschemeng.5b00771.

Peng, Z., Han, X., Li, S., Al-Youbi, A.O., Bashammakh, A.S., El-Shahawi, M.S., Leblanc, R. M., 2017. Carbon dots: biomacromolecule interaction, bioimaging and nanomedicine. Coord. Chem. Rev. 343, 256–277. https://doi.org/10.1016/j.ccr.2017.06.001.

Poursani, A.S., Nilchi, A., Hassani, A., Shariat, S.M., Nouri, J., 2016. The synthesis of nano TiO_2 and its use for removal of lead ions from aqueous solution. J. Water Resour. Protect. 438–448. https://doi.org/10.4236/jwarp.2016.84037, 08.

Qu, S., Wang, X., Lu, Q., Liu, X., Wang, L., 2012. A biocompatible fluorescent ink based on water-soluble luminescent carbon nanodots. Angew. Chem. 124, 12381–12384. https://doi.org/10.1002/ange.201206791.

Rahbar, M., Mehrzad, M., Behpour, M., Mohammadi-Aghdam, S., Ashrafi, M., 2019. S, N co-doped carbon quantum dots/TiO_2 nanocomposite as highly efficient visible light photocatalyst. Nanotechnology 30, 505702. https://doi.org/10.1088/1361-6528/ab40dc.

Ren, W., Ai, Z., Jia, F., Zhang, L., Fan, X., Zou, Z., 2007. Low temperature preparation and visible light photocatalytic activity of mesoporous carbon-doped crystalline TiO_2. Appl. Catal. B Environ. 69, 138–144. https://doi.org/10.1016/j.apcatb.2006.06.015.

Rodell, M., Velicogna, I., Famiglietti, J.S., 2009. Satellite-based estimates of groundwater depletion in India. Nature 460, 999–1002. https://doi.org/10.1038/nature08238.

Roy, N., Sohn, Y., Pradhan, D., 2013. Synergy of low-energy {101} and high-energy {001} TiO_2 crystal facets for enhanced photocatalysis. ACS Nano 7, 2532–2540. https://doi.org/10.1021/nn305877v.

Sabri, M., Habibi-Yangjeh, A., Vadivel, S., 2019. Activation of persulfate ions by TiO_2/carbon dots nanocomposite under visible light for photocatalytic degradations of organic contaminants. J. Mater. Sci. Mater. Electron. 30, 12510–12522. https://doi.org/10.1007/s10854-019-01611-7.

Sendão, R., Yuso, M.d.V.M.d., Algarra, M., Esteves da Silva, J.C.G., Pinto da Silva, L., 2020. Comparative life cycle assessment of bottom-up synthesis routes for carbon dots derived from citric acid and urea. J. Clean. Prod. 254 https://doi.org/10.1016/j.jclepro.2020.120080.

Sendao, R.M.S., Crista, D.M.A., Afonso, A.C.P., Martinez de Yuso, M.D.V., Algarra, M., Esteves da Silva, J.C.G., Pinto da Silva, L., 2019. Insight into the hybrid luminescence showed by carbon dots and molecular fluorophores in solution. Phys. Chem. Chem. Phys. 21, 20919–20926. https://doi.org/10.1039/c9cp03730f.

Seo, M.K., Park, S.J., 2009. Surface characteristics of carbon fibers modified by direct oxyfluorination. J. Colloid Interface Sci. 330, 237–242. https://doi.org/10.1016/j.jcis.2008.10.005.

Shaban, Y.A., Fallata, H.M., 2019. Sunlight-induced photocatalytic degradation of acetaminophen over efficient carbon doped TiO_2 (CTiO_2) nanoparticles. Res. Chem. Intermed. 45, 2529–2547. https://doi.org/10.1007/s11164-019-03750-2.

Sharma, S., Ibhadon, A.O., Francesconi, M.G., Mehta, S.K., Elumalai, S., Kansal, S.K., Umar, A., Baskoutas, S., 2020. Bi_2WO_6/C-Dots/TiO_2: a novel Z-scheme photocatalyst for the degradation of fluoroquinolone levofloxacin from aqueous medium. Nanomaterials 10 (5), 910. https://doi.org/10.3390/nano10050910.

Sharma, S., Mehta, S.K., Kansal, S.K., 2017. N doped ZnO/C-dots nanoflowers as visible light driven photocatalyst for the degradation of malachite green dye in aqueous

phase. J. Alloys Compd. 699, 323–333. https://doi.org/10.1016/j.jallcom.2016.12.408.
Sharma, S., Umar, A., Mehta, S.K., Ibhadon, A.O., Kansal, S.K., 2018. Solar light driven photocatalytic degradation of levofloxacin using TiO_2/carbon-dot nanocomposites. New J. Chem. 42, 7445–7456. https://doi.org/10.1039/c7nj05118b.
Shi, R., Li, Z., Yu, H., Shang, L., Zhou, C., Waterhouse, G.I.N., Wu, L.Z., Zhang, T., 2017. Effect of nitrogen doping level on the performance of N-doped carbon quantum dot/TiO_2 composites for photocatalytic hydrogen evolution. ChemSusChem 10, 4650–4656. https://doi.org/10.1002/cssc.201700943.
Si, W., Yang, Z., Wang, X., Lv, Q., Zhao, F., Li, X., He, J., Long, Y., Gao, J., Huang, C., 2019. Fe,N-Codoped graphdiyne displaying efficient oxygen reduction reaction activity. ChemSusChem 12, 173–178. https://doi.org/10.1002/cssc.201802170.
Simoes, E.F.C., da Silva, L.P., da Silva, J., Leitao, J.M.M., 2020. Hypochlorite fluorescence sensing by phenylboronic acid-alizarin adduct based carbon dots. Talanta 208, 120447. https://doi.org/10.1016/j.talanta.2019.120447.
Somalingam, K., McDonagh, A., Zhou, J.L., Johir, M.A.H., Ahmed, M.B., 2018. Photocatalysis of estrone in water and wastewater: Comparison between Au-TiO_2 nanocomposite and TiO_2, and degradation by-products. Sci. Total Environ. 610–611, 521–530. https://doi.org/10.1016/j.scitotenv.2017.08.097.
Sun, Y.P., Zhou, B., Lin, Y., Wang, W., Fernando, K.A., Pathak, P., Meziani, M.J., Harruff, B.A., Wang, X., Wang, H., Luo, P.G., Yang, H., Kose, M.E., Chen, B., Veca, L. M., Xie, S.Y., 2006. Quantum-sized carbon dots for bright and colorful photoluminescence. J. Am. Chem. Soc. 128, 7756–7757. https://doi.org/10.1021/ja062677d.
Tan, J., Zou, R., Zhang, J., Li, W., Zhang, L., Yue, D., 2016. Large-scale synthesis of N-doped carbon quantum dots and their phosphorescence properties in a polyurethane matrix. Nanoscale 8, 4742–4747. https://doi.org/10.1039/c5nr08516k.
Thakur, A., Devi, P., Saini, S., Jain, R., Sinha, R.K., Kumar, P., 2018. Citrus limetta organic waste recycled carbon nanolights: photoelectro catalytic, sensing, and biomedical applications. ACS Sustain. Chem. Eng. 7, 502–512. https://doi.org/10.1021/acssuschemeng.8b04025.
Thakur, A., Kumar, P., Kaur, D., Devunuri, N., Sinha, R.K., Devi, P., 2020. TiO_2 nanofibres decorated with green-synthesized PAu/Ag@CQDs for the efficient photocatalytic degradation of organic dyes and pharmaceutical drugs. RSC Adv. 10, 8941–8948. https://doi.org/10.1039/c9ra10804a.
Tian, M., Liu, Y., Wang, Y., Zhang, Y., 2019. Yellow-emitting carbon dots for selective detecting 4-NP in aqueous media and living biological imaging. Spectrochim. Acta Mol. Biomol. Spectrosc. 220, 117117. https://doi.org/10.1016/j.saa.2019.05.022.
Tian, N., Zhang, Y., Li, X., Xiao, K., Du, X., Dong, F., Waterhouse, G.I.N., Zhang, T., Huang, H., 2017. Precursor-reforming protocol to 3D mesoporous g-C_3N_4 established by ultrathin self-doped nanosheets for superior hydrogen evolution. Nano Energy 38, 72–81. https://doi.org/10.1016/j.nanoen.2017.05.038.
Tollefson, J., 2011. How green is my future? Nature 473, 134–135. https://doi.org/10.1038/473134a.
Toth, Z.R., Pap, Z., Danciu, V., Cosoveanu, V., Baia, L., Kovacs, G., 2019. Detailed investigation of phenol degradation on Au/TiO_2 composite materials. J. Nanosci. Nanotechnol. 19, 407–413. https://doi.org/10.1166/jnn.2019.15793.
Tu, W., Zhou, Y., Liu, Q., Yan, S., Bao, S., Wang, X., Xiao, M., Zou, Z., 2013. An in situ simultaneous reduction-hydrolysis technique for fabrication of TiO_2-graphene 2D sandwich-like hybrid nanosheets: graphene-promoted selectivity of photocatalytic-driven hydrogenation and coupling of CO_2 into methane and ethane. Adv. Funct. Mater. 23, 1743–1749. https://doi.org/10.1002/adfm.201202349.
Vale, N., Silva, S., Duarte, D., Crista, D.M.A., Pinto da Silva, L., Esteves da Silva, J.C.G., 2021. Normal breast epithelial MCF-10A cells to evaluate the safety of carbon dots. RSC Med. Chem. 12, 245–253. https://doi.org/10.1039/d0md00317d.
Wang, F., Wu, Y., Wang, Y., Li, J., Jin, X., Zhang, Q., Li, R., Yan, S., Liu, H., Feng, Y., Liu, G., Lv, W., 2019. Construction of novel Z-scheme nitrogen-doped carbon dots/{001} TiO_2 nanosheet photocatalysts for broad-spectrum-driven diclofenac degradation: mechanism insight, products and effects of natural water matrices. Chem. Eng. J. 356, 857–868. https://doi.org/10.1016/j.cej.2018.09.092.
Wang, J., Rao, P., An, W., Xu, J., Men, Y., 2016. Boosting photocatalytic activity of Pd decorated TiO_2 nanocrystal with exposed (001) facets for selective alcohol oxidations. Appl. Catal. B Environ. 195, 141–148. https://doi.org/10.1016/j.apcatb.2016.05.018.
Wang, K., Gao, Z., Gao, G., Wo, Y., Wang, Y., Shen, G., Cui, D., 2013. Systematic safety evaluation on photoluminescent carbon dots. Nanoscale Res. Lett. 8, 122. https://doi.org/10.1186/1556-276X-8-122.
Wang, K., Liang, L., Zheng, Y., Li, H., Niu, X., Zhang, D., Fan, H., 2021. Visible light-driven photocatalytic degradation of organic pollutants via carbon quantum dots/TiO_2. New J. Chem. 45, 16168–16178. https://doi.org/10.1039/d1nj02387j.
Wang, Q., Zheng, Q., Jin, R., Gao, S., Yuan, Q., Rong, W., Wang, R., 2017a. Photoelectrocatalytic removal of organic dyes and Cr(VI) ions using Ag_3PO_4 nanoparticles sensitized TiO_2 nanotube arrays. Mater. Chem. Phys. 199, 209–215. https://doi.org/10.1016/j.matchemphys.2017.06.051.
Wang, R., Lu, K. Q., Tang, Z. R., Xu, Y. J., 2017b. Recent progress in carbon quantum dots: synthesis, properties and applications in photocatalysis. J. Mater. Chem. 5, 3717–3734. https://doi.org/10.1039/c6ta08660h.
Wang, Z., Liu, J., Wang, W., Wei, Z., Wang, F., Gong, P., Wang, J., Li, N., Liu, B., Zhang, Z., Wang, W., Sun, L., 2017c. Photoluminescent carbon quantum dot grafted silica nanoparticles directly synthesized from rice husk biomass. J. Mater. Chem. B 5, 4679–4689. https://doi.org/10.1039/c7tb00811b.
Webb, S., Ternes, T., Gibert, M., Olejniczak, K., 2003. Indirect human exposure to pharmaceuticals via drinking water. Toxicol. Lett. 142, 157–167. https://doi.org/10.1016/s0378-4274(03)00071-7.
Wongso, V., Chung, H.K., Sambudi, N.S., Sufian, S., Abdullah, B., Wirzal, M.D.H., Ang, W.L., 2020. Silica–carbon quantum dots decorated titanium dioxide as sunlight-driven photocatalyst to diminish acetaminophen from aquatic environment. J. Photochem. Photobiol. Chem. 394, 112436. https://doi.org/10.1016/j.jphotochem.2020.112436.
Xu, X., Ray, R., Gu, Y., Ploehn, H.J., Gearheart, L., Raker, K., Scrivens, W.A., 2004. Electrophoretic analysis and purification of fluorescent single walled carbon nanotube fragments. J. Am. Chem. Soc. 126, 12736–12737. https://doi.org/10.1021/ja040082h.
Yang, H.G., Sun, C.H., Qiao, S.Z., Zou, J., Liu, G., Smith, S.C., Cheng, H.M., Lu, G.Q., 2008. Anatase TiO_2 single crystals with a large percentage of reactive facets. Nature 453, 638–641. https://doi.org/10.1038/nature06964.
Yang, S.T., Cao, L., Luo, P.G., Lu, F., Wang, X., Wang, H., Meziani, M.J., Liu, Y., Qi, G., Sun, Y.P., 2009. Carbon dots for optical imaging in vivo. J. Am. Chem. Soc. 131, 11308–11309. https://doi.org/10.1021/ja904843x.
Yin, S., Zhang, Q., Saito, F., Sato, T., 2003. Preparation of visible light-activated titania photocatalyst by mechanochemical method. Chem. Lett. 32, 358–359. https://doi.org/10.1246/cl.2003.358.
Yu, J., Jin, J., Cheng, B., Jaroniec, M., 2014a. A noble metal-free reduced graphene oxide–CdS nanorod composite for the enhanced visible-light photocatalytic reduction of CO_2 to solar fuel. J. Mater. Chem. 2, 3407–3416. https://doi.org/10.1039/c3ta14493c.
Yu, J., Zhang, C., Yang, Y., Yi, G., Fan, R., Li, L., Xing, B., Liu, Q., Jia, J., Huang, G., 2019. Lignite-derived carbon quantum dot/TiO_2 heterostructure nanocomposites: photoinduced charge transfer properties and enhanced visible light photocatalytic activity. New J. Chem. 43, 18355–18368. https://doi.org/10.1039/c9nj04860j.
Yu, S., Wang, Y., Sun, F., Wang, R., Zhou, Y., 2018. Novel npg-C_3N_4/TiO_2 nanocomposite photocatalytic membrane reactor for sulfamethoxazole photodegradation. Chem. Eng. J. 337, 183–192. https://doi.org/10.1016/j.cej.2017.12.093.
Yu, S., Zhong, Y.-Q., Yu, B.-Q., Cai, S.-Y., Wu, L.-Z., Zhou, Y., 2016. Graphene quantum dots to enhance the photocatalytic hydrogen evolution efficiency of anatase TiO_2 with exposed {001} facet. Phys. Chem. Chem. Phys. 18, 20338–20344. https://doi.org/10.1039/c6cp02561g.
Yu, X., Liu, J., Yu, Y., Zuo, S., Li, B., 2014b. Preparation and visible light photocatalytic activity of carbon quantum dots/TiO_2 nanosheet composites. Carbon 68, 718–724. https://doi.org/10.1016/j.carbon.2013.11.053.
Yuan, S.F., Liu, Z.H., Yin, H., Dang, Z., Wu, P.X., Zhu, N.W., Lin, Z., 2019. Trace determination of sulfonamide antibiotics and their acetylated metabolites via SPE-LC-MS/MS in wastewater and insights from their occurrence in a municipal wastewater treatment plant. Sci. Total Environ. 653, 815–821. https://doi.org/10.1016/j.scitotenv.2018.10.417.
Zeng, Y., Chen, D., Chen, T., Cai, M., Zhang, Q., Xie, Z., Li, R., Xiao, Z., Liu, G., Lv, W., 2019. Study on heterogeneous photocatalytic ozonation degradation of ciprofloxacin by TiO_2/carbon dots: kinetic, mechanism and pathway investigation. Chemosphere 227, 198–206. https://doi.org/10.1016/j.chemosphere.2019.04.039.
Zhang, B., Maimaiti, H., Zhang, D.-D., Xu, B., Wei, M., 2017a. Preparation of coal-based C-Dots/TiO_2 and its visible-light photocatalytic characteristics for degradation of pulping black liquor. J. Photochem. Photobiol. Chem. 345, 54–62. https://doi.org/10.1016/j.jphotochem.2017.05.031.
Zhang, F., Wang, X., Liu, H., Liu, C., Wan, Y., Long, Y., Cai, Z., 2019a. Recent advances and applications of semiconductor photocatalytic technology. Appl. Sci. 9 (12), 2489. https://doi.org/10.3390/app9122489.
Zhang, H., Liu, P., Feng, Y., Yang, F., 2013a. Fate of antibiotics during wastewater treatment and antibiotic distribution in the effluent-receiving waters of the Yellow Sea, northern China. Mar. Pollut. Bull. 73, 282–290. https://doi.org/10.1016/j.marpolbul.2013.05.007.
Zhang, J., Cao, Y., Zhao, P., Xie, T., Lin, Y., Mu, Z., 2020. Visible-light-driven pollutants degradation with carbon quantum dots/N-TiO_2 under mild condition: facile preparation, dramatic performance and deep mechanism insight. Colloids Surf. A Physicochem. Eng. Asp. 601, 125019. https://doi.org/10.1016/j.colsurfa.2020.125019.
Zhang, J., Liu, Q., He, H., Shi, F., Huang, G., Xing, B., Jia, J., Zhang, C., 2019b. Coal tar pitch as natural carbon quantum dots decorated on TiO_2 for visible light photodegradation of rhodamine B. Carbon 152, 284–294. https://doi.org/10.1016/j.carbon.2019.06.034.
Zhang, J., Ma, Y., Du, Y., Jiang, H., Zhou, D., Dong, S., 2017b. Carbon nanodots/WO_3 nanorods Z-scheme composites: remarkably enhanced photocatalytic performance under broad spectrum. Appl. Catal. B Environ. 209, 253–264. https://doi.org/10.1016/j.apcatb.2017.03.017.
Zhang, X., Jin, M., Liu, Z., Nishimoto, S., Saito, H., Murakami, T., Fujishima, A., 2006. Preparation and photocatalytic wettability conversion of TiO_2-based superhydrophobic surfaces. Langmuir 22, 9477–9479. https://doi.org/10.1021/la0618869.
Zhang, Y.-Q., Ma, D.-K., Zhang, Y.-G., Chen, W., Huang, S.-M., 2013b. N-doped carbon quantum dots for TiO_2-based photocatalysts and dye-sensitized solar cells. Nano Energy 2, 545–552. https://doi.org/10.1016/j.nanoen.2013.07.010.
Zheng, Z., Huang, B., Qin, X., Zhang, X., Dai, Y., 2010. Strategic synthesis of hierarchical TiO_2 microspheres with enhanced photocatalytic activity. Chemistry 16, 11266–11270. https://doi.org/10.1002/chem.201001280.
Zhou, M., Li, M., Hou, C., Li, Z., Wang, Y., Xiang, K., Guo, X., 2018. Pt nanocrystallines/TiO_2 with thickness-controlled carbon layers: preparation and activities in CO oxidation. Chin. Chem. Lett. 29, 787–790. https://doi.org/10.1016/j.cclet.2018.03.010.
Zulfiqar, M., Chowdhury, S., Sufian, S., Omar, A.A., 2018. Enhanced photocatalytic activity of Orange II in aqueous solution using solvent-based TiO_2 nanotubes: kinetic, equilibrium and thermodynamic studies. J. Clean. Prod. 203, 848–859. https://doi.org/10.1016/j.jclepro.2018.08.324.

1.3. Aim and objectives

The number of organic pollutants entering aqueous systems is growing every year as new compounds are discovered, produced, and sold for various applications. Worryingly, conventional water treatment techniques are ineffective when it comes to the removal of this class of pollutants, which includes compounds such as organic dyes and antibiotics.

Given this context, this project aims to develop an alternative to these methods based on advanced oxidation techniques by synthesizing sustainable TiO_2/CDs nanocomposites with good visible-light activity that are highly efficient under solar irradiation, creating a process in line with the United Nations Sustainable Development Goals 6 (Clean Water), 9 (Industry and Infrastructure), 12 (Responsible Consumption and Production) and 14 (Life Underwater). TiO_2 will be the photocatalytic component given its oxidizing power, low cost, low toxicity, and photostability. CDs will enhance the photocatalytic efficiency by extending the absorption of light into the visible region and enhancing the photonic efficiency, thus solving TiO_2's main limitations regarding sunlight-driven photocatalysis. To improve the sustainability of the process, we also studied the incorporation of corn stover, a by-product of the corn industry, as a carbon source for the preparation of the CDs, thus upcycling this otherwise discarded organic material.

This doctoral project had four objectives:

1. Sustainable synthesis of CDs incorporating corn stover following the green methodologies developed by our research group;
2. Development of visible-light-active nanocomposites obtained from the deposition of CDs into TiO_2 nanoparticles, thus enhancing TiO_2's visible-light absorption and photonic efficiency;
3. Sunlight-driven photodegradation of organic pollutants by the nanocomposites, including a study of their effectiveness, mechanism, and characterization of the photocatalysts;
4. Life Cycle Assessment studies of the developed photocatalysts to obtain data concerning the environmental impact of the production processes and optimize their environmental performance.

2. Results and discussion

2.1. Development of visible-light active photocatalytic nanocomposites

2.1.1. Preparation of first catalytic nanocomposite from commercial reagents

Article

Carbon Dots–TiO_2 Nanocomposites for the Enhanced Visible-Light Driven Photodegradation of Methylene Blue

Sendão, Ricardo M. S.; Algarra, Manuel; Ribeiro, Eduarda; Pereira, Mariana; Gil, Antonio; Vale, Nuno; Esteves da Silva, Joaquim C. G.; Pinto da Silva, Luís. "Carbon Dots–TiO_2 Nanocomposites for the Enhanced Visible-Light Driven Photodegradation of Methylene Blue". *Advanced Sustainable Systems* 8(1) (**2023**): 2300317. http://doi.org/10.1002/adsu.202300317.

2.1.1.1. Introduction and contributions to this work

This work reports the development of a visible-light-active photocatalytic nanocomposite toward the photocatalytic removal of organic pollutants from aqueous samples. Herein, we observed how adding CDs to TiO_2 increased the photocatalytic efficiency by improving the visible-light absorption, photonic efficiency, and adsorption of organic pollutants. The CDs used in the process were commercially available CA and ethylenediamine (EDA) and were prepared via a hydrothermal process. Methylene blue (MB) was employed as a model pollutant, and a 367% enhancement of the catalytic performance was observed when compared to bare TiO_2. Scavenger assays were performed to unravel the reactive species behind the photodegradation mechanism, in *vitro* studies were used to assess the toxicity of the CDs toward human cells, and life cycle assessment (LCA) studies were performed to compare the relative environmental impacts of using TiO_2/CDs nanocomposites compared to using TiO_2.

In this work, I was responsible, under supervisor from my supervisors, for synthesizing the CDs and the nanocomposite, their characterization in terms of UV-Vis DRS and fluorescence spectroscopy, band gap and quantum yield calculations, photocatalytic assays, COD analysis, scavenger studies, comparison with other reports available in the literature, and environmental impact assessment via LCA studies. I also conducted the analysis and interpretation of the results and wrote the first draft of the paper, which was

then reviewed and edited by Professor Dr. Luís Pinto da Siva and Professor Dr. Joaquim Esteves da Silva, who supervised the process from end-to-end. The remaining experiments were performed by partners from other institutions and external service providers. Namely, the CDs' toxicity assay was conducted by Eduarda Ribeiro, Mariana Pereira and supervised by Prof. Dr. Nuno Vale at CINTESIS – Faculty of Medicine of the University of Porto, SEM and AFM analysis were done by CEMUP, FTIR analysis at FCUP | DQB – Lab&Services, and finally, XPS and XRD were performed by Dr. Manuel Algarra and Dr. Antonio Gil from INAMAT^2 at the Public University of Navarra. It should be noted that while SEM, AFM, and FTIR analyses were performed by external service providers, I was the one responsible for data treatment and analysis.

RESEARCH ARTICLE

ADVANCED SUSTAINABLE SYSTEMS
www.advsustainsys.com

Carbon Dots–TiO_2 Nanocomposites for the Enhanced Visible-Light Driven Photodegradation of Methylene Blue

*Ricardo M. S. Sendão, Manuel Algarra, Eduarda Ribeiro, Mariana Pereira, Antonio Gil, Nuno Vale, Joaquim C. G. Esteves da Silva, and Luís Pinto da Silva**

Herein, the conjugation of carbon dots (CDs) with TiO_2 nanoparticles is reported to prepare a photocatalytic nanocomposite for an enhanced visible-light-driven photodegradation of methylene blue (MB). CDs are prepared from citric acid (CA) and ethylenediamine (EDA) via hydrothermal treatment. Using MB as a model pollutant, it is observed that, under visible-light irradiation, the nanocomposite presents an increment of the catalytic performance of 367% when compared to bare TiO_2. This is achieved because the addition of CDs leads to increased visible-light absorption and hinders the recombination of photogenerated charge carriers. Thus, CDs are capable of bridging some of the limitations posed by TiO_2. Tests using reactive species scavengers indicate that the main active species involved in the photodegradation by the nanocomposites are superoxide radicals followed by hydroxyl radicals, which differs from bare TiO_2. Lastly, a life cycle assessment (LCA) study shows that, when accounting for performance, the nanocomposites have lower relative environmental impacts than bare TiO_2. In addition, the safety of the produced CDs is shown by in vitro assays. In summary, due to conjugation with CDs, a relevant increment in the catalytic performance of TiO_2 is achieved; providing an important step toward the sustainable rational design of active visible-light-driven photocatalysts.

1. Introduction

Water is arguably the most crucial resource on Earth. Predictably, the contamination of water fit for human consumption may lead to the scarcity of this essential resource.[1,2] In particular, organic compounds, including dyes, are the major pollutants found in aquatic environments. These pollutants are capable of generating damaging by-products through hydrolysis, oxidation or other reactions that may take place in aqueous media.[3] Thus, the efficient removal of these pollutants is essential to preserve and assure the safety of our water resources. Conventional methods of treating wastewater include physical adsorption, coagulation, and biodegradation, all of which present serious limitations when regarding organic pollutants. More recently, photocatalysis and the treatment of wastewater via advanced oxidation processes (AOPs) have been under the

R. M. S. Sendão, J. C. G. Esteves da Silva, L. Pinto da Silva
Chemistry Research Unit (CIQUP)
Institute of Molecular Sciences (IMS)
Department of Geosciences, Environment and Territorial Planning
Faculty of Sciences
University of Porto
Rua do Campo Alegre s/n, Porto 4169-007, Portugal
E-mail: luis.silva@fc.up.pt

M. Algarra, A. Gil
INAMAT^2-Institute for Advanced Materials and Mathematics
Science Department
Public University of Navarre
Campus of Arrosadía, Pamplona 31006, Spain

E. Ribeiro, M. Pereira, N. Vale
PerMed Research Group
Center for Health Technology and Services Research (CINTESIS)
Rua Doutor Plácido da Costa, Porto 4200-450, Portugal

E. Ribeiro, M. Pereira, N. Vale
CINTESIS@RISE
Faculty of Medicine
University of Porto
Alameda Professor Hernâni Monteiro, Porto 4200-319, Portugal

N. Vale
Department of Community Medicine
Information and Health Decision Sciences (MEDCIDS)
Faculty of Medicine
University of Porto
Rua Doutor Plácido da Costa, Porto 4200-450, Portugal

J. C. G. Esteves da Silva, L. Pinto da Silva
LACOMEPHI
GreenUPorto
Department of Geosciences, Environment and Territorial Planning
Faculty of Sciences
University of Porto
Rua do Campo Alegre s/n, Porto 4169-007, Portugal

The ORCID identification number(s) for the author(s) of this article can be found under https://doi.org/10.1002/adsu.202300317

DOI: 10.1002/adsu.202300317

 © 2023 Wiley-VCH GmbH

ADVANCED SCIENCE NEWS
www.advancedsciencenews.com

ADVANCED SUSTAINABLE SYSTEMS
www.advsustainsys.com

focus of the scientific community as an alternative to those conventional methods. Photocatalysis focuses on the conversion of photoenergy into chemical energy. The use of photocatalytic technologies has several advantages: it can achieve a near complete degradation of pollutants, it can be a greener alternative to traditional chemical oxidation, and absence of by-products originating from the catalyst.[4,5]

One of the most studied photocatalysts is titanium dioxide (TiO_2), a stable and inexpensive material with potential for use in a variety of applications.[6,7] Namely, TiO_2 was already used for applications such as hydrogen generation via water splitting, metal removal via photoreduction (e.g., Zn, Cd and Pb), and photodegradation of organic pollutants (e.g., pharmaceuticals and organic dyes such as ibuprofen and methylene blue (MB), respectively).[8–11]

By using solar light as an energy source, it is possible to promote the catalytic process by using a clean and inexhaustible energy source, resulting in a less environmentally harmful process.[6,7] Solar light is comprised of UV, visible, and NIR (≈6%, 39%, and 55% of the radiation, respectively).[12] However, TiO_2 requires high-energy irradiation (band gap of 2.8–3.2 eV) due to the narrow photocatalytic region ($\lambda < 400$ nm),[13] making this photocatalyst only useful under UV irradiation. Thus, the lack of satisfactory photocatalytic efficiency under visible light hinders its industrial application and prevents TiO_2 photocatalysts from taking advantage of solar light as a clean energy source. Furthermore, TiO_2 suffers from rapid charge recombination, reducing its photonic efficiency.[14] Its surface also has a poor affinity toward organic pollutants, limiting the photocatalytic rate as the pollutants do not reach the active site easily.[15]

Given this, there has been active research in trying to enhance the visible-light-absorption and photocatalytic efficiency of TiO_2. More specifically, different strategies have been studied, such as metal and non-metal doping (e.g., platinum and nitrogen/fluorine, respectively)[16,17] and coupling the photocatalyst to other materials, such as carbon nitride and graphene.[18–20] These techniques could increase the surface affinity of TiO_2 toward pollutants and make it easier for them to reach the active site. In addition, they can allow the use of TiO_2 under visible-light by enabling new energy levels and a more stable nanocrystalline structure.[20–22] However, they rely mostly on costly and toxic metal elements and tend to accelerate the recombination of photogenerated charge carriers, decreasing the photocatalytic potential.[22]

Carbon dots (CDs) are carbon-based nanoparticles that were first found in 2004.[23–26] CDs are typically sized between 1 and 10 nm and present a spherical or quasi-spherical shape. Depending on the synthesis, they may present an sp^2-conjugated amorphous or crystalline core and a surface covered with functional groups (e.g., —OH and —COOH).[27,28] CDs present several interesting characteristics, such as photoluminescence, broadband absorption, chemical stability, high water solubility, low toxicity, and being easy and inexpensive to synthesize.[27,29–34] Due to their properties, practical applications for CDs include bioimaging,[35,36] sensing and biosensing,[36–38] drug delivery systems,[39] photodynamic therapy,[40] light-emitting devices,[41] nanothermometry,[42] photovoltaic devices,[43] and photocatalysis (including several cases of TiO_2/CDs nanocomposites).[43–47]

Combining the semiconductor with CDs may be a way to overcome the TiO_2 limitations.[46,48] In general, CDs are a nontoxic and less expensive alternative to the more conventional doping with metals and rare earth elements.[16,17] Unlike doping strategies,[22] the use of CDs for the nanocomposites does not tend to promote the recombination of charge carriers. Instead, the high electron storage capacity and the electron transfer properties of CDs allow them to accept photoexcited electrons in TiO_2's conduction band,[49] resulting in a better separation of photogenerated charge carriers; and thus, an improved photonic efficiency. Additionally, the addition of CDs may also extend the nanocomposites' absorption into the visible range, allowing a better utilization of solar light.[22,46,47,50] Finally, the CDs' functionalized surface provides a higher pollutant adsorption capacity due to the diversity of functional groups present; thus, increasing the amount of pollutants reaching the photocatalytic site and increasing the efficiency of the process.[47,51] It is worth nothing that CDs already showed great potential applicability in photocatalytic applications by themselves, be it for hydrogen generation, photodegradation or metal photoreduction, confirming their potential in the field.[52–55]

In this work, we report the preparation of TiO_2-CDs nanocomposites for the visible-light-only photocatalytic degradation of the organic dye methylene blue (MB) and their comparison to bare TiO_2. While there are some reports concerning the use of TiO_2-CDs systems for the catalytic degradation of MB, nearly all of them either use radiation other than visible-light alone[56–58] or have components other than TiO_2 and CDs (e. g. Ag, Fe_2O_3, and H_2O_2).[59–61] Our work yielded a catalytic nanocomposite prepared from TiO_2 and CDs with the capacity to convert low-energy visible-light irradiation into the catalytic degradation of MB. In fact, the TiO_2-CDs nanocomposite presented an increment of the catalytic performance of 367% when compared to bare TiO_2, confirming that the addition of the CDs successfully improved the virtually negligible activity of TiO_2 under visible-light irradiation. Tests with scavengers were made to identify the reactive species behind the photodegradation. Characterization of the nanomaterials was made to compare between the nanocomposites and TiO_2. Namely, the morphology and composition of the nanocomposite were studied via SEM, XRD, and FT-IR, whereas the optical properties were evaluated via UV–vis and fluorescence spectroscopy. Further, the CDs were also characterized (UV–vis and fluorescence spectroscopy, AFM, and XPS) and evaluated in terms of toxicity toward human cells. Finally, a life cycle assessment (LCA) study was made to verify if the enhanced performance of the nanocomposites was worth the potential environmental impacts resulting from the inclusion of the CDs.

2. Results and Discussion

2.1. Characterization of TiO_2–CDs Nanocomposites and Respective CDs

To better understand the properties of the nanocomposites and to evaluate in which ways they could affect the photocatalytic activity in comparison to bare TiO_2, we characterized the catalysts. Bare TiO_2 and TiO_2–CDs nanocomposites were compared in terms of optical properties. First, the UV–vis spectra were obtained. It was observed that the absorption spectra of TiO_2

© 2023 Wiley-VCH GmbH

ADVANCED SCIENCE NEWS
www.advancedsciencenews.com

ADVANCED SUSTAINABLE SYSTEMS
www.advsustainsys.com

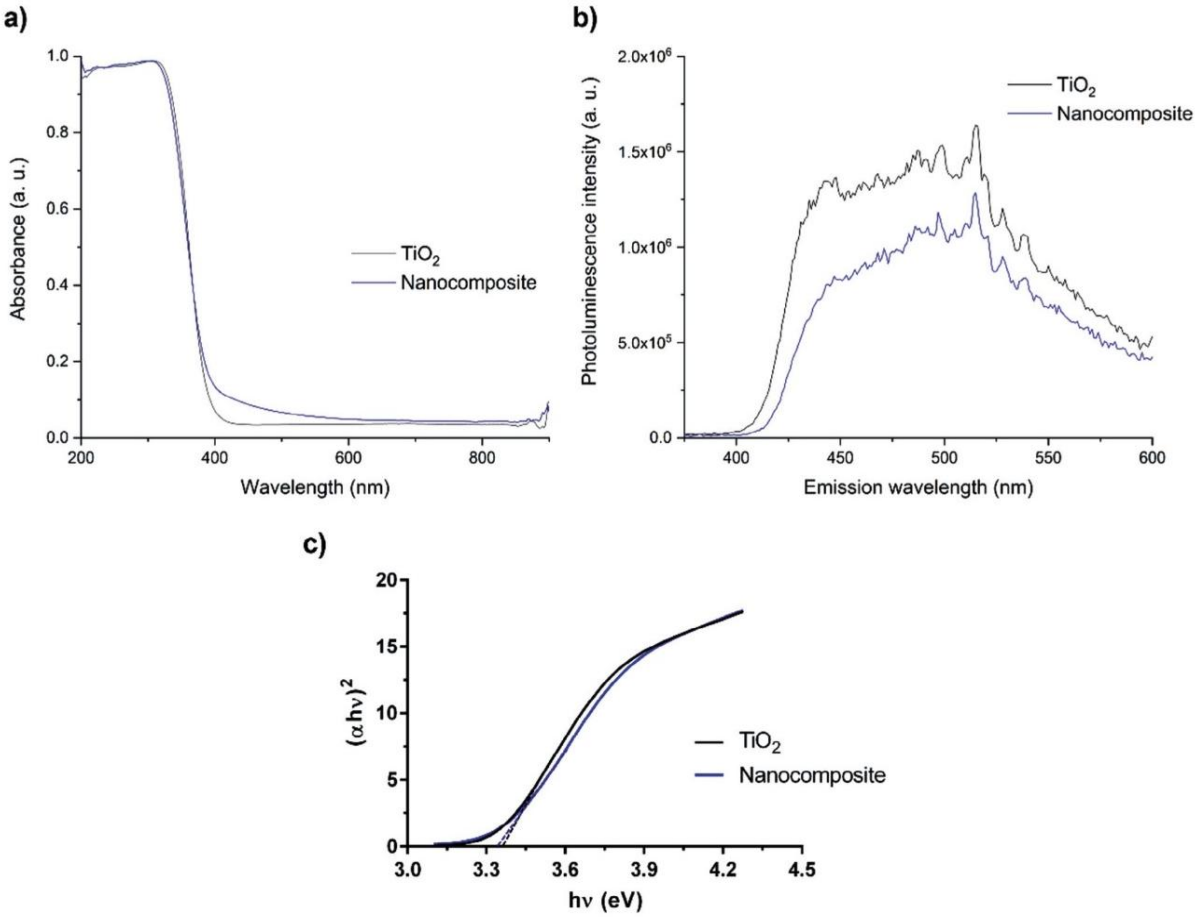


Figure 1. a) UV-Vis spectra, b) steady-state photoluminescence spectra, and c) Tauc plot of TiO_2 and TiO_2–CDs nanocomposites.

and the nanocomposites (**Figure 1**a) presented roughly the same profile. Bare TiO_2 absorption was confined to the UV region, with an absorption edge located at around 410 nm. However, this changed upon conjugation with CDs, which enhanced the absorption between 400 and 600 nm. Regarding the origin of the increased visible absorption, it was previously reported that Ti^{3+} ions, which could be formed due to electron exchange with the CDs, could arouse optical absorption at $\lambda > 600$ nm.[8] However, this was not observed in our samples, indicating that no residual Ti^{3+} ions existed in the samples and that the increased light absorption in the visible should be due to addition of the CDs. Thus, the addition of CDs seemed to enhance the visible-light harvesting ability in the nanocomposites, which was one of the main parameters affecting the catalytic efficiency.

To evaluate the role of the CDs in hindering the recombination of photogenerated charge carriers, the photoluminescence spectra of both bare TiO_2 and TiO_2-CDs nanocomposites were recorded. As observed in Figure 1b, both compounds presented a broad emission ranging from 400 to 600 nm. However, the emission intensity of the nanocomposites was considerably lower than that of bare TiO_2, suggesting that the interaction between CDs and TiO_2 provides a rapid electron transfer interface in which there is a transference of electrons between CDs and TiO_2, likely via the Ti—O—C bond.[62] This favors the photocatalytic process by preventing the recombination of photogeneration charge carriers; thus, diminishing the dissipation of the energy as radiation, which is consistent with previous reports.[63,64]

The UV–vis absorption data were processed to estimate the band gap energies by applying Tauc's formula (Figure 1c): $(\alpha h\nu)^2 = h\nu$, where α and $h\nu$ are the absorbance and the energy of the photon, respectively. The estimated band energies of both TiO_2 and the nanocomposites were similar (3.32 and 3.31 eV, respectively). Even though there was a higher absorption in the visible spectrum for the nanocomposites, the photocatalysts' band gap was not narrowed. This suggests that there was no formation of a "dyad" structure between the CDs and TiO_2.[43,65] These structures had been associated with an improved TiO_2 h^+ activity and an uptake of electrons by the carbon component (which delays the recombination of photogenerated charge carriers); thus, improving photocatalytic efficiency.[65,66]

To evaluate the morphological properties of both TiO_2 and TiO_2–CDs nanocomposites, both catalysts were analyzed via SEM (**Figure 2**). The two catalysts presented different characteristics as the nanocomposites presented a significantly larger

 © 2023 Wiley-VCH GmbH

ADVANCED SCIENCE NEWS
www.advancedsciencenews.com

ADVANCED SUSTAINABLE SYSTEMS
www.advsustainsys.com

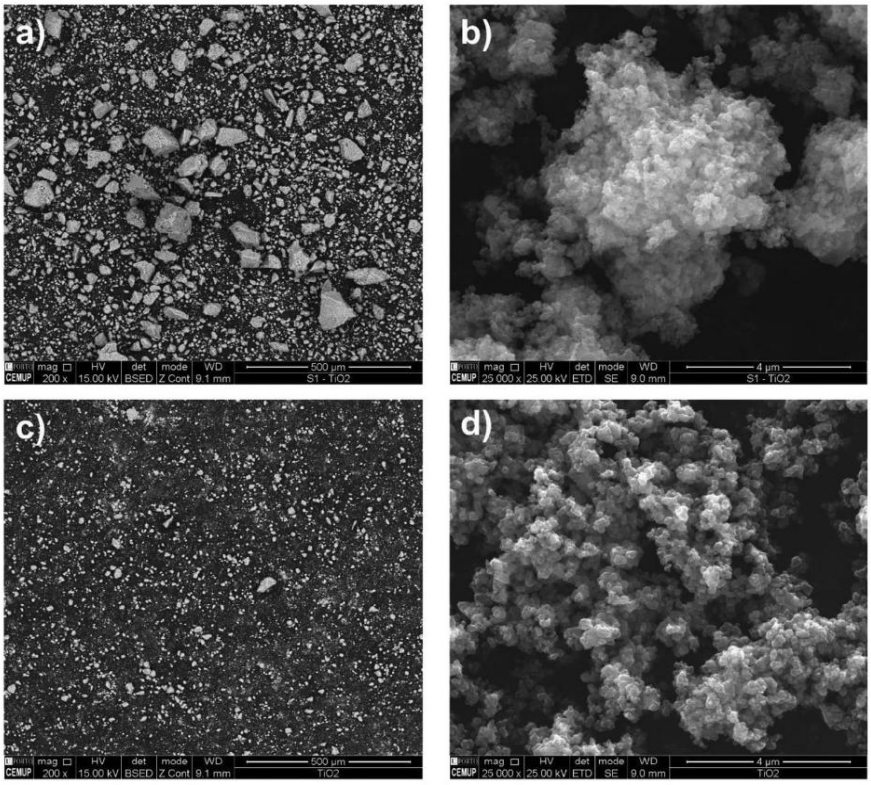


Figure 2. SEM images of TiO_2–CDs nanocomposites at a) 200× and b) 25 000× magnification and TiO_2 at c) 200× and d) 25 000× magnification.

number of aggregates than TiO_2 (Figure 2a,c). This may be due to the surface groups present in the CDs in the nanocomposites. CDs' surfaces commonly include carboxyl, carbonyl, and amine groups, which result in the formation of electrostatic interactions and hydrogen-bonds between one another; thus, leading to the agglomeration of the nanocomposite's particles.[67,68] The average size measured for the nanocomposites was ≈85 nm (Figure 2a,b), which was in line with other TiO_2-based catalysts.[69,70] Moreover, the nanocomposites were smaller than bare TiO_2 (Figure 2c,d, ≈140 nm in size). It is known that, for TiO_2, smaller sizes result in a better catalytic performance.[62] Thus, the fact that upon the addition of CDs we obtained smaller catalyst particles, would contribute to the catalytic performance of the nanocomposites, possibly being one of the reasons behind its enhancement.

The XRD patterns of TiO_2 and the nanocomposites were obtained and analyzed (**Figure 3**a). By analyzing the XRD profile, we observed a small shoulder at 26.1°, which could be attributed to the carbon nanoparticles in the nanocomposite composition (magnified inset in Figure 3a), anatase being the main assignment of it. The diffraction peaks of both samples matched those of (101), (004), (200), (105), (211), (204), (220), and (215) crystal planes of the anatase phase of TiO_2.[71] For TiO_2–CDs nanocomposites, typical diffraction peaks of CDs were not well observed, which was ascribed to the high dispersion and low content of CDs in the nanocomposites.[72] Thus, the addition of CDs did not change the structure of the semiconductor catalyst.

Using FTIR (Figure 3b), it was observed that both TiO_2 and TiO_2–CDs nanocomposites presented similar spectra with the same peaks/bands. Namely, in both cases, a small band was found at 1641 cm^{-1} and was assigned to the carbonyl group, —OH functional groups, as well as water adsorbed to the catalysts' surface.[71] The main band centered at 3344 cm^{-1} was attributed to —OH groups, confirming the presence of carboxylic acid as the main decoration of the nanocomposite.[73] Finally, the peak near the 500 cm^{-1} border was ascribed to Ti—O—Ti bonds, which was expected, given the nature of the catalysts.[73]

Having characterized the nanocomposites, it was now necessary to study the properties of the CDs. AFM analysis was performed (Figure S1, Supporting Information), revealing that the CDs presented a spherical shape with an average particle size of 1.87 ± 0.49 nm. XPS analysis was done to analyze the surface composition of the CDs. The XPS atomic composition (atomic wt%) was C: 74.1%, N: 12.7%, and O: 13.2%, respectively (Figure S2a, Supporting Information). The high-resolution C 1*s* spectra could be split into four peaks for all samples presenting binding energies of 284.8 eV (attributed to C—C/C—H groups, 54.65%), 286.1 eV (C—O/C—N groups, 27.1%), 287.6 eV (C=O groups, 14.72%), and 289.1 eV (O—C = O, 3.54%) (Figure S2b, Supporting Information). For the N 1*s* spectra (Figure S2c, Supporting Information), bonding energies of 399.9 and 401.3 eV

 © 2023 Wiley-VCH GmbH

ADVANCED SCIENCE NEWS
www.advancedsciencenews.com

ADVANCED SUSTAINABLE SYSTEMS
www.advsustainsys.com

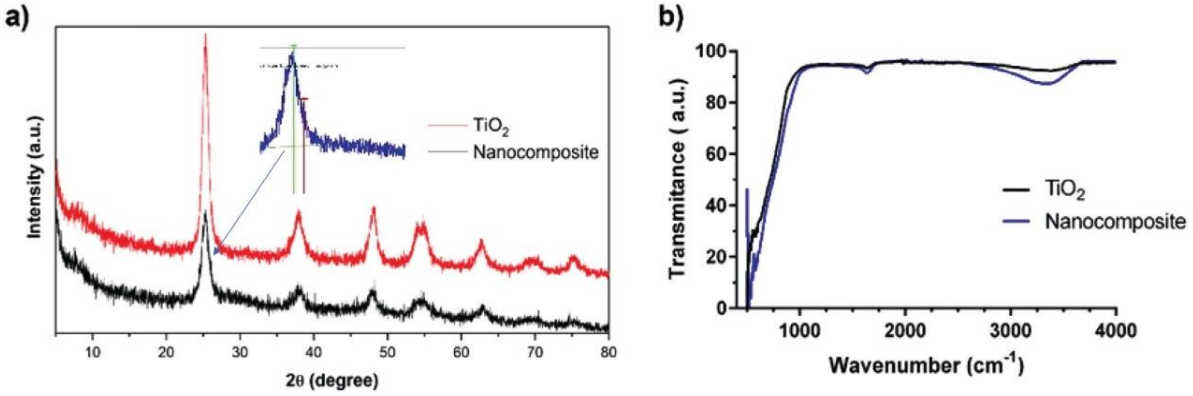


Figure 3. a) XRD patterns and b) FT-IR spectra of TiO_2 TiO_2–CDs nanocomposites.

were observed, being related to the bonds involving primary amines (—CH_2—NH_2) and amide carbonyl groups (—N—C=O), respectively. Figure S2d, Supporting Information shows the O 1*s* deconvolution, which shows a C=O contribution at 531.1 eV from carbonyl and carboxylate groups and a peak at 532.5 eV, attributed to C—OH/C—O—C This shows that their surface is dominated by carbonyl group (up to 2.5 times), indicating the high level of electron oxidation process. The optical characterization of the CDs was also made. The absorption spectrum of the CDs (Figure S3a, Supporting Information) displays a typical absorption profile of CDs. A well-defined band can be found at around 350 nm (ascribed to n→π^* transitions) and a shoulder is observed at 230 nm (attributed to $\pi \rightarrow \pi^*$ transitions).[74] The photoluminescent properties of the CDs were also evaluated. From the excitation-emission matrix (Figure S3b, Supporting Information), we observed that the CDs present a single emissive center, with an emission peak at 440 nm for an excitation of 350 nm. The corresponding excitation and emission spectra at these wavelengths (Figure S3a, Supporting Information) reveal that the maximum excitation occurs in the UV region, in a zone which overlaps the radiation primarily absorbed by TiO_2, whereas the emission extends from around 375 to 600 nm. The QY_{PL}, as calculated using quinine sulphate as a reference,[75] was 63.5%, a relatively high value for CDs.

2.2. Photocatalytic Studies

2.2.1. Evaluation of the Photocatalytic Performance

In this work, we used CDs prepared via a hydrothermal methodology (200 °C for 24 h) using citric acid (CA) and ethylenediamine (EDA) as precursors. Bare TiO_2 was obtained from titanium (IV) isopropoxide (TTIP) using a methodology previously used by our group.[76,77] The nanocomposites were prepared in a similar manner but with the addition of CDs.

Different nanocomposites were initially prepared with different CDs wt% (1%, 2%, and 4%) and their catalytic efficiency was evaluated by degrading MB (2.5 mg L^{-1}) under visible-light irradiation. Toward that end, we started with some preliminary tests (60 min of irradiation time) to compare the nanocomposite to bare TiO_2 and assess the best CDs wt% to be used in the nanocomposites. As indicators of the catalytic performance, we calculated the percentage of dye removal for a given period of time (%DR, Equation (1))[78,79] and the reaction rate constant (Equation (2)). For the %DR, the following equation was used:

$$\%\mathrm{DR} = \frac{C_0 - C_t}{C_0} \times 100 \quad (1)$$

Here, %DR is the percentage of MB degraded during a given period of time, C_0 corresponds to the initial concentration of MB and C_t to the concentration of MB at the time *t*. The MB concentration was calculated by measuring the absorbance at 665 nm (corresponding to the absorption peak of MB, $\epsilon_m = 73460\ M^{-1}\ cm^{-1}$) via UV–vis spectrophotometry.[80,81]

Further, we proceeded to evaluate the degradation rate constant of MB. The kinetic equation of the photodegradation followed a pseudo-first-order reaction that could be expressed as follows:[82]

$$-\ln\left(\frac{C_t}{C_0}\right) = kt \quad (2)$$

C_t corresponds to the concentration of MB at different reaction times, C_0 indicates the initial concentration of MB, *k* is the estimated reaction rate constant, and *t* is the time of exposure to visible-light irradiation.

The initial tests revealed that, upon 60 min of visible light irradiation, and using the same amount of catalyst (20 mg), the 2 wt% TiO_2-CDs nanocomposites performance was better than that of the 1 wt% and 4 wt% nanocomposites (Table S1, Supporting Information). In these conditions, the 2 wt% nanocomposites achieved a %DR of 41.6% ± 1.9%, whereas bare TiO_2 achieved a %DR of 16.6% ± 1.6%. Furthermore, the rate constant of the nanocomposites, up to 60 min of irradiation, was 0.0078 min^{-1} versus 0.0023 min^{-1} for TiO_2. These results clearly demonstrated that the introduction of CDs significantly increased the catalytic efficiency of the catalysts under visible-light irradiation and that further tests should be made. In another preliminary test, already using a 2 wt% nanocomposite, the effect of the MB concentration on the photodegradation was

 © 2023 Wiley-VCH GmbH

ADVANCED SCIENCE NEWS
www.advancedsciencenews.com

ADVANCED SUSTAINABLE SYSTEMS
www.advsustainsys.com

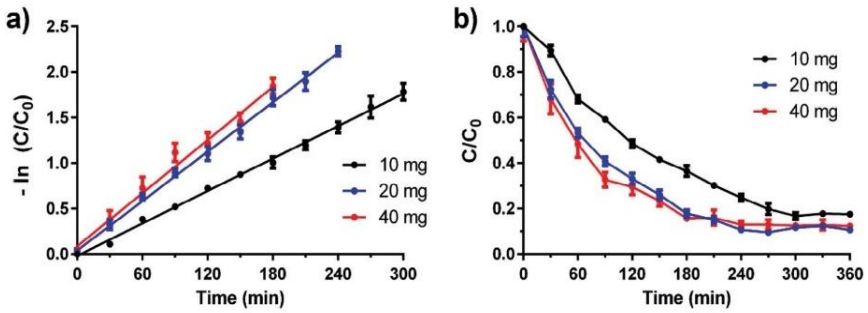


Figure 4. a) Plot of $-\ln(C_t/C_0)$ versus visible-light irradiation time for different catalysts amounts. Plot represented until degradation plateau is reached. b) C_t/C_0 values for the catalytic degradation of MB under visible-light irradiation.

evaluated (Table S2, Supporting Information). The optimal concentration of pollutant for the catalytic degradation was 2.5 mg L^{-1}, presenting both the higher rate constant and %DR of the tested concentrations, being thus chosen for the subsequent tests.

After the preliminary tests made to evaluate the effectiveness of the nanocomposite compared to the benchmark, TiO_2, we started by assessing the effect of the nanocomposite amount on the photodegradation rate (**Figure 4**) by testing three different photocatalyst amounts (10, 20, and 40 mg, corresponding to 0.1, 0.2, and 0.4 g L^{-1} of catalyst). It was observed that for the three tested amounts (10, 20, and 40 mg), the highest amount yielded the best rate constant ($k = 0.00972$ min^{-1}), whereas the 10 and 20 mg amounts presented rate constants of 0.00594 and 0.00934 min^{-1}, respectively (Figure 4a). Moreover, the time required to reach the degradation plateau was also dependent on the amount (Figure 4b), with the 40 mg amount resulting in the fastest time (180 min), followed by the 20 mg (240 min) and 10 mg (300 min) amounts. The 20 and 40 mg amounts achieved virtually the same final pollutant %DR (89.2% and 87.7%, respectively), whereas the amount of 10 mg seemed to be somewhat less effective in the same conditions (%DR of 82.3%). Adsorption in the dark phase (30 min before irradiation) was similar for all tests. However, when we normalized the rate constants by the amount of photocatalyst, the results were fully inverted, with the rate constants for the 10, 20, and 40 mg amounts being 0.594, 0.467, and 0.243 min^{-1} g^{-1}, respectively. Considering that similar %DR and rate constants were observed for the 20 and 40 mg amounts, the lower amount was chosen for subsequent studies.

Following that, the nanocomposites' efficiency was compared to that of visible-light-driven photolysis, CDs, and bare TiO_2 under the same conditions, namely 20 mg catalyst loading (or the calculated equivalent amount of CDs contained in 20 mg of nanocomposite), MB concentration of 2.5 mg L^{-1}, and pH 5 (**Figure 5**). Firstly, the effect of photolysis on the photodegradation of MB under visible light irradiation was quite limited, both in terms of rate constant and %DR. In fact, the estimated rate constant was 0.0012 min^{-1}, and the %DR was 35.5% after 360 min of irradiation. From this follows that photolysis was not the major responsible in the process. Secondly, after 360 min of visible-light irradiation, the CDs did not show any catalytic activity by themselves. The estimated rate constant and %DR of the photodegradation of MB in their presence were 0.011 min^{-1} and 33.5%, respectively, virtually equal to the values obtained for photolysis, suggesting that all photodegradation observed in this case may be a direct result of irradiation alone. Finally, both the catalytic rate constant and %DR of the TiO_2–CDs nanocomposite were clearly superior to that of TiO_2. Namely, the rate constant of the nanocomposites was 0.00934 min^{-1} versus 0.0020 min^{-1} for TiO_2 (which is relatively close to that of photolysis, confirming the poor efficiency of TiO_2 under visible-light irradiation).

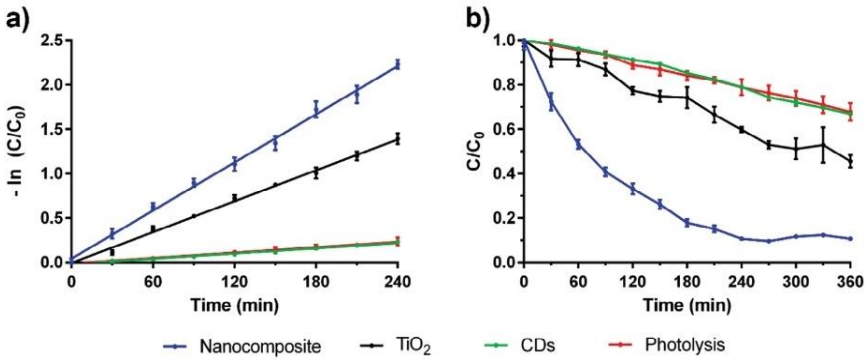


Figure 5. a) Plot of $-\ln(C_t/C_0)$ versus visible-light irradiation time for TiO_2–CDs nanocomposites (20 mg), TiO_2 (20 mg), CDs (quantity equal to that present in 20 mg of nanocomposite), and photolysis. b) C_t/C_0values for the catalytic degradation of MB under visible-light.

 © 2023 Wiley-VCH GmbH

ADVANCED SCIENCE NEWS
www.advancedsciencenews.com

ADVANCED SUSTAINABLE SYSTEMS
www.advsustainsys.com

Considering the higher %DR and rate constants of the nanocomposite, we quantified the increment of the catalytic performance upon the addition of CDs by using Equation (3)[78,79]:

$$\%\ \ln(C) = 100 \times \frac{k_{NC} - k_{TiO_2}}{k_{TiO_2}} \quad (3)$$

Here, % ln(C) is a relative measure of the increment of the catalytic performance of TiO_2 upon the addition of CDs, k_{NC} is the rate constant in the presence of the respective nanocomposite, and k_{TiO2} is the rate constant of TiO_2 in the same conditions.

The calculated % ln(C) for our TiO_2–CDs nanocomposite was 367%, indicating a considerable increment of catalytic activity of TiO_2 upon the addition of CDs. Regarding the %DR, for the nanocomposites, it reached 89.2% after 240 min of irradiation (a value still maintained at 360 min of irradiation), whereas for TiO_2, it was near 53.4% after 360 min of irradiation. The photodegradation of MB was further confirmed using FTIR and chemical oxygen demand (COD) analysis. The FTIR spectra (Figure S4, Supporting Information) after background correction for water, showed a decrease of the initial peaks after the photodegradation process; thus, confirming the degradation of the initial pollutant. As for COD (Figure S5, Supporting Information), it is a measure of the oxygen necessary to oxidize the organic material present in an aqueous sample, having already been used to confirm the photocatalytic degradation of MB samples.[83,84] By COD analysis, we observed that there is a clear decrease in the oxidizable content of the MB sample after the irradiation period. The obtained values indicate a degradation of the pollutant of an extent similar to that observed via absorbance at 665 nm (84.1% vs 89.2%, respectively). Finally, by comparing the full UV–vis absorption profile of the MB samples before and after the irradiation (Figure S6, Supporting Information), we can observe, as expected, a clear decrease in the absorption peaks associated with MB, confirming the success of the catalytic degradation. Furthermore, no new peaks appear after the process, suggesting that there are no UV–vis absorbing sub-products originating from the degradation of MB.

2.2.2. Scavenger Studies

To obtain more information about the mechanism behind the enhanced catalytic performance of TiO_2–CDs nanocomposites when compared to bare TiO_2, experiments with free radical scavengers were conducted. In a study aiming to reveal which oxidative species were responsible for the photocatalytic reaction, IPA (10 mM),[76] *p*-Benzoquinone (1 mM),[85] potassium iodide (10 mM),[76] potassium nitrate (10 mM),[86] and sodium azide (1 mM)[63] were used as scavengers for hydroxyl radicals (·OH), superoxide radicals ($O_2^{\cdot-}$), holes (h^+), electrons (e^-), and singlet oxygen ($^1O_2$), respectively. These reactive species were targeted as they are known to be participants in the mechanism behind the catalytic performance of TiO_2 and its respective composites.[48] Particular attention should be given to tests with IPA and *p*-Benzoquinone, which are the scavengers for the two most reactive species typically involved in the mechanism of TiO_2, hydroxyl and superoxide radicals, respectively.[76,85]

The variation of the %DR in the presence of the different reactive species scavengers was calculated using Equation (4):

$$\%DRV = \%DR_{test} - \%DR_{control} \quad (4)$$

Here, %DRV corresponds to the %DR variation in the presence of the scavenger ($\%DR_{test}$) in comparison to a control test ($\%DR_{control}$, standard photodegradation with TiO_2 or the TiO_2–CDs nanocomposite).

The test regarding the TiO_2–CDs nanocomposites (**Figure 6**a) shows a negative %DRV under visible light irradiation, suggesting that the photodegradation is inhibited in the presence of both *p*-Benzoquinone and IPA. While the reduction of the %DR in the presence of IPA is small (%DRV of −5.6% ± 0.5%); and thus, the role of hydroxyl radicals in the photodegradation seems to be limited, it is of considerable extent in the presence of *p*-Benzoquinone (%DRV of −29.3% ± 0.4%). Further, as observed in Figure 6a, tests with potassium iodide, potassium nitrate, and sodium azide did not result in any statistically significant change in the %DR, indicating that the corresponding reactive species (h^+, e^-, and $^1O_2$, respectively) are not involved in the reaction. It is worth noting that photolysis by itself can be responsible for a %DR of around 20% in the same conditions, even in the absence of the nanocomposites, and so, should be taken into consideration in the scavenger tests.

For TiO_2–CDs nanocomposites, under visible-light irradiation, when both superoxide and hydroxyl radicals are scavenged, the photocatalytic efficiency is affected. Superoxide radicals, in addition to hydroxyl radicals, seem to be the main reactive species involved in the photocatalytic reaction promoted by TiO_2–CDs nanocomposites. To date, several reports concerning TiO_2–CDs nanocomposites indicate that the superoxide radical may play a major role in the process and be the primary reactive specie promoting the photodegradation.[76,64] In fact, studies reporting specifically the dominance of superoxide-driven over hydroxyl-driven photodegradation of MB by TiO_2–CDs nanocomposites have already been reported by other authors and are in line with our results.[59,60,87]

The same test was made for bare TiO_2 (Figure 6b) with the scavengers corresponding to the most relevant reactive species observed for the nanocomposites (IPA and *p*-Benzoquinone). Similar to before, IPA again seems to present a slightly negative %DRV (−8.0% ± 1.4% compared to TiO_2 alone), indicating that the hydroxyl radical can be involved in the catalytic process, to an extent comparable to that observed with the nanocomposite. However, unexpectedly, *p*-Benzoquinone now seems to be enhancing the catalytic efficiency, with a %DRV of 33.2% ± 3.1% when compared to the control. While this was not expected, it could be explained by the fact that the photoreduction of quinones in water was already reported to originate hydroxyl radicals.[88] Moreover, due to being easily reduced, quinones enable electron trapping in the conduction band of the catalyst and can easily hinder electron–hole recombination, leaving the hole free to oxidize water to hydroxyl radicals.[17] To test this hypothesis and see if there was production of hydroxyl radicals in the presence of *p*-Benzoquinone, tests were made with the same concentration of *p*-Benzoquinone and an increasing concentration of hydroxyl radicals' scavenger (IPA) (Figure 6c). We observed that when the concentration of IPA was increased,

 © 2023 Wiley-VCH GmbH

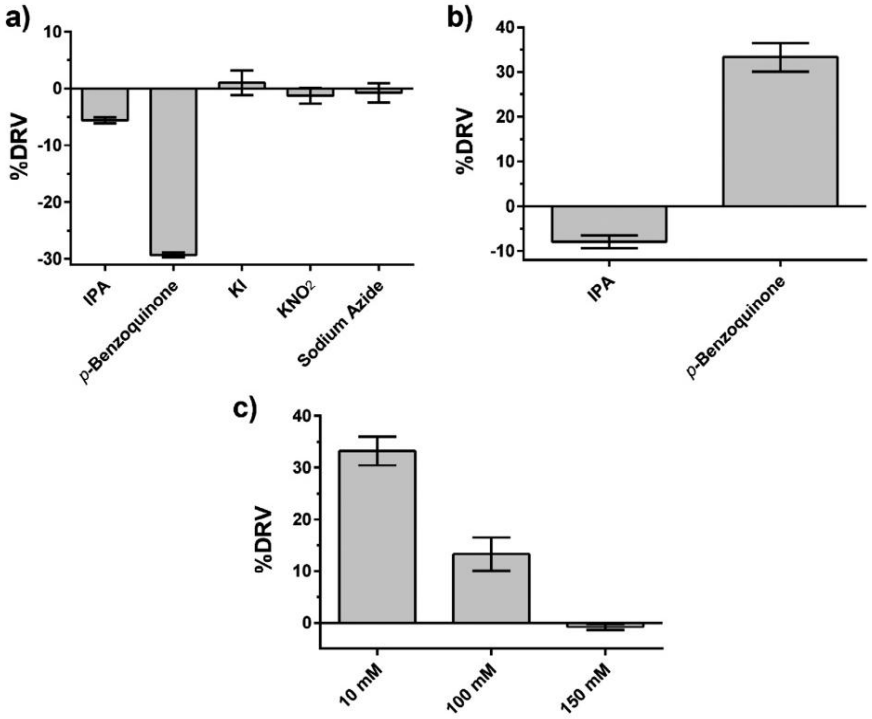


Figure 6. a) MB photodegradation tests with nanocomposites in the presence of reactive species scavengers. b) Scavengers test with TiO_2 in the presence of scavengers for species of relevance for the TiO_2–CDs nanocomposite. c) Scavenger tests with TiO_2 and a combination of a constant concentration of *p*-Benzoquinone with various concentrations of IPA. Results for (a,b,c) are presented in the form of %DRV. Positive values indicate an increase in the photocatalytic efficiency in the test when compared to the control, whereas negative values indicate a decrease.

the enhancing effect induced by *p*-Benzoquinone was gradually reduced. In fact, for the highest tested IPA concentration, the %DRV was virtually negligible (−0.8% ± 0.6% difference). At this point, all *p*-Benzoquinone-derived hydroxyl radicals would interact with IPA, and their effect would be nullified.

In summary, the superoxide anion is the major responsible for the photocatalytic effect of the nanocomposites. This differs from TiO_2, whose major contributing species is the hydroxyl radical, indicating that the CDs' addition alters the photocatalytic mechanism of the nanocomposite when compared to bare TiO_2. Differences in the mechanism of bare TiO_2 CDs-based nanocomposites have already been reported by Zhang et al.,[60] who reported different primary reactive species before and after the addition of CDs to the nanocomposite. Prior to the addition of CDs, only hydroxyl radicals and h^+ appear to have a relevant role in the photodegradation, whereas after adding CDs, the superoxide radical is almost as important as the hydroxyl radical for the photodegradation.[60] This change in the photodegradation mechanism upon the addition of CDs is well in line with our own results with our nanocomposite.

2.2.3. Comparison With Literature

Our work focuses on the improvement of the catalytic performance upon the addition of CDs to TiO_2. We evaluated the extent and the degree to which adding CDs increased the resulting nanocomposites' catalytic potential. Toward this, we compared the enhancement of the catalytic performance (% ln(C)) of our nanocomposite with other similar composites in the literature, before and after the addition of CDs. The comparison parameter, % ln(C), accounts for the fact that the conditions in which different studies were performed may vary in terms of several parameters (e.g., lamp intensity and light profile, pollutant concentration and identity, catalyst amount, reaction volume, and properties of used bare TiO_2, among others). This is important as these different conditions may affect the absolute photocatalytic efficiency; and thus, it may not be the most accurate way of evaluating the enhancement effect directly exerted by the addition of CDs. Furthermore, as our goal is to study the enhancing effect of CDs when considering a multi-component system, the % ln(C) was calculated to showcase the difference originated by the addition of CDs alone. The nanocomposites' performance increase upon CDs addition is reported in **Table 1**, along with other works available in the literature.

From the data summarized in Table 1, it is observable that in our nanocomposite, the addition of CDs to TiO_2 led to an increase of considerable extent of the catalytic performance of the resulting nanocomposite. The calculated % ln(C) for our nanocomposite was 367%, which is superior to all studies reported in the table. It should be further highlighted that the calculated % ln(C) of our nanocomposite, while higher, was quite similar to that presented by another nanocomposite in which the CDs were also obtained by CA and EDA.[60] Thus, these works indicate that this pair of

 © 2023 Wiley-VCH GmbH

ADVANCED SCIENCE NEWS
www.advancedsciencenews.com

ADVANCED SUSTAINABLE SYSTEMS
www.advsustainsys.com

Table 1. Summary of studies concerning the visible-light photodegradation of organic dyes by CDs-based TiO_2 nanocomposites. Catalyst dosage and MB concentration are presented in g L^{-1} and mg L^{-1}, respectively. NA – information not available. * – Estimated from a figure.

Nanocomposite	CDs precursors	CD wt%	Pollutant	Catalyst dosage	MB conc.	Time [min]	% ln(C)	Ref.
TiO_2–CDs	CA + EDA	2	MB	0.2	2.5	240	367	This work
Molecularly imprinted TiO_2–CDs	Lignite + H_2O_2 + Formic acid	NA	MB	0.5	10	120	64	[64]
TiO_2–Ag–CDs	Ethylene glycol	NA	MB	0.5	10	120	233	[59]
TiO_2–Fe_2O_3–CDs	CA + EDA	NA	MB	0.5	20	180	366	[60]
Oxygen-rich TiO_2_Peroxo–CDs	CA + Urea	0.9	MB	0.4	3.2	NA	130	[61]
Oxygen-rich TiO_2–Peroxo–CDs	CA + Urea	NA	Methyl orange	0.4	3.2	NA	200	[61]
TiO_2 microspheres–CDs	Glucose	NA	Rhodamine B	2.0	10	90	160*	[89]

carbon precursor and N-dopant show relevant potential to generate CDs with enhancing properties for photocatalysis. This finding should be further pursued in future research.

2.3. CDs' Toxicity Assay

Thus far, in this work, we have described a potential TiO_2–CDs nanocomposite for photocatalytic applications. As with any potential product, the possibility of the nanocomposites being toxic to human health needs to be considered and properly assessed as it could directly or indirectly affect human health. Nanomaterials are starting to be detected as contaminants in the environment, surface waters, and sewers.[90–92] Whether being released via spillage or leakage, they could also indirectly reach humans by contaminating agricultural soil, and thus, the food chain.[90–92] While there are already several studies concerning the contamination and human health impacts of TiO_2,[93,94] the toxicity of our CDs still needs to be evaluated.

To determine the cytotoxicity of CDs, we treated A549 cells with increasing concentrations (0.1 to 2.35 g L^{-1}) of CDs for 24 and 72 h. The results were obtained by an MTT viability assay (**Figure 7**). Morphological evaluations were also conducted to assess any observable changes in the phenotype of the cells (Figure S7, Supporting Information).

The effect of CDs on cell viability was not statistically significant. No significant CDs-derived cytotoxic effect was observed for both the 24 and 72 h incubation periods. This is well in line with other reports that attribute very low toxicity to CDs, making them suitable for biological applications.[32,33]

2.4. LCA Studies

Considering the intended application of the nanocomposite, its associated environmental impacts must be investigated. LCA studies are a tool that aims to quantify the environmental impacts of a process/product during its life cycle. Thus far, they have already been used in the environmental evaluation of several nanomaterials, including both CDs[95,96] and TiO_2.[97,98] A LCA study was made to assess if the enhanced catalytic performance of the nanocomposite was worth the potential additional impacts that result from the inclusion of the CDs in the system. To this end, the environmental impacts resulting from TiO_2 and TiO_2–CDs nanocomposites were evaluated and compared using both a weight-based functional unit and a function-based functional unit, scaled based on the rate constant of each catalyst.[95,99]

We started by performing a comparison between the impacts using a weight-based functional unit of 1 kg of produced material. It should be noted that our aim is not to make quantitative appreciations of the environmental impacts of each input. Rather,

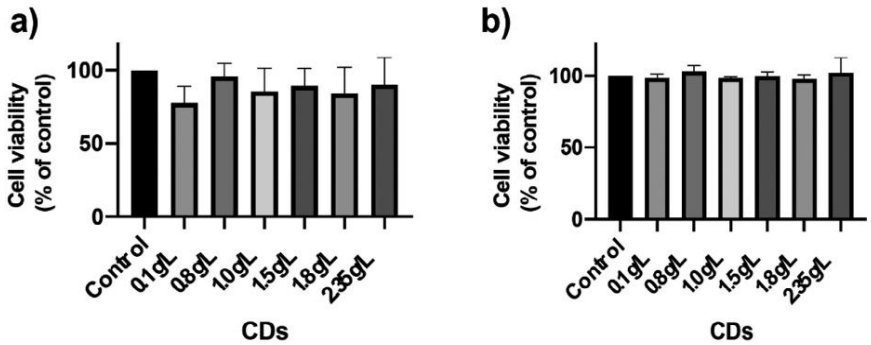


Figure 7. Cell viability of A549 cancer cells treated with CDs for a) 24 h and b) 72 h. Cultured cells were seeded in 96-well plates and treated with CDs (0.1–2.35 g L^{-1}). Cells treated with vehicle (0.1% DMSO) were used as the control. Values are expressed as percentages of control and represent means ± SEM. Each experiment was done three times independently ($n = 3$). *Statistically significant versus control at $p < 0.1$. ** Statistically significant versus control at $p < 0.01$. *** Statistically significant versus control at $p < 0.001$. ****Statistically significant versus control at $p < 0.0001$.

 © 2023 Wiley-VCH GmbH

ADVANCED SCIENCE NEWS
www.advancedsciencenews.com

ADVANCED SUSTAINABLE SYSTEMS
www.advsustainsys.com

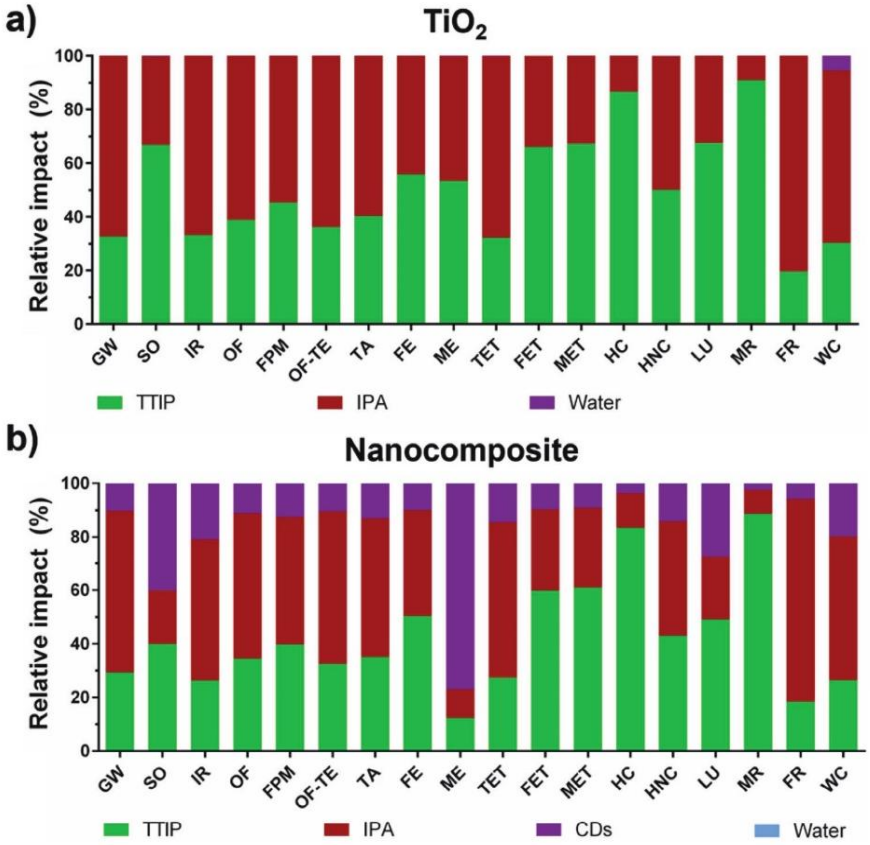


Figure 8. Relative environmental impacts of a) TiO_2 and b) TiO_2–CD nanocomposite with the ReCiPe2016 LCIA using a weight-based unit of 1 kg of photocatalyst.

we aim to compare the contributions to the different impact categories of the input resources involved in the preparation of each catalyst and compare the relative resource-derived impacts between TiO_2 and TiO_2–CDs nanocomposite. Impacts associated with energy-usage were not directly considered in this study as they do not vary between the different nanomaterials, and so, do not affect their relative impacts.

First, regarding TiO_2 (**Figure 8**a), the environmental impacts are almost entirely due to TTIP and IPA, with a small fraction being attributed to deionized water in the category of water consumption. TTIP is of particular importance for the categories of stratospheric ozone depletion, freshwater ecotoxicity, marine ecotoxicity, human carcinogenic toxicity, and mineral resource scarcity, whereas IPA is a major contributor to the categories of global warming, ionization radiation, ozone formation (human health and terrestrial ecosystems), fine particular matter formation, terrestrial acidification, terrestrial ecotoxicity, fossil resource scarcity, and water consumption. Regarding the nanocomposites (Figure 8b) and considering the addition of CDs, the relative ratios between the impacts of TTIP and IPA remain more or less the same. The 2 wt% of CDs contributes with particular emphasis to the impact categories of marine eutrophication, in which CDs are responsible for nearly 80% of the impacts, and stratospheric ozone depletion, in which the impact contribution of CDs is similar to that of TTIP. The small scale of the impacts associated with CDs, for most categories, can be ascribed to the small amount of CDs used for the nanocomposite when compared to TTIP and IPA.

To facilitate the comparison between TiO_2 and the nanocomposites, they are compared in **Figure 9** in terms of endpoint impact categories: human health, ecosystems, and resources. When considering the weight-based functional unit (Figure 9a), the relative environmental impacts of TiO_2 are slightly smaller than those of the nanocomposites (91.9%, 90.2%, and 97.6% of those of the nanocomposites for human health, ecosystems, and resources categories, respectively). This is explained by the fact that the difference in inputs between TiO_2 and the nanocomposites is just a small decrease in the quantity of TTIP and IPA and the addition of a small quantity of CDs (2 wt%). As the synthesis of CDs is associated with a low yield (2.35%), this can lead to a slightly higher relative impact associated with the making of the nanocomposite when compared to TiO_2.

The environmental impact profiles of the photocatalysts were also rescaled with respect to the reaction rate constant obtained with both TiO_2 and the TiO_2–CDs nanocomposite on the same conditions (Figure 9b). The rescaling was made by considering

 © 2023 Wiley-VCH GmbH

ADVANCED SCIENCE NEWS
www.advancedsciencenews.com

ADVANCED SUSTAINABLE SYSTEMS
www.advsustainsys.com

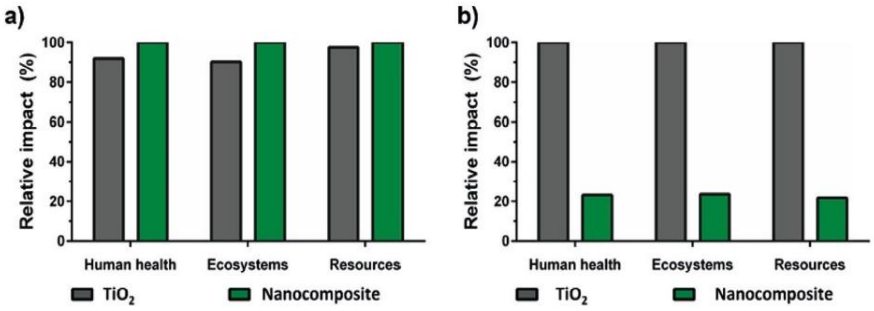


Figure 9. Comparative environmental profiles for TiO2 and TiO_2–CDs nanocomposites were obtained using ReCiPe 2016 v1.1 as LCIA. Comparison made using a) a weight-based functional unit and b) a rate constant-based functional unit.

the highest rate constant (0.00934 min^{-1} for the nanocomposite) as the reference. The functional unit by which the rescaling of the impacts concerning TiO_2 was made was obtained by dividing 000934 min^{-1} by the rate constant of bare TiO_2 (0.0020 min^{-1}); thus, obtaining a normalized functional unit of 4.67. With the rescaling, the environmental impact profiles change drastically. Now, due to the considerably higher performance in terms of MB photodegradation, the nanocomposites present a lower impact than TiO_2. For the human health, ecosystems, and resources impact categories, the impacts of the nanocomposite were 23.3%, 23.7%, and 21.9% of those of TiO_2, respectively.

In summary, due to the higher photocatalytic potential of the nanocomposites, even though they have a slightly higher relative environmental impact than TiO_2 when considering a weight-based functional unit of 1 kg, this changes when we consider an application-based functional unit. This indicates that the nanocomposite is an environmentally friendlier alternative to TiO_2 for the purpose of photocatalysis.

3. Conclusions and Outlook

By using CDs to bridge the limitations of TiO_2 as a visible-light photocatalyst, we have synthesized a TiO_2–CDs nanocomposite with enhanced visible-light catalytic performance for the photodegradation of MB. The CDs, synthesized from CA and EDA via hydrothermal treatment, were added to TiO_2, resulting in the nanocomposite. The as-synthesized nanocomposite catalyst exhibits a superior catalytic performance when compared to bare TiO_2, presenting a % ln(C) of 367% upon the addition of CDs to the semiconductor. Furthermore, the %DR also increased from 53.4% (360 min of irradiation) to 89.2% (240 min of irradiation). Tests with scavengers for reactive species revealed that the species behind the catalytic activity of the nanocomposite were the superoxide radical, followed by the hydroxyl radical, which differed from the results obtained with bare TiO_2. Characterization of the CDs, TiO_2, and TiO_2–CDs nanocomposites was performed. It was observed that the addition of CDs does not alter the semiconductor's structure as the crystal planes of TiO_2 were not changed after adding the CDs. Further, the overall visible-light absorption capacity was improved and the recombination of photogenerated charge carriers was hindered. This results in an enhanced catalytic performance by the nanocomposite when compared to TiO_2. In terms of human toxicity, the CDs presented no cytotoxicity toward the tested human cellular line, which is important as their intended application could result in emissions into both the environment and domestic systems. Finally, working toward environmental sustainability, we performed an LCA study to evaluate the relative environmental impacts associated with both TiO_2 and the nanocomposite. When only the weight of the catalyst was considered, the nanocomposite presented a slightly higher impact due to using a small quantity of CDs. However, when taking into consideration the intended application of the catalysts, those impacts were greatly offset by its enhanced potential. The current study demonstrates that the addition of CDs to TiO_2 may produce composites with enhanced activity; thus, providing an important step toward the design and development of highly-active, under visible-light-irradiation, and environmentally sustainable photocatalysts.

4. Experimental Section

Materials: TTIP (99.99%), CA (99.5%), EDA (99%), sodium azide (99.5%), and *p*-benzoquinone were purchased from Sigma–Aldrich. IPA (99.9%) was obtained from Fisher Chemical. MB was acquired from Carlo Erba. Potassium nitrate (99%) and potassium iodide (99%) were purchased from Merck. All reagents were used as received without further purification.

CDs Synthesis and Purification: The synthesis was made following a hydrothermal methodology.[100–102] Briefly, CA (0.15 g) and EDA (166.9 µL) were mixed and dissolved in NaOH 0.01 M (10 mL). The mixture was then transferred into a *Teflon*-lined recipient which was inserted into a steel outer shell, and then subjected to a temperature of 200 °C for 24 h in an oven (VWR DL 112 Prime oven, 2500 W power consumption). After this period, the recipient was allowed to cool down to room temperature and then the reaction products were subjected to centrifugation (6000 rpm, 30 min) to remove insoluble components. Afterward, it was subjected to dialysis (24 h, MWCO of 3.5 kDa) to remove soluble by-products, formed during the synthesis, that may affect the nanoparticles' properties and photoreactivity.[103] The synthesis yield of the whole process was 2.35%. Finally, to ascertain the mass concentration of the CDs, the purified CDs solution was subjected to lyophilization, weighted, and dissolved in deionized water (5 mL). The CDs were then kept in the cold (4 °C) until use.

TiO_2/CDs Nanocomposites Preparation: The preparation of the nanocomposites starts with the preparation of TiO_2, followed by the synthesis of the nanocomposites. For TiO_2,[77,104] for an expected yield of 0.5 g of TiO_2, TTIP (1.855 mL) was added dropwise to IPA (11.975 mL, 1:25 TTIP:H_2O ratio), and the mixture was left to stir for 30 min. Afterward, deionized H_2O (11.25 mL, 1:100 TTIP:H_2O ratio) was added dropwise and the mixture stirred for an extra 2 h. Simultaneously, the quantity of CDs solution needed for a mass equivalent of 1% to 4% of that of TiO_2 was diluted in deionized H_2O (5 mL) and put under stirring

 © 2023 Wiley-VCH GmbH

ADVANCED SCIENCE NEWS
www.advancedsciencenews.com

ADVANCED SUSTAINABLE SYSTEMS
www.advsustainsys.com

at 70 °C for 90 min. The CDs solution was then added dropwise to the TiO_2 suspension, which was followed by another 2 h of magnetic stirring. After stirring, the resulting product was washed with H_2O and vacuum filtered and dried in an oven (VWR DL 112 Prime oven, 2500 W) overnight at 100 °C. The dried product was powdered in a mortar and subjected to a temperature of 300 °C (in a Thermolyne 47900 muffle furnace, 1000 W) for 3 h (heating rate of 5 °C min^{-1}), resulting in a nanocomposite ready to be used. Bare TiO_2 was prepared in a similar manner but without the addition of the CDs solution. Both TiO_2/CDs nanocomposites and bare TiO_2 were kept in the dark until use.

Materials Characterization: Morphologic analyses of TiO_2 and TiO_2/CDs nanocomposites were obtained using a high-resolution scanning electron microscope (SEM) system (FEI Quanta 400 ESEM FEG). For this purpose, powder samples were dispersed in carbon tape. Sizes were calculated by averaging the measurements of 100 individual particles.

Absorption of the TiO_2–CDs nanocomposites was recorded via UV–vis spectroscopy in a Jasco V-760 spectrophotometer, equipped with an integration sphere (Jasco ILV-924), using $BaSO_4$ as a reference. For the CDs' absorption studies, the absorption spectra were recorded using a VWR UV3100PC spectrophotometer (with the UV–vis Analyst software) and standard 10 mm quartz cells.

The photoluminescence spectra of the CDs were obtained using a Horiba Jovin Yvon Fluoromax-4 spectrofluorimeter while employing the FluorEssence software to analyze the results. Standard 10 mm fluorescence quartz cells were used.

Infrared spectra were recorded in a Vertex70 FTIR spectrometer by Bruker in solid state and by means of an attenuated total reflectance (ATR) golden gate single reflection diamond ATR system accessory. A standard spectral resolution of 4 cm^{-1}, a spectral range of 4000–500 cm^{-1}, and 64 accumulations were employed, measuring air background.

Laboratory X-ray powder diffraction (XRPD) patterns were collected on a PANanalytical EMPYREAN automated diffractometer. Powder patterns were recorded in Bragg–Brentano reflection configuration by using the PIXcel 3D detector with a step size of 0.017° (2θ). The powder patterns were recorded between 5 and 70 in 2θ with a total measuring time of 60 min.

AFM analysis was carried out using a Veeco Metrology Multimode / Nanoscope IVA by tapping. A silica plate was used to deposit the sample for analysis and an AFM TESP-SS cantilever (curvature radius of 2 nm) was used. Samples were prepared via drop evaporation of a diluted CDs solution. The software used for the AFM data analysis was NanoScope. Particle size measurements were made based on the height of the particles. The average size was calculated by averaging the measurements of 100 individual particles.

X-ray photoelectron spectroscopy (XPS) was carried out using a Kratos Axis Ultra HSA spectrometer utilizing Al monochromatic radiation with a hemispherical multichannel detector (90 W and 15 kV). The analyzed sample was prepared upon a silicon wafer by dropping a drop of CDs solution and letting it dry, forming a uniform layer on top of the wafer. CasaXPS software was used to analyze the results and the carbon C 1s signal, 285.0 eV, was used as a reference to obtain the binding energy values, using Gauss–Lorentz curves and Shirley-type background.

Photoluminescent Quantum Yield (QY_{PL}) Calculations: The QY_{PL} was calculated via a standard procedure based on the comparison of the integrated photoluminescence intensities and absorbance values of the prepared CDs with those of a reference fluorophore. The QY_{PL} value in percentage was obtained by using the following equation:

$$QY_{PL}^{Sample} = QY_{PL}^{Ref} \times \frac{Grad_{Sample}}{Grad_{Ref}} \times \frac{\eta_{Sample}^2}{\eta_{Ref}^2} \times 100 \quad (5)$$

In the above equation, Grad corresponds to the gradient of the plot of integrated fluorescence intensity versus absorbance for both the sample and the reference fluorophore and η is the refractive index of the medium. Quinine sulphate was chosen as the reference fluorophore (QY_{PL} = 54%) for the quantum yield calculations due to the similarities of its photoluminescent properties to those of our CDs.[105]

Photocatalytic Activity Assays: The photocatalytic performance of both TiO_2–CDs nanocomposites and bare TiO_2 were assessed with a visible-light lamp (MainHouse energy saving lamp, 23 W, 6400 K, 1311 Lm) previously used by our team.[76,77] The photodegradation of 2.5 mg L^{-1} of MB under visible-light irradiation was analyzed and used to compare both catalysts. In a typical experiment, 10 to 40 mg of catalyst was suspended in 100 mL of a MB aqueous solution (2.5 mg L^{-1}). Before irradiation, the mixture was subjected to 1 min of ultrasonic treatment to better disperse the catalyst and 30 min of magnetic stirring to establish adsorption–desorption equilibrium.[106] After that, the irradiation source was turned on and aliquots were collected at $t = 0$ and every 30 min after. An additional aliquot was collected before 30 min of magnetic stirring to observe the extent of the pollutant adsorption by the photocatalysts. After collection, the aliquots were subjected to centrifugation (10 000 rpm for 10 min) to separate the catalyst from the remaining MB. The catalytic photodegradation efficiency was evaluated by monitoring the MB concentration variation at 665 nm (corresponding to the absorption peak of MB, ϵ_m = 73460 M^{-1} cm^{-1})[80,81] via UV–vis spectrophotometry and comparing it to the concentration corresponding to $t = 0$.

COD analysis was made using Hanna Instruments COD Reactor (HI 839800), Multiparameter Bench Photometer (HI 83214), and Chemical Oxygen Demand – Medium Range reagents kit (HU 94754B-25). The kit was utilized following the protocol. Briefly, 2 mL of each sample was mixed with the reagents kit (containing dichromate ion), heated in the reactor (150 °C for 2 h), and allowed to cool down to room temperature. Samples were then analyzed using the photometer, allowing the measure of the oxygen demand of each sample.

Free Radical Scavenger Tests: To determine the contribution of the active species during the photodegradation of MB, the effects of various free radicals' scavengers on the photocatalytic efficiency of the nanocomposites were evaluated. In this experiment, to the previously described photocatalytic mixture, a certain quantity of scavengers previously used in other reports concerning photocatalysis was introduced. IPA (10 mM),[76] *p*-Benzoquinone (1 mM),[85] potassium iodide (10 mM),[76] potassium nitrate (10 mM),[86] and sodium azide (1 mM)[63] were used as scavengers for hydroxyl radicals (·OH), superoxide radicals (O_2–), holes (h^+), electrons (e^-) and singlet oxygen ($^1O_2$), respectively. Similar to before, the mixture was allowed to stir in the dark for 30 min to achieve adsorption–desorption equilibrium and then irradiated with visible light for 240 min, after which the degradation rate was calculated.

CDs' Toxicity Assays—Cell, Media, and Compounds: A549 adenocarcinomic human alveolar basal epithelial cancer cell line was obtained from the American Type Culture Collection (ATCC; Manassas, VA, USA) and grown in a humidified incubator with 5% CO_2 at 37 °C in DMEM medium (PAN-Biotech, Aidenbach, Germany) supplemented with 10% fetal bovine serum (FBS) and 1% penicillin–streptomycin (pen-strep) solution. These reagents were purchased on Millipore Sigma (Merck KGaA, Darmstadt, Germany). The medium was changed every 2–3 days.

CDs' Toxicity Assays—Cell Viability Assays: Cell viability was measured using the MTT (Thiazolyl blue tetrazolium bromide; cat. no. M5655; Sigma–Aldrich; Merck KGaA, Darmstadt, Germany) assay in 96-well plates. For the protocol, 5000 cells in 200 µL of medium were grown per well for 24 h at 37 °C. Then, cells were treated with CDs in the following concentrations: 0.1, 0.8, 1.0, 1.5, 1.8, and 2.35 g L^{-1}. The controls were treated with 0.1% H_2O and 0.1% DMSO (vehicles). After incubation for 24 and 72 h at 37 °C, cell media were aspirated and 100 µL of MTT solution (0.5 mg mL^{-1} in PBS) was added to each well. After incubation for 3 h at 37 °C protected from light, MTT solution was removed from each well and 100 µL of DMSO was added to solubilize the formazan crystals. Absorbance was measured on a Tecan Infinite M200 plate reader (Tecan Group Ltd., Männedorf, Switzerland) at 570 nm. Cell viability was calculated relative to the absorbance of carrier controls. Average values were obtained by performing three independent cell viability assays ($n = 3$).

CDs' Toxicity Assays—Morphological Analysis: Changes in cell morphology were evaluated after cell treatment using a Leica DMI 6000B microscope equipped with a Leica DFC350 FX camera (Leica Microsystems, Wetzlar, Germany). Images were analyzed with the Leica LAS X imaging software (v3.7.4) (Leica Microsystems, Wetzlar, Germany).

 © 2023 Wiley-VCH GmbH

ADVANCED SCIENCE NEWS
www.advancedsciencenews.com

ADVANCED SUSTAINABLE SYSTEMS
www.advsustainsys.com

CDs' Toxicity Assays—Statistical Analysis: Cell viability graphs were obtained using the software GraphPad Prism 9 (GraphPad Software Inc., San Diego, CA, USA) after conducting three independent experiments ($n = 3$). Results are represented as the mean ± SEM for n experiments performed. Statistical analysis was performed with one-way ANOVA tests by Dunnett's multiple comparisons between the control and treatment groups. Results were considered statistically significant for p values < 0.05.

LCA Studies—Scope and System Boundaries: This cradle-to-gate LCA study aims to compare the relative environmental impacts associated with the preparation of TiO_2 and TiO_2–CDs nanocomposites. This was done considering a laboratory-scale manufacturing of the target photocatalysts, considering the direct emissions and indirect impacts associated with the upstream resource extraction. The impacts associated with electricity were not considered. The production schemes for TiO_2 and the nanocomposites were as described in *TiO_2/CDs Nanocomposites Preparation*, and in a first stage, the environmental impacts were analyzed and compared based on a functional unit of 1 kg of produced material. As previously reported, using a weight or volume-based functional unit makes sense to compare the manufacturing of an equivalent quantity of similar nanomaterials.[107,108] On a later stage, the impacts were normalized by considering the rate constants obtained with each photocatalyst as a weight-based functional unit does not consider the utility for which the materials were produced. Thus, it may not account for the possibility that a more resource and energy-intensive synthesis may be justified by a higher functionality of the resulting material. The rate constant was chosen as the normalization factor as it is a good indicator of the purpose for which the materials were made, namely, photocatalysis.

LCA Studies—Life Cycle Inventory (LCI): TiO_2 and nanocomposites' environmental impacts were evaluated using foreground data from the synthesis procedure described in Section 2.3, previously prepared processes, and the LCI data for the foreground system consisted of average data found in the Ecoinvent 3.9.1 database. The foreground system was based on the Ecoinvent 3.9.1 database information for IPA (Isopropanol [RER]| market for isopropanol | Cut-off, S) and deionized water (Water, deionized, from tap water, at user [Europe without Switzerland] | market for), as well as processes, created by us, for the CDs and TTIP, which were not available on the Ecoinvent database. The process for CDs was modeled considering the methodology developed by us and described in Section 2.2 (background data on Table S3, Supporting Information), whereas the process concerning TTIP was made considering the methodology found in ref. [109] (background data on Table S3, Supporting Information).

In this study, the same electricity input was required by both processes (TiO_2 and the nanocomposites), meaning that the comparative results were not affected by this parameter. In addition, the procedures were made at a laboratory scale in which neither the oven or furnace nor the stirring plate were used to their full capacity in terms of quantity. Thus, it can be difficult to accurately calculate the real electricity usage as the equipment used was not adjusted to the small quantities of catalysts produced by us. Given that the scope of the study was merely to compare TiO_2 and TiO_2–CDs nanocomposites in terms of relative environmental impacts and that both processes would consume the same amount of electricity, the contribution of electricity-related impacts was not included in this LCA study.

LCA Studies—Life Cycle Impact Assessment (LCIA): The LCA study was based on a cradle-to-gate approach, from the production of precursor materials/resources to the fabrication of TiO_2 and TiO_2/CDs nanocomposites. Environmental impacts were modeled using the ReCiPe 2016 v1.1 LCIA, Hierarchist Version, which evaluates the environmental impacts in three main categories of potential environmental impacts (endpoints): human health, ecosystems, and resources. Midpoint indicators were also evaluated: global warming (GW), stratospheric ozone depletion (SO), ionization radiation (IR), ozone formation – human health (OF), fine particulate matter formation (FPM), ozone formation – terrestrial ecosystems (OF-TE), terrestrial acidification (TA), freshwater eutrophication (FE), marine eutrophication (ME), terrestrial ecotoxicity (TET), freshwater ecotoxicity (FET), marine ecotoxicity (MET), human carcinogenic toxicity (HC), human non-carcinogenic toxicity (HNC), land use (LU), mineral resource scarcity (MR), fossil resource scarcity (FR), and water consumption (WC). The LCA study was performed by using the SimaPro 9.5.0.0 software.

Supporting Information

Supporting Information is available from the Wiley Online Library or from the author.

Acknowledgements

The Portuguese "Fundação para a Ciência e Tecnologia" (FCT, Lisbon) is acknowledged for funding of project PTDC/QUI-QFI/2870/2020, R&D Units CIQUP (UIDB/00081/2020) and GreenUPorto (UIDB/05748/2020), and the Associated Laboratory IMS (LA/P/0056/2020). L.P.d.S. acknowledges funding from FCT under the Scientific Employment Stimulus (CEECINST/00069/2021). R.M.S.S. acknowledges FCT for his Ph.D. grant (2021.06149.BD). M.A. thanks the Spanish Ministry of Science and Innovation (MCIN/AEI/10.13039/501100011033) though the project PID2021-122613OB-I00. N.V. thanks Fundo Europeu de Desenvolvimento Regional (FEDER) funds through the COMPETE 2020 Operational Programme for Competitiveness and Internationalisation (POCI), Portugal 2020 and by FCT in the framework of projects IF/00092/2014/CP1255/CT0004 and CHAIR in Onco-Innovation from the Faculty of Medicine, University of Porto (FMUP). E.R. thanks CHAIR in Onco-Innovation from FMUP for her Ph.D. grant, and M.P. acknowledges FCT for funding her PhD grant (2021.07450.BD). "Centro de Materiais da Universidade do Porto – CEMUP" is also acknowledged (www.cemup.up.pt).

Conflict of Interest

The authors declare no conflict of interest.

Data Availability Statement

The data that support the findings of this study are available from the corresponding author upon reasonable request.

Keywords

carbon dots, life cycle assessment, nanocomposites, photocatalysis, TiO_2

Received: July 20, 2023
Revised: October 12, 2023
Published online: November 1, 2023

[1] M. M. Mekonnen, A. Y. Hoekstra, *Sci. Adv.* **2016**, *2*, e1500323.
[2] J. Tollefson, *Nature* **2011**, *473*, 134.
[3] I. K. Konstantinou, T. A. Albanis, *Appl. Catal., B* **2004**, *49*, 1.
[4] S. Malato, P. Fernández-Ibáñez, M. I. Maldonado, J. Blanco, W. Gernjak, *Catal. Today* **2009**, *147*, 1.
[5] D. Spasiano, R. Marotta, S. Malato, P. Fernandez-Ibañez, I. Di Somma, *Appl. Catal., B* **2015**, *170–171*, 90.
[6] K. Kabra, R. Chaudhary, R. L. Sawhney, *Ind. Eng. Chem. Res.* **2004**, *43*, 7683.
[7] F. Meng, F. Lu, Z. Sun, J. Lü, *Sci. China: Technol. Sci.* **2010**, *53*, 3027.
[8] F. Zuo, L. Wang, T. Wu, Z. Zhang, D. Borchardt, P. Feng, *J. Am. Chem. Soc.* **2010**, *132*, 11856.
[9] Y.-C. Lee, J.-W. Yang, *J. Ind. Eng. Chem.* **2012**, *18*, 1178.
[10] T. M. Khedr, S. M. El-Sheikh, A. A. Ismail, D. W. Bahnemann, *Opt. Mater.* **2019**, *88*, 117.
[11] I. H. Chowdhury, S. Ghosh, M. K. Naskar, *Ceram. Int.* **2016**, *42*, 2488.
[12] D. Barolet, F. Christiaens, M. R. Hamblin, *J. Photochem. Photobiol., B* **2016**, *155*, 78.

 © 2023 Wiley-VCH GmbH

[13] W. Ren, Z. Ai, F. Jia, L. Zhang, X. Fan, Z. Zou, *Appl. Catal., B* **2007**, *69*, 138.
[14] R. Daghrir, P. Drogui, D. Robert, *J. Photochem. Photobiol.* **2012**, *238*, 41.
[15] H. Dong, G. Zeng, L. Tang, C. Fan, C. Zhang, X. He, Y. He, *Water Res.* **2015**, *79*, 128.
[16] O. Elbanna, P. Zhang, M. Fujitsuka, T. Majima, *Appl. Catal., B* **2016**, *192*, 80.
[17] A. Edreva, *Agric. Ecosyst. Environ.* **2005**, *106*, 119.
[18] J. Ni, W. Wang, D. Liu, Q. Zhu, J. Jia, J. Tian, Z. Li, X. Wang, Z. Xing, *J. Hazard. Mater.* **2021**, *408*, 124432.
[19] P. M. Martins, C. G. Ferreira, A. R. Silva, B. Magalhães, M. M. Alves, L. Pereira, P. A. A. P. Marques, M. Melle-Franco, S. Lanceros-Méndez, *Composites, Part B* **2018**, *145*, 39.
[20] A. Singh, P. Khare, S. Verma, A. Bhati, A. K. Sonker, K. M. Tripathi, S. K. Sonkar, *ACS Sustainable Chem. Eng.* **2017**, *5*, 8860.
[21] W. Tu, Y. Zhou, Q. Liu, S. Yan, S. Bao, X. Wang, M. Xiao, Z. Zou, *Adv. Funct. Mater.* **2013**, *23*, 1743.
[22] D. Pan, J. Jiao, Z. Li, Y. Guo, C. Feng, Y. Liu, L. Wang, M. Wu, *ACS Sustainable Chem. Eng.* **2015**, *3*, 2405.
[23] X. Xu, R. Ray, Y. Gu, H. J. Ploehn, L. Gearheart, K. Raker, W. A. Scrivens, *J. Am. Chem. Soc.* **2004**, *126*, 12736.
[24] D. Choi, S. Ham, D.-J. Jang, *J. Environ. Chem. Eng.* **2018**, *6*, 1.
[25] J. Chen, J. Shu, Z. Anqi, H. Juyuan, Z. Yan, J. Chen, *Diamond Relat. Mater.* **2016**, *70*, 137.
[26] Y. Li, Z. Liu, Y. Wu, J. Chen, J. Zhao, F. Jin, P. Na, *Appl. Catal., B* **2018**, *224*, 508.
[27] J. C. G. Esteves Da Silva, H. M. R. Gonçalves, *TrAC, Trends Anal. Chem.* **2011**, *30*, 1327.
[28] K. Holá, M. Sudolská, S. Kalytchuk, D. Nachtigallová, A. L. Rogach, M. Otyepka, R. Zboril, *ACS Nano* **2017**, *11*, 12402.
[29] R. Wang, K.-Q. Lu, Z.-R. Tang, Y.-J. Xu, *J. Mater. Chem. A* **2017**, *5*, 3717.
[30] Z. Peng, X. Han, S. Li, A. O. Al-Youbi, A. S. Bashammakh, M. S. El-Shahawi, R. M. Leblanc, *Coord. Chem. Rev.* **2017**, *343*, 256.
[31] S. Y. Lim, W. Shen, Z. Gao, *Chem. Soc. Rev.* **2015**, *44*, 362.
[32] N. Vale, S. Silva, D. Duarte, D. M. A. Crista, L. Pinto Da Silva, J. C. G. Esteves Da Silva, *RSC Med. Chem.* **2021**, *12*, 245.
[33] K. Wang, Z. Gao, G. Gao, Y. Wo, Y. Wang, G. Shen, D. Cui, *Nanoscale Res. Lett.* **2013**, *8*, 122.
[34] Y. Deng, M. Chen, G. Chen, W. Zou, Y. Zhao, H. Zhang, Q. Zhao, *ACS Omega* **2021**, *6*, 4247.
[35] H. Belkahla, R. Boudjemaa, V. Caorsi, D. Pineau, A. Curcio, J. S. Lomas, P. Decorse, A. Chevillot-Biraud, T. Azaïs, C. Wilhelm, H. Randriamahazaka, M. Hémadi, *Nanoscale Adv.* **2019**, *1*, 2571.
[36] J. Li, K. Tang, J. Yu, H. Wang, M. Tu, X. Wang, *R. Soc. Open Sci.* **2019**, *6*, 181557.
[37] E. F. C. Simões, L. P. Da Silva, J. C. G. E. Da Silva, J. M. M. Leitão, *Talanta* **2020**, *208*, 120447.
[38] A. C. P. Afonso, A. S. Correia, D. Duarte, A. T. S. C. Brandão, M. D. V. M. De Yuso, J. Jiménez-Jiménez, N. Vale, C. M. Pereira, M. Algarra, L. Pinto Da Silva, *Chemosensors* **2021**, *9*, 191.
[39] S. D. Hettiarachchi, R. M. Graham, K. J. Mintz, Y. Zhou, S. Vanni, Z. Peng, R. M. Leblanc, *Nanoscale* **2019**, *11*, 6192.
[40] H. He, X. Zheng, S. Liu, M. Zheng, Z. Xie, Y. Wang, M. Yu, X. Shuai, *Nanoscale* **2018**, *10*, 10991.
[41] J. Joseph, A. A. Anappara, *ChemPhysChem* **2017**, *18*, 292.
[42] S. Kalytchuk, K. Poláková, Y. Wang, J. P. Froning, K. Cepe, A. L. Rogach, R. Zboril, *ACS Nano* **2017**, *11*, 1432.
[43] Y.-Q. Zhang, D.-K Ma, Y.-G Zhang, W. Chen, S.-M. Huang, *Nano Energy* **2013**, *2*, 545.
[44] H. Li, X. He, Z. Kang, H. Huang, Y. Liu, J. Liu, S. Lian, C. H. A. Tsang, X. Yang, S.-T. Lee, *Angew. Chem., Int. Ed.* **2010**, *49*, 4430.
[45] M. Sabri, A. Habibi-Yangjeh, S. Vadivel, *J. Mater. Sci.* **2019**, *30*, 12510.
[46] H. Zhou, B. Zhang, Z. Jiang, H. Zhao, Y. Zhang, *Langmuir* **2023**, *39*, 7184.
[47] D. Saini, A. K. Garg, C. Dalal, S. R. Anand, S. K. Sonkar, A. K. Sonker, G. Westman, *ACS Appl. Nano Mater.* **2022**, *5*, 3087.
[48] R. M. S. Sendão, J. C. G. Esteves Da Silva, L. Pinto Da Silva, *Chemosphere* **2022**, *301*, 134731.
[49] J. Tian, Y. Leng, Z. Zhao, Y. Xia, Y. Sang, P. Hao, J. Zhan, M. Li, H. Liu, *Nano Energy* **2015**, *11*, 419.
[50] M. Rahbar, M. Mehrzad, M. Behpour, S. Mohammadi-Aghdam, M. Ashrafi, *Nanotechnology* **2019**, *30*, 505702.
[51] P. Chen, F. Wang, Z.-F. Chen, Q. Zhang, Y. Su, L. Shen, K. Yao, Y. Liu, Z. Cai, W. Lv, G. Liu, *Appl. Catal., B* **2017**, *204*, 250.
[52] P. Yang, J. Zhao, J. Wang, H. Cui, Li Li, Z. Zhu, *RSC Adv.* **2015**, *5*, 21332.
[53] G. S. Das, J. P. Shim, A. Bhatnagar, K. M. Tripathi, T. Kim, *Sci. Rep.* **2019**, *9*, 15084.
[54] A. Bhati, S. R. Anand, D. Saini, Gunture, S. K. Sonkar, *npj Clean Water* **2019**, *2*, 12.
[55] R. M. S. Sendão, J. C. G. Esteves Da Silva, L. Pinto Da Silva, *Catalysts* **2023**, *13*, 179.
[56] Y. Jin, W. Tang, J. Wang, F. Ren, Z. Chen, Z. Sun, P.-G. Ren, *J. Alloys Compd.* **2023**, *932*, 167627.
[57] J. Gong, Y. Guo, J. Lu, Yi Cheng, H. Wang, *Chem. Phys. Lett.* **2022**, *788*, 139297.
[58] H. Safardoust-Hojaghan, M. Salavati-Niasari, *J. Cleaner Prod.* **2017**, *148*, 31.
[59] C. Wang, K. Yang, X. Wei, S. Ding, F. Tian, F. Li, *Ceram. Int.* **2018**, *44*, 22481.
[60] J. Zhang, M. Kuang, J. Wang, R. Liu, S. Xie, Z. Ji, *Chem. Phys. Lett.* **2019**, *730*, 391.
[61] S. Feizpoor, A. Habibi-Yangjeh, I. Ahadzadeh, K. Yubuta, *Adv. Powder Technol.* **2019**, *30*, 1183.
[62] N. Xu, Z. Shi, Y. Fan, J. Dong, J. Shi, M. Z.-C. Hu, *Ind. Eng. Chem. Res.* **1999**, *38*, 373.
[63] M. Bancirova, *Luminescence* **2011**, *26*, 685.
[64] J. Yu, C. Zhang, Y. Yang, T. Su, G. Yi, X. Zhang, *Appl. Surf. Sci.* **2021**, *551*, 149476.
[65] Li Zhao, X. Chen, X. Wang, Y. Zhang, W. Wei, Y. Sun, M. Antonietti, M.-M. Titirici, *Adv. Mater.* **2010**, *22*, 3317.
[66] C. Siegers, J. Hohl-Ebinger, B. Zimmermann, U. Würfel, R. Mülhaupt, A. Hinsch, R. Haag, *ChemPhysChem* **2007**, *8*, 1548.
[67] Y. Ru, G. I. N. Waterhouse, S. Lu, *Aggregate* **2022**, *3*, e296.
[68] D. Crista, M. Algarra, M. V. Martínez De Yuso, J. C. G. Esteves Da Silva, L. Pinto Da Silva, *J. Mater. Chem. B* **2023**, *11*, 1131.
[69] R. Hatefi, H. Younesi, A. Mashinchian-Moradi, S. Nojavan, *Adv. Powder Technol.* **2021**, *32*, 2410.
[70] Z. Guo, H. Wu, M. Li, T. Tang, J. Wen, X. Li, *Appl. Surf. Sci.* **2020**, *526*, 146724.
[71] S. Feizpoor, A. Habibi-Yangjeh, K. Yubuta, *J. Photochem. Photobiol.* **2018**, *367*, 94.
[72] Q. Que, Y. Xing, Z. He, Y. Yang, X. Yin, W. Que, *Mater. Lett.* **2017**, *209*, 220.
[73] Y. Fang, Y. Huang, Z. Ni, Z. Wang, S. Kang, Y. Wang, Xi Li, *Int. J. Electrochem. Sci.* **2017**, *12*, 5951.
[74] V. Hinterberger, C. Damm, P. Haines, D. M. Guldi, W. Peukert, *Nanoscale* **2019**, *11*, 8464.
[75] W. H. Melhuish, *J. Phys. Chem.* **1961**, *65*, 229.
[76] A. El Mragui, O. Zegaoui, J. C. G. Esteves Da Silva, *Chemosphere* **2021**, *266*, 128931.
[77] A. El Mragui, Y. Logvina, L. Pinto Da Silva, O. Zegaoui, J. C. G. Esteves Da Silva, *Materials* **2019**, *12*, 3874.
[78] I. M. F. Cardoso, R. M. F. Cardoso, L. Pinto Da Silva, J. C. G. Esteves Da Silva, *Nanomaterials* **2022**, *12*, 2116.

 © 2023 Wiley-VCH GmbH

[79] R. M. F. Cardoso, I. M. F. Cardoso, L. P. Da Silva, J. C. G. Esteves Da Silva, *Nanomaterials* **2022**, *12*, 1211.
[80] D. Melgoza, A. Hernández-Ramírez, J. M. Peralta-Hernández, *Photochem. Photobiol. Sci.* **2009**, *8*, 596.
[81] S. F. Baranovskii, P. A. Bolotin, M. P. Evstigneev, *J. Appl. Spectrosc.* **2006**, *73*, 171.
[82] G. Rajender, J. Kumar, P. K. Giri, *Appl. Catal., B* **2018**, *224*, 960.
[83] T. Zhao, R. Liu, J. Lu, X. Zhu, X. Zhu, K. Lu, H. Zhu, *J. Phys. Org. Chem.* **2017**, *30*, e3712.
[84] A. V. Borhade, D. R. Tope, B. K. Uphade, *J. Chem.* **2012**, *9*, 705.
[85] J. Zhang, Q. Liu, He He, F. Shi, G. Huang, B. Xing, J. Jia, C. Zhang, *Carbon* **2019**, *152*, 284.
[86] B. Pastina, J. A. Laverne, S. M. Pimblott, *J. Phys. Chem. A* **1999**, *103*, 5841.
[87] S. Tong, J. Zhou, L. Ding, C. Zhou, Yi Liu, S. Li, J. Meng, S. Zhu, S. Chatterjee, F. Liang, *Colloids Surf., A* **2022**, *648*, 129342.
[88] A. I Ononye, A. R. Mcintosh, J. R. Bolton, *J. Phys. Chem.* **1986**, *90*, 6266.
[89] R. Liu, H. Li, L. Duan, H. Shen, Y. Zhang, X. Zhao, *Ceram. Int.* **2017**, *43*, 8648.
[90] K. Tiede, A. B. A. Boxall, S. P. Tear, J. Lewis, H. David, M. Hassellöv, *Food Addit. Contam.: Part A* **2008**, *25*, 795.
[91] R. J. B. Peters, G. Van Bemmel, N. B. L. Milani, G. C. T. Den Hertog, A. K. Undas, M. Van Der Lee, H. Bouwmeester, *Sci. Total Environ.* **2018**, *621*, 210.
[92] M. J. Riding, F. L. Martin, K. C. Jones, K. T. Semple, *Soil* **2015**, *1*, 1.
[93] F. Fiordaliso, P. Bigini, M. Salmona, L. Diomede, *Environ. Sci.: Nano* **2022**, *9*, 1199.
[94] A. D. Racovita, *Int. J. Environ. Res. Public Health* **2022**, *19*, 5681.
[95] R. Sendão, M. D. V. M. D. Yuso, M. Algarra, J. C. G. Esteves Da Silva, L. Pinto Da Silva, *J. Cleaner Prod.* **2020**, *254*, 120080.
[96] Christé, Esteves Da Silva, Pinto Da Silva, *Materials* **2020**, *13*, 504.
[97] S. Middlemas, Z. Z Fang, P. Fan, *J. Cleaner Prod.* **2015**, *89*, 137.
[98] F. Wu, Z. Zhou, A. L. Hicks, *Environ. Sci. Technol.* **2019**, *53*, 4078.
[99] S. Fernandes, J. C. G. Esteves Da Silva, L. Pinto Da Silva, L. Pinto da Silva, *NanoImpact* **2021**, *23*, 100332.
[100] C. Campalani, E. Cattaruzza, S. Zorzi, A. Vomiero, S. You, L. Matthews, M. Capron, C. Mondelli, M. Selva, A. Perosa, *Nanomaterials* **2021**, *11*, 524.
[101] D. M. A. Crista, J. C. G. Esteves Da Silva, L. Pinto Da Silva, *Nanomaterials* **2020**, *10*, 1316.
[102] D. M. A. Crista, G. P. C. Mello, O. Shevchuk, R. M. S. Sendão, E. F. C. Simões, J. M. M. Leitão, L. P. Da Silva, J. C. G. Esteves Da Silva, *J. Fluoresc.* **2019**, *29*, 265.
[103] R. M. S. Sendão, D. M. A. Crista, A. C. P. Afonso, M. D. V. Martínez De Yuso, M. Algarra, J. C. G. Esteves Da Silva, L. Pinto Da Silva, *Phys. Chem. Chem. Phys.* **2019**, *21*, 20919.
[104] A. El Mragui, I. Daou, O. Zegaoui, *Catal. Today* **2019**, *321–322*, 41.
[105] D. F. Eaton, *Pure Appl. Chem.* **1988**, *60*, 1107.
[106] S. Farjadfar, M. Ghiaci, S. A. Kulinch, W. Wunderlich, *Mater. Res. Bull.* **2022**, *155*, 111963.
[107] R. Hischier, T. Walser, *Sci. Total Environ.* **2012**, *425*, 271.
[108] S. Feijoo, S. González-García, Y. Moldes-Diz, C. Vazquez-Vazquez, G. Feijoo, M. T. Moreira, *J. Cleaner Prod.* **2017**, *143*, 528.
[109] J. Falbe, H. Bahrmann, W. Lipps, D. Mayer, in *Ullmann's Encyclopedia of Industrial Chemistry* (Ed: C. Ley), Wiley-VCH, Weinheim, Germany **2003**.

 © 2023 Wiley-VCH GmbH

2.1.1.2. Supplementary information

ADVANCED SUSTAINABLE SYSTEMS

Supporting Information

for *Adv. Sustainable Syst.*, DOI 10.1002/adsu.202300317

Carbon Dots–TiO_2 Nanocomposites for the Enhanced Visible-Light Driven Photodegradation of Methylene Blue

*Ricardo M. S. Sendão, Manuel Algarra, Eduarda Ribeiro, Mariana Pereira, Antonio Gil, Nuno Vale, Joaquim C. G. Esteves da Silva and Luís Pinto da Silva**

Carbon dots-TiO_2 nanocomposites for the visible-light driven photodegradation of methylene blue

Ricardo M. S. Sendão[1], Manuel Algarra[2], Eduarda Ribeiro[3,4], Mariana Pereira[3,4], Antonio Gil[2], Nuno Vale[3,4,5], Joaquim C. G. Esteves da Silva[1,6], Luís Pinto da Silva[1,6,*]

[1] Chemistry Research Unit (CIQUP), Institute of Molecular Sciences (IMS), Department of Geosciences, Environment and Territorial Planning, Faculty of Sciences, University of Porto, Rua do Campo Alegre s/n, 4169-007 Porto, Portugal.
[2] INAMAT^2-Institute for Advanced Materials and Mathematics. Science Department. Public University of Navarre. Campus of Arrosadía. 31006 Pamplona, Spain.
[3] PerMed Research Group, Center for Health Technology and Services Research (CINTESIS), Rua Doutor Plácido da Costa, Porto, 4200-319, Portugal.
[4] CINTESIS@RISE, Faculty of Medicine, University of Porto, Alameda Professor Hernâni Monteiro, Porto, 4200-319, Portugal.
[5] Department of Community Medicine, Information and Health Decision Sciences (MEDCIDS), Faculty of Medicine, University of Porto, Rua Doutor Plácido da Costa, Porto, 4200-319, Portugal.
[6] LACOMEPHI, GreenUPorto, Department of Geosciences, Environment and Territorial Planning, Faculty of Sciences, University of Porto, Rua do Campo Alegre s/n, 4169- 007 Porto, Portugal.
* luis.silva@fc.up.pt

Table S1 – Comparison of preliminary data concerning different wt% of CDs incorporated in TiO_2-CDs nanocomposites. Data collected for a visible-light irradiation period of 60 minutes with samples collected every 15 minutes.

CDs wt%	%DR	Rate constant (min^{-1})
0 (bare TiO_2)	16.6 ± 1.6%	0.0023 ± 0.0002
1	25.6 ± 0.7%	0.0049 ± 0.0001
2	41.6 ± 1.9%	0.0078 ± 0.0001
4	31.0 ± 3.5%	0.0065 ± 0.0011

Table S2 – Comparison of preliminary data concerning different tested MB concentrations for photocatalytic degradation with the nanocomposite. Data collected for a visible-light irradiation period of 60 minutes with samples collected every 15 minutes.

MB concentration	%DR	Rate constant (min^{-1})
1 mg L^{-1}	24.1 ± 2.6%	0.0043 ± 0.0005
2.5 mg L^{-1}	41.6 ± 1.9%	0.0078 ± 0.0001
5 mg L^{-1}	10.0 ± 0.9%	0.0017 ± 0.0003

Table S3 - Summary of Ecoinvent® 3.9.background data used to create the processes for CDs and TTIP.

Process	Background data
CDs	Citric acid {GLO}| market for | Cut-off, S
	Ethylenediamine {RER}| market for ethylenediamine | Cut-off, S
	Sodium hydroxide, without water, in 50% solution state {GLO}| market for | Cut-off, S
	Water, deionized, from tap water, at user {Europe without Switzerland} | market for

	Electricity, medium voltage {PT}| market for | Cut-off, S
TTIP	Ammonia, liquid {RER}| market for | Cut-off, S
	Isopropanol {RER}| production | Cut-off, S
	Titanium tetrachloride {GLO}| production | Cut-off, S
	Transport, freight train {RER}| market group for transport, freight train | Cut-off, S
	Transport, freight, lorry 16-32 metric ton, EURO3 {RER}| transport, freight, lorry 16-32 metric ton, EURO3 | Cut-off, S
	Electricity, medium voltage {RER}| market group for | Cut-off, S

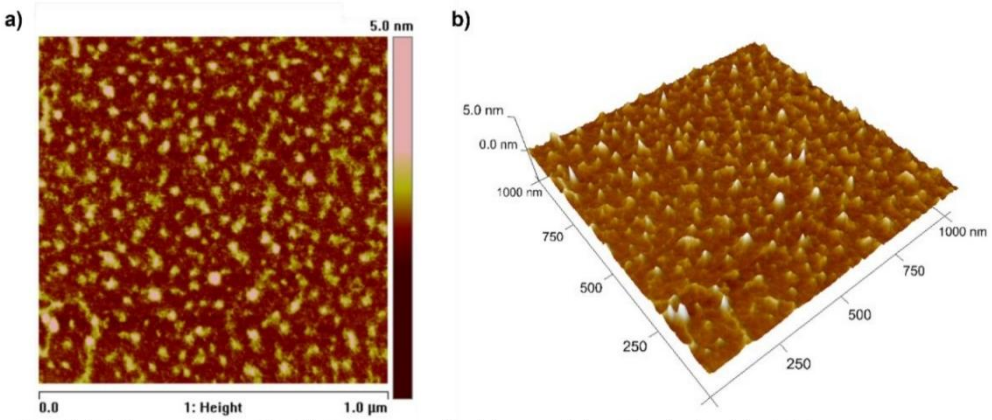


Figure S1 - a) AFM image of the CDs; b) 3D topographical image of the CDs obtained by AFM.

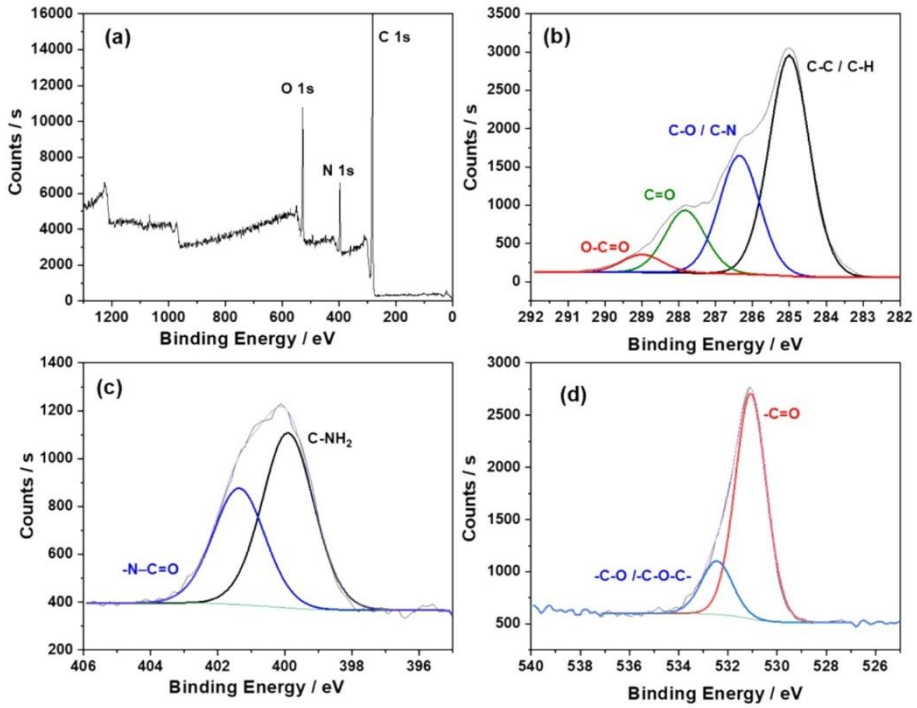


Figure S2 - a) XPS full survey and core level spectra of b) C 1*s*, c) N 1*s* and d) O 1*s* core level spectra of CA and EDA-based CDs.

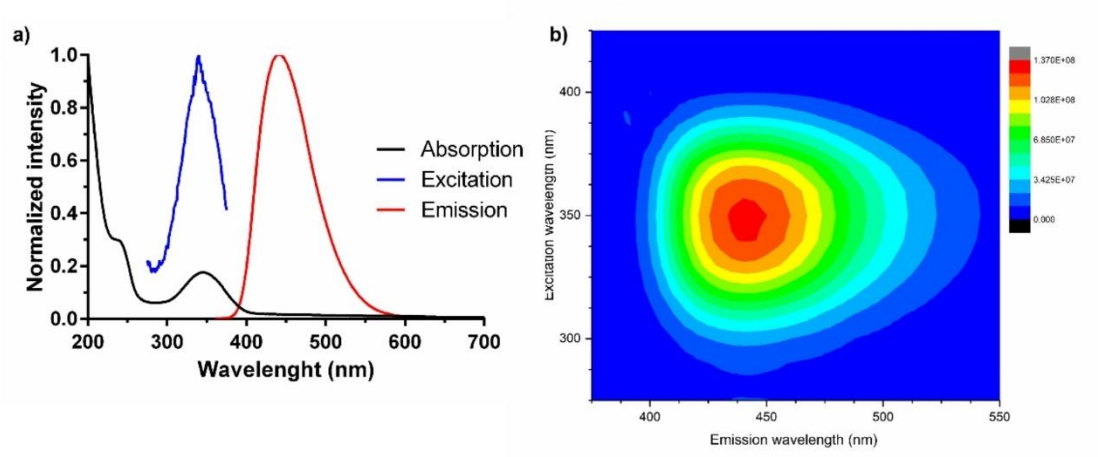


Figure S3 - Optical characterization of the CDs at a concentration of 8.5 mg L^{-1}: a) normalized absorption, excitation and emission spectra and b) photoluminescence excitation-emission matrix.

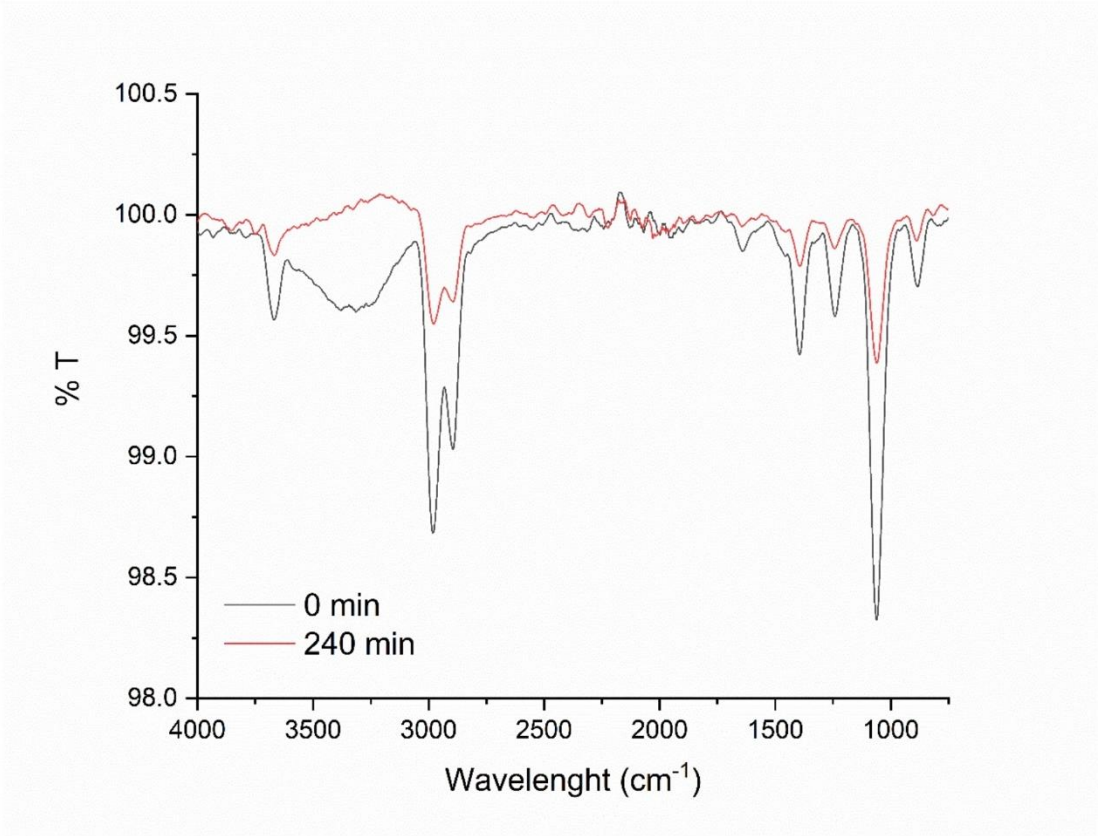


Figure S4 – FTIR spectra of the MB sample before and after 240 minutes of visible-light irradiation in the presence of the TiO_2-CDs nanocomposite.

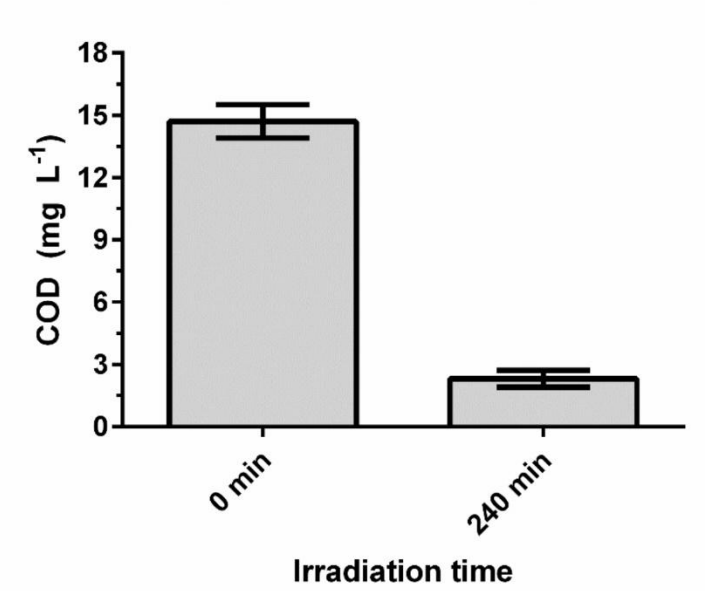


Figure S5 – COD analysis for MB samples before and after 240 minutes of visible-light irradiation in the presence of TiO_2-CDs nanocomposites.

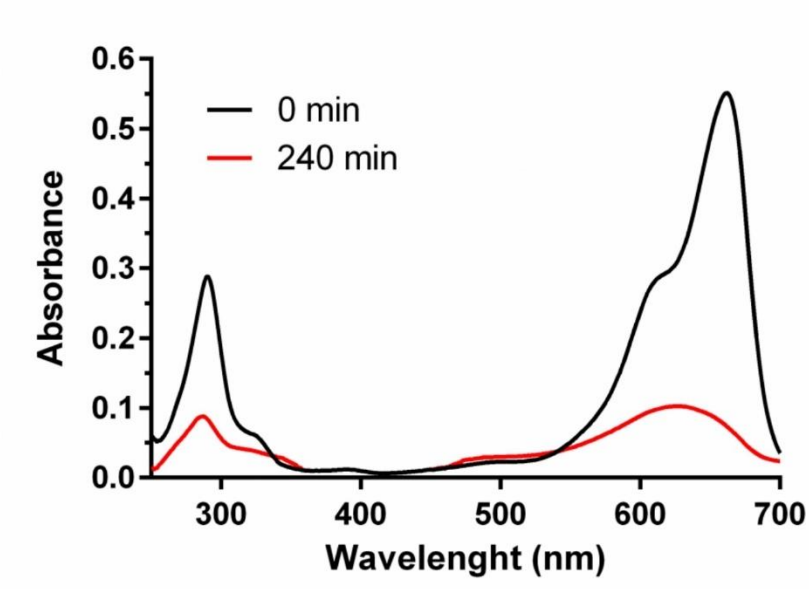


Figure S6 – Absorption spectra of MB samples before and after irradiation in the presence of TiO_2-CDs nanocomposite.

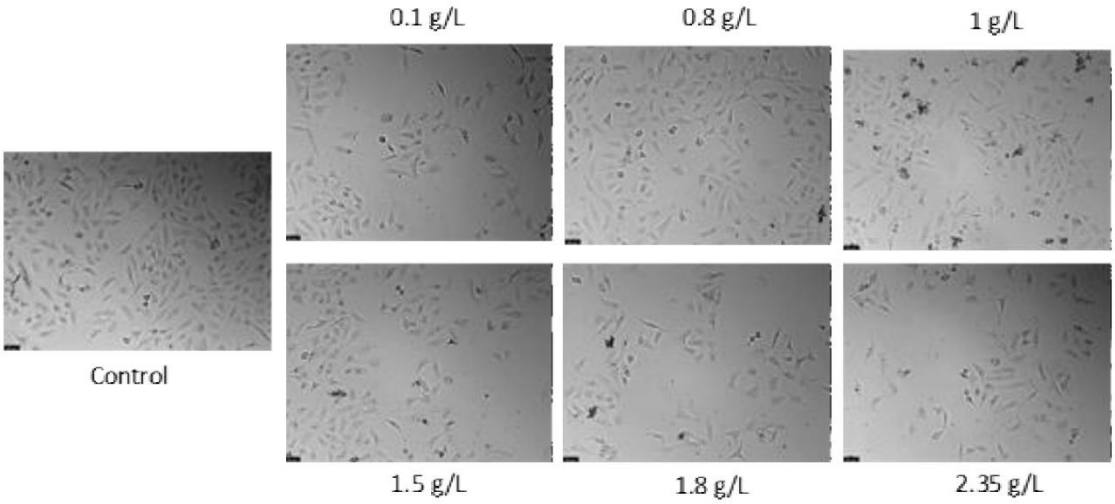


Figure S7 – Morphological analysis of A549 cells treated with increasing concentrations of CDs.

2.1.1.3. Conclusion

The development of visible-light-active photocatalysts is essential to achieve sustainable photocatalysis under solar irradiation. In this study, CDs synthesized from citric acid and ethylenediamine were successfully incorporated into TiO_2 to overcome its intrinsic limitations, such as its narrow absorption range and poor photonic efficiency. As a result of the incorporation of CDs, the nanocomposite exhibited enhanced photocatalytic performance under visible-light irradiation, achieving a 367% increase in catalytic activity compared to bare TiO_2 regarding the photodegradation of MB. This is primarily attributed to the CDs' ability to extend the nanocomposites' absorption into the visible range and to improve the separation of photogenerated electrons and holes, which is translated into a higher photocatalytic efficiency under visible-light irradiation.

Interestingly, as observed in the scavenger studies, the introduction of CDs also changed the reactive species involved in the catalytic process. While bare TiO_2 primarily relied on hydroxyl radicals for photodegradation, superoxide radicals were the dominant reactive species for the nanocomposite. Furthermore, LCA studies showed that, while the nanocomposites have slightly higher impacts when considering a weight-based FU, those impacts are greatly offset by their enhanced potential when compared to TiO_2, resulting in lower environmental impacts when considering a performance-based FU. Finally, cytotoxicity assessments also confirmed the safety of the synthesized CDs toward human cells, enabling their use in applications directly impacting human health. Altogether, these findings affirm that CDs are an effective, low-toxicity, and scalable additive to transform TiO_2 into a highly active and sustainable photocatalyst for sunlight-driven processes for the removal of organic pollutants.

2.1.2. Incorporation of corn stover as a carbon source in visible-light active photocatalytic TiO_2-CDs nanocomposites

Article

Visible-light-driven photocatalytic degradation of organic dyes using a TiO_2 and waste-based Carbon Dots nanocomposite

Sendão, Ricardo M. S.; Algarra, Manuel; Martínez, Juan; Brandão, Ana; Gil, Antonio; Pereira, Carlos; Esteves da Silva, Joaquim C. G.; Pinto da Silva, Luís. "Visible-light-driven photocatalytic degradation of organic dyes using a TiO_2 and waste-based Carbon Dots nanocomposite". *Colloids and Surfaces A: Physicochemical and Engineering Aspects* 713 (**2025**): 136475. https://doi.org/10.1016/j.colsurfa.2025.136475.

2.1.2.1. Introduction and contributions to this work

This work further develops the visible-light active TiO_2/CDs nanocomposite presented in section 2.1.1. and improves its sustainability by substituting part of the commercial reagents used in the hydrothermal synthesis of the CDs by incorporating corn stover, a major by-product of the corn industry. By doing so, we not only avoid part of the impacts associated with the production of citric acid, the typical carbon source used in traditional CDs synthesis, but also improve the circularity of the process by creating added value from a biomass that would otherwise be discarded. Furthermore, the preparation of the nanocomposites with these biomass-incorporating CDs ($NC_{50:50}$) even led to a slight increase of the catalytic potential when compared to NC_{100}, the first iteration of the nanocomposite (374% versus 367% increment over bare TiO_2 for MB, respectively), with $NC_{50:50}$ also being capable of removing other dyes, such as Rhodamine B (RhB), Orange II and Methyl Orange (MO) from aqueous samples. As before, a significant increase of the visible-light absorption capacity and photonic efficiency was observed upon adding the CDs, and tests with reactive species scavengers were performed to unravel the photodegradation mechanism of $NC_{50:50}$. Finally, LCA studies confirmed that $NC_{50:50}$ was the least impactful alternative when compared to TiO_2 and nanocomposites made fully from commercially available reagents.

In this work, I was responsible, under supervision from my supervisors, for synthesizing the CDs and $NC_{50:50}$, their characterization in terms of UV-Vis DRS and fluorescence spectroscopy, band gap calculations, photocatalytic assays, COD analysis,

scavenger studies, comparison with other reports available in the literature and environmental impact assessment via LCA studies. I was also responsible for the first draft of the paper, which was then reviewed and edited by Professor Dr. Luís Pinto da Siva and Professor Dr. Joaquim Esteves da Silva, who supervised the process from end-to-end. The remaining experiments were performed by partners from other institutions and external service providers. Namely, SEM analysis was done at CEMUP, FTIR, XPS, XRD and ss-NMR were performed by Dr. Manuel Algarra and Dr. Antonio Gil from INAMAT^2 at the Public University of Navarra, and Juan Lázaro-Martínez from the University of Buenos Aires, and finally, EIS experiments were conducted by Dr. Ana Brandão and supervised by Prof. Dr. Carlos Pereira from CIQUP – IMS, Faculty of Sciences – University of Porto. While SEM analysis was performed by an external service provider, I was the one responsible for data treatment and interpretation.

Colloids and Surfaces A: Physicochemical and Engineering Aspects 713 (2025) 136475

Contents lists available at ScienceDirect

Colloids and Surfaces A: Physicochemical and Engineering Aspects

journal homepage: www.elsevier.com/locate/colsurfa

Visible-light-driven photocatalytic degradation of organic dyes using a TiO_2 and waste-based carbon dots nanocomposite

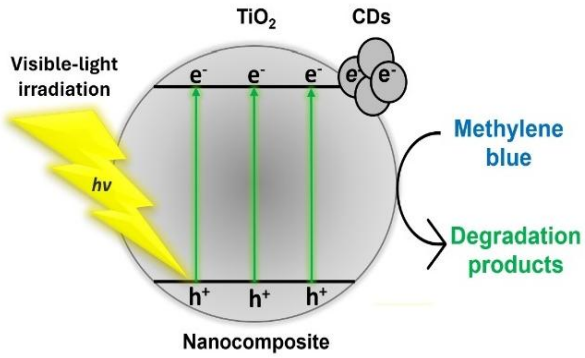
Ricardo M.S. Sendão [a], Manuel Algarra [b], Juan Lázaro-Martínez [c], Ana T.S.C. Brandão [d], Antonio Gil [b], Carlos Pereira [d], Joaquim C.G. Esteves da Silva [a,e], Luís Pinto da Silva [a,e,*]

[a] Chemistry Research Unit (CIQUP), Institute of Molecular Sciences (IMS), Department of Geosciences, Environment and Spatial Plannings, Faculty of Sciences, University of Porto, Rua do Campo Alegre s/n, Porto 4169-007, Portugal
[b] INAMAT2 - Institute for Advanced Materials and Mathematics, Department of Science, Public University of Navarra, Campus de Arrosadia, Pamplona 31006, Spain
[c] Universidad de Buenos Aires, Facultad de Farmacia y Bioquímica, Departamento de Ciencias Químicas and Instituto de Química y Metabolismo del Fármaco (IQUIMEFA UBA CONICET), Ciudad Autónoma de Buenos Aires, Argentina
[d] Chemistry Research Unit (CIQUP), Institute of Molecular Sciences (IMS), Department of Chemistry and Biochemistry, Faculty of Sciences, University of Porto, Rua do Campo Alegre s/n, Porto 4169-007, Portugal
[e] LACOMEPHI, GreenUPorto, Department of Geosciences, Environment and Spatial Plannings, Faculty of Sciences, University of Porto, Rua do Campo Alegre s/n, Porto 4169- 007, Portugal

HIGHLIGHTS

- Visible-light active photocatalysts ($NC_{50:50}$) were made from TiO_2 and Carbon Dots.
- Waste upcycling was achieved by incorporating corn stover in the Carbon Dots.
- $NC_{50:50}$ presented an improved visible-light absorption and photonic efficiency.
- $NC_{50:50}$ presented a 374 % enhancement of the catalytic efficiency compared to TiO_2.
- The relative environmental impact of $NC_{50:50}$ was much lower than those of TiO_2.

GRAPHICAL ABSTRACT



ARTICLE INFO

Keywords:
TiO_2
Carbon dots
Photocatalysis
Waste upcycling
Wastewater treatment

ABSTRACT

Herein we report a visible-light-active photocatalytic nanocomposite ($NC_{50:50}$) prepared from carbon dots (CDs) and TiO_2 nanoparticles, which was applied to the photodegradation of organic dyes in water. The CDs incorporated corn stover, a major agricultural waste, and were prepared via hydrothermal treatment. Using a visible-light irradiation source and the dye methylene blue as a representative of the organic dyes class, we observed that a 374 % enhancement of the catalytic performance was achieved by adding CDs relative to bare TiO_2. This was possible due to increased visible-light absorption and better photonic efficiency. Tests using reactive species scavengers indicated that three active species (superoxide anion, hydroxyl radicals, and electrons) were

* Corresponding author at: Chemistry Research Unit (CIQUP), Institute of Molecular Sciences (IMS), Department of Geosciences, Environment and Spatial Plannings, Faculty of Sciences, University of Porto, Rua do Campo Alegre s/n, Porto 4169-007, Portugal
E-mail address: luis.silva@fc.up.pt (L. Pinto da Silva).

https://doi.org/10.1016/j.colsurfa.2025.136475
Received 27 December 2024; Received in revised form 6 February 2025; Accepted 19 February 2025
Available online 20 February 2025
0927-7757/© 2025 The Authors. Published by Elsevier B.V. This is an open access article under the CC BY license (http://creativecommons.org/licenses/by/4.0/).

responsible for the photodegradation process, differing from bare TiO_2 in which only the hydroxyl radical has a relevant role. Photocatalytic degradation was also observed toward Rhodamine B, Orange II and Methyl Orange. Finally, we performed a life cycle assessment (LCA) study to assess and analyse the associated environmental impacts of $NC_{50:50}$ compared with other alternatives, which revealed that $NC_{50:50}$ is the alternative resulting in the least environmental impacts. In summary, $NC_{50:50}$ could, under visible-light irradiation, efficiently remove different organic dyes while incorporating organic waste materials and reducing the impacts associated with their use. We expect that this study provides a base for a more environmentally sustainable design of visible-light-active photocatalysts via waste upcycling.

1. Introduction

The preservation of the drinkable water supply is of paramount importance for mankind. Thus, the contamination of Earth's drinkable water supply could lead to severe water scarcity, a catastrophic outcome that could negatively impact global health, environmental, and economic standards [1,2]. Persistent organic pollutants are particularly important across the several classes of pollutants found in aquatic environments due to their long-lasting nature and possible damaging by-products [3]. Currently, conventional wastewater treatment methods frequently include physical adsorption, coagulation, and biodegradation, all of which can be ineffective when it comes to removing these persistent pollutants that include classes of commonly used compounds such as organic dyes and antibiotics [4,5].

More recently, methods based on advanced oxidation processes (AOPs), like the use of photocatalytic technologies, have been extensively studied as potential alternative treatment methodologies. Photocatalysis can be described as the promotion of a chemical reaction due to the action of a photocatalyst activated upon the absorption of suitable irradiation and can be achieved with different types of photocatalysts, such as semiconductors [6–10], carbon-based nanomaterials [11,12] or organophotocatalysts [13,14]. Compared to traditional water treatment methods, using photocatalytic technologies presents several advantages. Namely, it can be less environmentally impactful than traditional chemical oxidation due to the possibility of using an inexhaustible energy source (solar irradiation), may achieve a virtually complete removal of the target pollutants, and there is no generation of catalyst by-products during the photocatalytic process [15,16].

Amongst the photocatalysts currently known to the scientific community, titanium dioxide (TiO_2) is particularly important. Not only is it the most widely used photocatalyst in today's world, but it is also inexpensive, stable, and used for an array of purposes, including the photocatalytic removal of persistent pollutants such as textile dyes and pharmaceuticals (e.g. methylene blue (MB) and ibuprofen, respectively), heavy toxic metals photoreduction and removal, and hydrogen generation via water splitting [17–22]. However, TiO_2 lacks in terms of efficient utilization of solar irradiation. This is due to its high energy bandgap (2.8–3.2 eV), limiting the photocatalytic region of the semiconductor to high-energy lower-wavelength radiation ($\lambda < 400$ nm) [23], which is around 6 % of the whole solar spectrum [24]. Furthermore, after photoexcitation, the semiconductor suffers from rapid charge carrier recombination, which reduces its photonic efficiency [25]. Finally, due to the composition of its surface, TiO_2 presents a poor affinity towards organic pollutants [26].

Active research has been conducted to improve the absorption of radiation in the visible range and the efficiency of TiO_2 under solar irradiation. Several methods have been tested and reported thus far, such as doping and coupling with metals/non-metals (e.g. platinum or nitrogen, respectively) [27,28], and conjugating the semiconductor with alternative materials, such as graphene [29,30]. Employing these methods led to a higher affinity towards organic pollutants, increasing the quantity of those reaching the active site and improving the activity of the catalysts under visible radiation due to higher stability of the nanocrystalline structure and enabling new energy levels [30–32]. However, in most cases, these techniques require expensive and highly toxic metal elements, resulting in a lower photonic efficiency, thus decreasing the catalytic potential [32].

Another possible alternative to address these limitations is conjugating the semiconductor with carbon dots (CDs). These nanometric carbon-based particles appear as spherical or quasi-spherical structures, including a sp^2-conjugated core (either amorphous or crystalline) surrounded by a functionalized surface [33]. CDs display a variety of properties worth noting. Chief among these is, in terms of photocatalytic applications, high photoluminescence, a broad absorption extending into the visible range, good solubility in aqueous media, and low toxicity [34–36]. Due to being relatively inexpensive, easy to prepare, and presenting interesting properties, CDs are used for applications such as sensing [37], light-emitting devices [38], photodynamic therapy [39] and photocatalysis (either by themselves or in conjugation with semiconductors such as TiO_2) [40–42].

The rationale behind the combination of TiO_2 with CDs is that, unlike strategies such as doping or coupling, it overcomes the difficulties posed by using the semiconductor for photocatalysis without compromising in terms of additional limitations or toxicity [43]. CDs, having a lower cost and toxicity than the alternatives, do not hinder TiO_2's photonic efficiency nor induce harmful effects on human health or the environment [27,28,32]. In fact, due to their electron transfer properties and high electron storage capacity, they can accept the photoexcited e^- from TiO_2's conduction band, preventing their recombination with h^+ and promoting a better separation of the photoinduced charge carriers [44]. Furthermore, because of their enhanced absorption, they can expand the nanocomposite's absorption toward the visible region, permitting a more efficient application when using solar irradiation [41,42]. Finally, the functionalized surface brings a higher affinity towards organic compounds, increasing pollutant adsorption and promoting access to the active sites [42].

Another advantage is that CDs can be prepared from a wide array of compounds, including using organic waste as carbon precursors. Thus, this type of material has the potential to address the problems associated with using TiO_2 in real-world photocatalytic applications while upcycling an organic waste that would otherwise remain unutilized. The preparation of nano-catalysts from waste could also yield additional benefits in terms of reducing the environmental impacts of their preparation. This is particularly important given that, regarding CDs, Life Cycle Assessment (LCA) studies have demonstrated that the carbon precursor used during the synthesis may be a major factor impacting the resulting environmental impacts [45–47]. Thus, to minimize the impacts associated with the compound used as the carbon precursor, one could either reduce the amount or replace the commercial chemicals with waste materials as alternative precursors. One example of this would be to use corn stover as part of the carbon precursor mixture for the CDs. Corn stover, a major by-product of the corn industry, consists of the leaves, stalk and cobs of the corn plant left after harvest. It is a major agricultural waste that makes up about half of the corn crop's yield, and of which only around 10 % is used in other applications [48]. Given its high volume, the upcycling of corn stover into a nanotechnology solution for wastewater treatment should be greatly appreciated.

Herein, we describe the making of visible-light-active photocatalytic nanocomposites prepared from TiO_2 and corn stover-based CDs. This nanocomposite was tested for the photodegradation of several textile

dyes, including MB. Tests employing reactive species scavengers were performed to assess the catalytic mechanism and identify the species involved in the process. Additionally, the nanocomposites were characterized using several techniques, including SEM, FT-IR, XPS, XRD, ss-NMR, EIS, UV-Vis, and photoluminescence spectroscopy. Finally, LCA studies were performed to investigate the environmental impacts of its preparation and use.

2. Materials and methods

2.1. Materials

Titanium (IV) isopropoxide (TTIP, 99.99 %), citric acid (CA, 99.5 %), ethylenediamine (EDA, 99 %), sodium azide (99.5 %), Rhodamine B (95 %), *p*-benzoquinone, Orange II (85 %), and Titanium dioxide nanoparticles (99.7 %, <25 nm particle size, anatase phase) were acquired from Sigma Aldrich. Isopropyl alcohol (IPA, 99.9 %) was bought from Fisher Chemical. Potassium nitrate (99 %) and potassium iodide (99 %) were purchased from Merck. Methylene blue (MB) was obtained from Carlo Erba. Methyl orange was obtained from Honeywell Fluka. All commercially acquired reagents were utilized as they were received.

Corn stover was collected in an agricultural field in Mindelo, Portugal. Before using the material, corn stover was first washed with deionized water before drying at 50 °C in a VWR DL 112 Prime oven (2500 W). Afterward, it was milled using a Laarmann CM50 mill and a sieve size of 0.5 mm. The resulting crushed corn stover was stored in a freezer (-80 °C) to prevent the growth of microorganisms.

2.2. CDs synthesis and purification

The CDs were prepared via a hydrothermal process (represented in Fig. 1) based on previous work by our team. Briefly, CA (0.075 g), corn stover (0.075 g), and EDA (166.9 μL) were mixed in a NaOH 0.01 M (10 mL). The resulting solution was inserted into a *Teflon*-lined vessel surrounded by a steel outer shell. Hydrothermal treatment ensued at 200 °C during 8 h. After allowing the reaction product to cool down to room temperature, they were centrifuged (6000 rpm, 30 min) and dialyzed (3.5 kDa MWCO for 24 h) to remove both insoluble and soluble impurities, respectively, which could alter the CDs properties and reactivity [49]. Finally, the CDs solution was lyophilized, weighted and then dissolved in deionized water, resulting in a CDs solution of known concentration that was kept in the cold (4 °C) until further use.

2.3. TiO_2/CDs nanocomposites preparation

For the preparation of 0.5 g of bare TiO_2, we followed a method previously used by our team [50,51]. We start by adding TTIP (1.855 mL) dropwise to IPA (11.975 mL) under stirring. After 30 min, deionized water was added (11.25 mL), precipitating TiO_2. The mixture was then stirred for two more hours before being vacuum-filtered and dried overnight in an oven (VWR DL 112 Prime, 2500 W). Finally, the catalyst was powdered in a mortar and annealed at 300 °C for 3 h (Thermolyne 47900 muffle, 1000 W). It was then stored in the dark until use.

For the preparation of the nanocomposites [52], the process was similar to that of TiO_2, but with the addition of the necessary quantity of CDs amounting to 2–4 % of the total expected mass being added dropwise to the suspension prior to the vacuum-filtering stage and the 2 h of stirring before [52]. The CDs solution was kept under stirring at 70 °C for 90 minutes before adding it to the TiO_2 suspension. Two different nanocomposites were prepared over the course of this work. The first one, termed $NC_{50:50}$, was prepared using the CDs described in the "2.2. CDs synthesis and purification" section, employing a CA – corn stover ratio of 50:50 as co-carbon precursors. The second composite, termed NC_{100}, was prepared using CDs employing only a commercially available reagent, namely CA, as a carbon precursor, as reported in [52].

2.4. Photocatalytic activity assays

The visible-light-driven catalytic potential of TiO_2, $NC_{50:50}$ and NC_{100} was assessed using a MainHouse energy saving lamp (23 W, 6400 K, 1311 Lm) as the irradiation source, having this lamp already been employed in similar tests [51,53]. For the test, 2.5 mg L^{-1} of MB was photodegraded, with the catalytic efficiency being monitored via analysis of the absorbance at 665 nm (MB's absorption peak, ε_m = 73460 M^{-1} cm^{-1}) solution [54,55], Briefly, in a normal experimental setting, 20 mg of the photocatalyst was mixed with 100 mL of MB solution (2.5 mg L^{-1} in H_2O). Afterward, the solution was put in an ultrasonic bath for 1 min to disperse the catalyst and, before switching the irradiation source on, was kept under magnetic stirring in the dark for 30 min to achieve adsorption-desorption equilibrium [56]. Then, the lamp was switched on, and aliquots were collected 30 min before irradiation (t = -30, used to measure the adsorption of the pollutant by the catalysts), at the initial time (t = 0) and every additional 30 min of irradiation time. Before analysis via UV-Vis spectrophotometry, the aliquots were centrifuged (10,000 rpm for 10 min) to separate the

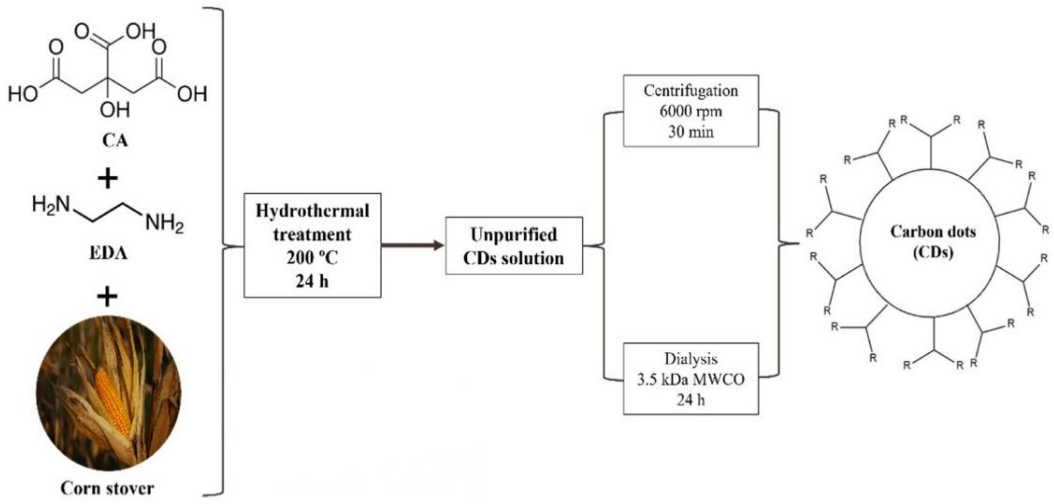


Fig. 1. Schematic representation of the synthesis and purification of the CDs employed in the photocatalytic nanocomposite.

heterogeneous catalyst from the treated sample. Tests with dyes other than MB were also made, with their respective concentrations being adjusted so that A = 0.5 at their absorption peak.

2.5. Free radical scavenger tests

To evaluate the role of each reactive species during the photodegradation of MB, tests were made employing scavengers for different free radicals' reactive species, with the effects of the presence of these scavengers in the catalytic mixture being monitored. Namely, hydroxyl radicals (·OH), superoxide radicals ($O_2^{\cdot-}$), electrons (e^-), holes (h^+) and singlet oxygen ($^1O_2$) were scavenged using isopropyl alcohol (IPA, 10 mM) [53], *p*-Benzoquinone (1 mM) [57], potassium nitrate (KNO_3, 10 mM) [58], potassium iodide (KI, 10 mM) [53], and sodium azide (1 mM) [59], respectively. For these tests, all reactional conditions were as described in the "Photocatalytic activity assays" (240 min of irradiation). Finally, the pollutant removal rate was compared to that of control tests performed without any scavenger.

2.6. Materials characterization

The morphology of bare TiO_2 and $NC_{50:50}$ was obtained via high-resolution scanning electron microscopy (SEM). Namely, a FEI Quanta 400 ESEM FEG system was used to analyze powder samples scattered in a carbon tape. Average sizes for the catalysts were obtained by calculating the average size of 100 individually measured particles.

The photocatalysts' absorption profiles were recorded using UV-Vis diffuse reflectance spectroscopy (DRS). The equipment used for this was a Jasco V-760 spectrophotometer with an integration sphere (Jasco ILV-924) addon. Barium sulfate was used as the reference.

Photoluminescence spectra were collected via a Horiba Jovin Yvon Fluoromax-4 spectrofluorometer in standard 10 nm fluorescence quartz cells. The data was processed and analyzed via the FluorEssence software provided with the equipment.

Electrochemical impedance spectroscopy (EIS) measurements were carried out using a computer-controlled VSP-300 multichannel potentiostat from BioLogic, controlled with EC-Lab V11.26 software. A screen-printed carbon electrode (C-SPE DropSens, reference DRP-110) was obtained from Metrohm Autolab (Utrecht, Netherlands). Electrochemical cleaning of the electrode was carried out using a 0.5 M H_2SO_4 aqueous solution and using the cyclic voltammetry (CV) technique (until it reached a profile i = f(t) stable over time). An average of 15 cycles was considered at a speed rate of 0.1 V s^{-1}, using an interval of potential of −0.45 to + 1.05 V vs. Ag. Once this procedure was completed, the electrodes were thoroughly washed with ultrapure water. To obtain the working electrode, 5 mg of samples were suspended in 0.5 mL deionized water with 0.05 mL of 5 wt% Nafion 117 dispersion, and then the mixture was sonicated for 30 min and spread onto the WE of the SPE. 0.1 M Na_2SO_4 aqueous solution was used as the electrolyte. A Main-House energy saving lamp (23 W, 6400 K, 1311 Lm) was used as the light source. The EIS measurements were performed applying a sinusoidal signal of 10 mV (rms) and with frequencies logarithmically distributed from 20 kHz to 1 Hz. The measurements were taken at 0.50 V.

Infrared spectra were collected using a Vertex70 (Bruker) FT-IT spectrophotometer coupled to a Specac Golden Gate Single Reflection Diamond Attenuated Total Reflectance addon. The spectra were analyzed in the range of 4000–500 cm^{-1} with a spectral resolution of 4 cm^{-1}.

X-Ray powder diffraction (XRPD) patterns were obtained using an automated diffractometer (PANanalatytical EMPYREAN) and recorded between 5 and 70 in 2θ (1 h of measuring time) in Bragg-Brentano reflection configuration with a PIXcel 3D detector with a step size of 0.017° (2θ).

XPS analysis was made using a Physical Electronics PHI VersaProbe II spectrometer employing monochromatic Al-K_α radiation (49.1 W, 15 kV and 1486.6 eV) with a hemispherical multichannel detector. A constant pass energy value of 29.35 eV and a 200 μm circular analysis area were used to record the spectra, which were then analyzed via the PHI SmartSoft software and processed using MultiPak 9.3 package. The adventitious carbon C 1 s signal (284.8 eV) was used as a reference for the binding energy values. Shirley-type background and Gauss-Lorentz curves were used to determine the binding energies.

Solid-state Nuclear Magnetic Resonance (*ss*-NMR) experiments were performed using a spectrometer equipped with a 14.1 T narrow bore magnet operating at Larmor frequencies of 600.09 MHz and 150.91 MHz for ^1H and ^{13}C, respectively. A powdered sample was packed in a 2.5 mm ZrO_2 rotor and rotated at room temperature at magic angle spinning (MAS) rates of 15 or 30 kHz. The recycling time was set at 5 s with a contact time during the cross-polarization of 2 ms for ^{13}C spectrum. ^1H-MAS and 2D homonuclear correlation experiments were recorded in a 2.5 mm MAS probe at a MAS rate of 30 kHz. The 2D ^1H-^1H SQ-DQ homonuclear correlation experiment was recorded using the back-to-back (BaBa) pulse sequence with excitation and reconversion times of two rotor periods. Chemical shifts (δ) for ^1H and ^{13}C (expressed in ppm) are relative to TMS ($\delta^1H = 0$ ppm) and adamantane ($\delta^{13}C = 38.5$ ppm), respectively.

2.7. LCA studies

2.7.1. Scope and system boundaries

This cradle-to-gate LCA study aimed to compare the relative environmental results from the production of TiO_2, NC_{100}, and $NC_{50:50}$. A laboratory-scale manufacturing of the photocatalysts was considered for this study, including the direct emissions and upstream impacts associated with resource extraction. Regarding the electricity used in the process, its impacts were not considered, as they are similar for the three processes. The production processes considered for TiO_2, NC_{100}, and $NC_{50:50}$ were as described in the "2.3. TiO_2/CDs nanocomposites preparation" section, building on a previous work by our team [52]. We started by analyzing and comparing the environmental impacts based on a functional unit (FU) of 1 kg of produced material. Selecting a weight-based FU is useful to compare the impacts associated with producing an equivalent quantity of similar nanomaterials [60,61]. Afterwards, the impacts were analyzed by considering a function-based FU depending on the reaction rate constants achieved by each catalyst. This is necessary given that the 1 kg FU cannot take into account that sometimes a more impactful process could be more beneficial due to higher applicability and functionality of the resulting material. In our case, given the intended purpose for which our nanocomposites were prepared, we chose the reaction rate constant as a measure of the functionality of our catalysts.

2.7.2. Life cycle inventory (LCI)

The LCA study was made using inventory (foreground) data inputs based on the process described in the "Materials and methods" section, with the foreground system using the database information from Ecoinvent® 3.9.1 for IPA (Isopropanol {RER}| market for isopropanol | Cut-off, S) and deionized water (Water, deionized, from tap water, at user {Europe without Switzerland} | market for). Additionally, some processes were not available in the database and were created by us based on information provided by us or found in the literature. Namely, for the CDs, the process was created based on a methodology we developed and used, whereas for TTIP we obtained the information required from ref [62]. A summary of the background data used in each case can be found in Table S1.

For this study, all three catalysts (TiO_2, $NC_{50:50}$ and NC_{100}) required the same electricity input during their synthesis, and so, the comparison between the relative environmental impacts of each catalyst does not depend on this parameter. Furthermore, a laboratory scale was considered for the purpose of our study, meaning that none of the equipment (such as the oven or furnace) was used to its full potential. Given this,

providing an accurate calculation of the energy required by the processes is difficult, as the equipment used is inefficient when processing small quantities. As our objective with this study is to make a comparison between the relative impacts of the three different processes, and the fact that the processes have similar energy requirements, the contribution of the impacts associated to this factor was not included in the present LCA study [52].

2.7.3. Life cycle impact assessment (LCIA)

The environmental impacts evaluated in this LCA study were modeled using the ReCiPe 2016 v1.1 LCIA, Hierarchist Version. The midpoint indicators taken into consideration in the ReCiPe method were: global warming – human health (GW - HH), global warming – terrestrial ecosystems (GW – TE), global warming – freshwater ecosystems (GW – FE), stratospheric ozone depletion (SO), ionization radiation (IR), ozone formation - human health (OF - HH), fine particulate matter formation (FPM), ozone formation - terrestrial ecosystems (OF-TE), terrestrial acidification (TA), freshwater eutrophication (FE), marine eutrophication (ME), terrestrial ecotoxicity (TET), freshwater ecotoxicity (FET), marine ecotoxicity (MET), human carcinogenic toxicity (HC), human non-carcinogenic toxicity (HNC), land use (LU), mineral resource scarcity (MR), fossil resource scarcity (FR), water consumption – human health (WC – HH), water consumption – terrestrial ecosystems (WC – TE) and water consumption – aquatic ecosystems (WC – AE). The LCA study was performed by using the SimaPro 9.5.0.0 software.

3. Results and discussion

3.1. Photocatalytic studies

3.1.1. Evaluation of the photocatalytic performance

Detailed information about the nanocomposite preparation may be found on the Supporting Information (SI). Bare TiO_2 nanoparticles were obtained from titanium (IV) isopropoxide (TTIP) in a sol-gel process and were analyzed previously by us in terms of photodegradation efficiency and characterization [52]. Hydrothermally-prepared CDs were made from a mixture of corn stover, citric acid (both as co-carbon precursors), and ethylenediamine (as N-dopant), with a mass ratio of 0.5:0.5:1, respectively. The TiO_2-CDs nanocomposite ($NC_{50:50}$) was prepared similarly to bare TiO_2, but with addition of the CDs' solution during the last stage of synthesis process, prior to annealing. In identifying the NC, 50:50 refers to the mass ratio of corn stover to citric acid used as co-carbon precursors for the waste-based CDs.

The visible-light-driven photodegradation potential was first analysed by measuring the photocatalytic degradation of MB via UV-Vis spectrophotometry. In an early stage, to optimize the system, preliminary tests (20 mg of photocatalyst, 2.5 mg L^{-1} MB, 60 minutes of irradiation) were made to decide the ratio of corn stover - citric acid to be incorporated and the hydrothermal reaction time to be used in the making of the CDs for inclusion in photocatalytic nanocomposites. The effect of varying the wt% of CDs including in the nanocomposite and the annealing stage temperature were also tested this way. To compare these results to those of bare TiO_2, we quantified the amount of pollutant removed over a set irradiation time (%DR, Eq. 1)[12] and calculated the associated rate constant (Eq. 2). To calculate the %DR, we employed the following equation:

$$\%DR = \frac{C_0 - C_t}{C_0} \times 100 \quad (1)$$

Here, %DR corresponds to the % of textile dye removed over a set time of irradiation, C_0 represents the initial concentration of MB in the mixture, and C_t is the concentration of MB after an irradiation period of t minutes. The dye concentration was obtained via analysis of the absorbance at 665 nm (ε_m = 73460 M^{-1} cm^{-1})[54,55] via UV-Vis spectrophotometry.

Furthermore, the kinetic equation of the degradation follows a pseudo-first-order reaction that can be written as follows [63]:

$$-\ln\left(\frac{C_t}{C_0}\right) = kt \quad (2)$$

C_t is the concentration of MB after an irradiation period of t minutes, C_0 corresponds to the initial MB concentration, k is the estimated rate constant, and t is the time of sample irradiation with a visible-light source.

For the first set of preliminary assays, CDs were prepared with both varying corn stover-citric acid ratios and different reaction times. After synthesis and purification, the CDs were conjugated with TiO_2, originating the catalytic nanocomposites. In terms of corn stover - citric acid ratio, we observed that, when using the same synthesis conditions (200 °C during 24 h), a 50:50 ratio yielded the best results (Table S2), both in terms of rate constant (0.0051 versus 0.0025 and 0.0036 min^{-1}) and % DR (26.4 versus 12.6 and 19.4 %). Considering this, we chose the 50:50 ratio. We tested the effects of different CDs' hydrothermal reaction times on the resulting nanocomposites, with the respective results indicating that an 8 h reaction time originates the CDs with the highest potential to be incorporated in a catalytic nanocomposite (Table S3). The respective nanocomposites, incorporating CDs made using a 50:50 ratio and 8 h of reaction time, presented a reaction rate constant of 0.0111 ± 0.0012 min^{-1} coupled to a %DR of 48.4 ± 3.7 %.

Afterward, we also evaluated the wt% of CDs to be integrated into the nanocomposites. We have opted for a 4 wt% CDs inclusion, given that it yielded a slightly higher rate constant and %DR (0.121 ± 0.0006 min^{-1} and 51.5 ± 1.7 %, respectively) when compared to a 2 wt% concentration (0.0111 ± 0.0012 min^{-1} and 48.4 ± 3.7 %). Finally, the effect of the nanocomposite's annealing temperature was also studied (Table S4). For temperatures between 300 and 500 °C, we observed that the catalytic performance of the nanocomposite worsens as the temperature is gradually increased. As an example, a 300 °C annealing temperature results in a rate constant and %DR (0.121 ± 0.0006 min^{-1} and 51.5 ± 1.7 %, respectively) more than 3 times higher than those resulting from a 350 °C annealing temperature (0.0029 ± 0.0002 min^{-1} and 16.0 ± 1.1 %). This could be due to the gradual degradation of the CDs in the nanocomposite at higher annealing temperatures, which removed the effect provided by the presence of the CDs.

Based on the preliminary studies, the following conditions were chosen for the nanocomposite preparation: CDs produced via hydrothermal treatment (200 °C for 8 h) using a 50:50 corn stover - citric acid ratio as carbon precursors mixed into TiO_2 prepared from TTIP, 4 wt% of CDs incorporated into TiO_2, annealing temperature of 300 °C, hereon described as $NC_{50:50}$. The corresponding nanocomposite resulted in a rate constant of 0.121 ± 0.0006 min^{-1} and %DR of 51.5 ± 1.7 % for an irradiation period of 60 minutes, which are significantly superior to those observed for similarly prepared bare TiO_2 previously analysed by our team (from TTIP, annealing at 300 °C, without the addition of CDs), 0.0023 ± 0.0003 min^{-1} and 16.6 ± 1.6 %, respectively [52]. Photocatalytic tests concerning TiO_2 annealed at 500 °C (0.0025 ± 0.0003 min^{-1} and 14.7 ± 1.4 %) and commercially available TiO_2 nanoparticles (0.0024 ± 0.0004 min^{-1} and 15.4 ± 1.2 %) further confirmed the increments obtained upon adding CDs. In summary, these results suggest that adding CDs to TiO_2 significantly increased the semiconductor's catalytic activity under visible-light irradiation and that additional tests are warranted.

Following that, the efficiency of $NC_{50:50}$ was compared to that of a benchmark consisting of commercially available TiO_2 nanoparticles over 5 h of visible-light irradiation (Fig. 2**a and b**). First and foremost, $NC_{50:50}$ is superior to commercial TiO2 regarding the reaction rate constant and %DR. Namely, $NC_{50:50}$ achieved a rate constant of 0.00949 min^{-1} versus 0.00192 min^{-1} for TiO_2. Regarding %DR, $NC_{50:50}$ managed to degrade 90.8 % of MB (240 min of irradiation), whereas TiO_2 had only removed 44.4 % after 300 min. Not only that, but $NC_{50:50}$

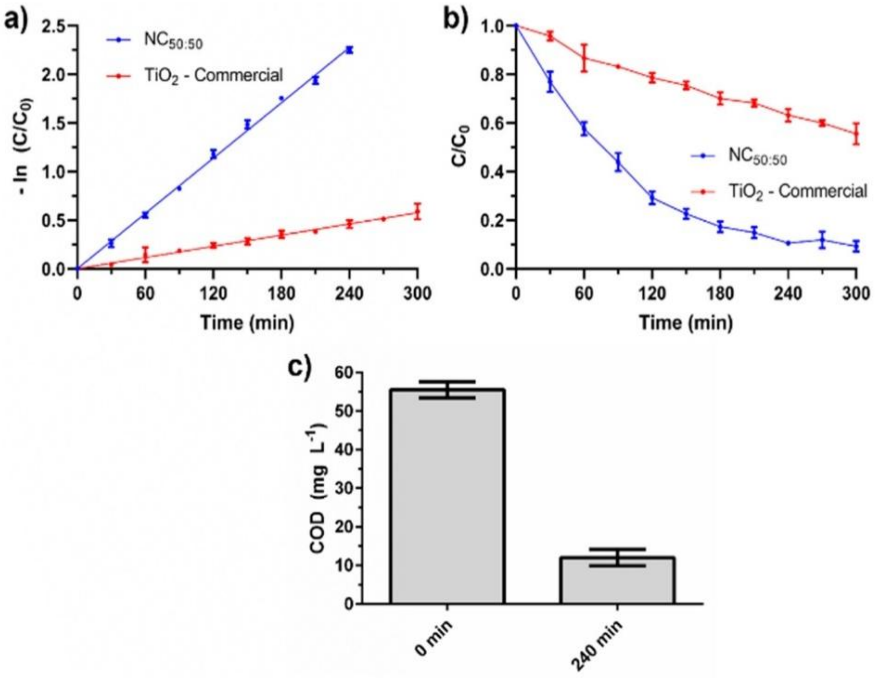


Fig. 2. a) representation of -ln (C_t/C_0) *versus* time of visible-light irradiation for $NC_{50:50}$ and commercial TiO_2; b) C_t/C_0values for the visible-light-driven photodegradation of MB; c) COD analysis for MB samples prior to and after irradiation (240 minutes, visible-light) in the presence of $NC_{50:50}$.

also presents higher rate constants than bare TiO_2 prepared in the same conditions as the nanocomposite and NC_{100} (containing CDs made solely of citric acid and ethylenediamine), which were 0.00200 and 0.00934 min^{-1}, as observed in a previous work [52]. The effect of photolysis is quite limited in these catalytic conditions, with a %DR of 35.5 % (360 min). Photodegradation in the presence of the CDs yielded similar results, suggesting that the CDs alone are insufficient to degrade MB in the same conditions.

To better evaluate the effect that adding CDs to TiO_2 has on the photocatalyst's %DR and reaction rate constant, we have calculated the extension of the enhancement of the catalytic efficiency induced by the addition of CDs via Eq. 3:

$$\%\ln(C) = 100 \quad x \quad \frac{k_{NC} - k_{TiO_2}}{k_{TiO_2}} \tag{3}$$

In this case, *% ln(C)* is a comparative measure of the enhancement of TiO_2's catalytic efficiency upon adding CDs, k_{NC} is the reaction rate constant obtained with the catalytic nanocomposite, and k_{TiO2} is the reaction rate constant of TiO_2 under similar conditions (annealing at 300 °C). Regarding $NC_{50:50}$, its calculated % ln(C) was 374 %, indicating that not only was there a significant performance enhancement upon adding the corn stover-containing CDs, but also that the catalytic performance was maintained even with the inclusion of an organic waste source as a co-carbon precursor for the CDs (using commercial reagents for CDs resulted in % ln(C) of 367 %) [52]. The pollutant removal was also evaluated via chemical oxygen demand (COD) analysis, which measures the oxygen necessary to fully oxidize the organic component found in contaminated aqueous samples and was already employed to quantify the degradation of MB from water-based samples [64,65]. COD analysis revealed a significant reduction in the oxidizable content after 240 minutes of irradiation (Fig. 2**c**), with the results demonstrating the removal of 82 % of the initial MB concentration, which is similar to the 90.8 % observed via spectrophotometry. Furthermore, a comparison between the absorption profiles of the samples before and after 240 minutes of visible-light irradiation (Figure S1) shows a clear decrease in MB's absorption peak. The absence of new peaks forming during the photodegradation suggests that no UV-Vis-absorbing by-products resulting are formed during MB's photodegradation.

$NC_{50:50}$ was also tested for the photodegradation of RhB, MO, and Orange II (same catalytic conditions but adjusting the concentration of each dye so that its absorbance was 0.5 at the maximum absorption wavelength) (Fig. 3**a** and **b**). First, it is worth noting that $NC_{50:50}$ could degrade all of the tested organic dyes under irradiation with visible light, albeit with varying catalytic potentials. In terms of rate constant (Fig. 3**a**), $NC_{50:50}$ was most effective for the degradation of MB (0.00949 min^{-1}), followed by RhB (0.00627 min^{-1}), Orange II (0.00328 min^{-1}), and finally, MO (0.00168 min^{-1}). The corresponding %DRs (Fig. 3**b**), 90.8, 81.7, 67.9, and 37.0, respectively, corroborated this.

Finally, to evaluate how $NC_{50:50}$ would perform in a more complex sample, we analysed its potential to photodegrade an aqueous mixture of MB and RhB (both at a 2.5 mg L^{-1} concentration). We observed that, under the same conditions, $NC_{50:50}$ maintained a good catalytic potential, achieving rate constants of 0.00810 and 0.00188 min^{-1} (Fig. 3**c**), respectively, with corresponding %DRs of 89.1 and 43.7 % (Fig. 3**d**). These results are quite interesting for two different reasons. First, even though we are now degrading a solution containing double the concentration of dyes (5 mg L^{-1} for MB and RhB together instead of 2.5 mg L^{-1} for tests with a single dye), $NC_{50:50}$ almost matched the rate constant and %DR obtained for MB when the dye was alone (0.00949 *vs* 0.00810 min^{-1} and 90.8 *vs* 89.1 %, respectively), suggesting that $NC_{50:50}$ retains its catalytic power even in more complex samples. Secondly, while the degradation parameters for MB remained nearly unchanged, this was not the case for RhB, whose %DR dropped from 81.7 % to 43.7 %. The degradation was considerably inhibited for this dye, as observed clearly by the different decrease of the absorption peaks corresponding to RhB and MB (Fig. 3**e**). This suggests a preference by $NC_{50:50}$ regarding the degradation targets, indicating that despite degrading both dyes, there is preference and selectivity toward MB when both dyes are together. Finally, the degradation was also assessed

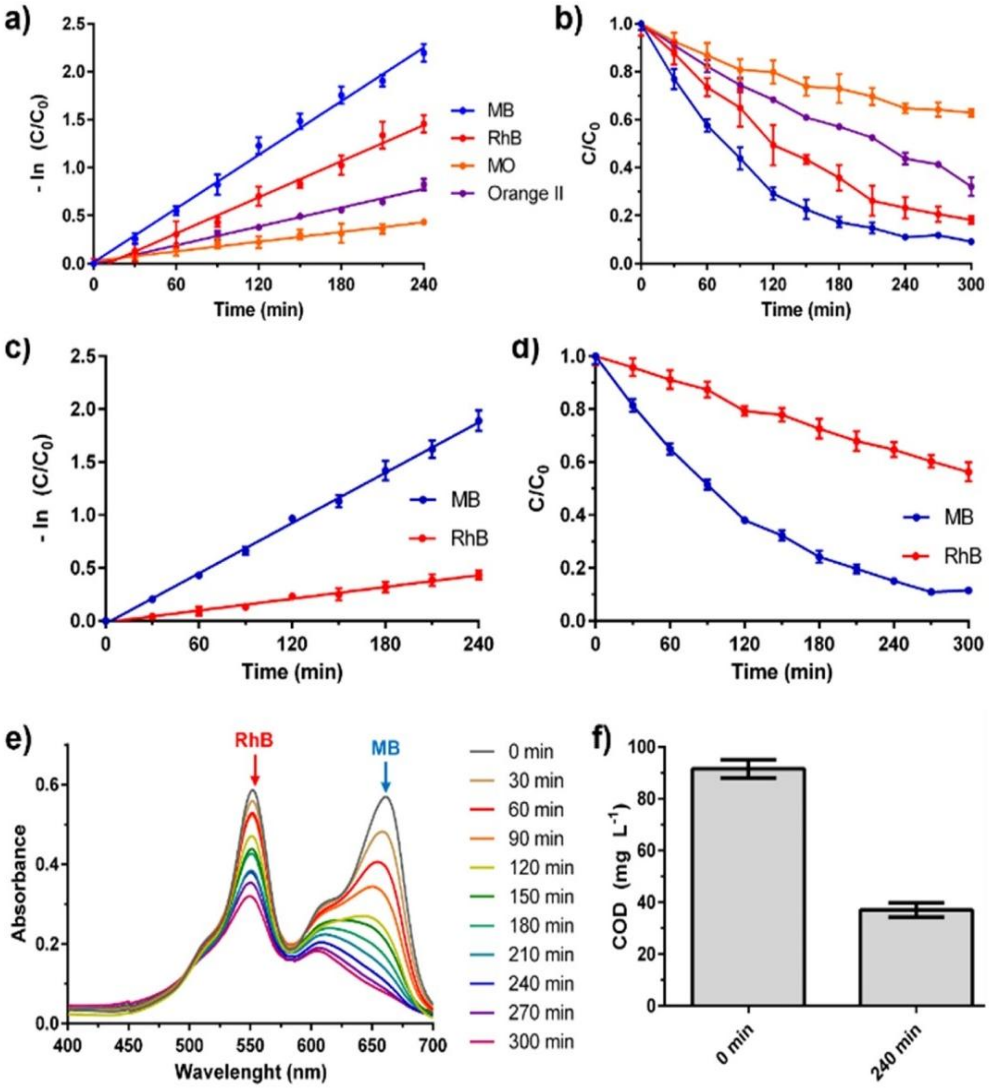


Fig. 3. a) plot of -ln(C_t/C_0) and b) C_t/C_0values *versus* irradiation time for the degradation of MB, RhB, MO and Orange II with $NC_{50:50}$; c) plot of -ln(C_t/C_0) and d) C_t/C_0 values *versus* visible-light irradiation time for the treatment of solution containing MB and RhB (2.5 mg L^{-1} each) with $NC_{50:50}$; e) full visible-range absorption spectra for $NC_{50:50}$-mediated MB/RhB samples degradation with increasing irradiation times; f) COD analysis for MB/RhB samples (2.5 mg L^{-1} each) prior to and after 240 minutes of irradiation with $NC_{50:50}$.

via COD (Fig. 3**f**), which indicated a 60 % decrease of the pollutants in the sample after irradiation.

3.1.2. Free radical scavenger studies

To gain insight into the reactive species behind the improved catalytic activity of $NC_{50:50}$, MB photodegradation experiments were made in the presence of free radical species. Namely, hydroxyl radicals (·OH), superoxide radicals ($O_2^{\cdot-}$), electrons (e^-), holes (h^+) and singlet oxygen ($^1O_2$) were scavenged using isopropyl alcohol (IPA, 10 mM), *p*-Benzoquinone (1 mM), potassium nitrate (KNO_3, 10 mM), potassium iodide (KI, 10 mM), and sodium azide (1 mM), respectively. The scavengers employed were chosen because the reactive species they target commonly participate in the catalytic mechanism of TiO_2 and its respective composites [43]. IPA and *p*-Benzoquinone are worthy of particular attention given that their respective target reactive species, hydroxyl and superoxide radicals, respectively, are the two most relevant species involved in bare TiO_2's mechanism [53,57].

The impact of each reactive species was gauged by quantifying the change in the %DR in the presence of the tested scavengers and is calculated as follows (Eq. 4) [52]:

$$\%DRV = \%DR_{test} - \%DR_{control} \quad (4)$$

Here, %DRV corresponds to the %DR variation when a scavenger (%DR_{test}) is added compared to a control test (%$DR_{control}$, standard photodegradation with the catalyst).

The test regarding the $NC_{50:50}$ composites (Fig. 4) yielded different outcomes depending on the reactive species tested. Tests using KI and sodium azide did not display any difference when compared to the control test (absence of scavengers), suggesting that their respective reactive species, h^+ and $^1O_2$, are not a part of the catalytic mechanism of $NC_{50:50}$. On the contrary, the %DR was considerably reduced in the presence of IPA (-14.5 ± 0.5 %), *p*-Benzoquinone (-17.6 ± 1.0 %), and KNO_3 (-12.8 ± 0.6 %). This demonstrates that their respective reactive species (hydroxyl radicals, superoxide radicals, and e^-, respectively) are

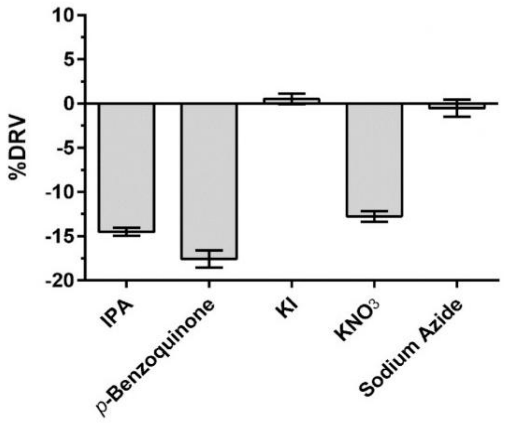


Fig. 4. Visible-light-driven $NC_{50:50}$-mediated p photodegradation of MB in the absence or presence of scavengers for reactive species. Results are presented in the form of %DRV. A negative %DRV value is an indication that the catalytic efficiency was hindered by the respective scavengers when compared to a control without scavengers.

part of the photocatalytic mechanism and that their absence due to the scavengers negatively impacted the photocatalytic performance of the nanocomposite. Finally, it is worth mentioning that photolysis alone can be responsive for up to 20 % of %DR, and so we must keep this in mind when analyzing the results of the scavengers' test.

In summary, under visible-light irradiation, three reactive species (·OH, $O_2^{\cdot-}$ and e^-) are responsible for the photocatalytic mechanism of the nanocomposite. When one or more of those species are scavenged, the photodegradation efficiency is negatively affected. Out of the three species, a slight prominence of the superoxide radical role is found compared to the other two species.

Interestingly, these results differ from those of another TiO_2/CDs nanocomposite. Namely, we have previously prepared one such nanocomposite (NC_{100}), and tested it toward MB degradation, in which the CDs had only citric acid (sole carbon precursor) and ethylenediamine as precursors [52]. In this case, the superoxide anion was the main contributor (%DRV of -29.3 ± 0.4 %) for the photodegradation, with only a small fraction of it being attributed to hydroxyl radical (%DRV of -5.6 ± 0.5 %) [52]. As for bare TiO_2, hydroxyl radicals were the main species behind the photodegradation mechanism, as previously observed [52].

This dominance of superoxide-driven photodegradation aligns well with previous studies concerning TiO_2/CDs nanocomposites using CDs made fully from commercially available reagents [66,67]. As for $NC_{50:50}$, including organic waste as part of the CDs led to a decrease in the predominance of the superoxide radical and the rise of the influence of the hydroxyl radical and the e^-.

3.1.3. Comparison to Literature

This emphasizes the sustainable development photocatalytic TiO_2/CDs nanocomposites with high visible-light efficiency. To evaluate the efficiency of our system, $NC_{50:50}$'s performance was compared with comparable composites available in the literature for the same purpose (MB photodegradation). The comparison was made in terms of % ln(C) (Table 1), as this value considers the benefits obtained with the addition of the CDs while also accounting for the variability of the conditions on which the different experiments may have been conducted (e.g. catalyst dosage, pollutant concentration, lamp intensity, among others). To make the results more comparable, for multi-component systems, the % ln(C) calculation was made considering only the presence and absence of CDs, ignoring the effect conferred by other components (e.g., TiO_2–Fe_2O_3–CDs *versus* TiO_2–Fe_2O_3, respectively). From the data available (Table 1), we observe that $NC_{50:50}$ achieved a very significant

Table 1
Literature reports regarding the photodegradation of organic dyes by different TiO_2-based nanocomposites under visible-light irradiation.

Nanocomposite	CDs precursors	Pollutant	% ln (C)	Ref.
TiO_2 – CDs	CA + Corn stover + EDA	MB	374	This work
TiO_2 – CDs	CA + EDA	MB	367	[52]
Molecularly imprinted TiO_2 - CDs	Lignite + H_2O_2 + Formic acid	MB	64	[68]
TiO_2 – Ag - CDs	Ethylene glycol	MB	233	[66]
TiO_2 – Fe_2O_3 – CDs	CA + EDA	MB	366	[67]
Oxygen rich TiO_2 – Peroxo - CDs	CA + Urea	MB	130	[69]
Oxygen rich TiO_2 – Peroxo - CDs	CA + Urea	Methyl Orange	200	[69]
TiO_2 microspheres - CDs	Glucose	Rhodamine B	160	[70]

enhancement of the catalytic efficiency despite including corn stover as a co-carbon precursor. When compared to other works in the literature, most studies presented % ln(C) between 64 % and 233 %, which was way below the 374 % enhancement obtained with $NC_{50:50}$. Aside from our own study, only one other team reported a close % ln(C) of 366 %, but that was using a composite including a third component (Fe_2O_3) that required a more resource- and time-intensive synthesis [67].

3.2. Materials characterization

After observing the enhancement of catalytic performance obtained with $NC_{50:50}$ compared to bare TiO2, it is now important to characterize catalysts to gain better insight regarding the basis of the superior performance obtained upon adding CDs. The CDs used for the making of $NC_{50:50}$ were prepared via a methodology previously developed by our laboratory, and their complete characterization may be found in [71].

We have started by comparing the photocatalysts in terms of optical properties. First, we investigated the optical absorption profile of bare TiO_2 (annealing stages at 300 and 500 °C), commercial TiO_2, NC_{100}, and $NC_{50:50}$, which includes corn stover as a co-carbon precursor for the CDs. By analyzing Fig. 5**a**, we can easily observe that the three types of TiO_2 present roughly the same profile, with TiO_2's absorption being limited to the UV range and an absorption edge at roughly 510 nm. The introduction of CDs alters the absorption profile, with both NC_{100} and $NC_{50:50}$, presenting an enhanced absorption between 400 and 600 nm. For $NC_{50:50}$, this effect is even more pronounced, with the nanocomposite absorbing radiation up to 700 nm and presenting a clear advantage regarding visible-light absorption. As for the reason behind the enhanced absorption in the visible region, reports have pointed out that Ti^{3+} ions can appear due to electron interchange with CDs, originating an enhanced absorption at $\lambda > 600$ nm [19]. For $NC_{50:50}$, there is a small, yet observable, absorption at wavelengths over 600 nm by $NC_{50:50}$, suggesting the presence of residual Ti^{3+} ions increases absorption at longer wavelengths. The enhanced absorption between 400 and 600 nm may be ascribed to the presence of the CDs themselves. Thus, either directly or indirectly (by originating Ti^{3+} ions), the CDs can improve the utilization of visible light by the nanocomposites, positively affecting its catalytic efficiency. Furthermore, the DRS data was used to calculate the band gap energies via Tauc's formula ($(\alpha h\nu)^2 = h\nu$), where α and $h\nu$ correspond to the absorbance and the energy of the photon at the corresponding wavelength, respectively). The calculated band gaps for TiO_2, 300 °C, and commercial, and NC50:50 are 3.32, 3.30, and 3.26 eV, respectively. This indicates that despite an improved visible irradiation uptake, the nanocomposite's bandgap remained unchanged.

The photoluminescence spectra of bare TiO_2 (300 °C), commercial TiO_2 and $NC_{50:50}$ was recorded and analysed to uncover the role of the CDs regarding the inhibition of the recombination of TiO_2's photoinduced charge carriers. As observable in Fig. 5**b**, TiO_2 and the

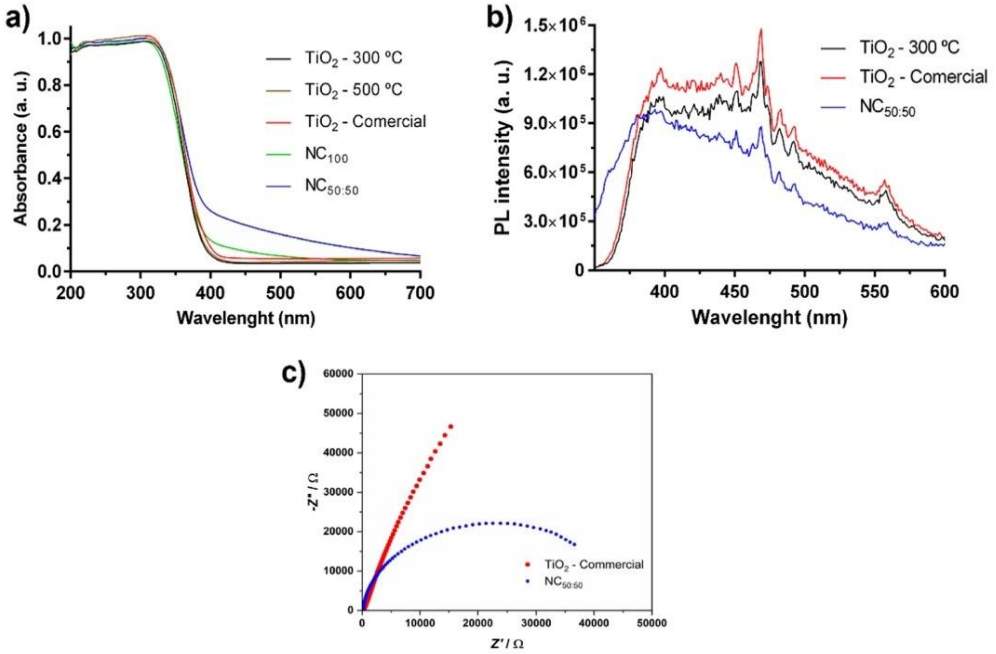


Fig. 5. a) UV-Vis DRS spectra of prepared bare TiO_2 (with annealing temperatures of 300 and 500 °C), commercial TiO_2, NC_{100} and $NC_{50:50}$; b) steady-state photoluminescence spectra of bare TiO_2 (annealing at 300 °C), commercial TiO_2 and $NC_{50.50}$ and c) electrochemical impedance spectroscopy of commercial TiO_2 and $NC_{50.50}$.

nanocomposites present a similar wide emission profile (350–600 nm). However, the addition of the CDs led to a significantly lower emission intensity in the respective nanocomposites when compared to TiO_2. This suggests that the interaction between TiO_2 and CDs results in a rapid transference of e^- via an electron transfer interface occurring between the CDs and TiO_2[52,72]. Given that after electron transfer, the CDs may act as a reservoir and retain the electron, the recombination of TiO_2's e^- and h^+ is prevented. As a result the catalytic process is favoured. The better catalytic efficiency and inhibition of the recombination means that there is less energy dissipated as radiation, resulting in a lower emission intensity, which is corroborated by previous reports[73,74]. Finally, the smaller impedance arc radius presented by $NC_{50:50}$ compared to commercial TiO_2 (Fig. 5**c**) indicates that the nanocomposite has a lower electron transfer resistance under visible-light irradiation. This, alongside the suggested improved optical absorption and delayed recombination of photogenerated charge carriers, demonstrates that adding the CDs can significantly promote the charge transfer and separation process.

To evaluate the morphology of $NC_{50:50}$, the catalyst was observed via SEM (Fig. 6). In line with other TiO_2-based compounds, $NC_{50:50}$ presented a rounded shape and an average size of 92.9 ± 16.5 nm [6,75]. Compared to similarly prepared bare TiO_2 (≈140 nm) [52], the smaller size of the nanocomposite may contribute towards a better catalytic efficiency upon the addition of CDs, as it was observed that for TiO_2, smaller sizes result in better catalytic efficiency [76]. Furthermore, $NC_{50:50}$ displays a certain tendency towards forming aggregates, which the CDs' functionalized surface may cause. Carboxyl, carbonyl, and amine groups, among others, are frequently present on these nanoparticles and may lead to electrostatic interactions and form hydrogen bonds between themselves, thus causing an agglomeration of particles

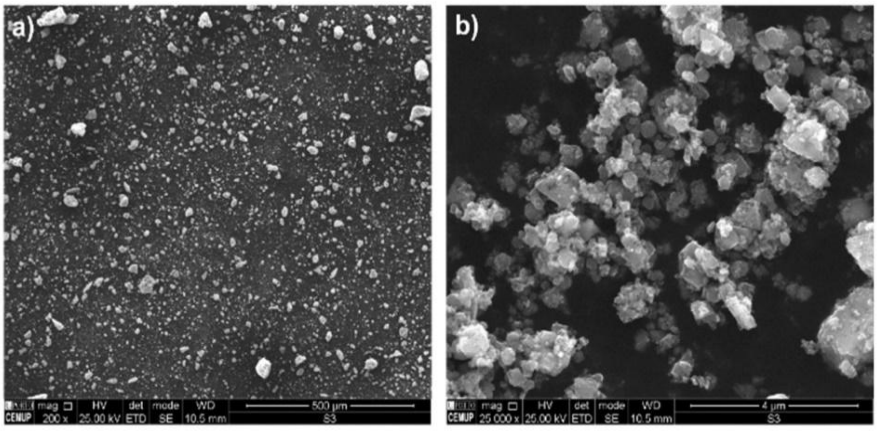


Fig. 6. SEM images of $NC_{50:50}$ at a) 200x and b) 25 000x magnification.

[77].

The XRD patterns of $NC_{50:50}$ were acquired and examined (Fig. 6**a**). The XRD pattern showed that $NC_{50:50}$ has the anatase crystal planes at (101) 25.12°, (004) 38.02°, (200) 47.83°, (105) 54.05° and (211) 54.98° and (204) 62.74° diffraction planes respectively [52,78]. Because of the great dispersion and low CDs content in $NC_{50:50}$, the usual diffraction peaks of CDs were not adequately seen [79]. FT-IR spectra was recorded for $NC_{50:50}$ and presented the expected signals (Fig. 6**b**). A small shoulder at 1629 cm^{-1} was attributed to carbonyl groups [78], while the wide band centered at 3311 cm^{-1} was attributed to the stretching vibration of -OH groups, confirming that carboxylic acid was the main group found on $NC_{50:50}$'s surface [80]. Finally, ~600 cm^{-1} we find a peak that can be attributed to the vibration of Ti-O-Ti bonds, which was not surprising considering the anatase structure described previously [80].

The surface of $NC_{50:50}$ was studied via XPS spectroscopy. We found that 46.5 and 30.4 % of it was O 1 s and C 1 s, respectively, as the main components, followed by a moderate content of Ti 2p, 22.2 %, and traces of N 1 s (0.8 %). When deconvoluted, the C 1s core level (Fig. 7**c**) revealed a major contribution (284.8 eV) attributed to the C-C/C-H bonds (89.9 %). The two bands found at 286.5 eV and 288.4 eV (C-N/C-O (5.84 %) and O═C-O (4.27 %) bonds, respectively), together with the high percentage of oxygen found (46.5 %) confirmed the existence of a surface covered with highly oxidized groups. Supporting this, the analysis and deconvolution of the O 1 s (Fig. 7**d**) presented bands at 530.1 (86.23 %) and 531.6 eV (13.77 %) ascribed to C–O/C–OH and carboxyl groups (-C═O), respectively (Fig. 7**b**). A small contribution from the N 1 s was observed at 400.1 eV related to the amine groups (Fig. 7**e**). Regarding the Ti 2p core level spectra, two bands were observed at 458.6 and 464.5 eV, being assigned to the Ti $2p_{3/2}$ and Ti $2p_{1/2}$ spin-orbital splitting photoelectrons, respectively (Fig. 7**f**).

To obtain information regarding the organic composition present in the nanocomposite at the atomic level, *ss*-^{1}H- and ^{13}C NMR studies were carried out. The ^{1}H MAS *ss*-NMR spectrum (Fig. 8**a**) for the nanoparticles

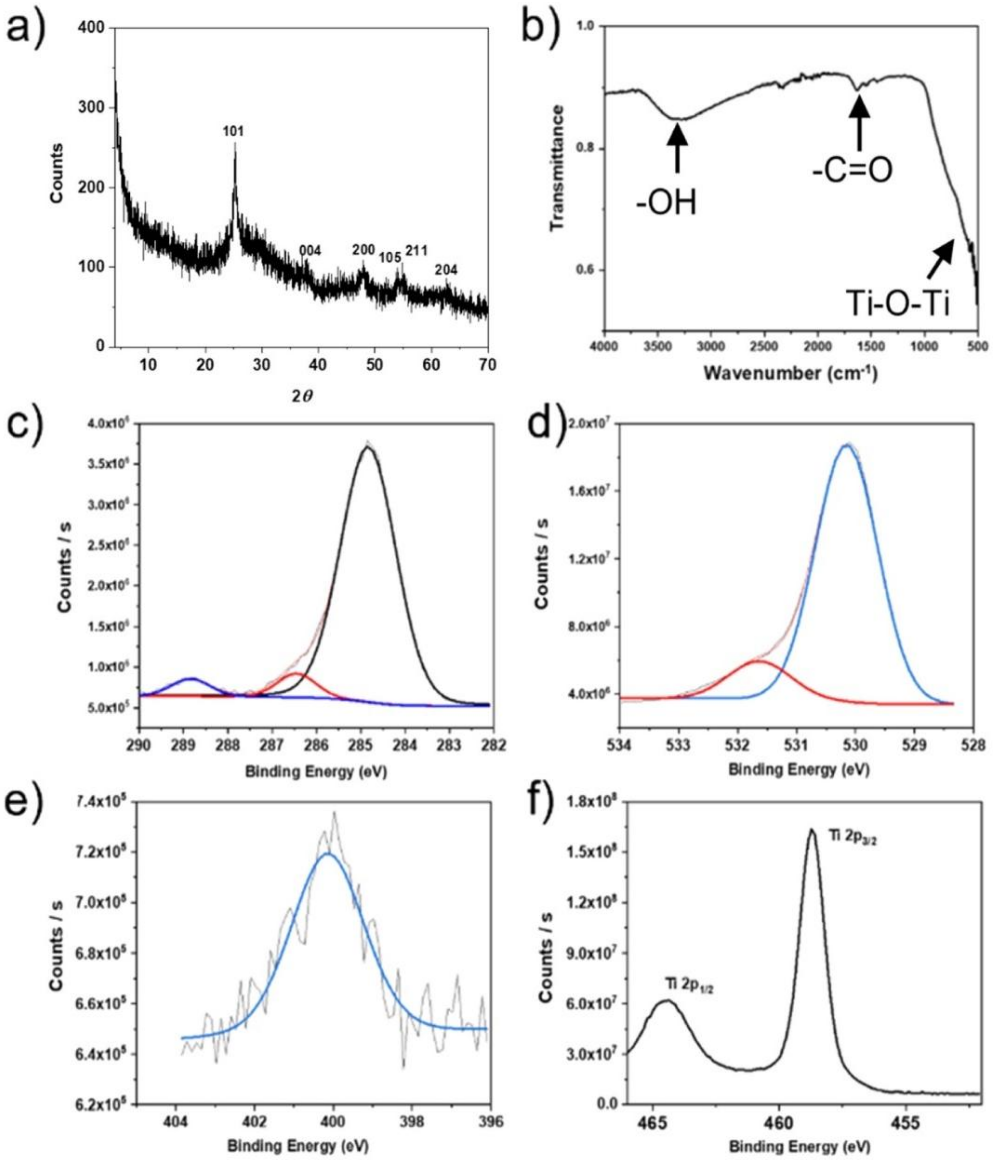


Fig. 7. a) XRD pattern; b) FT-IR spectra of $NC_{50:50}$; XPS core level spectra c) C 1 s d) O 1 s, e) N 1 s and f) Ti 2p of $NC_{50:50}$.

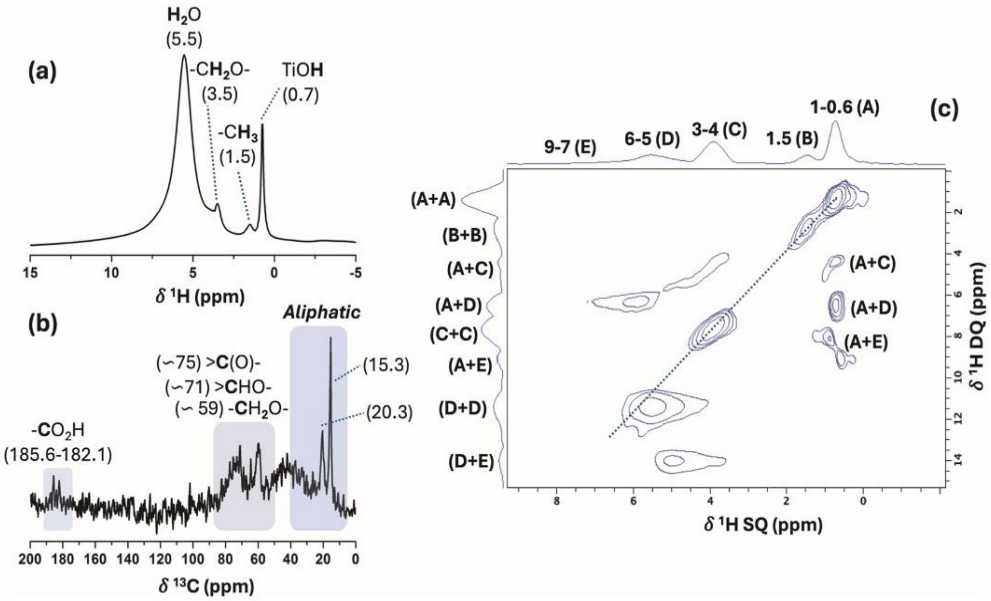


Fig. 8. **a)** ^{1}H MAS (MAS rate: 30 kHz), **b)** ^{13}C CP-MAS (MAS rate: 15 kHz) and **c)** 2D ^{1}H-^{1}H SQ-DQ (MAS rate: 30 kHz) spectra for the $NC_{50:50}$.

showed two main signals usually found in TiO_2 materials at a proton chemical shift (δ^1H) of ~0.7 and 5.5 ppm assigned to titanol groups and adsorbed water molecules, respectively [81,82]. The ^{13}C-CP-MAS spectrum shows the chemical surrounding of CD nanoparticles conjugated to TiO_2 nanocomposites (Fig. 8**b**). The organic content was mainly attributed to sp^3 hybridization carbon atoms, as determined by the NMR signal at a ^{13}C chemical shift (δ^{13}C) located between 0 and 80 ppm, being the signals at 80–60 ppm and 50–0 ppm assigned to oxygenated (>C(O)-, >CH-O- or -CH_2-OH) and aliphatic hydrocarbons (CH_3-, -CH_2-, >CH- or >C<), respectively. Besides, two low-intensity ^{13}C resonance signals were present at 185 and 182 ppm, which were ascribed to carboxylic acid carbons. The latter results agree with those obtained in XPS and FTIR experiments. Interestingly, important bulk chemical information was obtained even with a low signal-to-noise ratio in the ^{13} C CP-MAS spectrum. Thus, the highly oxygenated aliphatic structure can be proposed for covering the CDs conjugated to the novel TiO_2 nanocomposite. Commonly, the sp^2-conjugated core of the CD structure is observed neither with ^{13}C CP-MAS nor with direct polarization experiments.

2D ^{1}H *ss*-NMR experiments were performed for $NC_{50:50}$ (Fig. 8**c**). Less intense ^{1}H resonance signals from the hydrocarbon chain were observed at δ^1H of 1.5 and 3.5 ppm, which are related to the ^{13}C *ss*-NMR signals at δ^{13}C of 50–10 and 80–60 ppm, respectively. Furthermore, 2D ^{1}H-^{1}H SQ-DQ experiments were done to increase the resolution of the proton dimension. In this experiment, additional ^{1}H contributions were observed at high-frequency values. These contributions were associated with acidic bridging hydroxyl groups at 6–9 ppm of the TiO_2 particles [81,82]. Interestingly, the presence of the A-B correlation between the titanol group at a δ^1H of 0.9–0.6 ppm and the oxygenated aliphatic regions (δ^1H of 3–4 ppm) from the covering of the CDs demonstrate the presence of the nanocomposite arising from the short-range interactions between TiO_2 and CDs determined by the 2D ^{1}H-^{1}H SQ-DQ experiment. Besides, other cross-peaks (A-D and A-E correlations) were present between the titanol and other OH groups of the TiO_2 particles.

3.3. LCA studies

Considering our intended target of developing a more environmentally sustainable photocatalytic nanocomposite, the evaluation of the environmental impacts is an important step that needs to be considered to assess if adding corn stover as a co-carbon precursor had an overall beneficial effect. An LCA study was performed to evaluate if enhancing the photocatalytic efficiency of TiO_2 by adding CDs is worth the possibility of potentially increasing the impacts associated with the inclusion of the carbon nanoparticles and if partially utilizing corn stover instead of citric acid decreases the overall environmental impacts. For this purpose, the impacts associated with producing $NC_{50:50}$ were evaluated regarding midpoint impacts. Furthermore, the relative impacts of $NC_{50:50}$ were compared to those of NC_{100} and bare TiO_2. A weight-based functional unit (FU) was used in the first stage, followed by a function-based FU based on the rate constant of their respective photocatalyst, which was used in a later stage.

We began our study by evaluating the impacts associated with $NC_{50:50}$ using a FU of 1 kg of catalyst produced (Fig. 9). Herein, we also compared the relative contributions of individual inputs for the impact categories tested for TiO_2, $NC_{50:50}$, and NC_{100}. Impacts associated with energy usage during the preparation of the photocatalyst were not considered, as they would not be accurate for laboratory-scale studies and would not impact a comparison between $NC_{50:50}$, NC_{100}, and TiO_2, as the three processes require the same electricity-consuming steps.

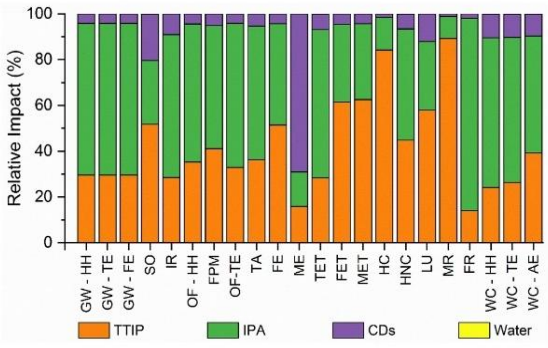


Fig. 9. The relative contribution of TTIP, IPA, CDs, and water toward different environmental impact categories of $NC_{50:50}$ calculated using the ReCiPe2016 LCIA and a weight-based FU of 1 kg of catalyst.

Regarding $NC_{50:50}$, the environmental impacts result mostly from TTIP and IPA for nearly all impact categories, apart from the marine eutrophication category, for which the CDs are the largest contributor. The categories of stratospheric ozone depletion, freshwater eutrophication, freshwater ecotoxicity, marine ecotoxicity, human carcinogenic toxicity, land use, and mineral resource scarcity are especially affected by TTIP. On the other hand, IPA contributes significantly to global warming (human health, terrestrial ecosystems, and freshwater ecosystems), ionization radiation, ozone formation (human health and terrestrial ecosystems), fine particular matter formation, terrestrial acidification, terrestrial ecotoxicity, fossil resource scarcity and water consumption (human health, terrestrial ecosystems, and aquatic ecosystems). When compared to similarly prepared bare TiO_2, published in ref [52], the impact distribution of $NC_{50:50}$ shows a mostly small contribution of the CDs towards all impact categories (and a major contribution towards marine eutrophication) which is not present in TiO_2 [52]. When compared to the results of NC_{100}, published in ref [52], we can see that, by employing corn stover as a co-carbon precursor and by relying in a lower hydrothermal reaction time (8 h versus 24 h), despite using 4 wt% instead of 2 wt% of CDs, the impacts ascribed to the presence of CDs in $NC_{50:50}$ are smaller than those found for the CDs in NC_{100}.

To facilitate the comparison between $NC_{50:50}$ and bare TiO_2/NC_{100}, we have compared regarding endpoint indicators, namely human health, ecosystems, and resources. First, when using a weight-based FU (Fig. 10**a**), $NC_{50:50}$'s impacts are lower than those of the alternatives, with TiO_2 being slightly less impactful than NC_{100}. From this, we can conclude two interesting facts: the synthesis of $NC_{50:50}$ is less impactful than that of NC_{100}, and thus, its respective CDs, due to requiring a lower reaction time and incorporating an organic waste source, appear to be more environmentally sustainable than those used for NC_{100}; and that the CDs included in $NC_{50:50}$ have slightly lower impacts than the bare TiO_2, given that substituting 4 wt% TiO_2 by those CDs led to a slight decrease of the impact in the three endpoint categories. The smaller impacts associated with $NC_{50:50}$ are even more pronounced when using a function-based FU (Fig. 10**b**). In this case, the FU was calculated by considering the highest rate constant (0.00949 min^{-1} for $NC_{50:50}$) and dividing it by the respective rate constants of NC_{100} (0.00934 min^{-1}) and bare TiO_2 (0.0020 min^{-1}). In terms of overall impacts, $NC_{50:50}$, when compared with bare TiO_2 and NC_{100}, presents lower relative environmental impacts due to having the lowest absolute environmental impacts (as observed when using a weight-based FU) while still achieving a considerable increase of the catalytic performance with the addition of the CDs. Thus, $NC_{50:50}$ is a more environmentally friendlier alternative to bare TiO_2 NC_{100} due to using CDs that require a lower reaction time and are prepared from an organic waste source, resulting in lower the endpoint impacts are diminished to the point that the inclusion of CDs decreases the impacts when compared to bare TiO_2. Including corn stover as a carbon precursor for CDs' fabrication is thus preferable in terms of performance and environmental sustainability.

4. Conclusion

In this work we have used CDs incorporating organic waste to address the limitations of using TiO_2 for the visible-light-driven degradation of MB. To this end, CDs were hydrothermally prepared using corn stover as a co-carbon precursor (with citric acid and the N-dopant ethylenediamine). The CDs were incorporated with TiO_2, resulting in a nanocomposite ($NC_{50:50}$) that presented a better performance under visible-light irradiation coupled to relatively environmental impacts compared to similar composites in the literature.

Regarding catalytic performance, $NC_{50:50}$ was more efficient than bare TiO_2, presenting a % ln (C) of 374 %, achieving a faster and more extensive photodegradation of MB. As for the catalytic mechanism, tests with reactive species scavengers revealed that the superoxide radical, hydroxyl radical, and e^-, by that order, are behind the photodegradation mechanism, differing from the results concerning bare TiO_2. $NC_{50:50}$ was also active towards RhB, Orange II, and MO. The optical characterization of $NC_{50:50}$ revealed that, by adding CDs, we managed to increase the uptake of radiation in the visible range and, at the same time, improve the photonic efficiency, both of which contribute towards the enhanced catalytic performance obtained with $NC_{50:50}$.

Finally, in a step toward developing a more environmentally sustainable process, we have prepared our CDs in a manner that led to the upcycling of organic waste, in this case by using corn stover, a major agricultural waste, as a carbon precursor. To study whether including these CDs is worth it in terms of environmental impacts, we have compared the environmental impacts associated with producing bare TiO_2, NC_{100}, and $NC_{50:50}$. Both when considering weight-based and function-based FUs, $NC_{50:50}$ presented the lowest relative environmental impacts, and so, was identified the best option for the photodegradation of MB. This study demonstrates that adding CDs to TiO_2 produces nanocomposites with enhanced photocatalytic properties, even when valuing organic waste as a co-carbon precursor, promoting a circular economy. Thus, this work provides a step toward a more environmentally sustainable design of visible-light-driven photocatalysts.

CRediT authorship contribution statement

Algarra Manuel: Writing – review & editing, Writing – original draft, Investigation, Funding acquisition. **Sendão Ricardo:** Writing – original draft, Visualization, Investigation. **Brandão Ana:** Investigation, Writing – original draft. **Lázaro-Martínez Juan:** Writing – review & editing, Writing – original draft, Visualization, Investigation. **Esteves da Silva Joaquim:** Writing – review & editing, Supervision. **Gil Antonio:** Writing – review & editing. **Pinto da Silva Luís:** Writing – review &

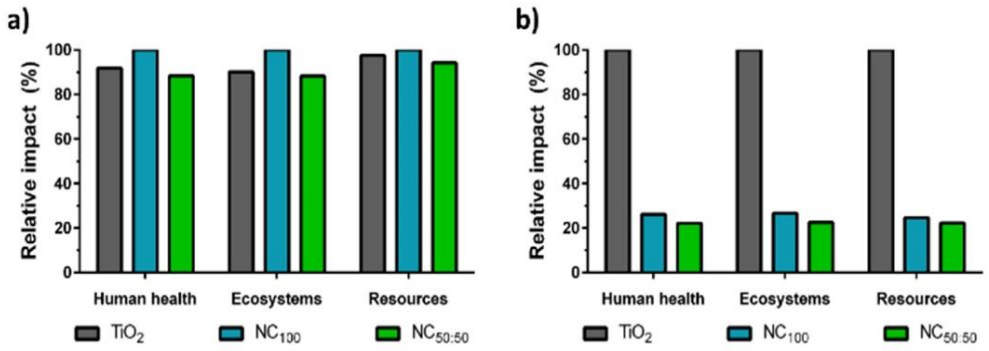


Fig. 10. Relative environmental profiles for TiO_2, $NC_{50:50}$ and NC_{100} obtained using ReCiPe 2016 v1.1 as LCIA. The comparison between the catalysts was made using a) a weight-based FU and b) a reaction rate constant-based FU.

editing, Supervision, Funding acquisition, Conceptualization. **Pereira Carlos M.:** Funding acquisition, Supervision, Writing – review & editing.

Declaration of Competing Interest

The authors declare that they have no known competing financial interests or personal relationships that could have appeared to influence the work reported in this paper.

Acknowledgements

The Portuguese "Fundação para a Ciência e Tecnologia" (FCT, Lisbon) is acknowledged for funding projects PTDC/QUI-QFI/2870/2020 and 2023.13127.PEX, R&D Units CIQUP (UIDB/00081/2020 and UIDP/00081/2020) and GreenUPorto (UIDB/05748/2020 and UIDP/05748/2020), and the Associated Laboratory IMS (LA/P/0056/2020). Carlos Pereira Portuguese acknowledges the Recovery and Resilience Plan and by the NextGeneration EU European funds in its component 12 – Sustainable Bioeconomy, Investment under project Bioshoes4All (TC-C12-i01). Luís Pinto da Silva acknowledges funding from FCT under the Scientific Employment Stimulus (CEECINST/00069/2021). Ricardo Sendão acknowledges FCT for his Ph.D. grant (2021.06149.BD). Manuel Algarra thanks the Spanish Ministry of Science and Innovation (MCIN/AEI/10.13039/501100011033) through the project PID2021–122613OB-I00.

Supporting information

The authors have included a summary of some background data inputs used for the LCA studies and some results (supporting tables and figures) for photocatalytic assays in the Supporting Information.

Appendix A. Supporting information

Supplementary data associated with this article can be found in the online version at doi:10.1016/j.colsurfa.2025.136475.

Data Availability

Data will be made available on request.

References

[1] M.M. Mekonnen, A.Y. Hoekstra, Four billion people facing severe water scarcity, Sci. Adv. 2 (2) (2016) e1500323, https://doi.org/10.1126/sciadv.1500323.
[2] J. Tollefson, How green is my future? Nature 473 (7346) (2011) 134–135, https://doi.org/10.1038/473134a.
[3] I.K. Konstantinou, T.A. Albanis, TiO_2-assisted photocatalytic degradation of azo dyes in aqueous solution: kinetic and mechanistic investigations, Appl. Catal. B. 49 (1) (2004) 1–14, https://doi.org/10.1016/j.apcatb.2003.11.010.
[4] P.E. Stackelberg, J. Gibs, E.T. Furlong, M.T. Meyer, S.D. Zaugg, R.L. Lippincott, Efficiency of conventional drinking-water-treatment processes in removal of pharmaceuticals and other organic compounds, Sci. Total Environ. 377 (2-3) (2007) 255–272, https://doi.org/10.1016/j.scitotenv.2007.01.095.
[5] L.F. Angeles, R.A. Mullen, I.J. Huang, C. Wilson, W. Khunjar, H.I. Sirotkin, A. E. McElroy, D.S. Aga, Assessing pharmaceutical removal and reduction in toxicity provided by advanced wastewater treatment systems, Environ. Sci.: Water Res. Technol. 6 (1) (2020) 62–77, https://doi.org/10.1039/c9ew00559e.
[6] Z. Guo, H. Wu, M. Li, T. Tang, J. Wen, X. Li, Phosphorus-doped graphene quantum dots loaded on TiO_2 for enhanced photodegradation, Appl. Surf. Sci. 526 (2020), https://doi.org/10.1016/j.apsusc.2020.146724.
[7] K.V. Karthik, A.V. Raghu, K.R. Reddy, R. Ravishankar, M. Sangeeta, N.P. Shetti, C. V. Reddy, Green synthesis of Cu-doped ZnO nanoparticles and its application for the photocatalytic degradation of hazardous organic pollutants, Chemosphere 287 (Pt 2) (2022) 132081, https://doi.org/10.1016/j.chemosphere.2021.132081.
[8] C.V. Reddy, R. Koutavarapu, K.R. Reddy, N.P. Shetti, T.M. Aminabhavi, J. Shim, Z-scheme binary 1D $ZnWO_4$ nanorods decorated 2D $NiFe_2O_4$ nanoplates as photocatalysts for high efficiency photocatalytic degradation of toxic organic pollutants from wastewater, J. Environ. Manag. 268 (2020) 110677, https://doi.org/10.1016/j.jenvman.2020.110677.
[9] C.V. Reddy, A. Nagar, N.P. Shetti, I.N. Reddy, S. Basu, J. Shim, R.R. Kakarla, Novel g $C_3N_4/BiVO_4$ heterostructured nanohybrids for high efficiency photocatalytic degradation of toxic chemical pollutants, Chemosphere 322 (2023) 138146, https://doi.org/10.1016/j.chemosphere.2023.138146.
[10] T. Fatima, S. Husain, J. Narang, M. Khanuja, N.P. Shetti, K.R. Reddy, Novel tungsten disulfide (WS_2) nanosheets for photocatalytic degradation and electrochemical detection of pharmaceutical pollutants, J. Water Process Eng. 47 (2022), https://doi.org/10.1016/j.jwpe.2022.102717.
[11] S.P. Smrithi, N. Kottam, B.R. Vergis, Heteroatom Modified Hybrid Carbon Quantum Dots Derived from Cucurbita pepo for the Visible Light Driven Photocatalytic Dye Degradation, Top. Catal. (2022), https://doi.org/10.1007/s11244-022-01581-x.
[12] I.M.F. Cardoso, R.M.F. Cardoso, L. Pinto da Silva, J.C.G. Esteves da Silva, UV-based advanced oxidation processes of remazol brilliant blue R dye catalyzed by carbon dots, Nanomaterials 12 (12) (2022), https://doi.org/10.3390/nano12122116.
[13] B. Zhang, H. Wu, S. Li, Y. Liu, P. Du, Z.-G. Wang, Enzyme-mimetic photodecarboxylation based on geometry-dependent supramolecular association, ACS Catal. 13 (10) (2023) 6763–6772, https://doi.org/10.1021/acscatal.3c01669.
[14] B.X. Li, D.K. Kim, S. Bloom, R.Y. Huang, J.X. Qiao, W.R. Ewing, D.G. Oblinsky, G. D. Scholes, D.W.C. MacMillan, Site-selective tyrosine bioconjugation via photoredox catalysis for native-to-bioorthogonal protein transformation, Nat. Chem. 13 (9) (2021) 902–908, https://doi.org/10.1038/s41557-021-00733-y.
[15] S. Malato, P. Fernández Ibáñez, M.I. Maldonado, J. Blanco, W. Gernjak, Decontamination and disinfection of water by solar photocatalysis: recent overview and trends, Catal. Today 147 (1) (2009) 1–59, https://doi.org/10.1016/j.cattod.2009.06.018.
[16] D. Spasiano, R. Marotta, S. Malato, P. Fernandez-Ibañez, I. Di Somma, Solar photocatalysis: materials, reactors, some commercial, and pre-industrialized applications. A comprehensive approach, Appl. Catal. B. 170-171 (2015) 90–123, https://doi.org/10.1016/j.apcatb.2014.12.050.
[17] K. Kabra, R. Chaudhary, R.L. Sawhney, Treatment of hazardous organic and inorganic compounds through aqueous-phase photocatalysis: a review, Ind. Eng. Chem. Res. 43 (24) (2004) 7683–7696, https://doi.org/10.1021/ie0498551.
[18] F. Meng, F. Lu, Z. Sun, J. Lü, A mechanism for enhanced photocatalytic activity of nano-size silver particle modified titanium dioxide thin films, Sci. China Technol. Sci. 53 (11) (2010) 3027–3032, https://doi.org/10.1007/s11431-010-4116-z.
[19] F. Zuo, L. Wang, T. Wu, Z. Zhang, D. Borchardt, P. Feng, Self-doped Ti^{3+} enhanced photocatalyst for hydrogen production under visible light, J. Am. Chem. Soc. 132 (34) (2010) 11856–11857, https://doi.org/10.1021/ja103843d.
[20] Y.-C. Lee, J.-W. Yang, Self-assembled flower-like TiO_2 on exfoliated graphite oxide for heavy metal removal, J. Ind. Eng. Chem. 18 (3) (2012) 1178–1185, https://doi.org/10.1016/j.jiec.2012.01.005.
[21] T.M. Khedr, S.M. El-Sheikh, A.A. Ismail, D.W. Bahnemann, Highly efficient solar light-assisted TiO_2 nanocrystalline for photodegradation of ibuprofen drug, Opt. Mater. 88 (2019) 117–127, https://doi.org/10.1016/j.optmat.2018.11.027.
[22] I.H. Chowdhury, S. Ghosh, M.K. Naskar, Aqueous-based synthesis of mesoporous TiO_2 and Ag–TiO_2 nanopowders for efficient photodegradation of methylene blue, Ceram. Int. 42 (2) (2016) 2488–2496, https://doi.org/10.1016/j.ceramint.2015.10.049.
[23] W. Ren, Z. Ai, F. Jia, L. Zhang, X. Fan, Z. Zou, Low temperature preparation and visible light photocatalytic activity of mesoporous carbon-doped crystalline TiO_2, Appl. Catal. B. 69 (3-4) (2007) 138–144, https://doi.org/10.1016/j.apcatb.2006.06.015.
[24] D. Barolet, F. Christiaens, M.R. Hamblin, Infrared and skin: friend or foe, J. Photochem. Photobiol. B. 155 (2016) 78–85, https://doi.org/10.1016/j.jphotobiol.2015.12.014.
[25] R. Daghrir, P. Drogui, D. Robert, Photoelectrocatalytic technologies for environmental applications, J. Photochem. Photobiol. A. 238 (2012) 41–52, https://doi.org/10.1016/j.jphotochem.2012.04.009.
[26] H. Dong, G. Zeng, L. Tang, C. Fan, C. Zhang, X. He, Y. He, An overview on limitations of TiO_2-based particles for photocatalytic degradation of organic pollutants and the corresponding countermeasures, Water Res 79 (2015) 128–146, https://doi.org/10.1016/j.watres.2015.04.038.
[27] O. Elbanna, P. Zhang, M. Fujitsuka, T. Majima, Facile preparation of nitrogen and fluorine codoped TiO_2 mesocrystal with visible light photocatalytic activity, Appl. Catal. B. 192 (2016) 80–87, https://doi.org/10.1016/j.apcatb.2016.03.053.
[28] A. Edreva, Generation and scavenging of reactive oxygen species in chloroplasts: a submolecular approach, Agric. Ecosyst. Environ. 106 (2-3) (2005) 119–133, https://doi.org/10.1016/j.agee.2004.10.022.
[29] J. Ni, W. Wang, D. Liu, Q. Zhu, J. Jia, J. Tian, Z. Li, X. Wang, Z. Xing, Oxygen vacancy-mediated sandwich-structural $TiO_{(2\,x)}$ /ultrathin g-$C_{(3)}N_{(4)}$/$TiO_{(2\,x)}$ direct Z-scheme heterojunction visible-light-driven photocatalyst for efficient removal of high toxic tetracycline antibiotics, J. Hazard. Mater. 408 (2021) 124432, https://doi.org/10.1016/j.jhazmat.2020.124432.
[30] A. Singh, P. Khare, S. Verma, A. Bhati, A.K. Sonker, K.M. Tripathi, S.K. Sonkar, Pollutant soot for pollutant dye degradation: soluble graphene nanosheets for visible light induced photodegradation of methylene blue, ACS Sustain. Chem. Eng. 5 (10) (2017) 8860–8869, https://doi.org/10.1021/acssuschemeng.7b01645.
[31] W. Tu, Y. Zhou, Q. Liu, S. Yan, S. Bao, X. Wang, M. Xiao, Z. Zou, An in situ simultaneous reduction-hydrolysis technique for fabrication of TiO_2-Graphene 2D sandwich-like hybrid nanosheets: graphene-promoted selectivity of photocatalytic-driven hydrogenation and coupling of CO_2 into methane and ethane, Adv. Funct. Mater. 23 (14) (2013) 1743–1749, https://doi.org/10.1002/adfm.201202349.
[32] D. Pan, J. Jiao, Z. Li, Y. Guo, C. Feng, Y. Liu, L. Wang, M. Wu, Efficient separation of electron–hole pairs in graphene quantum dots by TiO_2 Heterojunctions for Dye

Degradation, ACS Sustain. Chem. Eng. 3 (10) (2015) 2405–2413, https://doi.org/10.1021/acssuschemeng.5b00771.
[33] Y. Li, Z.M. Liu, Y.C. Wu, J.T. Chen, J.Y. Zhao, F.M. Jin, P. Na, Carbon dots-TiO_2 nanosheets composites for photoreduction of Cr(VI) under sunlight illumination: favorable role of carbon dots, Appl. Catal. B. 224 (2018) 508–517, https://doi.org/10.1016/j.apcatb.2017.10.023.
[34] R. Wang, K.-Q. Lu, Z.-R. Tang, Y.-J. Xu, Recent progress in carbon quantum dots: synthesis, properties and applications in photocatalysis, J. Mater. Chem. A. 5 (8) (2017) 3717–3734, https://doi.org/10.1039/c6ta08660h.
[35] N. Vale, S. Silva, D. Duarte, D.M.A. Crista, L. Pinto da Silva, J.C.G. Esteves da Silva, Normal breast epithelial MCF-10A cells to evaluate the safety of carbon dots, RSC Med. Chem. 12 (2) (2021) 245–253, https://doi.org/10.1039/d0md00317d.
[36] Y. Deng, M. Chen, G. Chen, W. Zou, Y. Zhao, H. Zhang, Q. Zhao, Visible-ultraviolet upconversion carbon quantum dots for enhancement of the photocatalytic activity of titanium dioxide, ACS Omega 6 (6) (2021) 4247–4254, https://doi.org/10.1021/acsomega.0c05182.
[37] J. Li, K. Tang, J. Yu, H. Wang, M. Tu, X. Wang, Nitrogen and chlorine co-doped carbon dots as probe for sensing and imaging in biological samples, R. Soc. Open Sci. 6 (1) (2019) 181557, https://doi.org/10.1098/rsos.181557.
[38] J. Joseph, A.A. Anappara, White-light-emitting carbon dots prepared by the electrochemical exfoliation of graphite, ChemPhysChem 18 (3) (2017) 292–298, https://doi.org/10.1002/cphc.201601020.
[39] H. He, X. Zheng, S. Liu, M. Zheng, Z. Xie, Y. Wang, M. Yu, X. Shuai, Diketopyrrolopyrrole-based carbon dots for photodynamic therapy, Nanoscale 10 (23) (2018) 10991–10998, https://doi.org/10.1039/c8nr02643b.
[40] M. Sabri, A. Habibi-Yangjeh, S. Vadivel, Activation of persulfate ions by TiO_2/carbon dots nanocomposite under visible light for photocatalytic degradations of organic contaminants, J. Mater. Sci. Mater. Electron. 30 (13) (2019) 12510–12522, https://doi.org/10.1007/s10854-019-01611-7.
[41] H. Zhou, B. Zhang, Z. Jiang, H. Zhao, Y. Zhang, Room-temperature synthesis of carbon dot/TiO_2 composites with high photocatalytic activity, Langmuir 39 (20) (2023) 7184–7191, https://doi.org/10.1021/acs.langmuir.3c00652.
[42] D. Saini, A.K. Garg, C. Dalal, S.R. Anand, S.K. Sonkar, A.K. Sonker, G. Westman, Visible-light-promoted photocatalytic applications of carbon dots: a review, ACS Appl. Nano Mater. 5 (3) (2022) 3087–3109, https://doi.org/10.1021/acsanm.1c04142.
[43] R.M.S. Sendão, J.C.G. Esteves da Silva, L. Pinto da Silva, Photocatalytic removal of pharmaceutical water pollutants by TiO_2 - Carbon dots nanocomposites: a review, Chemosphere 301 (2022) 134731, https://doi.org/10.1016/j.chemosphere.2022.134731.
[44] J. Tian, Y. Leng, Z. Zhao, Y. Xia, Y. Sang, P. Hao, J. Zhan, M. Li, H. Liu, Carbon quantum dots/hydrogenated TiO_2 nanobelt heterostructures and their broad spectrum photocatalytic properties under UV, visible, and near-infrared irradiation, Nano Energy 11 (2015) 419–427, https://doi.org/10.1016/j.nanoen.2014.10.025.
[45] D.M.A. Crista, J.C.G. Esteves da Silva, L. Pinto da Silva, Evaluation of different bottom-up routes for the fabrication of carbon dots, Nanomaterials 10 (7) (2020), https://doi.org/10.3390/nano10071316.
[46] R. Sendão, Md.V.Md Yuso, M. Algarra, J.C.G. Esteves da Silva, L. Pinto da Silva, Comparative life cycle assessment of bottom-up synthesis routes for carbon dots derived from citric acid and urea, J. Clean. Prod. 254 (2020), https://doi.org/10.1016/j.jclepro.2020.120080.
[47] S. Fernandes, J.C.G. Esteves da Silva, L. Pinto da Silva, Comparative life cycle assessment of high-yield synthesis routes for carbon dots, NanoImpact 23 (2021), https://doi.org/10.1016/j.impact.2021.100332.
[48] W. Zhao, Y. Cui, X. Sun, H. Wang, X. Teng, Corn stover biochar increased edible safety of spinach by reducing the migration of mercury from soil to spinach, Sci. Total Environ. 758 (2021) 143883, https://doi.org/10.1016/j.scitotenv.2020.143883.
[49] R.M.S. Sendão, D.M.A. Crista, A.C.P. Afonso, M.D.V. Martinez de Yuso, M. Algarra, J.C.G. Esteves da Silva, L. Pinto da Silva, Insight into the hybrid luminescence showed by carbon dots and molecular fluorophores in solution, Phys. Chem. Chem. Phys. 21 (37) (2019) 20919–20926, https://doi.org/10.1039/c9cp03730f.
[50] A. El Mragui, I. Daou, O. Zegaoui, Influence of the preparation method and ZnO/(ZnO + TiO_2) weight ratio on the physicochemical and photocatalytic properties of ZnO-TiO_2 nanomaterials, Catal. Today 321-322 (2019) 41–51, https://doi.org/10.1016/j.cattod.2018.01.016.
[51] A. El Mragui, Y. Logvina, L. Pinto da Silva, O. Zegaoui, J.C.G. Esteves da Silva, Synthesis of Fe- and Co-doped TiO_2 with improved photocatalytic activity under visible irradiation toward carbamazepine degradation, Materials 12 (23) (2019), https://doi.org/10.3390/ma12233874.
[52] R.M.S. Sendão, M. Algarra, E. Ribeiro, M. Pereira, A. Gil, N. Vale, J.C.G. Esteves da Silva, L. Pinto da Silva, Carbon dots–TiO_2 nanocomposites for the enhanced visible-light driven photodegradation of methylene blue, Adv. Sustain. Syst. (2023), https://doi.org/10.1002/adsu.202300317.
[53] A. El Mragui, O. Zegaoui, J.C.G. Esteves da Silva, Elucidation of the photocatalytic degradation mechanism of an azo dye under visible light in the presence of cobalt doped TiO_2 nanomaterials, Chemosphere 266 (2021) 128931, https://doi.org/10.1016/j.chemosphere.2020.128931.
[54] D. Melgoza, A. Hernandez-Ramirez, J.M. Peralta-Hernandez, Comparative efficiencies of the decolourisation of Methylene Blue using Fenton's and photo-Fenton's reactions, Photochem. Photobiol. Sci. 8 (5) (2009) 596–599, https://doi.org/10.1039/b817287k.
[55] S.F. Baranovskii, P.A. Bolotin, M.P. Evstigneev, Aggregation of 1,3,7-trimethylxanthine with methylene blue in aqueous solution, J. Appl. Spectrosc. 73 (2) (2006) 171–177, https://doi.org/10.1007/s10812-006-0054-8.
[56] S. Farjadfar, M. Ghiaci, S.A. Kulinich, W. Wunderlich, Efficient photocatalyst for the degradation of cationic and anionic dyes prepared via modification of carbonized mesoporous TiO_2 by encapsulation of carbon dots, Mater. Res. Bull. 155 (2022), https://doi.org/10.1016/j.materresbull.2022.111963.
[57] J. Zhang, Q. Liu, H. He, F. Shi, G. Huang, B. Xing, J. Jia, C. Zhang, Coal tar pitch as natural carbon quantum dots decorated on TiO_2 for visible light photodegradation of rhodamine B, Carbon 152 (2019) 284–294, https://doi.org/10.1016/j.carbon.2019.06.034.
[58] B. Pastina, J.A. LaVerne, S.M. Pimblott, Dependence of molecular hydrogen formation in water on scavengers of the precursor to the hydrated electron, J. Phys. Chem. A. 103 (29) (1999) 5841–5846, https://doi.org/10.1021/jp991222q.
[59] M. Bancirova, Sodium azide as a specific quencher of singlet oxygen during chemiluminescent detection by luminol and Cypridina luciferin analogues, Luminescence 26 (6) (2011) 685–688, https://doi.org/10.1002/bio.1296.
[60] R. Hischier, T. Walser, Life cycle assessment of engineered nanomaterials: state of the art and strategies to overcome existing gaps, Sci. Total Environ. 425 (2012) 271–282, https://doi.org/10.1016/j.scitotenv.2012.03.001.
[61] S. Feijoo, S. González-García, Y. Moldes-Diz, C. Vazquez-Vazquez, G. Feijoo, M. T. Moreira, Comparative life cycle assessment of different synthesis routes of magnetic nanoparticles, J. Clean. Prod. 143 (2017) 528–538, https://doi.org/10.1016/j.jclepro.2016.12.079.
[62] J. Falbe, H. Bahrmann, W. Lipps, D. Mayer, Ullmann's Encyclopedia of Industrial Chemistry, ed. Wiley-VCH. Weinheim: Wiley-VCH.
[63] G. Rajender, J. Kumar, P.K. Giri, Interfacial charge transfer in oxygen deficient TiO_2 graphene quantum dot hybrid and its influence on the enhanced visible light photocatalysis, Appl. Catal. B. 224 (2018) 960–972, https://doi.org/10.1016/j.apcatb.2017.11.042.
[64] A.V. Borhade, D.R. Tope, B.K. Uphade, An efficient photocatalytic degradation of methyl blue dye by using synthesised PbO nanoparticles, E-J. Chem. 9 (2) (2012) 705–715, https://doi.org/10.1155/2012/362680.
[65] T. Zhao, R. Liu, J. Lu, X. Zhu, X. Zhu, K. Lu, H. Zhu, Photocatalytic degradation of methylene blue solution by diphenylanthrazoline compounds, J. Phys. Org. Chem. 30 (12) (2017), https://doi.org/10.1002/poc.3712.
[66] C. Wang, K. Yang, X. Wei, S. Ding, F. Tian, F. Li, One-pot solvothermal synthesis of carbon dots/Ag nanoparticles/TiO_2 nanocomposites with enhanced photocatalytic performance, Ceram. Int. 44 (18) (2018) 22481–22488, https://doi.org/10.1016/j.ceramint.2018.09.017.
[67] J. Zhang, M. Kuang, J. Wang, R. Liu, S. Xie, Z. Ji, Fabrication of carbon quantum dots/TiO_2/Fe_2O_3 composites and enhancement of photocatalytic activity under visible light, Chem. Phys. Lett. 730 (2019) 391–398, https://doi.org/10.1016/j.cplett.2019.06.011.
[68] J. Yu, C. Zhang, Y. Yang, T. Su, G. Yi, X. Zhang, Facile synthesis of molecularly imprinted black TiO_{2-x}/carbon dots nanocomposite and its recognizable photocatalytic performance under visible-light, Appl. Surf. Sci. 551 (2021), https://doi.org/10.1016/j.apsusc.2021.149476.
[69] S. Feizpoor, A. Habibi-Yangjeh, I. Ahadzadeh, K. Yubuta, Oxygen-rich TiO_2 decorated with C-Dots: highly efficient visible-light-responsive photocatalysts in degradations of different contaminants, Adv. Powder Technol. 30 (6) (2019) 1183–1196, https://doi.org/10.1016/j.apt.2019.03.014.
[70] R. Liu, H. Li, L. Duan, H. Shen, Y. Zhang, X. Zhao, In situ synthesis and enhanced visible light photocatalytic activity of C-TiO_2 microspheres/carbon quantum dots, Ceram. Int. 43 (12) (2017) 8648–8654, https://doi.org/10.1016/j.ceramint.2017.03.184.
[71] S. Fernandes, M. Algarra, A. Gil, J. Esteves da Silva, L. Pinto da Silva, Development of a facile and green synthesis strategy for brightly fluorescent carbon dots from various waste materials, ChemSusChem (2024) e202401702, https://doi.org/10.1002/cssc.202401702.
[72] S. Tong, J. Zhou, L. Ding, C. Zhou, Y. Liu, S. Li, J. Meng, S. Zhu, S. Chatterjee, F. Liang, Preparation of carbon quantum dots/TiO_2 composite and application for enhanced photodegradation of rhodamine B, Colloids Surf. A Physicochem. Eng. Asp. 648 (2022), https://doi.org/10.1016/j.colsurfa.2022.129342.
[73] R.J.B. Peters, G. van Bemmel, N.B.L. Milani, G.C.T. den Hertog, A.K. Undas, M. van der Lee, H. Bouwmeester, Detection of nanoparticles in Dutch surface waters, Sci. Total Environ. 621 (2018) 210–218, https://doi.org/10.1016/j.scitotenv.2017.11.238.
[74] M.J. Riding, F.L. Martin, K.C. Jones, K.T. Semple, Carbon nanomaterials in clean and contaminated soils: environmental implications and applications, Soil 1 (1) (2015) 1–21, https://doi.org/10.5194/soil-1-1-2015.
[75] R. Hatefi, H. Younesi, A. Mashinchian Moradi, S. Nojavan, A facile decoration of anatase Fe_3O_4/TiO_2 nanocomposite with graphene quantum dots: Synthesis, characterization, and photocatalytic activity, Adv. Powder Technol. 32 (7) (2021) 2410–2422, https://doi.org/10.1016/j.apt.2021.05.020.
[76] N. Xu, Z. Shi, Y. Fan, J. Dong, J. Shi, M.Z.C. Hu, Effects of particle size of TiO_2 on photocatalytic degradation of methylene blue in aqueous suspensions, Ind. Eng. Chem. Res. 38 (2) (1999) 373–379, https://doi.org/10.1021/ie980378u.
[77] Y. Ru, G.I.N. Waterhouse, S. Lu, Aggregation in carbon dots, Aggregate 3 (6) (2022), https://doi.org/10.1002/agt2.296.
[78] S. Feizpoor, A. Habibi-Yangjeh, K. Yubuta, Integration of carbon dots and polyaniline with TiO_2 nanoparticles: Substantially enhanced photocatalytic activity to removal various pollutants under visible light, J. Photochem. Photobiol. A. 367 (2018) 94–104, https://doi.org/10.1016/j.jphotochem.2018.08.017.
[79] Q. Que, Y. Xing, Z. He, Y. Yang, X. Yin, W. Que, Bi_2O_3/Carbon quantum dots heterostructured photocatalysts with enhanced photocatalytic activity, Mater. Lett. 209 (2017) 220–223, https://doi.org/10.1016/j.matlet.2017.07.115.

[80] Y. Fang, Co modified commercial P25 TiO_2 by Fe doping and g C_3N_4 coating as high performance photocatalyst under visible light irradiation, Int. J. Electrochem. Sci. (2017) 5951–5963, https://doi.org/10.20964/2017.07.77.
[81] M. Crocker, R.H.M. Herold, A.E. Wilson, M. Mackay, C.A. Emeis, A. M. Hoogendoorn, ^{1}H NMR spectroscopy of titania. Chemical shift assignments for hydroxy groups in crystalline and amorphous forms of TiO_2, J. Chem. Soc. Faraday Trans. 92 (15) (1996), https://doi.org/10.1039/ft9969202791.
[82] F. Ding, C.L. Tavera Méndez, J.P. Grass, R.W. Crisp, M.K.S. Barr, D. Wisser, Solid state NMR spectroscopic investigation of TiO_2 GRown on silica nanoparticles by solution atomic layer deposition, Adv. Mater. Interfaces 10 (17) (2023), https://doi.org/10.1002/admi.202202131.

2.1.2.2. Supplementary information

Visible-light photodegradation of organic dyes by Titanium Dioxide – Carbon Dots nanocomposites incorporating corn stover

Ricardo M.S. Sendão,[1] Manuel Algarra,[2] Juan Lázaro-Martínez,[3] Ana T. S. C. Brandão,[4] Antonio Gil,[2] Carlos Pereira,[4] Joaquim C.G. Esteves da Silva,[1,5] and Luís Pinto da Silva*[,1,5]

[1] Chemistry Research Unit (CIQUP), Institute of Molecular Sciences (IMS), Department of Geosciences, Environment and Territorial Planning, Faculty of Sciences, University of Porto, Rua do Campo Alegre s/n, 4169-007 Porto, Portugal

[2] INAMAT[2] - Institute for Advanced Materials and Mathematics. Department of Science. Public University of Navarra. Campus de Arrosadia, 31006 Pamplona, Spain

[3] Universidad de Buenos Aires, Facultad de Farmacia y Bioquímica, Departamento de Ciencias Químicas and Instituto de Química y Metabolismo del Fármaco (IQUIMEFA-UBA-CONICET), Ciudad Autónoma de Buenos Aires, Argentina

[4] Chemistry Research Unit (CIQUP), Institute of Molecular Sciences (IMS), Department of Chemistry and Biochemistry, Faculty of Sciences, University of Porto, Rua do Campo Alegre s/n, 4169-007 Porto, Portugal

[5] LACOMEPHI, GreenUPorto, Department of Geosciences, Environment and Territorial Planning, Faculty of Sciences, University of Porto, Rua do Campo Alegre s/n, 4169- 007 Porto, Portugal

* luis.silva@fc.up.pt

Materials and methods

Table S1. Summary of Ecoinvent® 3.9.background data used to create the processes for CDs and TTIP.

Process	Background data
CDs	Citric acid [1]| market for | Cut-off, S
	Ethylenediamine {RER}| market for ethylenediamine | Cut-off, S
	Sodium hydroxide, without water, in 50% solution state [1]| market for | Cut-off, S
	Water, deionized, from tap water, at user {Europe without Switzerland} | market for
	Electricity, medium voltage {PT}| market for | Cut-off, S
TTIP	Ammonia, liquid {RER}| market for | Cut-off, S
	Isopropanol {RER}| production | Cut-off, S
	Titanium tetrachloride [1]| production | Cut-off, S
	Transport, freight train {RER}| market group for transport, freight train | Cut-off, S
	Electricity, medium voltage {RER}| market group for | Cut-off, S
	Transport, freight, lorry 16-32 metric ton, EURO3 {RER}| transport, freight, lorry 16-32 metric ton, EURO3 | Cut-off, S

Results and discussion

Photocatalytic studies

Evaluation of the photocatalytic performance

Table S2. Preliminary test data regarding the making of catalytic nanocomposites made from TiO_2 and 2 wt% CDs with different corn stover : citric acid ratios as co-carbon precursors. CDs were prepared via hydrothermal treatment (200 ºC for 24 h).

Corn stover : Citric acid ratio	k (min^{-1})	%DR
75 : 25	0.0025 ± 0.0005	12.6 ± 2.2
50 : 50	0.0051 ± 0.0004	26.4 ± 1.2
25 : 75	0.0036 ± 0.0003	19.4 ± 1.1

Table S3. Preliminary test data regarding the making of catalytic nanocomposites made from TiO_2 and 2 wt% CDs. CDs were prepared via hydrothermal treatment at 200 ºC, with reaction times between 4 and 24 h being tested. Corn stover : citric acid ratio was 50:50.

Reaction time (h)	k (min^{-1})	%DR
4	0.0090 ± 0.0011	41.5 ± 3.9
8	0.0111 ± 0.0012	48.4 ± 3.7
16	0.0081 ± 0.0003	38.6 ± 0.8
24	0.0051 ± 0.0004	26.4 ± 1.2

Table S4. Preliminary test data regarding the making of catalytic nanocomposites made from TiO_2 and 4 wt% CDs using different annealing temperatures.

Annealing temperature (ºC)	k (min^{-1})	%DR
300	0.0121 ± 0.0006	51.5 ± 1.7
350	0.0029 ± 0.0002	16.0 ± 1.1
400	0.0027 ± 0.0001	14.4 ± 0.8
450	0.0029 ± 0.0004	15.6 ± 1.5
500	0.0012 ± 0.0001	7.2 ± 0.7

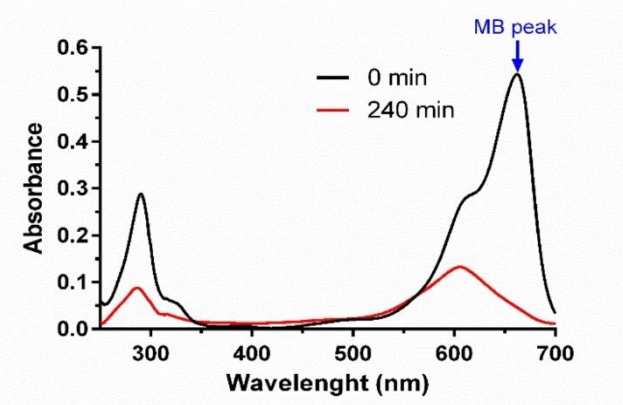


Figure S1. Absorption spectra of MB samples before and after visible-light irradiation in the presence of $NC_{50:50}$.

References

1. F. Yuan, Y.-K. Wang, G. Sharma, Y. Dong, X. Zheng, P. Li, A. Johnston, G. Bappi, J.Z. Fan, H. Kung, B. Chen, M.I. Saidaminov, K. Singh, O. Voznyy, O.M. Bakr, Z.-H. Lu, E.H. Sargent, Bright high-colour-purity deep-blue carbon dot light-emitting diodes via efficient edge amination, Nature Photonics. 14(3) (2019) 171-176, https://doi.org/10.1038/s41566-019-0557-5

2.1.2.3. Conclusion

This work presents the successful development of $NC_{50:50}$, a nanocomposite that integrates CDs that embody corn stover, an agricultural waste that consists of a by-product of the corn industry. $NC_{50:50}$ managed to achieve a substantial enhancement in photocatalytic efficiency when compared to TiO_2, achieving a 374% increase in the catalytic efficiency despite partly substituting commercial reagents with an organic waste. Notably, the incorporation of corn stover as a co-carbon precursor did not compromise the functionality of the CDs regarding their conjugation with TiO_2. On the contrary, the nanocomposite outperformed both bare TiO_2 and NC_{100} (corresponding to the nanocomposite described in section 2.1.1.), highlighting the potential of employing biomass as a carbon source.

Furthermore, LCA studies confirmed that $NC_{50:50}$ had lower environmental impacts than both NC_{100} and bare TiO_2, particularly when considering a function-based FU that accounts for the fact that a more resource and energy-intensive synthesis may be offset by a higher efficiency in the resulting material. These improvements are attributed to the fact that $NC_{50:50}$ displays a high photocatalytic efficiency and that using corn stover instead of CA reduces the need for commercial reagents, minimizing the environmental impacts associated with their production. Furthermore, the CDs were also synthesized using a hydrothermal process that required a lower reaction time, further decreasing the associated impacts.

By demonstrating that an abundant waste material can be upcycled into a high-performing nanocomposite, this work provides a basis for how to improve the sustainability of TiO_2/CDs nanocomposites by reducing the impacts associated with the procurement of the raw materials required for their production. $NC_{50:50}$ highlights that it is possible to decrease the environmental impacts of a product without compromising its performance.

2.2. Sunlight-driven photodegradation of ciprofloxacin

Article

Enhanced Photocatalytic Degradation of Ciprofloxacin Under Natural Sunlight Using a Waste-Derived Carbon Dots–TiO_2 Nanocomposite

Sendão, Ricardo M. S.; Brandão, Ana; Pereira, Carlos, Esteves da Silva, Joaquim C. G.; Pinto da Silva, Luís. "Enhanced Photocatalytic Degradation of Ciprofloxacin Under Natural Sunlight Using a Waste-Derived Carbon Dots–TiO_2 Nanocomposite". *Catalysts* 16(2) (**2026**): 142. http://doi.org /10.3390/catal16020142.

2.2.1. Introduction and contributions to this work

This works consists of the main objective of my doctoral project. Namely, herein we report a high efficiency sunlight-driven photodegradation of the antibiotic CIP using $NC_{50:50}$, a photocatalytic nanocomposite prepared from TiO_2, and CDs made from corn stover, CA and EDA via hydrothermal treatment. The resulting nanocomposites, aside from presenting an enhanced absorption of visible light and an improved photonic efficiency, also presented a larger specific surface area than TiO_2. As a result, in laboratory conditions, after adding the CDs to TiO_2, a 217% enhancement of the catalytic efficiency was observed regarding the photodegradation of CIP under solar irradiation. In fact, CIP was virtually fully degraded under 20 minutes of irradiation, presenting a rate constant of 0.2372 min^{-1}, which is higher than any other TiO_2-based system available in the literature with similar or higher catalyst dosages and CIP concentrations. Furthermore, while potential degradation by-products were detected via HPLC-DAD, these subsequently virtually disappear under irradiation. $NC_{50:50}$ also demonstrated to be stable, as it maintained good photocatalytic activity after three cycles. Finally, in order to assess $NC_{50.50}$'s ability to work under real-world irradiation, tests were made under natural sunlight. Under these conditions, $NC_{50:50}$ managed to achieve virtually full degradation within 30 minutes of irradiation, even under different meteorological conditions, with the UV factor appearing to affect the photodegradation efficiency the most (temperature and sky conditions appear to have virtually no effect). In summary, this work lays a pathway to achieve enhanced photocatalytic efficiency under natural sunlight while upcycling an otherwise discarded organic waste and promoting a circular economy.

In this work, I was responsible, under supervision from my supervisors, for synthesizing the CDs and $NC_{50:50}$ and performing the photocatalytic assays (both under simulated and natural sunlight), scavenger studies, recycling studies, and comparison with other reports available in the literature. I also conducted the analysis and interpretation of the results and wrote the draft of the paper, which was then reviewed and edited by Professor Dr. Luís Pinto da Siva and Professor Dr. Joaquim Esteves da Silva, who supervised the process from end-to-end. BET experiments were conducted by Dr. Ana Brandão and supervised by Prof. Dr. Carlos Pereira from CIQUP – IMS, Faculty of Sciences – University of Porto.

catalysts

MDPI

Article

Enhanced Photocatalytic Degradation of Ciprofloxacin Under Natural Sunlight Using a Waste-Derived Carbon Dots–TiO_2 Nanocomposite

Ricardo M. S. Sendão [1], Ana T. S. C. Brandão [2], Carlos M. Pereira [2], Joaquim C. G. Esteves da Silva [1] and Luís Pinto da Silva [1,*]

[1] Chemistry Research Unit (CIQUP), Institute of Molecular Sciences (IMS), Department of Geosciences, Environment and Spatial Planning, Faculty of Sciences, University of Porto, Rua do Campo Alegre s/n, 4169-007 Porto, Portugal; up201405083@edu.fc.up.pt (R.M.S.S.); jcsilva@fc.up.pt (J.C.G.E.d.S.)
[2] Chemistry Research Unit (CIQUP), Institute of Molecular Sciences (IMS), Department of Chemistry and Biochemistry, Faculty of Sciences, University of Porto, Rua do Campo Alegre s/n, 4169-007 Porto, Portugal; ana.brandao@fc.up.pt (A.T.S.C.B.); cmpereir@fc.up.pt (C.M.P.)
* Correspondence: luis.silva@fc.up.pt

Abstract

The presence of emerging organic contaminants in water and effluents, including antibiotics, poses significant environmental and health risks. Moreover, while photocatalysis is a promising approach for their removal, the inefficient utilization of natural sunlight by common photocatalysts limits its large-scale use. This work demonstrates the enhanced sunlight-driven photodegradation of the antibiotic Ciprofloxacin (CIP) using a nanocomposite composed of carbon dots (CDs) and TiO_2 ($NC_{50:50}$). The CDs were obtained from corn stover, a major agricultural waste product. Initial testing was performed under artificial solar radiation: CIP was virtually fully degraded within 20 min, with a rate constant of 0.2372 min^{-1} and a 217% enhancement of catalytic activity over commercial TiO_2. Validation under real-world irradiation conditions was subsequently made by performing photocatalytic assays under natural sunlight on different days under diverse meteorological conditions. The performance of $NC_{50:50}$ was retained, degrading CIP within 30 min under natural conditions. Notably, while degradation by-products were identified under both artificial and natural sunlight, they were subsequently photodegraded by the nanocomposite under these conditions. This enhanced performance was attributed to a combination of effects resulting from CDs' incorporation, namely, improved absorption of visible light, enhanced charge separation, and increased specific surface area. Furthermore, the addition of CDs resulted in changes in the reactive species generation profile, which can alter the available degradation pathways. Thus, this study provides insight that can be useful for strategies aimed at the rational design of sunlight-active TiO_2-based photocatalysts with tunable surface reactivity.

Keywords: sunlight-driven photocatalysis; TiO_2-carbon dots nanocomposite; reactive species modulation; waste-based carbon dots; surface reactivity

Check for updates

Academic Editors: Shujuan Zhang, Ioannis Konstantinou and Vincenzo Vaiano

Received: 29 December 2025
Revised: 10 January 2026
Accepted: 14 January 2026
Published: 2 February 2026

Copyright: © 2026 by the authors. Licensee MDPI, Basel, Switzerland. This article is an open access article distributed under the terms and conditions of the Creative Commons Attribution (CC BY) license.

1. Introduction

Water is an essential resource for humanity, and thus, its contamination by persistent organic pollutants, such as antibiotics, is a significant concern, especially when we consider that conventional water treatment techniques are unable to efficiently remove this type

of pollutant from water supplies [1]. The ineffectiveness stemming from the complex structure of antibiotics allows these pollutants to reach water streams through the effluents of wastewater treatment plants, resulting in their widespread presence in countries worldwide [2]. Batt et al. detected ciprofloxacin (CIP), sulfamethoxazole, trimethoprim, tetracycline, and clindamycin in wastewater effluents from three treatment plants in New York State, USA [3]. Liu et al. found that quinolone antibiotics were major pollutant factors in Chinese lakes [4]. Rodriguez-Mozaz et al. reported the detection of ciprofloxacin in several European countries, with concentrations as high as 1435.5 ng L^{-1} being detected in Portugal [5].

The widespread presence of antibiotics in aquatic systems is further exacerbated by the absence of policies regulating their consumption in several countries, leading to excessive use. Ultimately, they reach wastewater treatment plants and are subsequently discharged into environmental water, where they range from the ng L^{-1} to the µg L^{-1} [6]. Additionally, industries such as pharmaceutics, agriculture, healthcare, and livestock farming can also lead to the infiltration of antibiotics into aquatic systems [7].

This widespread presence of traceable amounts of human and veterinary antibiotics poses a significant threat to public health, as it contributes to the development and dissemination of antibiotic resistance [8–10]. In aquatic ecosystems, the continuous release of antibiotics facilitates the selection of antibiotic-resistant bacteria and promotes the spread of antibiotic resistance genes, which are subsequently transferred within microbial communities [2]. As a result, bacterial infections become more difficult to treat, leading to higher healthcare costs and increased mortality. Moreover, the accumulation of antibiotics in aquatic environments also exerts toxic effects on non-target organisms, disrupting ecological balance and biodiversity [11]. Given these critical consequences, the effective degradation of antibiotics and their removal from aquatic systems is of paramount importance to mitigate their resulting environmental and public health impacts.

Among the antibiotics present in aquatic systems, we find CIP, a synthetic fluoroquinolone with antibacterial activity against both Gram-positive and Gram-negative bacteria, such as *Escherichia coli* and *Staphylococcus aureus* [12]. Regarding CIP, despite its broad-spectrum efficacy and widespread use in aquatic environments, concerns exist regarding its ecological impact and potential contribution to antibiotic resistance. As with most antibiotics, conventional wastewater treatment methods are often ineffective at fully degrading CIP, leading to its accumulation in surface water, groundwater, and sediments.

Considering the limitations and ineffectiveness of conventional wastewater treatment methods regarding removing antibiotics, it is no surprise that the scientific community has focused its efforts on alternative technologies. Photocatalysis is a potentially clean technology that has been widely studied for various applications, utilizing light irradiation as the energy source behind the intended catalytic reaction [13–16]. It is frequently a less impactful method than conventional alternatives for removing organic pollutants, as it exhibits high redox performance, produces minimal amounts of sludge, and can utilize a clean energy source, such as solar irradiation, to drive the degradation process [17].

Thus far, several photocatalysts have been investigated for environmental remediation and pollutant removal, primarily focusing on metal oxides and sulfides [16,18–20]. Among those studied by the scientific community, TiO_2 is particularly important due to its widespread application, cost-effectiveness, and chemical stability. Furthermore, it is already extensively utilized in photocatalytic technologies for environmental remediation, including the degradation of organic pollutants such as pharmaceutical contaminants (e.g., ibuprofen), the photoreduction and removal of toxic heavy metals, and the generation of hydrogen via water splitting [13,14,16,21]. Despite these advantages, TiO_2 presents several limitations that restrict its use in a wider range of applications. First and foremost,

it exhibits a wide bandgap (around 3.2 eV) that prevents efficient utilization under sunlight (of which only around 5% is UV radiation) [22,23]. Additionally, TiO_2 suffers from a rapid recombination of photogenerated holes (h^+) and electrons (e^-), [24] and presents a poor affinity for organic pollutants [25].

Given these challenges, recent research efforts have focused on optimizing photocatalytic materials via methods using doping with both metals [26] and non-metals [27] and conjugation with alternative materials such as graphene [28]. Due to the increased structural stability of the crystalline framework and the introduction of new energy levels, which extend the light absorption capabilities, applying these strategies may significantly enhance photocatalytic efficiency under visible-light irradiation [26–29]. However, many of these techniques rely on incorporating potentially toxic metal elements, which, in addition to being expensive, can raise health and environmental concerns. Additionally, such modifications often lead to increased charge carrier recombination, ultimately reducing photonic efficiency and diminishing the overall catalytic performance [30].

An alternative approach to overcoming these limitations is the conjugation of semiconductors with carbon dots (CDs). These nanometric carbon-based particles exhibit spherical or quasi-spherical morphologies, possess either an amorphous or crystalline core, and a functionalized surface [31]. CDs possess several advantageous properties relevant to photocatalysis, including strong photoluminescence, a broadband absorption range that extends into the visible range, high water solubility, and low toxicity [32–35]. Due to being low cost, easy to prepare, and presenting versatile physicochemical properties, CDs have been tested and employed in various applications, such as sensing, [36] light-emitting devices, [37] photodynamic therapy, [38] and photocatalysis [15,16,39,40]. In the latter, CDs can function as independent photocatalysts or in conjunction with semiconductors, such as TiO_2, to enhance light absorption and improve photonic efficiency, thereby improving overall photocatalytic performance.

The conjugation of CDs with TiO_2 has the potential to enhance the sunlight-driven photocatalytic performance while avoiding the drawbacks associated with doping or coupling with metal-based materials. Unlike these strategies, adding CDs to TiO_2 does not introduce additional toxicity or compromise the photonic efficiency of TiO_2, making it a more environmentally and economically viable alternative [30,41,42]. CDs enhance photocatalytic activity through several mechanisms. For one, CDs can effectively accept photoexcited e^- from the conduction band of TiO_2, thereby improving the separation of photoexcited e^-/h^+ pairs [43]. Additionally, the broadband absorption range of CDs allows for an absorption range that extends into the visible region, enabling a more efficient utilization of solar irradiation [15,44,45]. Finally, the functionalized surface of CDs increases the affinity of the nanocomposites' surface toward organic pollutants, enhancing adsorption onto the photocatalyst and facilitating their interaction with active sites. All these factors contribute to improved sunlight-driven photodegradation, making CD-TiO_2 composites a highly effective and sustainable solution for photocatalytic applications [45].

Another significant advantage of using CDs over other methods is their versatility in synthesis, as they can be produced from a diverse range of carbon precursors, including organic waste. This can help to upcycle these residues into valuable nanomaterials. Moreover, life cycle assessment studies indicate that the most impactful stage of the life cycle of nanomaterials is their synthesis, and that the identity of the carbon precursor employed in the synthesis of CDs significantly influences the resulting potential environmental impacts of the process [46–48]. By using organic waste such as corn stover instead of commercially available reagents, we can avoid the impacts associated with the preparation of these chemicals and thus reduce the overall impact of the CDs. Corn stover, a major agricultural waste product consisting of the leaves, stalks, and cobs left after corn harvest, represents

approximately 50% of the total corn crop yield; yet, only about 10% is repurposed for other applications [49]. Given its abundance, upcycling corn stover into a nanotechnology-based solution for wastewater treatment presents a promising opportunity for both environmental remediation and resource sustainability.

Herein, we report how the efficient and virtually complete sunlight-driven photodegradation of the emerging contaminant CIP can be achieved with a CDs and TiO_2 nanocomposite ($NC_{50:50}$), under both artificial and natural irradiation conditions. The CDs were prepared from corn stover, thereby combining circular-economy principles with solar-driven approaches to develop more environmentally sustainable wastewater treatment processes.

While this nanocomposite was characterized earlier [16], its sunlight-driven photocatalytic activity (under real-world irradiation and artificial conditions) and its performance as a catalyst toward the photodegradation of pharmaceutical contaminants were investigated here for the first time. This type of investigation, conducted under real-world conditions, is essential for future large-scale applications of TiO_2-based photocatalysis for (waste)water treatment.

More specifically, when first using a solar simulator for assays in artificial conditions, $NC_{50:50}$ was able to virtually fully degrade CIP within 20 min (k of 0.2372 min^{-1}), while showing a 217% enhancement of photocatalytic activity toward commercial TiO_2. Some potential degradation by-products were identified by HPLC-DAD and subsequently shown to be photodegraded by $NC_{50:50}$. The photocatalyst was found to be stable over multiple photocatalytic cycles, and scavenger assays identified the reactive species involved. Finally, assays conducted under real-world irradiation conditions with natural sunlight showed that $NC_{50:50}$ consistently fully degrades CIP within 30 min, even when prepared on different days under diverse meteorological conditions.

Furthermore, we observed that the addition of CDs led to a shift in the reactive species generation profile, with CIP being degraded by a combination of different reactive species (superoxide anion, h^+, e^-, and singlet oxygen). This approach can then enable a strategy to tune the reactivity of TiO_2-based photocatalysts and broaden their application to a wide range of contaminant classes.

2. Results and Discussion

2.1. Description of the Photocatalyst and Prior Characterization

The TiO_2—CDs nanocomposite ($NC_{50:50}$) used in this study was previously developed by our group and comprehensively characterized, including by XRD, SEM, XPS, solid-state (ss) NMR, FTIR, PL, and UV-Vis spectroscopy, as reported in [16]. In the present work, this material was reproduced following the previously reported synthesis and evaluated for the first time as a sunlight-driven photocatalyst for the degradation of pharmaceutical contaminants.

$NC_{50:50}$ was prepared from TiO_2 and CDs (prepared using corn stover and citric acid (CA) as co-carbon sources, and ethylenediamine (EDA) as N-dopant in a 1:1:2 ratio, respectively) [16]. Both $NC_{50:50}$ and commercially available TiO_2, thereon employed as a benchmark, were tested here as photocatalysts for the sunlight-driven photodegradation of CIP in aqueous solution. It should be noted that while $NC_{50:50}$ was previously obtained, its photocatalytic performance under sunlight irradiation, either artificial or natural, had not been investigated prior to this work, nor had its application to pharmaceutical contaminants.

Given that the nanocomposite was first developed in a previous study, the results of its previous comprehensive characterization are summarized here for the benefit of the reader, with the full datasets being found in [16].

Regarding optical properties, the introduction of carbon dots (CDs) led to an extended absorption range up to 700 nm [16], enhancing their visible-light absorption capability without changing the bandgap of $NC_{50:50}$ (3.26 eV) [16]. By their turn, photoluminescence studies suggested that adding CDs leads to suppressing the recombination of TiO_2's photoinduced charge carriers [16], due to lower photoluminescence than that measured for sole TiO_2 [16]. Electrochemical impedance spectroscopy further supported this finding by indicating lower electron transfer resistance under irradiation [15,16]. These results indicate that CDs enhance visible-light absorption and facilitate more efficient charge separation [16], ultimately improving the photocatalytic performance of the nanocomposite.

In terms of structural and chemical composition, $NC_{50:50}$ was assessed using various characterization techniques, including SEM, XRD, FTIR, XPS, and ss-NMR spectroscopy [16]. SEM analysis revealed that $NC_{50:50}$ exhibited a spherical morphology with an average diameter of approximately 92.9 nm. XRD patterns were consistent with anatase-phase TiO_2, while FTIR and XPS analysis identified functional groups such as carbonyl, hydroxyl, and amines, which may influence the nanocomposite's interaction with pollutants and confirm the presence of the CDs on the TiO_2. ss-NMR spectroscopy provided further insights into the organic structure of the CDs, revealing highly oxygenated aliphatic chains that interact with TiO_2. These findings suggest that the CDs play a crucial role in modifying the nanocomposite's surface properties, thereby further enhancing its photocatalytic performance and providing a foundation for our work [16].

2.2. Photocatalytic Optimization and Assays

The photocatalytic efficiency of $NC_{50:50}$ under simulated sunlight toward CIP was evaluated via RP-HPLC-DAD. Before optimizing the photocatalytic conditions, preliminary tests were conducted with 20 mg of photocatalyst and 20 ppm of CIP under 60 min of irradiation, with samples collected every 15 min. Additionally, the same assay was performed using commercial TiO_2 (<25 nm particle size, anatase phase, from Sigma-Aldrich), which served as a benchmark.

To evaluate $NC_{50:50}$'s performance relative to TiO_2, we quantified the percentage of CIP removed over a fixed irradiation period (%DR, Equation (1)) [50] and determined the corresponding rate constant (Equation (2)). The %DR was calculated using the following equation:

$$\%DR = \frac{C_0 - C_t}{C_0} \times 100 \quad (1)$$

Here, %DR corresponds to the % of CIP removed, C_0 represents the initial CIP concentration, and C_t is the concentration of CIP after an irradiation period of t minutes.

Moreover, the kinetic equation of the degradation follows a pseudo-first-order reaction that can be expressed as follows [51]:

$$-\ln\left(\frac{C_t}{C_0}\right) = kt \quad (2)$$

In this case, k corresponds to the estimated reaction rate constant.

The analysis of the initial results obtained revealed that, even prior to optimization, $NC_{50:50}$ presented a significantly better CIP photodegradation potential than TiO_2, both in terms of reaction rate constant (0.0536 min^{-1} vs. 0.0283 min^{-1}, enhancement of 89.4%, depicted in Figure S1a) and degradation extent, with $NC_{50:50}$ managing achieving a virtually complete removal of the initial CIP concentration within 60 min (Figure S1b).

Afterwards, we tested the effect of different CIP concentrations, pH level, and catalyst dosage on the efficiency of the catalytic process (Table 1 and Figure S1c–h). Starting with the initial CIP concentration, we found, as expected, that the lowest CIP concentration led to

the highest reaction rate constant (0.0823 min^{-1} for 10 ppm versus 0.0537 and 0.0200 min^{-1} for 20 and 30 ppm, respectively). Although using 10 ppm of CP resulted in a higher rate constant, 20 ppm was selected for subsequent assays because it still achieved near-complete degradation using a higher pollutant concentration within a relatively short time frame.

Table 1. *k* and %DR data regarding the optimization of the CIP concentration, pH level and catalyst dosage of the photodegradation of CIP with $NC_{50:50}$. The corresponding plots are found in Figure S1.

Test	Parameter Value	*k* (min^{-1})	%DR	Time (min)
CIP concentration	10 ppm	0.0823	96.4	40
	20 ppm	0.0537	96.2	60
	30 ppm	0.0200	69.7	60
pH level	5	0.0256	78.5	60
	7	0.0828	99.1	60
	9	0.0765	98.8	60
Catalyst dosage	10 mg	0.0218	73.4	60
	20 mg	0.0763	99.1	60
	40 mg	0.1114	98.0	40
	60 mg	0.2372	98.2	16

Regarding the pH level, and already using a CIP concentration of 20 ppm, the results revealed that a pH of 7 resulted in the highest catalytic efficiency, achieving a rate constant of 0.0828 min^{-1} and a %DR of 99.1% within 60 min of irradiation (Figure S1e,f). Finally, regarding the catalyst dosage, using 20 ppm of CIP at pH 7, we found that a 60 mg dosage led to the best results, resulting in a rate constant over double that of second-best performer (0.2372 min^{-1} versus 0.1114 min^{-1} for a 40 mg dosage) and achieving a virtually complete degradation of the initial pollutant within 16 min of irradiation (Figure S1g,h).

While this dosage was the highest amount we tested, we decided not to continue the test further, as higher concentrations resulted in a large amount of catalyst being deposited at the bottom of the reaction mixture. Thus, there was no advantage in adding more material. In summary, for subsequent tests, we selected the following reaction conditions: 20 ppm of CIP, pH 7, and 60 mg of catalyst, with a total reaction volume of 100 mL.

Based on these reaction parameters, the photocatalytic efficiency of $NC_{50:50}$ was compared to that of commercial TiO_2, photolysis, and CDs by themselves (Figure 1a,b). Under the same conditions, $NC_{50:50}$ exhibited a rate constant of 0.2372 $\pm$ 0.0032 min^{-1} and a %DR of 98.2 $\pm$ 0.6% within 16 min of irradiation, outperforming commercial TiO_2, which achieved a rate constant of 0.0749 $\pm$ 0.0002 min^{-1} and a %DR of 89.2 $\pm$ 1.7% after 30 min under simulated sunlight. Furthermore, the effect of photolysis was minimal, with only 5.8% degradation observed after 30 min. Photodegradation experiments using CDs alone yielded comparable results to photolysis, indicating that CDs by themselves are not sufficient to degrade CIP under the same conditions. These findings demonstrate that incorporating the CDs into TiO_2 substantially enhances the semiconductor's photocatalytic performance under solar irradiation.

By analyzing the evolution of the chromatogram (Figure 1c) with increasing reaction times, we can observe that CIP's initial peak, found at around retention time (RT) of 3.65 min, disappears quite rapidly (within 16 min of irradiation). Several peaks ascribed to potential degradation by-products appear during the course of the process. However, they also disappear as the photocatalytic process continues. Namely, when we prolonged the duration of the photocatalytic assay (Figure 1d), we observed that no significant peaks (with

over 1% of initial CIP peak area) are found for an irradiation time of 300 min, suggesting that even the produced by-products are also degraded by $NC_{50:50}$. To better demonstrate this, a full overview of the evolution of chromatogram peaks areas appearing over the course of the degradation and their evolution over time can be found in Figure 1e (with specific data on Table S1), which clearly demonstrated that all additional peaks appearing over the course of the experiment (P2–P6) tend to disappear when compared to the initial CIP peak (P1).

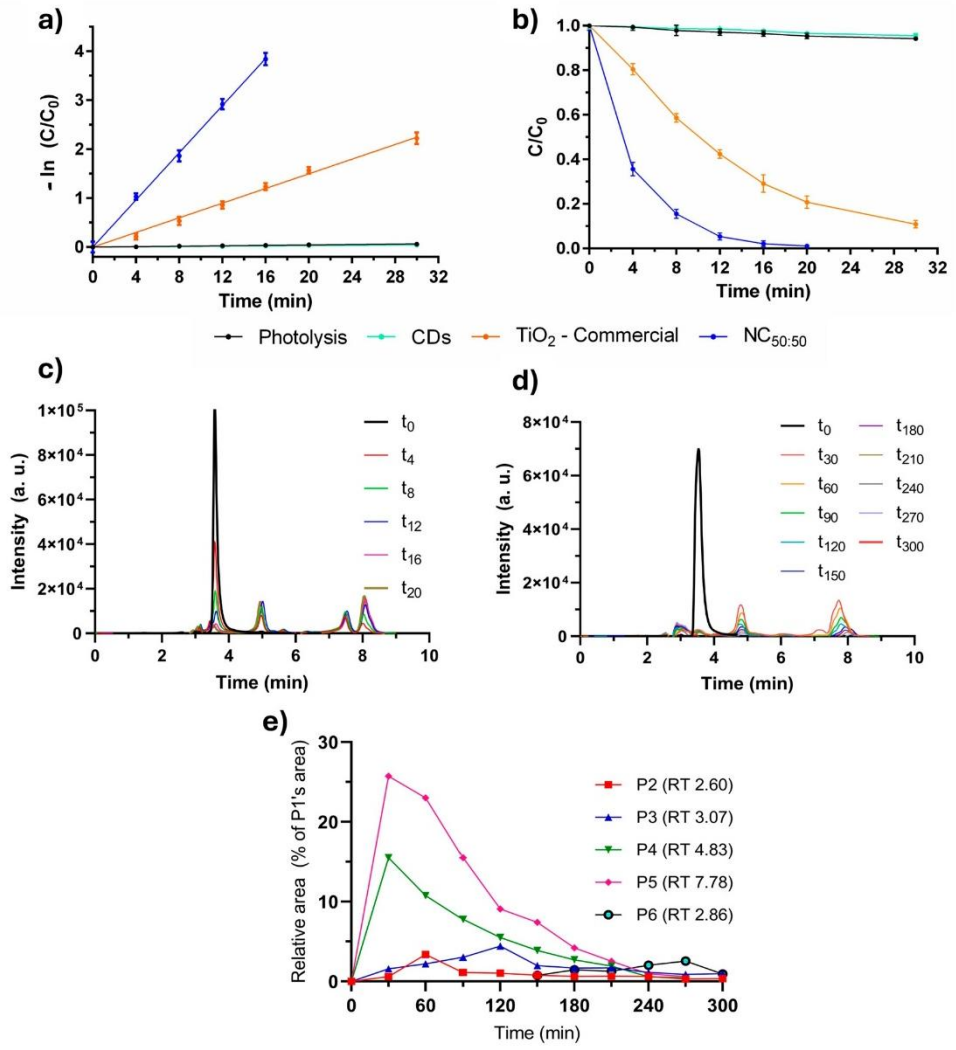


Figure 1. Representation of (**a**) −ln (C_t/C_0) and (**b**) C_t/C_0 versus time of irradiation for $NC_{50:50}$, commercial TiO_2, CDs and photolysis regarding the sunlight-driven photodegradation of CIP. (**c**,**d**) represent the evolution of the chromatograms depicting CIP's photodegradation by $NC_{50:50}$ over time for total irradiation periods of 20 and 300 min, respectively. (**e**) represents the area evolution of the additional peaks appearing during the photodegradation process (P2–P6) when compared to the area of the initial CIP peak (P1). Error bars for (**a**,**b**) represent uncertainty as calculated via the propagation of the standard error.

To further assess the impact of incorporating CDs into TiO_2 on the catalytic performance, we quantified the enhancement of TiO_2's catalytic efficiency upon the incorporation of CDs by using Equation (3):

$$\%\ln(C) = 100 \times \frac{k_{NC} - k_{TiO_2}}{k_{TiO_2}} \quad (3)$$

In this context, %ln(C) serves as a comparative metric for evaluating the enhancement of TiO_2's catalytic efficiency upon the incorporation of CDs regarding the photodegradation of CIP, k_{NC} represents the reaction rate constant of $NC_{50:50}$, while k_{TiO_2} corresponds to the reaction rate constant of commercial TiO_2. By applying this formula, we estimated the % ln(C) to be 217%, demonstrating a very significant enhancement in catalytic performance compared to that of commercial TiO_2. This was achieved by adding CDs, which, in addition to improving the catalytic performance, utilized corn stover in a manner that upcycled this otherwise discarded material.

However, aside from the increased photocatalytic efficiency, it is also worth noting that adding CDs also increased the adsorption of CIP to $NC_{50:50}$ in the dark compared to TiO_2 (Figure S2a). In fact, nearly half of the initial CIP concentration seems to be adsorbed by $NC_{50:50}$ during the 30 min period in the dark. This is relevantly higher than what is observed for TiO_2, where only around 4.1% of the initial CIP appears to be adsorbed. To assess if this higher adsorption could be responsible for the observed photodegradation with the lamp on, we compared the variation in C_t/C_0 of CIP in the presence of $NC_{50:50}$ both with the lamp on and off (Figure S2b). These results indicate that while there is a significant adsorption of CIP into the $_{NC50:50}$ during the 30 min dark period before turning on the lamp, the adsorption is stabilized thereafter. That is, after the 30 min dark period, when the lamp is still off, the C_t/C_0 ratio remains constant. While the lamp is on, a significant decrease in CIP levels is observed during the same period. These results confirm that the degradation observed during photocatalytic assays is due to photocatalysis itself, and not just continuous adsorption into $NC_{50:50}$.

The different degrees of adsorption between $NC_{50:50}$ and TiO_2 can be explained by the fact that by adding a nanoparticle with a highly functionalized surface [31] with different functional groups that confer a better affinity towards organic compounds than that inherent to TiO_2, the photocatalyst facilitates the adsorption of CIP, enhancing its interaction with active sites.

In fact, data from BET analysis revealed that $NC_{50:50}$ presents a higher specific area (S_{BET}) than TiO_2 (Table 2). Namely, the results suggest that both TiO_2 and $NC_{50:50}$ exhibit Type III isotherms (Figure 2a), with the nanocomposite showing an SBET of 269.9 $m^2\ g^{-1}$, over 2.5× higher than that of TiO_2 (105.2 $m^2\ g^{-1}$). This increased surface area helps to explain the higher CIP adsorption observed with $NC_{50:50}$. Regarding pore size, both TiO_2 and $NC_{50:50}$ are classified as mesoporous, presenting pore widths of 13.1 and 4.1 nm, respectively (estimated via the BJH method with pore size distribution represented in Figure 2b) [52].

Table 2. Surface area, pore volume and pore size for TiO_2 and $NC_{50:50}$.

Sample	S_{BET} ($m^2\ g^{-1}$)	V_{total} ($cm^3\ g^{-1}$)	D_p (nm)
TiO_2	105.2	0.276	13.1
$NC_{50:50}$	269.9	0.212	4.1

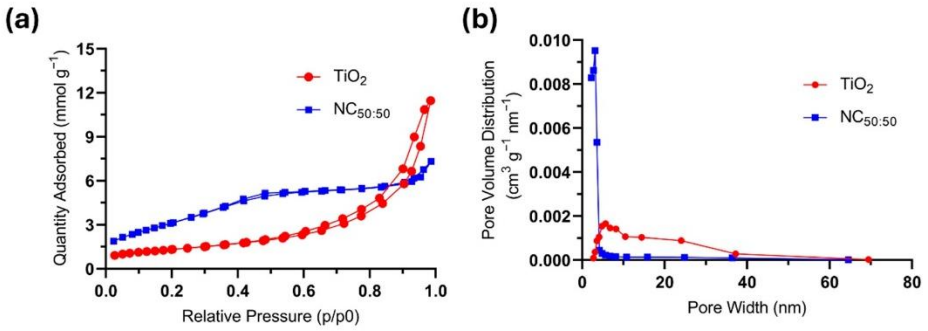


Figure 2. (**a**) N2 adsorption–desorption isotherms and (**b**) pore volume distribution calculated by the BJH (Barrett–Joyner–Halenda) pore size distribution method for TiO_2 and $NC_{50:50}$. Measured values for surface area, pore volume, and pore size can be found in Table 2.

2.3. Scavenger Assays

To investigate the reactive species responsible for the enhanced catalytic activity of $NC_{50:50}$, sunlight-driven CIP degradation assays were conducted in the presence of specific radical scavengers. Hydroxyl radicals (·OH), superoxide radicals (O_2^-), electrons (e^-), holes (h^+), and singlet oxygen ($^1O_2$) were selectively scavenged using isopropyl alcohol (IPA, 10 mM), 1,2-dihydroxybenzene-3,5-disulfonate (Tiron, 10 mM), potassium nitrate (KNO_3, 10 mM), potassium iodide (KI, 10 mM), and sodium azide (1 mM), respectively. These scavengers were selected based on their established roles in targeting reactive species commonly associated with TiO_2 and TiO_2-composites [41]. IPA and Tiron were of particular interest, as hydroxyl and superoxide radicals, their respective target species, are typically among the primary reactive species in the photocatalytic mechanism of bare TiO_2 [26,53].

The influence of each reactive species was assessed by measuring the change in the %DR in the presence of the scavengers, as calculated using Equation (4) [15]:

$$\%DRV = \%DR_{test} - \%DR_{control} \quad (4)$$

In this equation, %DRV represents the variation in %DR when a scavenger is introduced ($\%DR_{test}$) relative to the control test ($\%DR_{control}$), which represents standard photodegradation without scavengers. Therefore, the magnitude of the %DRV allows for a quantitative assessment of each species' contribution: a higher degree of inhibition (more negative %DRV) corresponds to a greater relative importance of that species in the degradation process.

The results from the scavengers' tests revealed that, for $NC_{50:50}$, all tested reactive species, except for the hydroxyl radical, participated in the photodegradation mechanism (Figure 3a). Namely, tests using IPA did not yield any significant %DRV value. For their turn, the %DR was diminished significantly in the presence of Tiron ($-51.1 \pm 5.4\%$), KI ($-40.9 \pm 3.5\%$), KNO_3 ($-22.3 \pm 0.8\%$) and sodium azide ($-19.0 \pm 1.0\%$). This indicates that the superoxide radical, h^+, e^- and $^1O_2$, by that order, have a role in the photocatalytic mechanism of $NC_{50:50}$. Regarding TiO_2 (Figure 3b), the reactive species responsible for the degradation mechanism were the superoxide radical, h^+, and $^1O_2$.

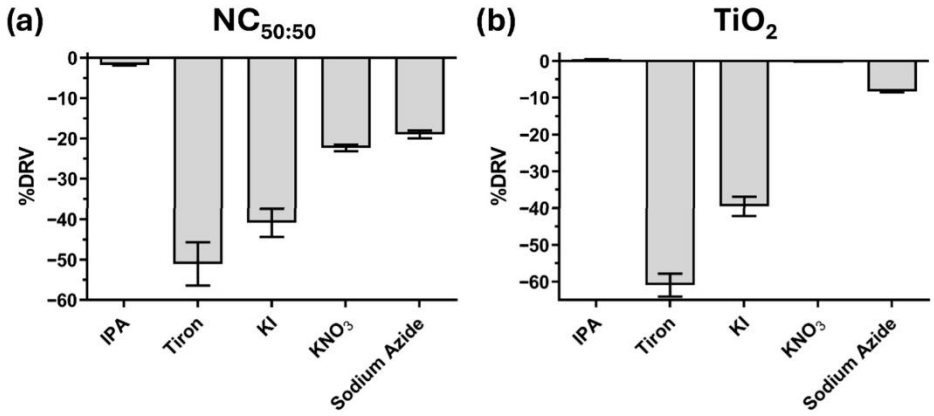


Figure 3. Solar light-driven (**a**) $NC_{50:50}$ and (**b**) TiO_2-mediated photodegradation of CIP in the absence or presence of scavengers for reactive species. Results are presented in the form of %DRV. Negative %DRV values indicate an inhibition of the photocatalytic efficiency. Error bars represent uncertainty as calculated via the propagation of the standard error.

2.4. Recycling Studies

Recycling experiments for the photodegradation of CIP under simulated solar irradiation were conducted to evaluate the stability and performance of $NC_{50:50}$ over three consecutive runs. In this experiment, consecutive cycles of CIP photodegradation were performed in 1 h periods of solar irradiation in the presence of $NC_{50:50}$. After each cycle, the composite was collected, dried, and reused repeatedly without further processing.

It was observed that the %DR obtained in the final cycle was still over 95%, compared to 99% in the first cycle (Figure 4). Given this, $NC_{50:50}$ is considered to have good performance stability and still achieves a nearly complete degradation of the target pollutant within the same time period. The number of considered cycles is also consistent with literature data [54–56].

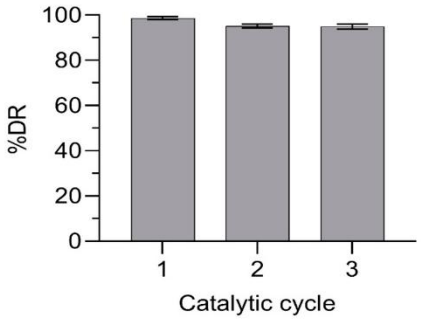


Figure 4. $NC_{50:50}$ recycling studies regarding the photodegradation of CIP. Error bars represent uncertainty as calculated via the propagation of the standard error.

It should be noted that there were mass losses during material recovery that made it difficult to perform additional cycles. For one, this issue is nevertheless common for powder-based photocatalysts. In that sense, it can be considered a general limitation for this type of photocatalyst, and further exploration should be the focus of future studies. Namely, the addition of the nanocomposite to lightweight materials to provide floating capability, which should allow for facile separation from the matrix to be treated by skimming.

Nevertheless, the obtained %DR variation over the performed cycles still allows us to characterize the photocatalytic activity of the material as stable.

2.5. Comparison to the Literature

To better evaluate the effectiveness of our composite, the photocatalytic performance of $NC_{50:50}$ was compared to other TiO_2-based systems reported for the photodegradation of CIP. The comparison (Table 3) was made regarding k and how much the k obtained by $NC_{50:50}$ is enhanced relative to literature entries (% ln(C)).

First, $NC_{50:50}$ presents the highest rate constant (0.2372 min^{-1}). In fact, the nanocomposite studied in this work presented a k that was enhanced, on average, by 1444% over all the other entries. Namely, the observed enhancement was over 500% for all entries (reaching enhancement values of 2691% and 5303%), except for entries 3 and 7. However, even considering those latter entries, the enhancement was also quite relevant (133% and 84%, respectively).

Furthermore, it should be noted that entry 3 only considered UV radiation (in which TiO_2 is known to be intrinsically more efficient), and not sunlight (as the present work did). Regarding entry 7, the measured k was obtained by considering about double the catalyst dosage and half of the CIP concentration in the present study. Finally, while entry 7 did employ artificial solar radiation as an irradiation source, contrary to our study, the performance of the photocatalyst was not validated under natural sunlight (Section 2.6).

Moreover, it is worth noting that this was achieved employing CDs partially prepared from corn stover. Meaning that by using our waste-incorporating carbon nanoparticles, we not only obtain a significantly higher catalytic potential than other alternatives, but we also use otherwise discarded organic material, thus providing a way to upcycle this organic waste.

Future work should include the evaluation of $NC_{50:50}$'s performance against other antibiotics, such as tetracycline and oxytetracycline [57–62].

Table 3. Comparison between the rate constant (k, min^{-1}) obtained by $NC_{50:50}$ and other TiO_2-based photocatalysts for the photodegradation of CIP. Here, % ln(C) is also calculated according to Equation (3), but considering the k of each literature entry as a reference. Namely, here, % ln(C) measures how enhanced the k of $NC_{50:50}$ is over each literature entry.

Photocatalyst	Cat. (g L^{-1})	CIP Conc. (ppm)	Lamp	k (min^{-1})	% ln(C)	DOI
TiO_2/CDs $NC_{50:50}$	0.6	20	Solar simulator	0.2372		This work
Glass-deposited TiO_2	0.13	20	365 nm 10 mW/cm^2	0.0085	2691	[63]
Graphitized carbon-TiO_2	0.35	15	254 nm 14 W	0.102	133	[64]
Glass-deposited TiO_2	1	3	UV	0.0197	1104	[65]
TiO_2 NPs	0.7	80	3 × 254 nm 8 W	0.00439	5303	[66]
TiO_2/SnO_2	1	2.5	3 × 253 nm 35 W	0.0311	663	[67]
TiO_2/CDs6 wt%	1	10	Xe Arc 350 W 290 Filter	0.129	84	[68]
TiO_2/H_2O_2	0.5	9	Solar 800 W Xe lamp	0.022	978	[69]
TiO_2/WO_3	0.5	20	Sunlight	0.034	598	[70]

2.6. Photocatalysis Under Natural Sunlight

Finally, the last stage of our experiment consisted of analyzing the photocatalytic potential of $NC_{50:50}$ under natural sunlight to further assess its practical applicability. Namely, an experiment was conducted on the roof of the FC3 Building of the Faculty of Sciences—University of Porto (Portugal), in which the photodegradation of CIP under direct sunlight irradiation was monitored (Figure 5 and Table 4). The assays were performed during three consecutive days with different meteorological conditions (Table 4).

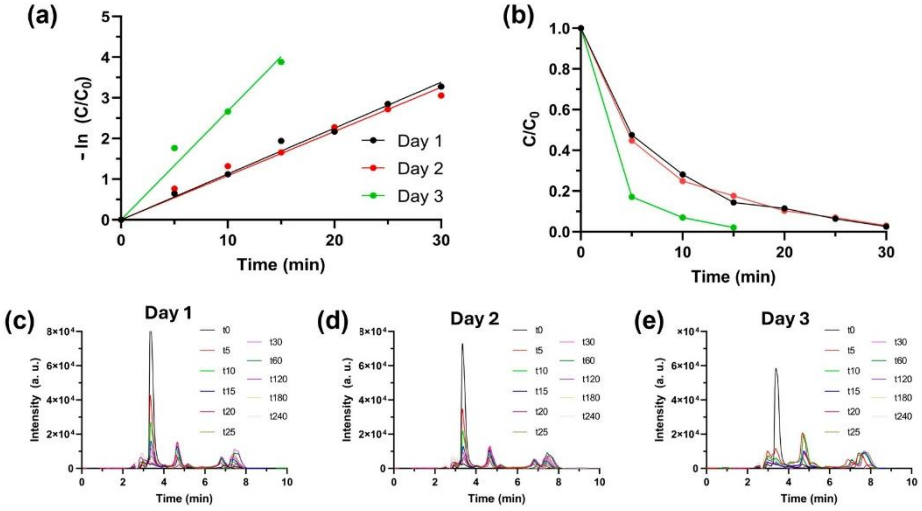


Figure 5. Graphic depiction of the (**a**) −ln (C/C_0) and (**b**) C/C_0 values for the sunlight-driven photodegradation of CIP by $NC_{50:50}$. (**c**–**e**) represent the evolution of the chromatograms with increasing sunlight irradiation times during the 1st, 2nd and 3rd day of assays under natural sunlight.

Table 4. Prevailing atmospheric conditions and %DR obtained concerning the photocatalytic degradation of CIP by $NC_{50:50}$ under direct sunlight. Meteorological data obtained from Instituto Português do Mar e da Atmosfera (IPMA).

Day	Time Period	Temperature Range	UV Index	Conditions	%DR	Time to ~100%DR
23 August 2024	11.00 to 15.00	30–32 °C	8	Sunny	~100%	30 min
24 August 2024	11.00 to 15.00	26–29 °C	8	Clouded	~100%	30 min
25 August 2024	11.00 to 15.00	23–26 °C	9	Clouded	~100%	15 min

The results demonstrate that, even under real sunlight, $NC_{50:50}$ is very efficient at degrading CIP. In fact, on the day experiencing the highest UV index (Day 3), $NC_{50:50}$ achieved an estimated reaction rate constant of 0.2676 min^{-1} (Figure 5a), which was even higher than that obtained with the solar simulator as the irradiation source (0.2372 min^{-1}). The photocatalytic potential was further confirmed over three different days, in which CIP was virtually fully degraded within 30 min of irradiation, with Day 3 recording a %DR of ~100% within 15 min of exposure to sunlight (Figure 5b).

Interestingly, neither the temperature nor the atmospheric conditions seem to affect catalytic efficiency significantly. Instead, photocatalytic activity appears to be more closely related to variations in the UV index, as increasing the index from 8 to 9 led to halving the irradiation time required to achieve a %DR of 100%. It should be noted that the UV index is a meteorological measure of the intensity of sunburn-producing UV radiation, which is used here as a proxy for the intensity of natural sunlight (which includes visible light). The

enhanced activity of the photocatalyst is attributed to its higher visible light absorption, which allows efficient utilization under sunlight.

In terms of degradation products, as observed in Figure 5c–e, the same peaks (with the same retention times) appear in the chromatograms in the same order as they did when using the solar simulator, suggesting that the degradation products are the same, independently of employing simulated solar irradiation or real sunlight. It should be noted that these potential degradation by-products were also degraded by $NC_{50:50}$ under natural sunlight, similar to what was observed under simulated sunlight.

The ability of $NC_{50:50}$ to degrade CIP under natural sunlight in an efficient manner can be attributed to the addition of CDs to TiO_2. Namely, CDs are known to be good electron acceptors during photoinduced electron transfer, leading to an improved separation of photoexcited e^-/h^+ pairs [43]. In fact, previously performed PL and EIS assays involved $NC_{50:50}$ (mentioned in Section 3.1) [16] indicated that the addition of CDs led to suppression of the recombination of TiO_2's photoinduced charge carriers and to lower photoinduced electron transfer resistance. The $NC_{50:50}$ was also previously shown to possess enhanced visible light absorption than TiO_2 [16], which can be a result of the typical broadband absorption range of CDs [15,44,45]. Given that the main individual component of sunlight is visible light, this enhancement in visible light absorption indicates a more efficient activation under visible light. Herein, the superior performance of $NC_{50:50}$ under real-world irradiation conditions can be explained by the addition of CDs, which enhances sunlight-driven photoactivation and facilitates efficient charge separation, ultimately improving the photonic efficiency of the photocatalyst.

2.7. Photocatalytic Mechanism

Scavenger assays indicated that superoxide radical, h^+, e^- and $^1O_2$ (in decreasing order of magnitude) all had a relevant role in the photodegradation of CIP (Figure 3a), when catalyzed by $NC_{50:50}$.

It should be noted that while TiO_2-based photocatalysts are mainly associated with the production of hydroxyl radicals (under UV radiation) [71], their reactive species generation profile can vary at different irradiation wavelengths. Namely, different groups observed that superoxide anion was the primary reactive oxygen species (ROS) in the visible light-driven activity of TiO_2-based photocatalysts [72,73]. Also under visible light, Zhou et al. found that $^1O_2$ to be a main reactive species in the studied TiO_2-based system [74]. By their turn, Guo et al. attributed the sunlight-driven degradation of organic dyes by TiO_2 photocatalysts to hole-mediated oxidation, rather than to hydroxyl radicals [75]. Thus, our results are consistent with existing literature.

As for the specific photocatalytic mechanism, as mentioned in Section 2.1 [16], the addition of CDs to $NC_{50:50}$ appeared to have led to an inhibited recombination of photo-generated charge carriers. This is attributed to the capacity of CDs (among other carbon nanomaterials) to act as electron reservoirs, thereby retaining photoexcited electrons transferred from TiO_2 upon light irradiation [15,43,76]. This enhances charge separation and suppresses the recombination of holes and electrons [43,77]. Therefore, effectively extending their lifetime and allowing them to have a more direct role in the photodegradation reaction. This can explain the more prominent role of both h^+ and e^- in the photodegradation of CIP observed in the study (Figure 3a).

The direct involvement of h^+ and e^- might also be facilitated by the enhanced adsorption capability of $NC_{50:50}$ (Figures 2 and S2, Table 2). Namely, it was observed that the addition of CDs led to a 2.5× increase in the specific surface area of the nanocomposite, which resulted in a large adsorption of CIP to $NC_{50:50}$ (Figure S2), during the dark period. This means that before the start of light irradiation, CIP molecules are already positioned at the surface of the photocatalyst, where they can interact more rapidly with photogenerated h^+ and e^-.

Furthermore, CDs are typically considered both photoinduced electron acceptors (which allows them to retain e^- from TiO_2) and donors [78]. The latter characteristic can also enable them to act as mediators/electron relays [79,80], and assist in the formation of superoxide anion. This latter ROS can then either induce the degradation of CIP or be oxidized in a hole-mediated process, to generate $^1O_2$ [81]. The efficiency of these processes is expected to be enhanced by the inhibited recombination rate of photogenerated charge carriers, which justifies the observed involvement of superoxide anion and $^1O_2$ in the degradation of CIP (Figure 3a).

In short (Figure 6), the addition of CDs allows for sunlight-driven photoexcitation and enhanced charge separation, by retaining photoexcited electrons from TiO_2. Given their extended lifetime, these e^- can generate superoxide anion, which is partially converted to $^1O_2$ via a h^+-mediated route. These two ROS, together with remaining h^+ and e^-, directly oxidize CIP. The degradation process is also expected to be enhanced by the larger surface area of $NC_{50:50}$, resulting from the addition of CDs, which allows for significant CIP adsorption prior to the irradiation phase. This pre-positions CIP in the reactive interface, which can enhance reaction rates once light irradiation starts.

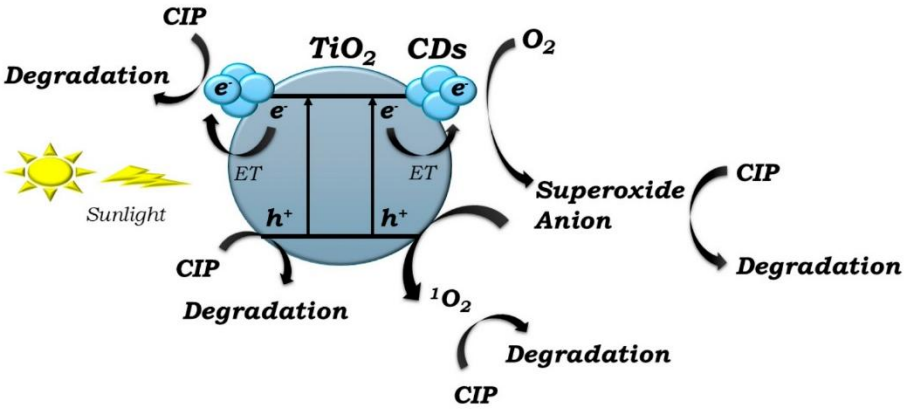


Figure 6. Proposed mechanism for the sunlight-driven degradation of CIP, when catalyzed by $NC_{50:50}$. ET: electron transfer.

It should also be highlighted that the addition of CDs also modulates the reactive species generation profile of the resulting photocatalytic nanocomposite. Namely, analysis of Figure 3 shows that the reactive species involved in CIP degradation differ for reactions catalyzed by $NC_{50:50}$ or commercial TiO_2. As mentioned, superoxide anion, h^+, e^- and $^1O_2$ are involved in photodegradation catalyzed by $NC_{50:50}$. However, only superoxide anion, h^+, and $^1O_2$ were found to be involved in the commercial TiO_2-catalyzed process.

Furthermore, the difference between reactive species profiles does not appear to end with the involvement or not of e^-. That is, the $NC_{50:50}$ appears to be more balanced in terms of the reactive species involved (Figure 3). While higher, the impact of superoxide anion is close to that of h^+. The impact of e^- is similar to that of $^1O_2$, and their combined

contribution to CIP degradation is still significant (about half of the combined contributions of superoxide anion and h^+).

The profile is different for commercial TiO_2 (Figure 3). Now, superoxide anion is more clearly the main contributor by a relevant margin to h^+, and that of $^1O_2$ is relatively residual. These differences can be ascribed to the charge separation-enhancing effect of CDs. Thereby, allowing the higher involvement of addition of h^+ and e^-, and of additional ROS (such as $^1O_2$).

Thus, the incorporation of CDs not only enhances photocatalytic efficiency but also appears to alter the charge-transfer dynamics of TiO_2. By modulating the reactive species generation profile, CDs can change the available degradation pathways. This finding potentially opens a pathway for the rational design of sunlight-active TiO_2-based photocatalysts with tunable surface reactivity and broader contaminant compatibility.

3. Materials and Methods

3.1. Preparation of CDs

The CDs were synthesized via a hydrothermal method, reproducing a synthesis procedure previously developed by us and thus, the morphological, structural, surface, and luminescent characterization of the material can be found in [16,82]. In summary, citric acid (CA), corn stover, and ethylenediamine (EDA) (1:1:2 mass ratio, in a total of 0.3 g) were dispersed in a NaOH solution (0.01 M). The reaction mixture was placed in a Teflon-lined autoclave reactor, which was then sealed stainless-steel outer shell. The mixture was subsequently subjected to a hydrothermal treatment (200 °C for 8 h), after which it was left to cool overnight. The resulting mixture was then subjected to purification by centri-fugation (6000 rpm for 30 min, while retaining the supernatant), and dialysis (3.5 kDa cutoff, 24 h). The former was performed to remove insoluble material, while the latter was performed to eliminate any remaining soluble contaminants that could interfere with the physicochemical properties [33]. Finally, the purified CD solution was lyophilized, weighed, and then redissolved in deionized water before being stored in the refrigerator (4 °C) until needed.

3.2. TiO_2/CDs Nanocomposites Preparation

To synthesize the TiO_2-CD nanocomposite, we modified a procedure previously developed by us [83,84], adapting it to include CDs [16]. In brief, titanium isopropoxide (TTIP) was initially added to IPA dropwise under continuous stirring. Afterwards, deionized water was introduced to precipitate TiO_2. A controlled amount of CDs, equivalent to 4% of the total expected mass, was then added dropwise under stirring. Before incorporation, the CD solution was maintained under stirring at 70 °C to ensure homogeneity. After adding the CDs, the suspension was stirred for an additional 2 h before filtration, followed by drying overnight and annealing at 300 °C in a muffle furnace (Thermolyne 47900, 1000 W, Thermo Scientific, Waltham, MA, USA, EUA), resulting in $NC_{50:50}$. In this nomenclature, 50:50 indicates that corn stover and CA were used in a 50:50 mass ratio as co-carbon precursors in the synthesis of CDs, which are then used in the preparation of the nanocomposite. $NC_{50:50}$ was then kept in the dark until further use.

3.3. Photocatalytic Activity Assays

The sunlight-driven photocatalytic efficiency of commercial TiO_2 and $NC_{50:50}$ was evaluated using an Ossila LED Solar Simulator (1000 W m^{-2}, Ossila, Sheffield, UK) as the irradiation source for the photodegradation of CIP. For these assays, 60 mg of photocatalyst was dispersed in 100 mL of CIP solution (20 mg L^{-1}). Afterwards, the mixture was exposed to 1 min of ultrasonic agitation. Prior to switching on the irradiation source, the suspension

was stirred in the dark for 30 min to reach an adsorption–desorption equilibrium [85]. Samples were collected at the beginning of that dark period (t = −30 min), to assess pollutant adsorption on the catalyst). Following this period, the solar simulator was turned on, and samples were collected at specific time intervals: at the start of irradiation (t = 0 min), and at several different irradiation times. To remove the catalyst from the sample prior to analysis, the aliquots were centrifuged at 10,000 rpm for 10 min and filtered using PTFE 0.45 µm syringe filters (LLG Labware).

The chromatographic analysis of the samples was performed using a reverse-phase HPLC with a diode array detector (RP HPLC-DAD) chromatographic system. The system employed a Thermo Scientific SpectraSystem P1000 pump (Thermo Scientific, Waltham, MA, USA, EUA), a Rheodyne manual injection valve, an Acclaim™ 120 column and a UV6000 LP diode array detector from Thermo Finnigan (San Jose, CA, USA). A mobile phase composed of 49.5% methanol, 49.5% deionized water, 1% acetic acid, and 1 mM ammonium acetate was used with a flow of 0.65 mL per minute.

3.4. Scavenger Assays

To gain insight into the potential participation of different reactive species in the photocatalytic degradation of CIP, additional photocatalytic assays were conducted using scavengers for each respective species, and the effect of the scavengers was monitored via RP-HPLC-DAD. Herein, IPA (10 mM) [26], Tiron (10 mM) [86], KNO_3 (10 mM) [87], KI (10 mM) [26], and sodium azide (1 mM) [88] were used to evaluate the roles of hydroxyl radicals (·OH), superoxide radicals (O_2^-), electrons (e^-), holes (h^+) and singlet oxygen ($^1O_2$), respectively.

3.5. BET Analysis

The surface area and pore parameters were determined using a nitrogen adsorption analyzer (TriStar Plus, Micromeritics, Norcross, GA, USA). Prior to conducting the N_2 adsorption–desorption measurements, the samples were degassed under N_2 flow at 200 °C for 6 h to remove adsorbed water and volatile impurities, ensuring that the measured surface area and pore characteristics reflect only the properties of the materials and not those of surface contaminants. The pore size distributions were calculated using the desorption branch of the N_2 isotherms, applying the Barrett–Joyner–Halenda (BJH) method.

4. Conclusions

This work demonstrates the efficient sunlight-driven degradation of the pharmaceutical contaminant CIP using a TiO_2/CDs nanocomposite under real-world irradiation conditions, a crucial step toward large-scale water-treatment applications. Furthermore, the used CDs were prepared from a major agricultural waste, corn stover.

Initial testing was performed under simulated sunlight. Under these conditions, $NC_{50:50}$ achieved a virtually full degradation of CIP within 20 min, with a rate constant of 0.2372 min^{-1}. Moreover, the photocatalytic activity of the nanocomposite was found to be 217% enhanced compared with commercial TiO_2. $NC_{50:50}$ also showed good stability. Finally, while some potential by-products were detected, they were also photodegraded by $NC_{50:50}$. When compared with other photocatalysts used for CIP degradation, $NC_{50:50}$ showed the most promising performance.

Subsequently, the performance of $NC_{50:50}$ was validated under real-world irradiation conditions. Namely, under natural sunlight over three consecutive days, with different meteorological conditions. This photocatalyst was found to retain its efficiency, fully photodegrading CIP under 30 min, irrespective of the day. Potential degradation by-

products were also formed but were subsequently degraded by $NC_{50:50}$. This indicates that the nanocomposite exhibits enhanced photodegradation catalytic effects even under real-world irradiation conditions.

The enhanced activity of $NC_{50:50}$ was attributed to a combination of effects that resulted from the incorporation of CDs. More specifically, their incorporation resulted in more efficient activation by sunlight, due to enhanced visible-light absorption. It was also concluded that CDs suppressed the recombination of holes and electrons, increasing the photodegradation efficiency. The incorporation of CDs also increased the specific surface area of the photocatalyst, which enhanced CIP adsorption before the photocatalysis stage. This pre-positioned CIP in the surface interface, which facilitated the photodegradation after starting the light irradiation phase.

Finally, the incorporation of CDs not only significantly improved the sunlight-driven photocatalytic activity but also modulated the reactive species generation profile of TiO_2. By altering the type and contribution magnitude of generated reactive species, CDs can modify the available degradation pathways. This finding potentially opens a pathway for the rational design of sunlight-active TiO_2-based photocatalysts with tunable surface reactivity and broader contaminant compatibility.

Supplementary Materials: The following supporting information can be downloaded at https://www.mdpi.com/article/10.3390/catal16020142/s1, Figure S1: Representation of the preliminary results of CIP photodegradation with $NC_{50:50}$ in terms of (a) ln (C/C_0) and (b) C/C_0 in function of different simulated sunlight irradiation times; (c) ln (C/C_0) and (d) C/C_0 values for different initial CIP concentrations; (e) ln (C/C_0) and (f) C/C_0 values at different pH and (g) ln (C/C_0) and (h) C/C_0 values for different catalyst dosages obtained during the optimization of the reactional conditions.; Figure S2: (a) CIP adsorption by $NC_{50:50}$ and TiO_2 occurred during the 30 min in the dark prior to turning on the lamp (corresponding to t_{-30} to t_0). Calculated by using the following equation: CIP adsorption = $((C - C_0)/C_0)$ *100. (b) Representation of the C/C_0 of CIP in the presence of $NC_{50:50}$ with and without an irradiation source. Variation with the lamp off corresponds to the effect of adsorption alone, whereas lamp on represents photocatalytic degradation. Table S1: Overview of chromatogram peaks appearing over the course of a 300 min CIP degradation photocatalytic assay with $NC_{50:50}$ under solar irradiation. Values are expressed as a percentage of the area of the initial CIP peak $(A(P1 - t_0)/A(P_x - t_y) * 100$.

Author Contributions: Conceptualization, L.P.d.S.; investigation, R.M.S.S. and A.T.S.C.B.; writing—original draft preparation, R.M.S.S.; writing—review and editing, A.T.S.C.B., C.M.P., L.P.d.S. and J.C.G.E.d.S.; supervision, C.M.P., L.P.d.S. and J.C.G.E.d.S.; funding acquisition, C.M.P., L.P.d.S. and J.C.G.E.d.S. All authors have read and agreed to the published version of the manuscript.

Funding: The Portuguese "Fundação para a Ciência e Tecnologia" (FCT, Lisbon) is acknowledged for funding project 2023.13127.PEX, R&D Unit CIQUP (UID/00081/2025) and the Associated Laboratory IMS (LA/P/0056/2020). "Programa Regional do Norte 2021–2027" (Norte 2030) is acknowledged for funding projects Restaura (NORTE 2030-FEDER-02704900), iChem4M (NORTE2030-FEDER-02706400), and AGRO-CIRN (NORTE2030-FEDER-02703200). For the purpose of Open Access, the authors have applied a CC-BY public copyright license to any Author's Accepted Manuscript (AAM) version arising from this submission. Carlos Pereira acknowledges the Portuguese Recovery and Resilience Plan and by the NextGeneration EU European funds in its component 12—Sustainable Bioeconomy, Investment under project Bioshoes4All (TC-C12-i01). Luís Pinto da Silva acknowledges funding from FCT under the Scientific Employment Stimulus (CEECINST/00069/2021). Ricardo Sendão acknowledges FCT for his Ph.D. grant (2021.06149.BD).

Data Availability Statement: The data that support the findings of this study are available from the authors upon reasonable request.

Acknowledgments: The Portuguese "Fundação para a Ciência e Tecnologia" (FCT, Lisbon) is acknowledged for funding project 2023.13127.PEX, R&D Unit CIQUP (UID/00081/2025) and the Associated Laboratory IMS (LA/P/0056/2020). "Programa Regional do Norte 2021–2027" (Norte 2030) is acknowledged for funding projects Restaura (NORTE 2030-FEDER-02704900), iChem4M (NORTE2030-FEDER-02706400), and AGRO-CIRN (NORTE2030-FEDER-02703200). For the purpose of Open Access, the authors have applied a CC-BY public copyright license to any Author's Accepted Manuscript (AAM) version arising from this submission. Carlos Pereira acknowledges the Portuguese Recovery and Resilience Plan and by the NextGeneration EU European funds in its component 12—Sustainable Bioeconomy, Investment under project Bioshoes4All (TC-C12-i01). Luís Pinto da Silva acknowledges funding from FCT under the Scientific Employment Stimulus (CEECINST/00069/2021). Ricardo Sendão acknowledges FCT for his Ph.D. grant (2021.06149.BD).

Conflicts of Interest: The authors declare that they have no known competing financial interests or personal relationships that could have appeared to influence the work reported in this paper.

References

1. Akhil, D.; Lakshmi, D.; Senthil Kumar, P.; Vo, D.-V.N.; Kartik, A. Occurrence and removal of antibiotics from industrial wastewater. *Environ. Chem. Lett.* **2021**, *19*, 1477–1507. [CrossRef]
2. Fayaz, T.; Renuka, N.; Ratha, S.K. Antibiotic occurrence, environmental risks, and their removal from aquatic environments using microalgae: Advances and future perspectives. *Chemosphere* **2024**, *349*, 140822. [CrossRef] [PubMed]
3. Batt, A.L.; Bruce, I.B.; Aga, D.S. Evaluating the vulnerability of surface waters to antibiotic contamination from varying wastewater treatment plant discharges. *Environ. Pollut.* **2006**, *142*, 295–302. [CrossRef] [PubMed]
4. Liu, X.; Lu, S.; Guo, W.; Xi, B.; Wang, W. Antibiotics in the aquatic environments: A review of lakes, China. *Sci. Total Environ.* **2018**, *627*, 1195–1208. [CrossRef]
5. Rodriguez-Mozaz, S.; Vaz-Moreira, I.; Varela Della Giustina, S.; Llorca, M.; Barcelo, D.; Schubert, S.; Berendonk, T.U.; Michael-Kordatou, I.; Fatta-Kassinos, D.; Martinez, J.L.; et al. Antibiotic residues in final effluents of European wastewater treatment plants and their impact on the aquatic environment. *Environ. Int.* **2020**, *140*, 105733. [CrossRef]
6. Zhang, X.; Xu, Y.; Liu, Y.; Wei, Y.; Lan, F.; Wang, R.; Yang, Y.; Chen, J. Research progress and trend of antibiotics degradation by electroactive biofilm: A review. *J. Water Process Eng.* **2024**, *58*, 104846. [CrossRef]
7. Yu, X.; Yu, F.; Li, Z.; Zhan, J. Occurrence, distribution, and ecological risk assessment of pharmaceuticals and personal care products in the surface water of the middle and lower reaches of the Yellow River (Henan section). *J. Hazard. Mater.* **2023**, *443*, 130369. [CrossRef]
8. Pan, M.; Chu, L.M. Occurrence of antibiotics and antibiotic resistance genes in soils from wastewater irrigation areas in the Pearl River Delta region, southern China. *Sci. Total Environ.* **2018**, *624*, 145–152. [CrossRef]
9. Salam, M.A.; Al-Amin, M.Y.; Salam, M.T.; Pawar, J.S.; Akhter, N.; Rabaan, A.A.; Alqumber, M.A.A. Antimicrobial Resistance: A Growing Serious Threat for Global Public Health. *Healthcare* **2023**, *11*, 1946. [CrossRef]
10. Biswas, S.; Bal, M.; Pati, S.; Rana, R.; Dixit, S.; Ranjit, M. Antibiotic resistance in toxigenic E. coli: A severe threat to global health. *Discov. Med.* **2024**, *1*, 72. [CrossRef]
11. Peltzer, P.M.; Lajmanovich, R.C.; Attademo, A.M.; Junges, C.M.; Teglia, C.M.; Martinuzzi, C.; Curi, L.; Culzoni, M.J.; Goicoechea, H.C. Ecotoxicity of veterinary enrofloxacin and ciprofloxacin antibiotics on anuran amphibian larvae. *Environ. Toxicol. Pharmacol.* **2017**, *51*, 114–123. [CrossRef]
12. Zhang, G.F.; Liu, X.; Zhang, S.; Pan, B.; Liu, M.L. Ciprofloxacin derivatives and their antibacterial activities. *Eur. J. Med. Chem.* **2018**, *146*, 599–612. [CrossRef]
13. Ansón-Casaos, A.; Hernández-Ferrer, J.; Vallan, L.; Xie, H.; Lira-Cantú, M.; Benito, A.M.; Maser, W.K. Functionalized carbon dots on TiO_2 for perovskite photovoltaics and stable photoanodes for water splitting. *Int. J. Hydrogen Energy* **2021**, *46*, 12180–12191. [CrossRef]
14. Aggarwal, R.; Saini, D.; Sonkar, S.K.; Sonker, A.K.; Westman, G. Sunlight promoted removal of toxic hexavalent chromium by cellulose derived photoactive carbon dots. *Chemosphere* **2022**, *287*, 132287. [CrossRef]
15. Sendão, R.M.S.; Algarra, M.; Ribeiro, E.; Pereira, M.; Gil, A.; Vale, N.; Esteves da Silva, J.C.G.; Pinto da Silva, L. Carbon Dots–TiO_2 Nanocomposites for the Enhanced Visible-Light Driven Photodegradation of Methylene Blue. *Adv. Sustain. Syst.* **2023**, *8*, 2300317. [CrossRef]

16. Sendão, R.M.S.; Algarra, M.; Lázaro-Martínez, J.; Brandão, A.T.S.C.; Gil, A.; Pereira, C.; Esteves da Silva, J.C.G.; Pinto da Silva, L. Visible-light-driven photocatalytic degradation of organic dyes using a TiO_2 and waste-based carbon dots nanocomposite. *Colloids Surf. A Physicochem. Eng. Asp.* **2025**, *713*, 136475. [CrossRef]
17. Song, D.; Li, M.; Liao, L.; Guo, L.; Liu, H.; Wang, B.; Li, Z. High-Crystallinity BiOCl Nanosheets as Efficient Photocatalysts for Norfloxacin Antibiotic Degradation. *Nanomaterials* **2023**, *13*, 1841. [CrossRef] [PubMed]
18. Singh, A.; Ahmed, A.; Sharma, A.; Sharma, C.; Paul, S.; Khosla, A.; Gupta, V.; Arya, S. Promising photocatalytic degradation of methyl orange dye via sol-gel synthesized Ag–CdS@Pr-TiO_2 core/shell nanoparticles. *Phys. B Condens. Matter* **2021**, *616*, 413121. [CrossRef]
19. Karthik, K.V.; Raghu, A.V.; Reddy, K.R.; Ravishankar, R.; Sangeeta, M.; Shetti, N.P.; Reddy, C.V. Green synthesis of Cu-doped ZnO nanoparticles and its application for the photocatalytic degradation of hazardous organic pollutants. *Chemosphere* **2022**, *287*, 132081. [CrossRef] [PubMed]
20. Koedsiri, Y.; Amornpitoksuk, P.; Randorn, C.; Rattana, T.; Tandorn, S.; Suwanboon, S. S-Schematic $CuWO_4$/ZnO nanocomposite boosted photocatalytic degradation of organic dye pollutants. *Mater. Sci. Semicond. Process.* **2024**, *177*, 108385. [CrossRef]
21. Khedr, T.M.; El-Sheikh, S.M.; Ismail, A.A.; Bahnemann, D.W. Highly efficient solar light-assisted TiO_2 nanocrystalline for photodegradation of ibuprofen drug. *Opt. Mater.* **2019**, *88*, 117–127. [CrossRef]
22. Ren, W.; Ai, Z.; Jia, F.; Zhang, L.; Fan, X.; Zou, Z. Low temperature preparation and visible light photocatalytic activity of mesoporous carbon-doped crystalline TiO_2. *Appl. Catal. B Environ.* **2007**, *69*, 138–144. [CrossRef]
23. Barolet, D.; Christiaens, F.; Hamblin, M.R. Infrared and skin: Friend or foe. *J. Photochem. Photobiol. B* **2016**, *155*, 78–85. [CrossRef]
24. Daghrir, R.; Drogui, P.; Robert, D. Photoelectrocatalytic technologies for environmental applications. *J. Photochem. Photobiol. A Chem.* **2012**, *238*, 41–52. [CrossRef]
25. Dong, H.; Zeng, G.; Tang, L.; Fan, C.; Zhang, C.; He, X.; He, Y. An overview on limitations of TiO_2-based particles for photocatalytic degradation of organic pollutants and the corresponding countermeasures. *Water Res.* **2015**, *79*, 128–146. [CrossRef]
26. El Mragui, A.; Zegaoui, O.; Esteves da Silva, J.C.G. Elucidation of the photocatalytic degradation mechanism of an azo dye under visible light in the presence of cobalt doped TiO_2 nanomaterials. *Chemosphere* **2021**, *266*, 128931. [CrossRef]
27. Eslami, A.; Amini, M.M.; Yazdanbakhsh, A.R.; Mohseni-Bandpei, A.; Safari, A.A.; Asadi, A. N,S co-doped TiO_2 nanoparticles and nanosheets in simulated solar light for photocatalytic degradation of non-steroidal anti-inflammatory drugs in water: A comparative study. *J. Chem. Technol. Biotechnol.* **2016**, *91*, 2693–2704. [CrossRef]
28. Ni, J.; Wang, W.; Liu, D.; Zhu, Q.; Jia, J.; Tian, J.; Li, Z.; Wang, X.; Xing, Z. Oxygen vacancy-mediated sandwich-structural $TiO_{(2-x)}$/ultrathin g-$C_{(3)}N_{(4)}$/$TiO_{(2-x)}$ direct Z-scheme heterojunction visible-light-driven photocatalyst for efficient removal of high toxic tetracycline antibiotics. *J. Hazard. Mater.* **2021**, *408*, 124432. [CrossRef]
29. Singh, A.; Khare, P.; Verma, S.; Bhati, A.; Sonker, A.K.; Tripathi, K.M.; Sonkar, S.K. Pollutant Soot for Pollutant Dye Degradation: Soluble Graphene Nanosheets for Visible Light Induced Photodegradation of Methylene Blue. *ACS Sustain. Chem. Eng.* **2017**, *5*, 8860–8869. [CrossRef]
30. Pan, D.; Jiao, J.; Li, Z.; Guo, Y.; Feng, C.; Liu, Y.; Wang, L.; Wu, M. Efficient Separation of Electron–Hole Pairs in Graphene Quantum Dots by TiO_2 Heterojunctions for Dye Degradation. *ACS Sustain. Chem. Eng.* **2015**, *3*, 2405–2413. [CrossRef]
31. Li, Y.; Liu, Z.; Wu, Y.; Chen, J.; Zhao, J.; Jin, F.; Na, P. Carbon dots-TiO_2 nanosheets composites for photoreduction of Cr(VI) under sunlight illumination: Favorable role of carbon dots. *Appl. Catal. B* **2018**, *224*, 508–517. [CrossRef]
32. Wang, R.; Lu, K.-Q.; Tang, Z.-R.; Xu, Y.-J. Recent progress in carbon quantum dots: Synthesis, properties and applications in photocatalysis. *J. Mater. Chem. A* **2017**, *5*, 3717–3734. [CrossRef]
33. Sendao, R.M.S.; Crista, D.M.A.; Afonso, A.C.P.; Martinez de Yuso, M.D.V.; Algarra, M.; Esteves da Silva, J.C.G.; Pinto da Silva, L. Insight into the hybrid luminescence showed by carbon dots and molecular fluorophores in solution. *Phys. Chem. Chem. Phys.* **2019**, *21*, 20919–20926. [CrossRef]
34. Vale, N.; Silva, S.; Duarte, D.; Crista, D.M.A.; Pinto da Silva, L.; Esteves da Silva, J.C.G. Normal breast epithelial MCF-10A cells to evaluate the safety of carbon dots. *RSC Med. Chem.* **2021**, *12*, 245–253. [CrossRef]
35. Deng, Y.; Chen, M.; Chen, G.; Zou, W.; Zhao, Y.; Zhang, H.; Zhao, Q. Visible-Ultraviolet Upconversion Carbon Quantum Dots for Enhancement of the Photocatalytic Activity of Titanium Dioxide. *ACS Omega* **2021**, *6*, 4247–4254. [CrossRef]
36. Crista, D.M.A.; Mello, G.P.C.; Shevchuk, O.; Sendao, R.M.S.; Simoes, E.F.C.; Leitao, J.M.M.; da Silva, L.P.; Esteves da Silva, J.C.G. 3-Hydroxyphenylboronic Acid-Based Carbon Dot Sensors for Fructose Sensing. *J. Fluoresc.* **2019**, *29*, 265–270. [CrossRef]
37. An, Y.; Liu, C.; Li, Y.; Chen, M.; Zheng, Y.; Tian, H.; Shi, R.; He, X.; Lin, X. Preparation of Multicolour Solid Fluorescent Carbon Dots for Light-Emitting Diodes Using Phenylethylamine as a Co-Carbonization Agent. *Int. J. Mol. Sci.* **2022**, *23*, 11071. [CrossRef]
38. Kong, T.; Liu, T.; Zhang, Y.; Wang, M. Carbon dots with intrinsic theranostic properties for photodynamic therapy of oral squamous cell carcinoma. *J. Biomater. Appl.* **2022**, *37*, 850–858. [CrossRef]

39. Zhu, Z.; Li, X.; Luo, M.; Chen, M.; Chen, W.; Yang, P.; Zhou, X. Synthesis of carbon dots with high photocatalytic reactivity by tailoring heteroatom doping. *J. Colloid Interface Sci.* **2022**, *605*, 330–341. [CrossRef]
40. Sendão, R.M.S.; Esteves da Silva, J.C.G.; Pinto da Silva, L. Applications of Fluorescent Carbon Dots as Photocatalysts: A Review. *Catalysts* **2023**, *13*, 179. [CrossRef]
41. Sendao, R.M.S.; Esteves da Silva, J.C.G.; Pinto da Silva, L. Photocatalytic removal of pharmaceutical water pollutants by TiO_2—Carbon dots nanocomposites: A review. *Chemosphere* **2022**, *301*, 134731. [CrossRef]
42. Elbanna, O.; Zhang, P.; Fujitsuka, M.; Majima, T. Facile preparation of nitrogen and fluorine codoped TiO_2 mesocrystal with visible light photocatalytic activity. *Appl. Catal. B Environ.* **2016**, *192*, 80–87. [CrossRef]
43. Tian, J.; Leng, Y.; Zhao, Z.; Xia, Y.; Sang, Y.; Hao, P.; Zhan, J.; Li, M.; Liu, H. Carbon quantum dots/hydrogenated TiO_2 nanobelt heterostructures and their broad spectrum photocatalytic properties under UV, visible, and near-infrared irradiation. *Nano Energy* **2015**, *11*, 419–427. [CrossRef]
44. Zhou, H.; Zhang, B.; Jiang, Z.; Zhao, H.; Zhang, Y. Room-Temperature Synthesis of Carbon Dot/TiO_2 Composites with High Photocatalytic Activity. *Langmuir* **2023**, *39*, 7184–7191. [CrossRef] [PubMed]
45. Saini, D.; Garg, A.K.; Dalal, C.; Anand, S.R.; Sonkar, S.K.; Sonker, A.K.; Westman, G. Visible-Light-Promoted Photocatalytic Applications of Carbon Dots: A Review. *ACS Appl. Nano Mater.* **2022**, *5*, 3087–3109. [CrossRef]
46. Crista, D.M.A.; Esteves da Silva, J.C.G.; Pinto da Silva, L. Evaluation of Different Bottom-up Routes for the Fabrication of Carbon Dots. *Nanomaterials* **2020**, *10*, 1316. [CrossRef] [PubMed]
47. Sendão, R.; Yuso, M.d.V.M.d.; Algarra, M.; Esteves da Silva, J.C.G.; Pinto da Silva, L. Comparative life cycle assessment of bottom-up synthesis routes for carbon dots derived from citric acid and urea. *J. Clean. Prod.* **2020**, *254*, 120080. [CrossRef]
48. Fernandes, S.; Esteves da Silva, J.C.G.; Pinto da Silva, L. Comparative life cycle assessment of high-yield synthesis routes for carbon dots. *NanoImpact* **2021**, *23*, 100332. [CrossRef]
49. Zhao, W.; Cui, Y.; Sun, X.; Wang, H.; Teng, X. Corn stover biochar increased edible safety of spinach by reducing the migration of mercury from soil to spinach. *Sci. Total Environ.* **2021**, *758*, 143883. [CrossRef]
50. Cardoso, I.M.F.; Cardoso, R.M.F.; Pinto da Silva, L.; Esteves da Silva, J.C.G. UV-Based Advanced Oxidation Processes of Remazol Brilliant Blue R Dye Catalyzed by Carbon Dots. *Nanomaterials* **2022**, *12*, 2116. [CrossRef]
51. Rajender, G.; Kumar, J.; Giri, P.K. Interfacial charge transfer in oxygen deficient TiO_2-graphene quantum dot hybrid and its influence on the enhanced visible light photocatalysis. *Appl. Catal. B Environ.* **2018**, *224*, 960–972. [CrossRef]
52. Barrett, E.P.; Joyner, L.G.; Halenda, P.P. The Determination of Pore Volume and Area Distributions in Porous Substances. I. Computations from Nitrogen Isotherms. *J. Am. Chem. Soc* **2002**, *73*, 373–380. [CrossRef]
53. Zhang, J.; Liu, Q.; He, H.; Shi, F.; Huang, G.; Xing, B.; Jia, J.; Zhang, C. Coal tar pitch as natural carbon quantum dots decorated on TiO_2 for visible light photodegradation of rhodamine B. *Carbon* **2019**, *152*, 284–294. [CrossRef]
54. Milojković, N.; Simović, B.; Žunić, M.; Radovanović, L.; Prekajski-Đorđević, M.; Dapčević, A. Modified Z-scheme heterojunction of TiO_2/polypyrrole recyclable photocatalyst. *J. Am. Ceram. Soc.* **2025**, *108*, e20431. [CrossRef]
55. Sorathiya, K.; Mishra, B.; Kalarikkal, A.; Reddy, K.P.; Gopinath, C.S.; Khushalani, D. Enhancement in Rate of Photocatalysis Upon Catalyst Recycling. *Sci. Rep.* **2016**, *6*, 35075. [CrossRef]
56. Mohamed, I.M.A.; Hossam, G.; Shaker, A.M.; Nassr, L.A.E. Surface functionalization of TiO_2 nanoparticles with hydrophobic tridentate Schiff base for a promising photocatalytic reduction of toxic Cr(VI) in aqueous solutions. *Ceram. Int.* **2025**, *51*, 16005–16016. [CrossRef]
57. Escareno-Torres, G.A.; Pinedo-Escobar, J.A.; De Haro-Del Rio, D.A.; Becerra-Castaneda, P.; Araiza, D.G.; Inchaurregui-Mendez, H.; Carrillo-Martinez, C.J.; Gonzalez-Rodriguez, L.M. Enhanced degradation of ciprofloxacin in water using ternary photocatalysts $TiO_2/SnO_2/g\text{-}C_3N_4$ under UV, visible, and solar light. *Environ. Sci. Pollut. Res.* **2024**, *31*, 40174–40189. [CrossRef]
58. Chen, Z.; Kuate, L.J.N.; Zhang, H.; Hou, J.; Wen, H.; Lu, C.; Li, C.; Shi, W. Photothermally enabled black $g\text{-}C_3N_4$ hydrogel with integrated solar-driven evaporation and photo-degradation for efficient water purification. *Sep. Purif. Technol.* **2025**, *355*, 129751. [CrossRef]
59. Gao, X.; Sun, L.; Hao, P.; Zhang, S.; Shen, Y.; Hou, J.; Guo, F.; Li, C.; Shi, W. Construction of black $g\text{-}C_3N_4$/loofah/chitosan hydrogel as an efficient solar evaporator for desalination coupled with antibiotic degradation. *Sep. Purif. Technol.* **2025**, *355*, 129615. [CrossRef]
60. Shi, W.; Hao, C.; Shi, Y.; Guo, F.; Tang, Y. Effect of different carbon dots positions on the transfer of photo-induced charges in type I heterojunction for significantly enhanced photocatalytic activity. *Sep. Purif. Technol.* **2023**, *304*, 122337. [CrossRef]
61. Shi, W.; Sun, W.; Liu, Y.; Zhang, K.; Sun, H.; Lin, X.; Hong, Y.; Guo, F. A self-sufficient photo-Fenton system with coupling in-situ production H_2O_2 of ultrathin porous $g\text{-}C_3N_4$ nanosheets and amorphous FeOOH quantum dots. *J. Hazard Mater.* **2022**, *436*, 129141. [CrossRef]

62. Pan, J.; Sun, H.; Chen, K.; Zhang, Y.; Shan, P.; Shi, W.; Guo, F. Nanodiamonds decorated yolk-shell $ZnFe_2O_4$ sphere as magnetically separable and recyclable composite for boosting antibiotic degradation performance. *Chin. J. Chem. Eng.* **2023**, *54*, 162–172. [CrossRef]
63. Triquet, T.; Tendero, C.; Latapie, L.; Manero, M.-H.; Richard, R.; Andriantsiferana, C. TiO_2 MOCVD coating for photocatalytic degradation of ciprofloxacin using 365 nm UV LEDs—Kinetics and mechanisms. *J. Environ. Chem. Eng.* **2020**, *8*, 104544. [CrossRef]
64. Zheng, X.; Xu, S.; Wang, Y.; Sun, X.; Gao, Y.; Gao, B. Enhanced degradation of ciprofloxacin by graphitized mesoporous carbon (GMC)-TiO_2 nanocomposite: Strong synergy of adsorption-photocatalysis and antibiotics degradation mechanism. *J. Colloid Interface Sci.* **2018**, *527*, 202–213. [CrossRef]
65. Malakootian, M.; Nasiri, A.; Amiri Gharaghani, M. Photocatalytic degradation of ciprofloxacin antibiotic by TiO_2 nanoparticles immobilized on a glass plate. *Chem. Eng. Commun.* **2019**, *207*, 56–72. [CrossRef]
66. Akter, S.; Islam, M.S.; Kabir, M.H.; Shaikh, M.A.A.; Gafur, M.A. UV/TiO_2 photodegradation of metronidazole, ciprofloxacin and sulfamethoxazole in aqueous solution: An optimization and kinetic study. *Arab. J. Chem.* **2022**, *15*, 103900. [CrossRef]
67. Costa, L.N.; Nobre, F.X.; Lobo, A.O.; de Matos, J.M.E. Photodegradation of ciprofloxacin using Z-scheme TiO_2/SnO_2 nanostructures as photocatalyst. *Environ. Nanotechnol. Monit. Manag.* **2021**, *16*, 100466. [CrossRef]
68. Zeng, Y.; Chen, D.; Chen, T.; Cai, M.; Zhang, Q.; Xie, Z.; Li, R.; Xiao, Z.; Liu, G.; Lv, W. Study on heterogeneous photocatalytic ozonation degradation of ciprofloxacin by TiO_2/carbon dots: Kinetic, mechanism and pathway investigation. *Chemosphere* **2019**, *227*, 198–206. [CrossRef]
69. Li, W.; Guo, C.; Su, B.; Xu, J. Photodegradation of four fluoroquinolone compounds by titanium dioxide under simulated solar light irradiation. *J. Chem. Technol. Biotechnol.* **2012**, *87*, 643–650. [CrossRef]
70. Moghni, N.; Boutoumi, H.; Khalaf, H.; Makaoui, N.; Colón, G. Enhanced photocatalytic activity of TiO_2/WO_3 nanocomposite from sonochemical-microwave assisted synthesis for the photodegradation of ciprofloxacin and oxytetracycline antibiotics under UV and sunlight. *J. Photochem. Photobiol. A Chem.* **2022**, *428*, 113848. [CrossRef]
71. Abdullah, A.M.; Gracia-Pinilla, M.A.; Pillai, S.C.; O'Shea, K. UV and Visible Light-Driven Production of Hydroxyl Radicals by Reduced Forms of N, F, and P Codoped Titanium Dioxide. *Molecules* **2019**, *24*, 2147. [CrossRef] [PubMed]
72. Parnicka, P.; Mazierski, P.; Grzyb, T.; Lisowski, W.; Kowalska, E.; Ohtani, B.; Zaleska-Medynska, A.; Nadolna, J. Influence of the preparation method on the photocatalytic activity of Nd-modified TiO_2. *Beilstein J. Nanotechnol.* **2018**, *9*, 447–459. [CrossRef]
73. Zhao, C.; Pelaez, M.; Dionysiou, D.D.; Pillai, S.C.; Byrne, J.A.; O'Shea, K.E. UV and visible light activated TiO_2 photocatalysis of 6-hydroxymethyl uracil, a model compound for the potent cyanotoxin cylindrospermopsin. *Catal. Today* **2014**, *224*, 70–76. [CrossRef]
74. Zou, M.; Kong, Y.; Wang, J.; Wang, Q.; Wang, Z.; Wang, B.; Fan, P. Spectroscopic analyses on ROS generation catalyzed by TiO_2, CeO_2/TiO_2 and Fe_2O_3/TiO_2 under ultrasonic and visible-light irradiation. *Spectrochim. Acta Part A* **2013**, *101*, 82–90. [CrossRef]
75. Guo, Y.; Cheng, C.; Wang, J.; Wang, Z.; Jin, X.; Li, K.; Kang, P.; Gao, J. Detection of reactive oxygen species (ROS) generated by TiO_2(R), TiO_2(R/A) and TiO_2(A) under ultrasonic and solar light irradiation and application in degradation of organic dyes. *J. Hazard. Mater.* **2011**, *192*, 786–793. [CrossRef]
76. Hoffmann, M.R.; Martin, S.T.; Choi, W.; Bahnemann, D.W. Environmental Applications of Semiconductor Photocatalysis. *Chem. Rev.* **2002**, *95*, 69–96. [CrossRef]
77. Tong, S.; Zhou, J.; Ding, L.; Zhou, C.; Liu, Y.; Li, S.; Meng, J.; Zhu, S.; Chatterjee, S.; Liang, F. Preparation of carbon quantum dots/TiO_2 composite and application for enhanced photodegradation of rhodamine B. *Colloids Surf. A* **2022**, *648*, 129342. [CrossRef]
78. Wang, X.; Cao, L.; Lu, F.; Meziani, M.J.; Li, H.; Qi, G.; Zhou, B.; Harruff, B.A.; Kermarrec, F.; Sun, Y.P. Photoinduced electron transfers with carbon dots. *Chem. Commun.* **2009**, *25*, 3774–3776. [CrossRef]
79. Chang, L.; Ahmad, N.; Zeng, G.; Ray, A.; Zhang, Y. N, S co-doped carbon quantum dots/TiO_2 composite for visible-light-driven photocatalytic reduction of Cr (VI). *J. Environ. Chem. Eng.* **2022**, *10*, 108742. [CrossRef]
80. Wang, H.; Zhang, L.; Chen, Z.; Hu, J.; Li, S.; Wang, Z.; Liu, J.; Wang, X. Semiconductor heterojunction photocatalysts: Design, construction, and photocatalytic performances. *Chem. Soc. Rev.* **2014**, *43*, 5234–5244. [CrossRef] [PubMed]
81. Nosaka, Y.; Daimon, T.; Nosaka, A.Y.; Murakami, Y. Singlet oxygen formation in photocatalytic TiO_2 aqueous suspension. *Phys. Chem. Chem. Phys.* **2004**, *6*, 2917–2918. [CrossRef]
82. Fernandes, S.; Algarra, M.; Gil, A.; Esteves da Silva, J.; Pinto da Silva, L. Development of a Facile and Green Synthesis Strategy for Brightly Fluorescent Carbon Dots from Various Waste Materials. *ChemSusChem* **2025**, *18*, e202401702. [CrossRef]
83. El Mragui, A.; Daou, I.; Zegaoui, O. Influence of the preparation method and ZnO/(ZnO + TiO_2) weight ratio on the physico-chemical and photocatalytic properties of ZnO-TiO_2 nanomaterials. *Catal. Today* **2019**, *321–322*, 41–51. [CrossRef]
84. El Mragui, A.; Logvina, Y.; Pinto da Silva, L.; Zegaoui, O.; Esteves da Silva, J.C.G. Synthesis of Fe- and Co-Doped TiO_2 with Improved Photocatalytic Activity Under Visible Irradiation Toward Carbamazepine Degradation. *Materials* **2019**, *12*, 3874. [CrossRef]

85. Farjadfar, S.; Ghiaci, M.; Kulinch, S.A.; Wunderlich, W. Efficient photocatalyst for the degradation of cationic and anionic dyes prepared via modification of carbonized mesoporous TiO_2 by encapsulation of carbon dots. *Mater. Res. Bull.* **2022**, *155*, 111963. [CrossRef]
86. Liubimovskii, S.O.; Ustynyuk, L.Y.; Tikhonov, A.N. Superoxide radical scavenging by sodium 4,5-dihydroxybenzene-1,3-disulfonate dissolved in water: Experimental and quantum chemical studies. *J. Mol. Liq.* **2021**, *333*, 115810. [CrossRef]
87. Pastina, B.; LaVerne, J.A.; Pimblott, S.M. Dependence of Molecular Hydrogen Formation in Water on Scavengers of the Precursor to the Hydrated Electron. *J. Phys. Chem. A* **1999**, *103*, 5841–5846. [CrossRef]
88. Bancirova, M. Sodium azide as a specific quencher of singlet oxygen during chemiluminescent detection by luminol and Cypridina luciferin analogues. *Luminescence* **2011**, *26*, 685–688. [CrossRef]

Disclaimer/Publisher's Note: The statements, opinions and data contained in all publications are solely those of the individual author(s) and contributor(s) and not of MDPI and/or the editor(s). MDPI and/or the editor(s) disclaim responsibility for any injury to people or property resulting from any ideas, methods, instructions or products referred to in the content.

2.2.2. Supplementary information

Enhanced Photocatalytic Degradation of Ciprofloxacin Under Natural Sunlight Using a Waste-Derived Carbon Dots–TiO_2 Nanocomposite

Ricardo M. S. Sendão[1], Ana T. S. C. Brandão[2], Carlos Pereira[2], Joaquim C. G. Esteves da Silva[1,3], Luís Pinto da Silva[1,3,*]

[1] Chemistry Research Unit (CIQUP), Institute of Molecular Sciences (IMS), Department of Geosciences, Environment and Territorial Planning, Faculty of Sciences, University of Porto, Rua do Campo Alegre s/n, 4169-007 Porto, Portugal
[2] Chemistry Research Unit (CIQUP), Institute of Molecular Sciences (IMS), Department of Chemistry and Biochemistry, Faculty of Sciences, University of Porto, Rua do Campo Alegre s/n, Porto 4169-007, Portugal
[3] LACOMEPHI, GreenUPorto, Department of Geosciences, Environment and Territorial Planning, Faculty of Sciences, University of Porto, Rua do Campo Alegre s/n, 4169- 007 Porto, Portugal
* luis.silva@fc.up.pt

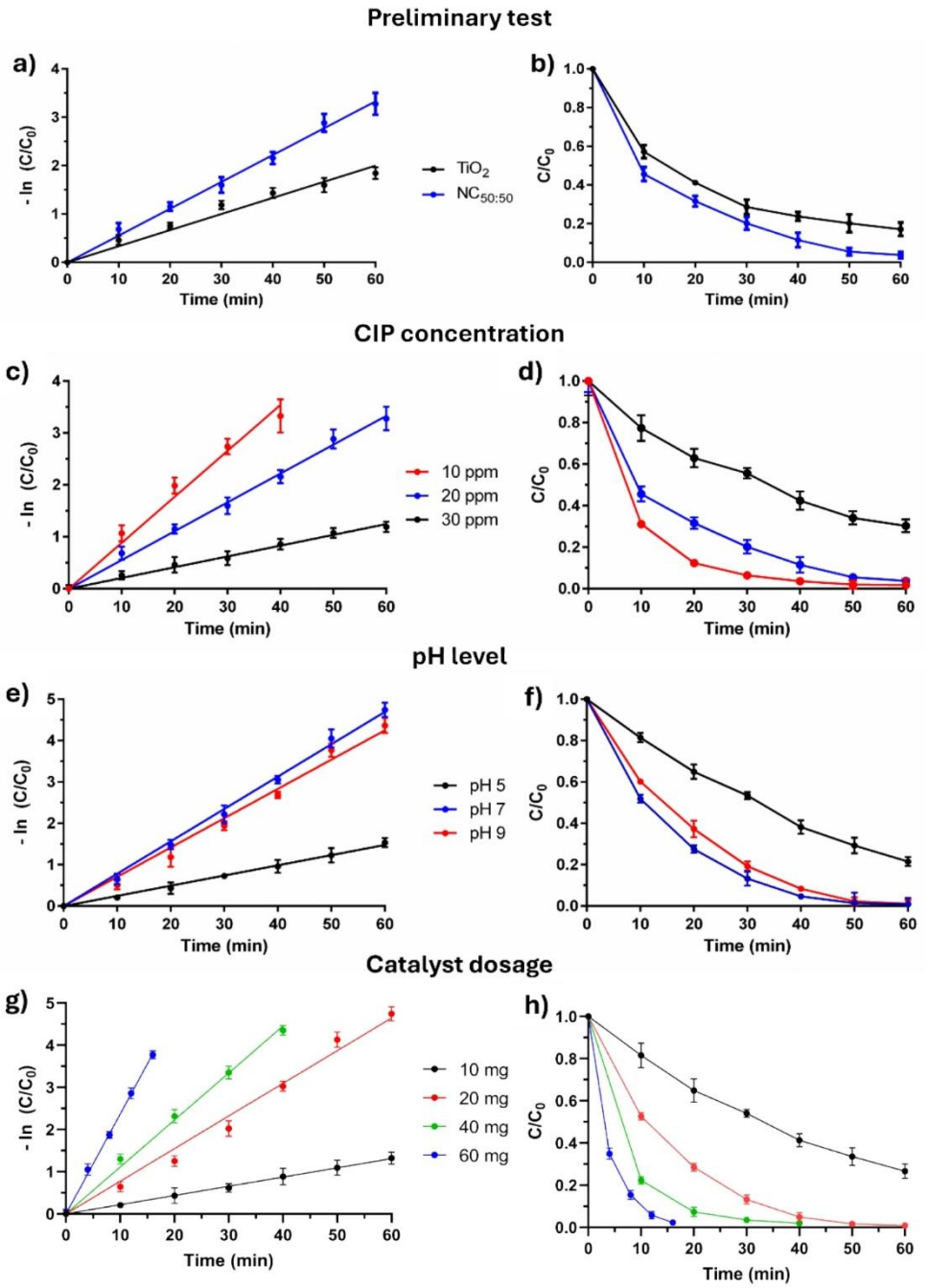


Figure S1 – Representation of the preliminary results of CIP photodegradation with $NC_{50:50}$ in terms of a) - ln (C/C_0) and b) C/C_0 in function of different simulated sunlight irradiation times; c) - ln (C/C_0) and d) C/C_0 values for different initial CIP concentrations; e) - ln (C/C_0) and f) C/C_0 values at different pH and g) - ln (C/C_0) and h) C/C_0 values for different catalyst dosages obtained during the optimization of the reactional conditions.

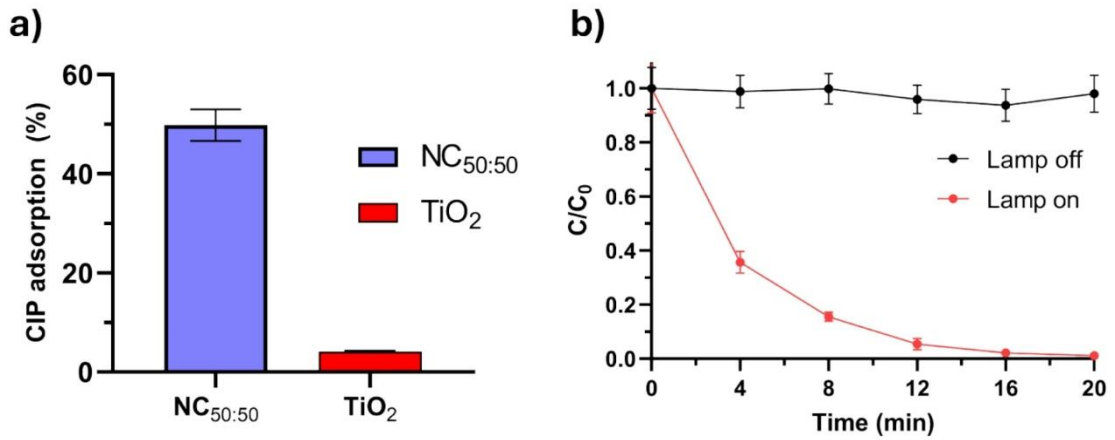


Figure S2 – a) CIP adsorption by $NC_{50:50}$ and TiO_2 occurred during the 30 minutes in the dark prior to turning on the lamp (corresponding to t_{-30} to t_0). Calculated by using the following equation: CIP adsorption = (($C - C_0$) / C_0) *100. B) Representation of the C/C_0 of CIP in the presence of $NC_{50:50}$ with and without an irradiation source. Variation with the lamp off corresponds to the effect of adsorption alone, whereas lamp on represents photocatalytic degradation.

Table S1 - Overview of chromatogram peaks appearing over the course of a 300 minutes CIp degradation photocatalytic assay with $NC_{50:50}$ under solar irradiation. Values are expressed as a percentage of the area of the initial CIP peak (A(P1-t_0) / A(Px-t_y) * 100.

IRRADIATION TIME (MIN)	PEAK					
	P1 (RT 3.53)	P2 (RT 2.60)	P3 (RT 3.07)	P4 (RT 4.83)	P5 (RT 4.83)	P6 (RT 2.86)
0	100.000					
30	2.477	0.619	1.583	15.505	25.737	
60	1.099	3.387	2.203	10.774	23.007	
90	0.663	1.126	3.030	7.777	15.504	
120	0.753	1.031	4.449	5.517	9.098	
150	0.728	0.787	1.980	3.889	7.405	0.762
180	0.822	0.645	1.696	2.709	4.220	1.466
210	0.910	0.658	1.724	1.930	2.530	1.280
240	0.852	0.643	1.141	0.599	0.972	2.041
270	0.792	0.311	0.884	0.467	0.621	2.567
300	0.752	0.363	0.987			0.945

2.2.3. Conclusion

This work reports the development of sunlight-active photocatalytic nanocomposites toward the photodegradation of CP under both simulated and natural sunlight. This was done using a nanocomposite prepared from TiO_2 and CDs, $NC_{50:50}$, which also incorporated corn stover, an organic waste, on its preparation. The resulting nanocomposite presented an enhanced absorption in the visible range, an inhibited recombination of photogenerated charge carriers and a larger specific surface area than commercial TiO_2.

Regarding its photocatalytic potential, under a solar simulator, $NC_{50:50}$ achieved a virtually complete removal of CIP within 20 minutes of irradiation and a rate constant of 0.2372 min^{-1}, which corresponds to a 217% enhancement when compared to the TiO_2 benchmark. Some by-products appearing during CIP degradation were also virtually fully degraded by $NC_{50:50}$. Furthermore, as observed in tests with reactive species scavengers, the superoxide radical, h^+, e^- and $^1O_2$, by that order, seem to be the species behind the photodegradation mechanism. During recycling studies, $NC_{50:50}$ also showed good stability, maintaining its photocatalytic activity during at least three catalytic cycles. Finally, tests under natural sunlight and varying atmospheric conditions revealed that $NC_{50:50}$ is efficient even under these conditions. Namely, under direct sunlight, it was capable of fully degrading CP within 30 minutes of irradiation, irrespective of the day, sky conditions, and temperature.

In summary, this work confirmed that the conjugation of TiO_2 and CDs is a valid approach to achieve a more sustainable yet efficient degradation of a relevant antibiotic, CIP, under both simulated and natural solar irradiation. As a confirmation of the potential of this strategy, when compared to other TiO_2-based systems, $NC_{50:50}$ presented the highest reaction rate constant of the literature works we could find and required the last amount of time to fully degrade the initial CIP in the reactional mixture. Moreover, this was achieved while employing corn stover, thus upcycling an otherwise discarded organic waste while maintaining a good catalytic efficiency. This indicates that using biomass-incorporating CDs to overcome the limitations of TiO_2 is feasible and can be achieved while also upcycling corn-stover, thus achieving a better catalytic efficiency and a more circular economy.

2.3. Life Cycle Assessment studies of photocatalytic TiO_2/CDs nanocomposites

Article

Comparative life cycle assessment of the fabrication of visible-light-driven photocatalytic TiO2 – Carbon dots nanocomposites for wastewater treatment

Sendão, Ricardo M. S.; Esteves da Silva, Joaquim C. G.; Pinto da Silva, Luís. "Comparative life cycle assessment of the fabrication of visible-light-driven photocatalytic TiO_2 – Carbon dots nanocomposites for wastewater treatment". *NanoImpact* 38(22) (**2025**): 100556. http://doi.org/10.3390/suschem4040024.

2.3.1. Introduction and contributions to this work

The final part of this thesis consists of a comprehensive study of three different TiO_2/CDs nanocomposites prepared toward the photodegradation of MB. As shown in the previous sections, the addition of CDs to TiO_2 has the potential to bridge TiO_2's poor visible-light absorption and photonic efficiency, thus expanding the real-world application of this known photocatalyst. However, given that this type of photocatalytic material is still at an early stage of development and that there are aspects of the process still requiring optimization, concrete and verified data regarding the sustainable development and fabrication of this type of nanomaterial is lacking. Toward this end, we performed a LCA study to understand the environmental impacts of different visible-light-active TiO_2/CDs nanocomposites produced toward the photodegradation of MB. From the data we obtained, we found that the nanocomposites with the highest photocatalytic activity were the ones whose synthesis was associated with lower environmental impacts, as a higher catalytic potential resulted in a lower mass of catalyst required for the process, and that the most critical parameter affecting the overall environmental impacts was the source of the TiO_2 used in the nanocomposites.

In this work, I was responsible for gathering the data concerning the different nanocomposites reported in the study, perform the LCA studies, analyzing and interpreting the results obtained and writing the first draft of the paper which was then reviewed and edited by Professor Dr. Luís Pinto da Siva and Professor Dr. Joaquim Esteves da Silva, who supervised the research from end-to-end.

NanoImpact 38 (2025) 100556

Contents lists available at ScienceDirect

NanoImpact

journal homepage: www.elsevier.com/locate/nanoimpact

Research Paper

Comparative life cycle assessment of the fabrication of visible-light-driven photocatalytic TiO_2 – Carbon dots nanocomposites for wastewater treatment

Ricardo M.S. Sendão [a], Joaquim C.G. Esteves da Silva [a,b], Luís Pinto da Silva [a,b,*]

[a] Chemistry Research Unit (CIQUP), Institute of Molecular Sciences (IMS), Department of Geosciences, Environment and Spatial Plannings, Faculty of Sciences, University of Porto, Rua do Campo Alegre s/n, 4169-007 Porto, Portugal
[b] LACOMEPHI, GreenUPorto, Department of Geosciences, Environment and Spatial Plannings, Faculty of Sciences, University of Porto, Rua do Campo Alegre s/n, 4169-007 Porto, Portugal

ARTICLE INFO

Editor: Bernd Nowack

Keywords:
Life cycle assessment
TiO_2
Carbon dots
Photocatalysis
Wastewater treatment
Advanced oxidation processes

ABSTRACT

TiO_2 nanoparticles are promising photocatalysts due to their oxidizing strength and inertness. However, their inability to efficiently absorb visible light limits industrial applications that could use sunlight. The addition of carbon dots to TiO_2 has been recently shown to have the potential to address this issue by enhancing the visible-light-driven photocatalytic efficiency of the resulting nanocomposites. However, concrete data on their sustainable development and fabrication is lacking. Herein, we performed a life cycle assessment (LCA) study to understand the environmental impacts of different TiO_2-carbon dots nanocomposites with enhanced visible-light-driven photocatalytic activity. It was found that the nanocomposites with the highest photocatalytic activity were the ones whose synthesis was associated with lower environmental impacts. Furthermore, the carbon dots generally have little to moderate contributions to most impact categories, except for marine eutrophication. Finally, the most critical parameter was found to be the source of TiO_2 for the nanocomposites.

1. Introduction

Water scarcity is a global challenge that is aggravated due to an ever-increasing demand for drinking water. (Pimentel et al., 2004) Because of this, it is estimated that over 40 % of the global population will endure severe water scarcity within the next 50 years. (Mekonnen and Hoekstra, 2016) Thus, the protection of existing freshwater resources is of paramount importance for future sustainability. (Tollefson, 2011) Textile industries that employ organic dyes are responsible for the utilization of a huge amount of potable water, (Sen et al., 2019) as they require highly water-intensive processes that pose an environmental challenge. Although textile wastewater can undergo treatment for subsequent reuse, it may contain high amounts of persistent organic pollutants, inorganic salts and heavy metals. (Sen et al., 2019) Organic dyes can be hazardous to human health and cause dysfunction in several systems of human beings. (Adegoke and Bello, 2015) Additionally, these pollutants may originate damaging by-products via hydrolysis, oxidation or other reactions associated with an aqueous medium. (Konstantinou and Albanis, 2004).

Several strategies have been studied regarding the treatment of textile wastewater effluents. In general, conventional treatment plants have not effectively removed dyes from textile wastewater. (Konstantinou and Albanis, 2004) Some alternatives offering higher efficiency, such as chemical precipitation, nanofiltration, and electrocoagulation, have been reported. (Arellano-Cárdenas et al., 2013; Chowdhury et al., 2011) However, these technologies have a very high cost and high energy demands and may require toxic components to function as intended. Another option would be advanced oxidation processes (AOPs), such as photocatalysis. These processes have gained the scientific community's attention due to offering a higher degradation efficiency of organic pollutants while being relatively low cost and safe to use.

Photocatalytic processes are based on converting photoenergy into chemical energy, promoting a reaction without consuming the catalyst. It can be a greener alternative to conventional treatment methods and presents several advantages. Namely, it may employ an inexhaustible

* Corresponding author at: Chemistry Research Unit (CIQUP), Institute of Molecular Sciences (IMS), Department of Geosciences, Environment and Spatial Plannings, Faculty of Sciences, University of Porto, Rua do Campo Alegre s/n, 4169-007 Porto, Portugal.
E-mail address: luis.silva@fc.up.pt (L. Pinto da Silva).

https://doi.org/10.1016/j.impact.2025.100556
Received 27 January 2025; Received in revised form 1 April 2025; Accepted 2 April 2025
Available online 2 April 2025
2452-0748/© 2025 The Authors. Published by Elsevier B.V. This is an open access article under the CC BY license (http://creativecommons.org/licenses/by/4.0/).

and widely available energy source (solar irradiation) and achieve virtually complete degradation of the target pollutant. (Daghrir et al., 2012) Out of the known photocatalysts, titanium dioxide is the most widely employed catalytic agent, as it offers a non-toxic and affordable catalysis that does not originate catalyst by-products and is corrosion resistant. (Sendão et al., 2023a; Sendão et al., 2022) Due to its nature, photocatalysis is a method that can present an highly efficient conversion of light into chemical energy. Thus, it is often the focus of environmental remediation and pollutant removal studies. (Chen et al., 2016; Das et al., 2019; Sendão et al., 2023a).

Despite being widely used, TiO_2 also presents some limitations that must be addressed to permit a broader range of applications. Namely, TiO_2 presents a poor solar light harvesting capacity, as it is only capable of utilizing UV irradiation due to its large bandgap and consequent narrow photocatalytic region ($\lambda < 400$ nm). This is troublesome given that solar irradiation is comprised mainly of visible and NIR irradiation, with UV accounting for only ≈ 6 % of the whole solar spectrum, and thus, the outdoor application of TiO_2 using only clean and inexhaustible solar irradiation is prevented. (Barolet et al., 2016; Ren et al., 2007) Moreover, TiO_2 also suffers from rapid recombination of photogenerated charge carriers, resulting in the dissipation of absorbed energy and poor photonic efficiency. (Daghrir et al., 2012) Finally, the semiconductor's surface presents poor affinity toward organic compounds such as dyes and drugs, limiting the reaction rate as the target pollutants do not reach the active sites easily. (Dong et al., 2015).

One of the strategies that has been gaining attention for addressing TiO_2's limitations is to create nanocomposites between it and carbon dots (CDs). The latter are carbon-based nanoparticles, typically sized under 10 nm, that display several interesting properties, such as a broadband absorption range, high photoluminescence, water solubility and low toxicity. They are also inexpensive and easy to prepare from simple compounds. (Deng et al., 2021; Vale et al., 2021) As a result, they have been employed in applications covering several areas, such as sensing, (Simoes et al., 2020) photovoltaic devices (Zhang et al., 2013) and photocatalysis. (Saini et al., 2022; Zhou et al., 2023).

In this specific area of TiO_2-based photocatalysis, including CDs has been shown to enhance visible light absorption (the main component of sunlight) and the affinity toward organic pollutants by the resulting nanocomposite. (Gong et al., 2022) Given this, combining TiO_2 with CDs is a promising approach to develop visible-light-driven photocatalysts that take better advantage of sunlight and show enhanced photocatalytic activity. In fact, several studies have shown that adding CDs to TiO_2 leads to enhanced efficiency in applications as varied as hydrogen splitting, catalytic photoreduction of metals or the photodegradation of organic pollutants. (Aghamali et al., 2018; Ansón-Casaos et al., 2021; Choi et al., 2018; Gong et al., 2022; Sendão et al., 2023a; Wang et al., 2018).

Despite the overall success of TiO_2 as a photocatalyst and considering applications like the photodegradation of organic pollutants, we must also consider the environmental impacts associated with preparing the photocatalyst itself. To achieve this, one can perform Life Cycle Assessment (LCA) studies to determine the environmental impacts associated with the life cycle of a product or process. (Finnveden et al., 2009) Thus far, several LCA studies have been conducted regarding consumer products containing nanomaterials. (Karan and Chakraborty, 2022; Li et al., 2024; Zhang et al., 2024).

It should be highlighted that different studies concerning nanomaterials have identified their production as of environmental concern, with the required reagents and energy being relevant contributors toward the product's environmental impacts during its life cycle. (Garcia Gonzalez et al., 2022; Pourzahedi and Eckelman, 2015b; Tollefson, 2011) Given this, research efforts aimed at improving the photocatalytic performance of TiO_2 must be coupled with studies identifying the environmental impacts of the preparation of novel materials so cleaner fabrication approaches can be identified and devised.

Despite this, only a fraction of studies developing TiO_2-based nanoparticles include an evaluation of associated environmental impacts. (Caramazana-González et al., 2017; Fernandes et al., 2020; Grubb and Bakshi, 2011; Pesqueira et al., 2021; Pesqueira et al., 2024; Pini et al., 2015; Sendão et al., 2023a; Tsang et al., 2018) Knowledge about the environmental impacts of producing TiO_2/CDs nanocomposites is even scarcer (Sendão et al., 2023a). Furthermore, this type of photocatalytic nanocomposites is still at an early stage of development, and so, there are still aspects of the overall process that were not focused on and require study and optimization. (Farjadfar et al., 2022; Zhang et al., 2021) Namely, aspects such as solvent optimization, materials recovery, and waste management are major uncertainties that need to be addressed to reach a viable commercial development. The absence of information regarding such parameters consists of a limitation regarding LCA studies of this type of nanocomposites that must also be addressed in the future when the process is optimized. Thus, there is a need for a more in-depth understanding of the environmental impacts associated with this promising type of nanomaterials so that, ultimately, better-performing photocatalytic nanomaterials can be obtained with lower environmental impacts.

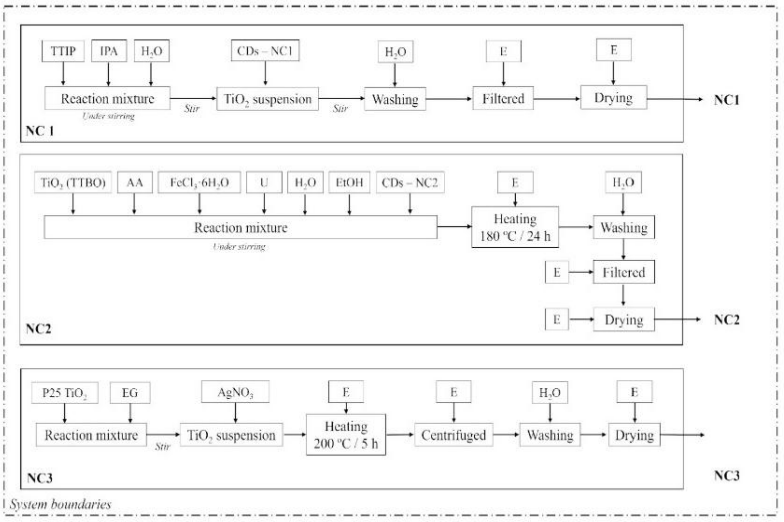
Herein, a "cradle-to-gate" LCA study was performed for the production of different TiO_2/CDs nanocomposites using three different CDs and production pathways, termed NC1 to NC3. These NCs were chosen due to displaying a significant enhancement of visible-light-driven photocatalytic activity, between 210 and 367 % over bare TiO_2, for the degradation of organic pollutants in water. (Sendão et al., 2023a; Wang et al., 2018; Zhang et al., 2019) Furthermore, these NCs were applied for the same pollutant, facilitating comparison between them, and the studies in which they were described provided all necessary data for performing an LCA study. NC1 is a nanocomposite previously prepared and reported by us, consisting of the conjugation of TiO_2 nanoparticles made from TTIP and CDs prepared from citric acid and ethylenediamine. (Sendão et al., 2023a) NC2 was reported by Zhang et al. and consists of a TiO_2/CDs/Fe_2O_3 nanocomposite. TiO_2 was obtained from titanium tetrabutoxide (TTBO), whereas the CDs were made from citric acid and ethylenediamine. (Zhang et al., 2019) Finally, NC3, prepared by Wang et al., consisted of the one-pot synthesis of TiO_2/CDs/Ag nanocomposites, using commercially available TiO_2, silver nitrate and ethylene glycol as the carbon source. (Wang et al., 2018) Based on these nanocomposites, the present study aims to compare synthetic methodologies and identify the major impact hotspots associated with each synthesis.

2. Methods

2.1. Nanocomposites synthesis procedure

This work is focused on the analysis of the environmental impact of three different nanocomposites published independently by different authors. (Sendão et al., 2023a; Wang et al., 2018; Zhang et al., 2019) To describe how each nanocomposite was synthesized, we provide the methods used by the authors, as reported by them in their respective works. These procedures were used as the basis from which we obtained the materials and energy consumed to produce the nanocomposites, as summarized in Fig. 1.

Regarding the methods used by the authors, NC1 was prepared via a sol-gel methodology. (Sendão et al., 2023a) First, the CDs were prepared via hydrothermal treatment from citric acid (0.15 g) and ethylenediamine (166.9 μL) dissolved in NaOH 0.01 M (10 mL). The reaction mixture was transferred into a Teflon-lined recipient in a stainless-steel outer shell and subjected to 200 °C for 24 h in an oven. After cooling to room temperature, the reaction products were centrifuged (6000 rpm, 30 min) and dialyzed (24 h, MWCO of 3.5 kDa) to remove possible by-products. Finally, the CDs were lyophilized, weighted and resuspended in deionized water to obtain a CDs solution of known concentration. Regarding the TiO_2/CDs nanocomposites, for an expected yield of 0.5 g of NC1, TTIP (1.855 mL) was added dropwise to isopropanol (11.975



Legend: TTIP – titanium isopropoxide; IPA – isopropyl alcohol; H_2O – deionized water; CDs – NC1 – CDs prepared previously for NC1; E – electricity; TiO_2 (TTBO) – TiO_2 nanoparticles prepared from titanium tetrabutoxide; AA – acetic acid; $FeCl_3 \cdot 6H_2O$ – iron chloride (III) hexahydrate; U – urea; EtOH – ethanol; CDs – NC2 – CDs prepared previously for NC2; P25 TiO_2 – commercially available P25 TiO_2 nanoparticles; EG – ethylene glycol; $AgNO_3$ – silver nitrate.

Fig. 1. Flowchart describing the system boundaries of the LCA study.

mL). The mixture was left stirring for 30 min, after which H_2O (11.25 mL) was added dropwise, followed by another 2 h of magnetic stirring. At the same time, the quantity of CDs solution equivalent to 0.01 g of nanoparticles (2 %) was diluted in H_2O (5 mL) and stirred at 70 °C for 90 min. The CDs were added to the TiO_2 nanoparticles suspension, followed by another 2 h of magnetic stirring. The final product was washed, vacuum-filtered and dried overnight. Finally, the dried nanocomposite was powdered and annealed at 300 °C for 3 h. (Sendão et al., 2023a).

NC2, reported by Zhang et al., started with the production of TiO_2 nanoparticles from TTBO and acetic acid. (Zhang et al., 2019) Briefly, 68 mL of TTBO was added to 50 mL of acetic acid, and the mixture was stirred for 30 min. Afterwards, it was transferred into a 200 mL Teflon-lined recipient and subjected to 100 °C for 12 h. The nanoparticles were then collected via centrifugation, washed, dried at 60 °C for 12 h and annealed in air at 450 °C for 2 h. By its turn, the CDs were hydrothermally-prepared (180 °C for 5 h) prepared from citric acid (6.3042 g) and ethylenediamine (2.01 mL) in deionized water (60 mL). After the reaction, the CDs were subjected to dialysis (3.5 kDa MWCO) and filtered. Finally, to prepare NC2, 2 g of previously prepared TiO_2 nanoparticles, 0.68 g of $FeCl_3 \cdot 6H_2O$ and 0.4 g of urea were dissolved in a mixture of 30 mL of ethanol and 70 mL of water. 10 mL of CDs solution was added to the mixture, which was kept at 40 °C for 1 h. The mixture was then inserted into a Teflon-lined autoclave and subjected to 180 °C for 24 h. Afterwards, it was washed, filtered, dried and stored until necessary. (Zhang et al., 2019)

Finally, NC3, prepared by Wang et al., was prepared via one-pot synthesis. (Wang et al., 2018) Briefly, 1 g of commercially available P25 TiO_2 nanoparticles was added to 25 mL of ethylene glycol. The mixture was stirred for 5 h until a homogeneous suspension was obtained. Then, 50 mg of silver nitrate were added to the mixture under stirring, after which the solution was transferred into a Teflon-lined autoclave and subjected to 200 °C for 5 h. The nanocomposite was collected via centrifugation, washed and dried overnight. (Wang et al., 2018) An overview of the inputs used to calculate the impacts associated with making 1 kg of NC1, NC2 and NC3 can be found on Table 1:

Table 1
Reference flows associated with the production of 1 kg of each nanocomposite.

Nanocomposite	Input
NC1	3.42 kg of TTIP
	18.07 kg of Isopropanol
	0.02 kg of CDs-NC1
	37.60 kg of Deionized Water
	2.67 kWh of electricity
NC2	0.51 kg of TiO_2 (from TTBO)
	0.16 kg of $FeCl_3$
	0.10 kg of Urea
	17.91 kg of Ethanol
	2.56 L of CDs NC2
	15.67 kWh
NC3	0.93 kg of TiO_2 (Commercial)
	25.82 kg of Ethylene Glycol
	0.05 kg of $AgNO_3$
	5.37 kWh of electricity

2.1.1. Scope and system boundaries

This cradle-to-gate LCA study was performed using the SimaPro 9.5.0.0 software and aims to compare the relative environmental impacts of preparing the three TiO_2/CDs-based nanocomposites considered in this study. This was done based on the reported synthesis process for the three target photocatalysts, considering the direct emissions and indirect impacts associated with the upstream resource extraction and energy generation. The production schemes for the nanocomposites were described in section 2.1.

In a first phase, the environmental impacts were analyzed and compared using a weight-based functional unit (FU) of 1 kg of produced material. As previously reported, using a weight or volume-based FU is useful to compare the manufacturing of an equivalent quantity of similar nanomaterials. (Feijoo et al., 2017; Hischier and Walser, 2012) The resulting impacts were normalized in a second phase by considering each photocatalysts' % ln (C) and k as function-based FUs. The former parameter measures the enhancement in photocatalytic activity over bare TiO_2 by adding CDs and is calculated according to Eq. 1 (Table 2). The latter parameter corresponds to the rate constant of the photodegradation reaction of target organic pollutants, as catalyzed by the NCs (Table 3). In short, k is a proportionality constant that quantifies the rate and direction of a chemical reaction. These were chosen as FUs, as

Table 2
% ln (C) and respective FU associated with NC1, NC2, and NC3.

Nanocomposite	% ln (C)	FU
NC1	367 %	1
NC2	366 %	1.003
NC3	210 %	1.748

Table 3
k and respective FU associated to NC1, NC2 and NC3.

Nanocomposite	k	FU
NC1	0.00934 min^{-1}	1.183
NC2	0.01105 min^{-1}	1
NC3	0.00200 min^{-1}	5.525

they are important indicators of the purpose for which the materials were made, thus accounting for the possibility that a higher functionality of the resulting material may justify a more resource and energy-intensive synthesis. Both function-based FUs were calculated by dividing the relevant property (% ln (C) or k) of the best-performing composite by those of the other composites. (Fernandes et al., 2020; Sendão et al., 2023a).

To make the comparison between NCs meaningful, when considering the function-based FUs, the considered % ln (C) and k should result from the same type of photocatalyzed reaction. For this study, we considered the visible-light-driven photodegradation reaction of the organic dye Methylene Blue (MB) in water, for which all NCs were previously employed. (Sendão et al., 2023a; Wang et al., 2018; Zhang et al., 2019) MB was chosen as a model pollutant due to the availability of different nanocomposites prepared toward its photodegradation and the fact that it is a widely used textile dye (among other applications), often found in the wastewater of this industry, and linked with several health and environmental problems. (Adegoke and Bello, 2015; Arias Arias et al., 2020; Sen et al., 2019).

Data concerning the k for NC1 and NC2 was obtained directly from their respective papers, whereas to obtain the data concerning NC3, we used the WebPlotDigitizer tool (https://automeris.io/wpd/?v=4_8), version 4.8, accessed on August 8th, 2024, from Porto, Portugal) to extract and quantify the relevant data points. The % ln (C) was calculated via the comparison of the reaction rate constant of each nanocomposite when compared to simple TiO_2, as shown below:

$$\%\ln(C) = 100\ x\ \frac{k_{NC} - k_{TiO_2}}{k_{TiO_2}} \quad (1)$$

2.1.2. Life cycle inventory (LCI)

The environmental impacts were evaluated using foreground data from the synthesis procedures described in section 2.1, while LCI data for the background system consisted of average data found in the Ecoinvent 3.9.1 database for isopropanol (Isopropanol [RER] | market for isopropanol | Cut-off, S), deionized water (Water, deionized, from tap water, at user [Europe without Switzerland] | market for water, deionized, from tap water, at user, Cut-off, S), electricity (Electricity, medium voltage [PT] | market for electricity, medium voltage | Cut-off, S), urea (Urea [RER] | market for urea | Cut-off, S), ethanol (Ethanol, without water, in 99.7 % solution state, from ethylene [RER] market for ethanol, without water, in 99.7 % solution state, from ethylene | Cut-off, S), iron (III) chloride (Iron (III) chloride, in 40 % solution state [GLO] | market for iron (III) chloride, in 40 % solution state | Cut-off, S), commercial titanium dioxide nanoparticles (Titanium dioxide [RER] | market for titanium dioxide | Cut-off, S), ethylene glycol (Ethylene glycol [GLO] | market for ethylene glycol | Cut-off, S) and glucose (Glucose [GLO] | market for glucose | Cut-off, S).

The processes for CDs-NC1 and CDs-NC2 were modelled considering the methodology reported by their authors (Sendão et al., 2023b; Zhang et al., 2019) and described in Section 2.1 (background data on Table S1). The process concerning TTIP was made considering the methodology found in ref. (Falbe et al., 2007) (background data in Table S1). Regarding the process of preparing TiO_2 nanoparticles from TTBO, the process was described in section 2.1, reported by (Zhang et al., 2019) and originated from the work of Jiang et al., (Jiang et al., 2008) with the method for the preparation of TTBO being obtained from (Caramazana-González et al., 2017) (background data in Table S1). Finally, the work of Pourzahedi and Eckelman (Pourzahedi and Eckelman, 2015a) provided us with the information necessary to create the process for silver nitrate (background data in Table S1).

For this study, whenever equipment was necessary and was of a common type across the studies, we considered that they had the same energy consumption. Namely, stages requiring heating were always considered to have a power requirement of 2500 W, independently of the nanocomposite. This was done to consider the fact that for the same task (*e. g.,* heating), the teams could have used different kinds of ovens with varying consumptions of power, thus affecting the environmental impact due to the equipment itself and not because one process was more impactful than the other if the same equipment was used. Additionally, the power consumption considered for the study was proportional to the capacity of the equipment used. This allows us to take into account that the equipment was not used to its full capacity due to the processes being done at a laboratory-scale. That is, the capacity for these equipment is not scaled to the amounts typically generated at the laboratory-scale (they can have more capacity than what is really needed). Finally, it is worth noting that, in this study, some steps common across all synthesis processes (e.g. 12 h drying stage in an oven) were omitted, given that the respective inputs would be similar. Thus, the comparative results were not affected.

2.1.3. Life cycle impact assessment (LCIA)

The LCA study was based on a cradle-to-gate approach, from raw material extraction to the fabrication of nanocomposites. Environmental impacts were modelled using the ReCiPe 2016 v1.1 LCIA endpoint method, Hierarchist Version, which evaluates the environmental impacts in three main categories of potential environmental impacts (endpoints): human health, ecosystems, and resources. Midpoint indicators were also evaluated: global warming (GW), stratospheric ozone depletion (SO), ionization radiation (IR), ozone formation – human health (OF), fine particulate matter formation (FPM), ozone formation – terrestrial ecosystems (OF-TE), terrestrial acidification (TA), freshwater eutrophication (FE), marine eutrophication (ME), terrestrial ecotoxicity (TET), freshwater ecotoxicity (FET), marine ecotoxicity (MET), human carcinogenic toxicity (HC), human non-carcinogenic toxicity (HNC), land use (LU), mineral resource scarcity (MR), fossil resource scarcity (FR), and water consumption (WC). Both midpoint and endpoint indicators were evaluated, as they provide different information on different aggregation levels. Namely, endpoint uses indicators at an higher level of impacts aggregation, while midpoint indicators are defined somewhere between the emission and the endpoint and are frequently based on a more robust modelling, thus providing more precise information regarding the respective impact categories. It is also worth noting that the Hierarchist model is commonly considered as the default model in scientific LCA studies (Chaurasiya and Singh, 2023; Diamanti et al., 2025) as it is based on the most common policy principles regarding time-frame and other issues, thus being the most suitable for our study.

2.2. Sensitivity analysis

Since the fabrication of photocatalytic TiO_2/CDs nanocomposites is still in the research and development stage, assessing the environmental impacts of their fabrication is still uncertain. Thus, we performed a sensitivity analysis to help determine such uncertainties for scale-up production (Kazemi et al., 2018). This was made by considering

"What-if" scenarios (Pianosi et al., 2016), achieved by varying the amount and type of materials used for the preparation of the CDs (± 30 % and using glucose as precursor instead, respectively), varying the electricity input (± 30 %) and altering the source of TiO_2 of NC1 and NC2 to the commercially available P25 TiO_2 used in NC3.

3. Results and discussion

To obtain a comprehensive understanding of the relative environmental impacts associated with the preparation of the nanocomposites, we must not only evaluate them from a synthesis-yield viewpoint (e.g. based on the production of 1 kg of catalyst) but also consider that differently prepared nanocomposites will probably present different catalytic efficiencies under a similar set of conditions. As such, in addition to studies employing a weight-based FU, we also did studies using FUs based on two different indicators of catalytic performance. For one, we employed an % ln (C)-based FU, which takes into consideration how much a given CDs enhance the photocatalytic activity of the respective NC over bare TiO_2. A k-based FU was also employed, which considers the different rate constants for the photodegradation of an organic pollutant (MB), under visible light irradiation, when catalyzed by the different NCs. Finally, a sensitivity analysis was conducted to evaluate the change in the environmental impacts under different sets of conditions posed by what-if scenarios.

3.1. Synthesis comparison by weight

We started our study by comparing the relative impacts of synthesizing 1 kg of photocatalytic NCs (weight-based FU). Herein, we aim to compare the contributions of each input in the process toward the different impact categories for each photocatalyst, thus identifying the environmental hotspots associated with each nanocomposite.

Analysis of the midpoint impact categories of NC1 (Fig. 2a, raw data available of Table S2) revealed that the highest contributors for most categories were TTIP and isopropanol, which are needed to prepare the TiO_2 nanoparticles to which the CDs are added. This is not surprising, as TiO_2 constitutes the vast majority of the material in NC1, with the CDs added in the synthesis stage as 2 % of mass equivalent to that of TiO_2. TTIP and isopropanol are responsible for at least 60 % of the impacts associated with all categories except for marine eutrophication. TTIP is of particular importance for the categories regarding freshwater eutrophication, freshwater ecotoxicity, marine ecotoxicity, and mineral resource scarcity (accounting for over 50 % of the impacts). In contrast, isopropanol is the most preponderant contributor toward global warming, terrestrial ecotoxicity, and fossil resource scarcity categories. As for the CDs, even though they amounted to only 2 % of the nanocomposites' mass, they still presented moderate impacts for most categories, except when regarding marine eutrophication, of which they are the highest contributors. The impacts associated with electricity and deionized water are negligible, with the latter only appearing for the water consumption category.

Regarding NC2 (Fig. 2b, raw data on Table S3), the source of TiO_2 (TTBO) is again responsible for at least 60 % of the resulting impacts for all categories except marine eutrophication, in which, again, the CDs are the most important input affecting the impacts. Impacts associated with CDs, ethanol, and electricity were found across all impact categories. CDs' biggest contribution was toward the marine eutrophication category, whereas ethanol and electricity's largest impacts were found in the categories of fossil resource scarcity and ionization radiation, respectively. The contributions of $FeCl_4$, deionized water, and urea were virtually negligible for all impact categories.

Finally, for NC3 (Fig. 2c, raw data on Table S4), unlike NC1 and NC2, we found that the largest contributor was not the TiO_2 source but ethylene glycol and $AgNO_3$. The drastic decrease in the impact associated with TiO_2 may result from the research team employing commercially available TiO_2 nanoparticles rather than fabricating their own

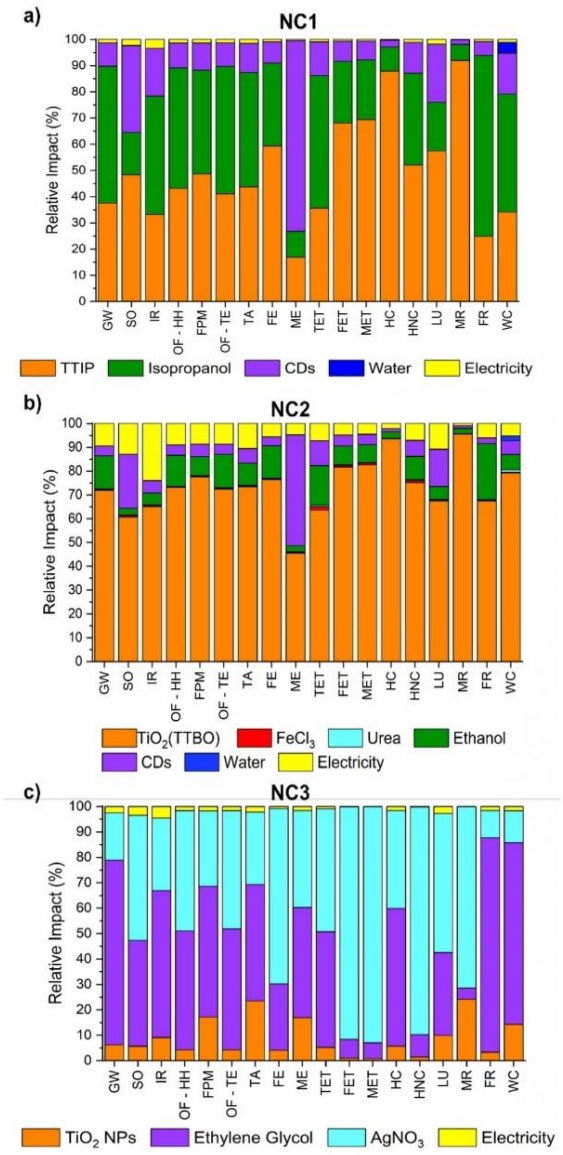


Fig. 2. Relative environmental impacts of the synthesis of 1 kg of: a) NC1, b) NC2, and c) NC3 with the ReCiPe 2016 LCIA, considering midpoint impact categories.

TiO_2. Ethylene glycol, the precursor used for the CDs, was found to be the major contributor to the categories of global warming, ionization radiation, human carcinogenic toxicity, fossil resource scarcity, and water consumption, whereas $AgNO_3$, used as the precursor for the silver dopant of NC3, affected freshwater eutrophication, freshwater ecotoxicity, marine ecotoxicity, human non-carcinogenic toxicity, land use, and mineral resource scarcity the most.

In summary, regarding midpoint impact categories for NC1 and NC2, the inputs associated with obtaining TiO_2 were responsible for most of the impacts for all categories (except marine eutrophication) by far, which is expected given the high amount of TiO_2 present in these nanocomposites. Similarly, in other reports concerning TiO_2 and TiO_2-composites, the source of TiO_2 was also the main contributor to most categories. Namely, Pesqueira et al. found that ammonium hexafluorotitanate was the major environmental hotspot in the preparation of graphene oxide – TiO_2 composites (Pesqueira et al., 2021), and Pini

et al. found that a significant portion of the impacts associated with the preparation of TiO_2 nanoparticles were a result of the organic precursors used in the synthesis. On the other hand, contrary to NC1 and NC2, the TiO_2-derived impacts of NC3 were limited. Instead, most of NC3's impacts resulted from the precursors for the CDs and the silver dopant, which were used in large quantities and had demanding requirements for their synthesis. Zuin et al. found similar results regarding the preparation of TiO_2 nanoparticles deposited on polyethersulfone membranes, for which the TiO_2 was a minor contributor toward all impact categories and the polymer responsible for over 70 % of all impacts. (Zuin et al., 2013)

The relative environmental impacts of the three nanocomposites are compared in Fig. 3, with the impact categories being divided into three main categories: human health, ecosystems, and resources. First and foremost, to produce the same mass of material, the relative environmental impact of NC3 is the largest for the human health and ecosystems categories and a very close second (96.5 % of those of NC1) in the resources category. This suggests that, overall, NC3 is the NC associated with the highest environmental impacts, likely due to using large quantities of ethylene glycol and silver nitrate, which are major inputs responsible for the impacts of NC3. On the other hand, the use of commercial TiO_2 led only to a small percentage of the impacts being associated with the semiconductor, differing from NC1 and NC2, which can attribute well over 60 % of its impacts in all categories (except for marine eutrophication) to the source of TiO_2. On the other hand, NC2 presented the lowest relative impacts for all three endpoint categories, indicating that its synthesis is associated with lower impacts (50.4 %, 62.3 %, and 66.1 % of those of the most impactful nanocomposite for the human health, ecosystems, and resources categories).

3.2. Synthesis comparison by % ln (C)

On a second stage, we again calculated the environmental impacts for endpoint categories of each nanocomposite. However, in this case, we considered a function-based FU based on the % ln (C) associated with the photodegradation of MB in water catalyzed by the nanocomposites. This FU was calculated by dividing the % ln (C) (calculated as shown in Eq. 1) of the best-performing nanocomposite by those of the alternatives, resulting in the FUs displayed in Table 2, which can be used to multiply the relative impacts of each photocatalyst based on how well they performed their intended function as measured by the % ln (C). This specific FU was chosen as it allows us to evaluate the enhancement of photocatalytic performance upon adding CDs to the TiO_2 nanoparticles over bare TiO_2 for each study. Thus, this section aims to assess if the enhancement in photocatalytic activity, originating from the addition of CDs, can offset environmental impacts that result from the synthesis stage.

The results revealed that, while NC3 is still the most impactful nanocomposite for the tested categories (Fig. 4), the scale of the discrepancy of its impacts when compared to NC1 and NC2 increased significantly. This is explained by the fact that, aside from having the most impactful synthesis based on the weight of produced nanocomposite, it also presented the lower % ln (C) (210 % versus 367 % and 366 % for NC1 and NC2, respectively). This resulted in a higher FU that furthers the difference in the relative impacts of each nanocomposite. Thus, it is no surprise that NC3 presents the highest endpoint environmental impacts out of the three nanocomposites. As for NC1 and NC2, because of their near-identical % ln (C) values, they present the same proportion of impacts observed with a weight-based FU, with NC2 presenting the lower relative impacts for all three endpoint categories closely followed by NC1. Once again, the impact associated with resources is considerably higher for NC1.

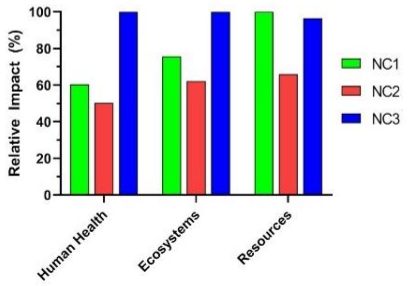


Fig. 3. Comparative environmental profiles for NC1, NC2 and NC3 obtained using the the ReCiPe 2016 v1.1 as LCIA and a weight-based FU of 1 kg of catalyst, when considering endpoint impact categories.

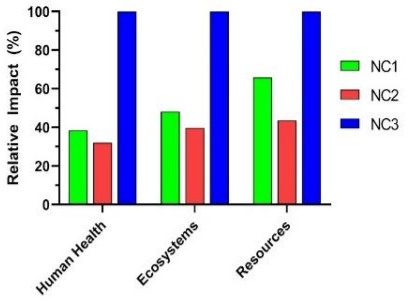


Fig. 4. Comparative endpoint impacts for NC1, NC2 and NC3 obtained using the the ReCiPe 2016 v1.1 as LCIA and a % ln (C)-based FU.

3.3. Synthesis comparison by k

Finally, we calculated the environmental impacts by considering an FU based on the k of the photodegradation of MB in water when catalyzed by the different NCs. k can be considered an absolute measurement of the efficiency of the studied photocatalytic reaction. This k-based FU was also considered because while % ln (C) measures the enhancement in performance of the specific NC over the corresponding bare TiO_2, it cannot show if the enhanced performance is significant when compared with other systems. That is, if the bare TiO_2 considered in a study has very poor catalytic performance, even significant enhancements might not lead to an overall efficient catalytic activity. To better assess this, k is the most relevant parameter. Like before, the FU was calculated by dividing the highest observed k out of the three nanocomposites by the respective k of each composite (Table 3).

The study revealed an even larger discrepancy between the impacts of NC3 and those of NC1 and NC2 (Fig. 5), deepening the effect already observed when using a % ln (C)-FU. This is because the proportional difference between k of the three nanocomposites (0.00200 min^{-1} versus 0.00934 min^{-1} and 0.01105 min^{-1} for NC1 and NC2, respectively) was considerably larger than the difference between their % ln

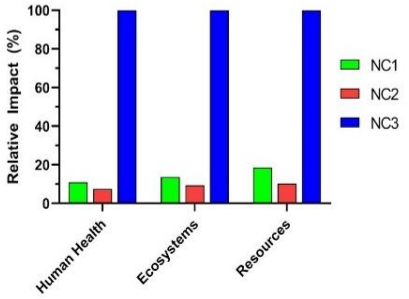


Fig. 5. Comparative environmental profiles for NC1, NC2 and NC3 obtained using the the ReCiPe 2016 v1.1 as LCIA and a k-based FU, when considering endpoint impact categories.

(C). This means that while NC3's % ln (C) - FU was 1.748, the FU when using the k as a reference was 5.525. This explains the larger difference found in the endpoint impacts of NC3 with this FU compared to the two previous studies. The relative impacts of NC1 and NC2 remain similar to what was previously observed, with NC1 presenting slightly higher relative impacts for the human health and ecosystems categories and considerably higher impacts in the resources category. This can be attributed to their respective k being somewhat close; thus, their respective FUs will be close and will not significantly alter the impact distribution.

3.4. Sensitivity analysis

A sensitivity analysis was performed with a focus on the functionality of the nanocomposites. Different scenarios were posed when considering k- and % ln (C)-based FUs. In each case, the scenarios included changing the input of the raw materials and electricity required for the making of the CDs by ±30 %, changing the identity of the carbon precursor used for the CDs (to glucose), and altering the source of TiO_2 of NC1 and NC2 to that of NC3 (commercially available TiO_2 nanoparticles).

Fig. 6a and b represent the results of the sensitivity evaluation regarding the variation of the inputs concerning the materials required

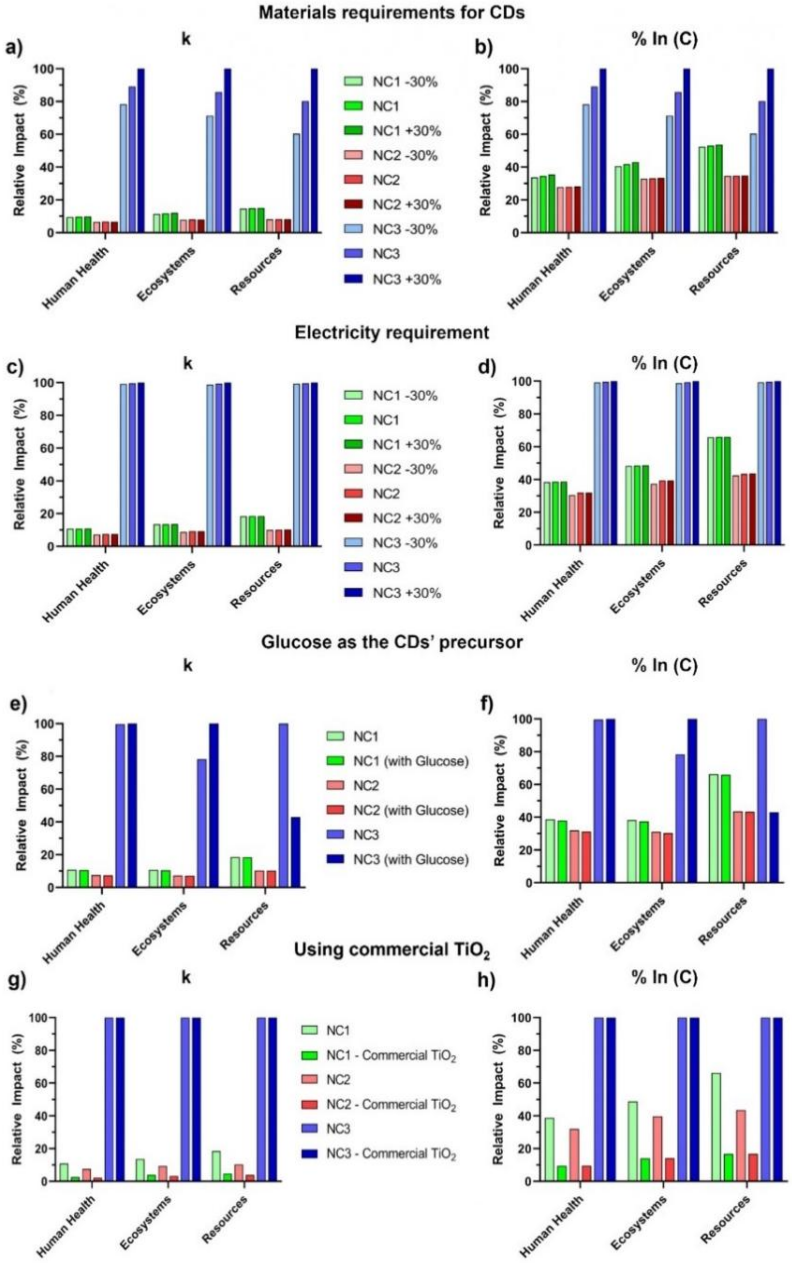


Fig. 6. Sensitivity analysis testing several "what-if" scenarios: ± 30 % materials requirement for CDs' synthesis for a) k- and b) % ln (C)-based FUs; ± 30 % electricity requirements for c) k- and d) % ln (C)-based FUs; replacing the precursors of the CDs by glucose for e) k- and f) % ln (C)-based FUs; and replacing the materials required to originate TiO_2 by the commercially available TiO_2 used in NC3 for g) k- and h) % ln (C)-based FUs.

for synthesizing the CDs. For both FUs, NC1 and NC2 display very little differences in impacts resulting from the 30 % variation. In fact, for NC1 and NC2 altogether, the biggest impact variation was found for NC1 in the human health category, varying less than 3 %, indicating that the synthesis of the respective CDs is irrelevant to the environmental impacts of the resulting nanocomposites. On the opposite hand, the resulting impacts of NC3 vary relevantly by altering the inputs by ±30 %, with the impacts associated with the human health, ecosystems and resources categories varying by ±11 %, ± 15 % and ± 20 %, respectively, for both FUs. This indicates that for NC3, the impact associated with the CDs can be significant, and small variations in this step will prompt relevant differences in the impacts.

As for electricity (Fig. 6c and d), altering its input did not significantly change the resulting environmental profile of any of the nanocomposites. This is not surprising when we consider that the contribution of electricity toward the midpoint impact categories was minimal for all three nanocomposites (Fig. 2).

Changing the CDs precursors to glucose (Fig. 6e and f) yields marginally smaller impacts, with decreases under 2 %, for NC1 and NC2, once again suggesting that the synthesis of the respective CDs is not of particular importance for the sustainability of these nanocomposites. As for NC3, substituting ethylene glycol for glucose led to a considerable decrease in the impacts in the categories of ecosystems and resources (22 % and 57 %, respectively).

Finally, the last "what-if" scenario tested the outcome of converting the source of TiO_2 of NC1 and NC2 to the commercial TiO_2 used in NC3 (Fig. 6g and h). Due to the nature of the sensitivity test, NC3 impacts did not change, as the TiO_2 source remains the same. On the other hand, NC1 and NC2 both presented significant changes in their environmental impacts, with their environmental impacts decreasing drastically with the change of TiO_2's source. Namely, the impacts of NC1 decreased by 75 %, 71 %, and 75 % for the human health, ecosystems, and resources categories, respectively, whereas the effects of NC2 decreased by 70 %, 65 %, and 62 %, respectively.

This reduction upon change of the TiO_2 source can be explained by the large amount of TiO_2 included in the composites and the much higher impact associated with the preparation of TiO_2 from TTIP and TTBO compared to commercially available TiO_2. In the employed version of Ecoinvent database, the input for commercially available TiO_2 considers a mix of 50 % TiO_2 prepared via the chloride method and 50 % via the sulfate method. By themselves, both methods result in significantly lower relative environmental impacts than preparing the semiconductor nanoparticles from TTIP or TTBO (Fig. S1). Preparation of TiO_2 from TTIP proved to be the most impactful for the category of resources, while TTBO led to the highest impacts on human health and ecosystems. The impacts of the sulfate and chloride method were never more than 12 % of those associated with the most impactful method for each category.

In summary, the most important factor affecting the environmental profile of the nanocomposites is the source of TiO_2. Thus, addressing this hotspot and correctly choosing the source of TiO_2 could severely improve the nanocomposites' environmental sustainability. Furthermore, in the case of NC3, where the prominence of the impacts derived from the CDs was larger, altering the amount and identity of the materials used for the CDs led to relevant changes in environmental impacts. So, addressing this could be useful for this specific nanocomposite. However, it is worth noting that the catalytic efficiency of a nanocomposite depends on its structure, which in turn is affected by the identity and ratio of the materials employed in its preparation. Thus, while the sensitivity evaluation demonstrated that the source of TiO_2 and the CDs are possible sensitive factors regarding the environmental impacts, further studies are recommended before varying the inputs and identity of the materials, as changing them will likely impact the catalytic efficiency of the resulting materials and may offset the expected environmental benefits.

4. Conclusion

This work provides a detailed LCA-based assessment of the environmental profiles of three different photocatalytic TiO_2/CDs nanocomposites (NC1, NC2, and NC3) prepared for the visible-light-driven photodegradation of MB. The studied nanocomposites include different synthetic strategies, CDs, sources of TiO_2, and catalytic efficiencies.

The analysis using a weight-based FU revealed that the nanocomposites with the highest photocatalytic activity were also those whose synthesis was associated with lower environmental impacts (NC2 and NC1). It was found that the main hotspot for the environmental impacts of those processes was the use of the chemical inputs needed to generate TiO_2. Interestingly, for NC1 and NC2, the addition of CDs was found to have little to moderate contributions in most impact categories, except for the marine eutrophication category (in which the contribution was significant).

The preparation of NC3 was found to be associated with the highest environmental impacts despite including the TiO_2 production process with the lowest impacts out of all 3 syntheses. However, the synthesis of NC3 included the addition of ethylene glycol and silver nitrate, which were the sources for CDs and Ag-doping, respectively. These inputs were found to have significant contributions to the environmental impacts of NC3, thereby helping to explain the worse environmental performance of its synthesis (compared to NC1 and NC2).

Different function-based FU were considered, but they did not lead to changes in conclusions over the analysis involving only a weight-based FU. A sensitivity analysis was also performed by considering several "what-if" scenarios. It was concluded that neither changes in electricity nor in the CDs led to significant changes in the relative impacts of the nanocomposites. On the contrary, the resulting impacts were quite sensitive to changes in the source of TiO_2.

In summary, it was demonstrated that CDs can be used to enhance the performance of TiO_2 without leading to significant environmental impacts during the synthesis step. Moreover, the generation of TiO_2 itself was found to be the critical step in the preparation of the nanocomposites, and so, it should become a focus of future studies regarding the cleaner production of nanocomposites with enhanced photocatalytic performance.

CRediT authorship contribution statement

Ricardo M.S. Sendão: Writing – original draft, Visualization, Investigation. **Joaquim C.G. Esteves da Silva:** Writing – review & editing, Supervision, Funding acquisition. **Luís Pinto da Silva:** Writing – review & editing, Supervision, Funding acquisition, Conceptualization.

Funding

This work was supported by the Portuguese "Fundação para a Ciência e Tecnologia" (FCT, Lisbon), who funded the project 2023.13127.PEX, R&D Units CIQUP (UIDB/00081/2020) and GreenUPorto (UIDB/05748/2020), and the Associated Laboratory IMS (LA/P/0056/2020). FCT is also acknowledged for funding Luís Pinto da Silva under the Scientific Employment Stimulus (CEECINST/00069/2021) and Ricardo Sendão on a Ph.D. grant (2021.06149.BD).

Declaration of competing interest

The authors declare that they have no known competing financial interests or personal relationships that could have appeared to influence the work reported in this paper.

Appendix A. Supplementary data

Supplementary data to this article can be found online at https://doi.

org/10.1016/j.impact.2025.100556.

Data availability

Data will be made available on request.

References

Adegoke, K.A., Bello, O.S., 2015. Dye sequestration using agricultural wastes as adsorbents. Water Resources Ind. 12, 8–24. https://doi.org/10.1016/j.wri.2015.09.002.

Aghamali, A., Khosravi, M., Hamishehkar, H., Modirshahla, N., Behnajady, M.A., 2018. Preparation of novel high performance recoverable and natural sunlight-driven nanocomposite photocatalyst of Fe3O4/C/TiO2/N-CQDs. Mater. Sci. Semicond. Process. 87, 142–154. https://doi.org/10.1016/j.mssp.2018.07.018.

Ansón-Casaos, A., Hernández-Ferrer, J., Vallan, L., Xie, H., Lira-Cantú, M., Benito, A.M., Maser, W.K., 2021. Functionalized carbon dots on TiO_2 for perovskite photovoltaics and stable photoanodes for water splitting. Int. J. Hydrog. Energy 46 (22), 12180–12191. https://doi.org/10.1016/j.ijhydene.2020.03.077.

Arellano-Cárdenas, S., López-Cortez, S., Cornejo-Mazón, M., Mares-Gutiérrez, J.C., 2013. Study of malachite green adsorption by organically modified clay using a batch method. Appl. Surf. Sci. 280, 74–78. https://doi.org/10.1016/j.apsusc.2013.04.097.

Arias Arias, F., Guevara, M., Tene, T., Angamarca, P., Molina, R., Valarezo, A., Salguero, O., Vacacela Gomez, C., Arias, M., Caputi, L.S., 2020. The adsorption of methylene blue on eco-friendly reduced graphene oxide. Nanomaterials (Basel) 10 (4). https://doi.org/10.3390/nano10040681.

Barolet, D., Christiaens, F., Hamblin, M.R., 2016. Infrared and skin: Friend or foe. J. Photochem. Photobiol. B 155, 78–85. https://doi.org/10.1016/j.jphotobiol.2015.12.014.

Caramazana-González, P., Dunne, P.W., Gimeno-Fabra, M., Zilka, M., Ticha, M., Stieberova, B., Freiberg, F., McKechnie, J., Lester, E.H., 2017. Assessing the life cycle environmental impacts of titania nanoparticle production by continuous flow solvo/hydrothermal syntheses. Green Chem. 19 (6), 1536–1547. https://doi.org/10.1039/c6gc03357a.

Chaurasiya, S., Singh, G., 2023. Life cycle assessment of nanocomposite manufactured using ultrasonic stir casting. J. Mater. Sci. 58 (12), 5298–5318. https://doi.org/10.1007/s10853-023-08363-0.

Chen, J., Shu, J., Anqi, Z., Juyuan, H., Yan, Z., Chen, J., 2016. Synthesis of carbon quantum dots/TiO2 nanocomposite for photo-degradation of Rhodamine B and cefradine. Diam. Relat. Mater. 70, 137–144. https://doi.org/10.1016/j.diamond.2016.10.023.

Choi, D., Ham, S., Jang, D.-J., 2018. Visible-light photocatalytic reduction of Cr(VI) via carbon quantum dots-decorated TiO_2 nanocomposites. J. Environ. Chem. Eng. 6 (1), 1–8. https://doi.org/10.1016/j.jece.2017.11.065.

Chowdhury, S., Mishra, R., Saha, P., Kushwaha, P., 2011. Adsorption thermodynamics, kinetics and isosteric heat of adsorption of malachite green onto chemically modified rice husk. Desalination 265 (1–3), 159–168. https://doi.org/10.1016/j.desal.2010.07.047.

Daghrir, R., Drogui, P., Robert, D., 2012. Photoelectrocatalytic technologies for environmental applications. J. Photochem. Photobiol. A Chem. 238, 41–52. https://doi.org/10.1016/j.jphotochem.2012.04.009.

Das, G.S., Shim, J.P., Bhatnagar, A., Tripathi, K.M., Kim, T., 2019. Biomass-derived carbon quantum dots for visible-light-induced photocatalysis and label-free detection of Fe(III) and ascorbic acid. Sci. Rep. 9 (1), 15084. https://doi.org/10.1038/s41598-019-49266-y.

Deng, Y., Chen, M., Chen, G., Zou, W., Zhao, Y., Zhang, H., Zhao, Q., 2021. Visible-ultraviolet upconversion carbon quantum dots for enhancement of the photocatalytic activity of titanium dioxide. ACS Omega 6 (6), 4247–4254. https://doi.org/10.1021/acsomega.0c05182.

Diamanti, M.V., Shinnur, M.V., Pedeferri, M., Ferrari, A.M., Rosa, R., Meroni, D., 2025. Toward sustainable photocatalysis: addressing deactivation and environmental impact of anodized and sol–gel photocatalysts. Adv. Sustain. Syst. https://doi.org/10.1002/adsu.202401017.

Dong, H., Zeng, G., Tang, L., Fan, C., Zhang, C., He, X., He, Y., 2015. An overview on limitations of TiO2 based particles for photocatalytic degradation of organic pollutants and the corresponding countermeasures. Water Res. 79, 128–146. https://doi.org/10.1016/j.watres.2015.04.038.

Falbe, J., Bahrmann, H., Lipps, W., Mayer, D., 2007. Ullmann's Encyclopedia of Industrial Chemistry. Wiley-VCH, Weinheim.

Farjadfar, S., Ghiaci, M., Kulinch, S.A., Wunderlich, W., 2022. Efficient photocatalyst for the degradation of cationic and anionic dyes prepared via modification of carbonized mesoporous TiO2 by encapsulation of carbon dots. Mater. Res. Bull. 155. https://doi.org/10.1016/j.materresbull.2022.111963.

Feijoo, S., González-García, S., Moldes-Diz, Y., Vazquez-Vazquez, C., Feijoo, G., Moreira, M.T., 2017. Comparative life cycle assessment of different synthesis routes of magnetic nanoparticles. J. Clean. Prod. 143, 528–538. https://doi.org/10.1016/j.jclepro.2016.12.079.

Fernandes, S., Esteves da Silva, J.C.G., Pinto da Silva, L., 2020. Life cycle assessment of the sustainability of enhancing the photodegradation activity of TiO(2) with metal-doping. Materials (Basel) 13 (7). https://doi.org/10.3390/ma13071487.

Finnveden, G., Hauschild, M.Z., Ekvall, T., Guinee, J., Heijungs, R., Hellweg, S., Koehler, A., Pennington, D., Suh, S., 2009. Recent developments in life cycle assessment. J. Environ. Manag. 91 (1), 1–21. https://doi.org/10.1016/j.jenvman.2009.06.018.

Garcia Gonzalez, M.N., Quiroga-Flores, R., Börjesson, P., 2022. Life cycle assessment of a nanomaterial-based adsorbent developed on lab scale for cadmium removal: comparison of the impacts of production, use and recycling. Clean. Environ. Syst. 4. https://doi.org/10.1016/j.cesys.2022.100071.

Gong, J., Guo, Y., Lu, J., Cheng, Y., Wang, H., 2022. TEMPO oxidized nanofiber carbon quantum dots/TiO_2 composites with enhanced photocatalytic activity for degradation of methylene blue. Chem. Phys. Lett. 788. https://doi.org/10.1016/j.cplett.2021.139297.

Grubb, G.F., Bakshi, B.R., 2011. Life cycle of titanium dioxide nanoparticle production. J. Ind. Ecol. 15 (1), 81–95. https://doi.org/10.1111/j.1530-9290.2010.00292.x.

Hischier, R., Walser, T., 2012. Life cycle assessment of engineered nanomaterials: state of the art and strategies to overcome existing gaps. Sci. Total Environ. 425, 271–282. https://doi.org/10.1016/j.scitotenv.2012.03.001.

Jiang, D., Xu, Y., Hou, B., Wu, D., Sun, Y., 2008. A simple non-aqueous route to anatase TiO_2. Eur. J. Inorg. Chem. 2008 (8), 1236–1240. https://doi.org/10.1002/ejic.200700650.

Karan, P., Chakraborty, R., 2022. E-waste derived silica-alumina for eco-friendly and inexpensive Mg-Al-Ti photocatalyst towards glycerol carbonate (electrolyte) synthesis: process optimization and LCA. Waste Manag. 140, 213–224. https://doi.org/10.1016/j.wasman.2021.11.022.

Kazemi, A., Bahramifar, N., Heydari, A., Olsen, S.I., 2018. Life cycle assessment of nanoadsorbents at early stage technological development. J. Clean. Prod. 174, 527–537. https://doi.org/10.1016/j.jclepro.2017.10.245.

Konstantinou, I.K., Albanis, T.A., 2004. TiO_2-assisted photocatalytic degradation of azo dyes in aqueous solution: kinetic and mechanistic investigations. Appl. Catal. B 49 (1), 1–14. https://doi.org/10.1016/j.apcatb.2003.11.010.

Li, Q., Vogt, M.R., Wang, H., Monticelli, C., Zanelli, A., 2024. Life cycle assessment of roll-to-roll produced chemical vapor deposition graphene transparent electrodes towards copper foil recycling. J. Clean. Prod. 468. https://doi.org/10.1016/j.jclepro.2024.143068.

Mekonnen, M.M., Hoekstra, A.Y., 2016. Four billion people facing severe water scarcity. Sci. Adv. 2 (2), e1500323. https://doi.org/10.1126/sciadv.1500323.

Pesqueira, J., Pereira, M.F.R., Silva, A.M.T., 2021. A life cycle assessment of solar-based treatments H_2O_2, TiO_2 photocatalysis, circumneutral photo-(Fenton) for the removal of organic micropollutants. Sci. Total Environ. 761, 143258. https://doi.org/10.1016/j.scitotenv.2020.143258.

Pesqueira, J.F.J.R., Pereira, M.F.R., Silva, A.M.T., 2024. Carbon-based composites in advanced wastewater treatment: a life cycle assessment of TiO2 and GO-TiO2 solar photocatalysis. J. Clean. Prod. 444. https://doi.org/10.1016/j.jclepro.2024.140845.

Pianosi, F., Beven, K., Freer, J., Hall, J.W., Rougier, J., Stephenson, D.B., Wagener, T., 2016. Sensitivity analysis of environmental models: a systematic review with practical workflow. Environ. Model Softw. 79, 214–232. https://doi.org/10.1016/j.envsoft.2016.02.008.

Pimentel, D., Berger, B., Filiberto, D., Newton, M., Wolfe, B., Karabinakis, E., Clark, S., Poon, E., Abbett, E., Nandagopal, S., 2004. Water resources: agricultural and environmental issues. BioScience 54 (10). https://doi.org/10.1641/0006-3568(2004)054[0909:Wraaei]2.0.Co;2.

Pini, M., Rosa, R., Neri, P., Bondioli, F., Ferrari, A.M., 2015. Environmental assessment of a bottom-up hydrolytic synthesis of TiO2 nanoparticles. Green Chem. 17 (1), 518–531. https://doi.org/10.1039/c4gc00919c.

Pourzahedi, L., Eckelman, M.J., 2015a. Comparative life cycle assessment of silver nanoparticle synthesis routes. Environ. Sci. Nano 2 (4), 361–369. https://doi.org/10.1039/c5en00075k.

Pourzahedi, L., Eckelman, M.J., 2015b. Environmental life cycle assessment of nanosilver-enabled bandages. Environ. Sci. Technol. 49 (1), 361–368. https://doi.org/10.1021/es504655y.

Ren, W., Ai, Z., Jia, F., Zhang, L., Fan, X., Zou, Z., 2007. Low temperature preparation and visible light photocatalytic activity of mesoporous carbon-doped crystalline TiO2. Appl. Catal. B Environ. 69 (3–4), 138–144. https://doi.org/10.1016/j.apcatb.2006.06.015.

Saini, D., Garg, A.K., Dalal, C., Anand, S.R., Sonkar, S.K., Sonker, A.K., Westman, G., 2022. Visible-light-promoted photocatalytic applications of carbon dots: a review. ACS Appl. Nano Mater. 5 (3), 3087–3109. https://doi.org/10.1021/acsanm.1c04142.

Sen, S.K., Patra, P., Das, C.R., Raut, S., Raut, S., 2019. Pilot-scale evaluation of bio-decolorization and biodegradation of reactive textile wastewater: an impact on its use in irrigation of wheat crop. Water Resources Ind. 21. https://doi.org/10.1016/j.wri.2019.100106.

Sendão, R.M.S., Esteves da Silva, J.C.G., Pinto da Silva, L., 2022. Photocatalytic removal of pharmaceutical water pollutants by TiO2 - carbon dots nanocomposites: a review. Chemosphere 301, 134731. https://doi.org/10.1016/j.chemosphere.2022.134731.

Sendão, R.M.S., Algarra, M., Ribeiro, E., Pereira, M., Gil, A., Vale, N., Esteves da Silva, J.C.G., Pinto da Silva, L., 2023a. Carbon dots–TiO_2 nanocomposites for the enhanced visible-light driven photodegradation of methylene blue. Adv. Sustain. Syst. https://doi.org/10.1002/adsu.202300317.

Sendão, R.M.S., Esteves da Silva, J.C.G., Pinto da Silva, L., 2023b. Applications of fluorescent carbon dots as photocatalysts: a review. Catalysts 13 (1). https://doi.org/10.3390/catal13010179.

Simoes, E.F.C., da Silva, L.P., da Silva, J., Leitao, J.M.M., 2020. Hypochlorite fluorescence sensing by phenylboronic acid-alizarin adduct based carbon dots. Talanta 208, 120447. https://doi.org/10.1016/j.talanta.2019.120447.

Tollefson, J., 2011. How green is my future? Nature 473 (7346), 134–135. https://doi.org/10.1038/473134a.

Tsang, M.P., Philippot, G., Aymonier, C., Sonnemann, G., 2018. Supercritical fluid flow synthesis to support sustainable production of engineered nanomaterials: case study

of titanium dioxide. ACS Sustain. Chem. Eng. 6 (4), 5142–5151. https://doi.org/10.1021/acssuschemeng.7b04800.

Vale, N., Silva, S., Duarte, D., Crista, D.M.A., Pinto da Silva, L., Esteves da Silva, J.C.G., 2021. Normal breast epithelial MCF-10A cells to evaluate the safety of carbon dots. RSC Med. Chem. 12 (2), 245–253. https://doi.org/10.1039/d0md00317d.

Wang, C., Yang, K., Wei, X., Ding, S., Tian, F., Li, F., 2018. One-pot solvothermal synthesis of carbon dots/Ag nanoparticles/TiO_2 nanocomposites with enhanced photocatalytic performance. Ceram. Int. 44 (18), 22481–22488. https://doi.org/10.1016/j.ceramint.2018.09.017.

Zhang, Y.-Q., Ma, D.-K., Zhang, Y.-G., Chen, W., Huang, S.-M., 2013. N-doped carbon quantum dots for TiO2 based photocatalysts and dye-sensitized solar cells. Nano Energy 2 (5), 545–552. https://doi.org/10.1016/j.nanoen.2013.07.010.

Zhang, J., Kuang, M., Wang, J., Liu, R., Xie, S., Ji, Z., 2019. Fabrication of carbon quantum dots/TiO_2/Fe_2O_3 composites and enhancement of photocatalytic activity under visible light. Chem. Phys. Lett. 730, 391–398. https://doi.org/10.1016/j.cplett.2019.06.011.

Zhang, Z., Yi, G., Li, P., Zhang, X., Fan, H., Wang, X., Zhang, C., Zhang, Y., Sun, Q., 2021. Construction of N doped carbon dots/macroporous TiO2 composites (N-CDs/m-TiO2) with dramatically enhanced photocatalytic activity. Ind. Eng. Chem. Res. 60 (32), 11954–11963. https://doi.org/10.1021/acs.iecr.1c02081.

Zhang, S., Gan, J., Lv, J., Shen, C., Xu, C., Li, F., 2024. Environmental impacts of carbon fiber production and decarbonization performance in wind turbine blades. J. Environ. Manag. 351, 119893. https://doi.org/10.1016/j.jenvman.2023.119893.

Zhou, H., Zhang, B., Jiang, Z., Zhao, H., Zhang, Y., 2023. Room-temperature synthesis of carbon dot/TiO_2 composites with high photocatalytic activity. Langmuir 39 (20), 7184–7191. https://doi.org/10.1021/acs.langmuir.3c00652.

Zuin, S., Scanferla, P., Brunelli, A., Marcomini, A., Wong, J.E., Wennekes, W., Genné, I., 2013. Layer-by-layer deposition of titanium dioxide nanoparticles on polymeric membranes: a life cycle assessment study. Ind. Eng. Chem. Res. 52 (39), 13979–13990. https://doi.org/10.1021/ie302979d.

2.3.2. Supplementary information

Comparative Life Cycle Assessment of the Fabrication of Visible-Light-Driven Photocatalytic TiO_2 – Carbon Dots Nanocomposites for Wastewater Treatment

Ricardo M. S. Sendão[1], Joaquim C. G. Esteves da Silva[1,2], Luís Pinto da Silva[1,2,*]

[1] Chemistry Research Unit (CIQUP), Institute of Molecular Sciences (IMS), Department of Geosciences, Environment and Territorial Planning, Faculty of Sciences, University of Porto, Rua do Campo Alegre s/n, 4169-007 Porto, Portugal
[2] LACOMEPHI, GreenUPorto, Department of Geosciences, Environment and Territorial Planning, Faculty of Sciences, University of Porto, Rua do Campo Alegre s/n, 4169- 007 Porto, Portugal
* luis.silva@fc.up.pt

Table S1 - Summary of Ecoinvent® background data used to create the additional processes not available on the database.

Process	Background data
CDs-NC1	Citric acid [GLO] | market for citric acid | Cut-off, S
	Ethylenediamine [RER] | market for ethylenediamine | Cut-off, S
	Sodium hydroxide, without water, in 50% solution state [GLO] | market for sodium hydroxide, without water, in 50% solution state | Cut-off, S
	Water, deionized, from tap water, at user [Europe without Switzerland] | market for water, deionized, from tap water, at user | Cut-off, S
	Electricity, medium voltage [PT] | market for | Cut-off, S
CDs-NC2	Citric acid [GLO] | market for citric acid | Cut-off, S
	Ethylenediamine [RER] | market for ethylenediamine | Cut-off, S
	Water, deionized, from tap water, at user [Europe without Switzerland] | market for water, deionized, from tap water, at user | Cut-off, S
	Electricity, medium voltage [PT] | market for | Cut-off, S
TTIP	Ammonia, liquid [RER] | market for ammonia | Cut-off, S
	Isopropanol [RER] | production | Cut-off, S
	Titanium tetrachloride [GLO] | production | Cut-off, S
	Transport, freight train [RER] | market group for transport, freight train | Cut-off, S
	Transport, freight, lorry 16-32 metric ton, EURO3 [RER] | transport, freight, lorry 16-32 metric ton, EURO3 | Cut-off, S
	Electricity, medium voltage [RER] | market group for | Cut-off, S
TiO_2 nanoparticles from TTBO	TTBO (process modeled by us)
	Acetic acid, without water, in 98% solution state [GLO] | market for acetic acid, without water, in 98% solution state, Cut-off, S
	Electricity, medium voltage [PT] | market for | Cut-off, S
TTBO	Titanium tetrachloride [GLO] | market for titanium tetrachloride | Cut-off, S

	Ammonia, liquid [RER] | market for ammonia | Cut-off, S
	Benzene [GLO] | market for benzene | Cut-off, S
	1-butanol [GLO] | market for 1-butanol | Cut-off, S
	Natural gas, high pressure [Europe without Switzerland] | market group for natural gas, high pressure | Cut-off, S
Silver nitrate	Nitric acid, without water, in 50% solution state [RER without UK] | market for nitric acid, without water, in 50% solution state | Cut-off, S
	Silver [GLO] | market for silver | Cut-off, S

Table S2 – Raw data concerning the relative midpoint impacts associated with the production of 1 kg of NC1.

Impact Cat.	*Unit*	*TTIP*	*Isopropanol*	*CDs – NC1*	*Water*	*Electricity*
GW	%	37.559	52.165	8.968	0.024	1.284
SO	%	48.326	16.129	33.175	0.091	2.280
IR	%	33.220	45.165	18.239	0.050	3.327
OF - HH	%	43.226	45.854	9.532	0.024	1.364
FPM	%	48.707	39.514	10.399	0.052	1.328
OF - TE	%	41.063	48.638	8.988	0.022	1.289
TA	%	43.763	43.676	11.044	0.051	1.466
FE	%	59.380	31.571	8.079	0.028	0.942
ME	%	16.870	9.922	72.682	0.018	0.508
TET	%	35.625	50.536	12.896	0.064	0.879
FET	%	68.146	23.561	7.567	0.032	0.694
MET	%	69.390	22.792	7.136	0.031	0.652
HC	%	87.892	9.162	2.614	0.015	0.316
HNC	%	52.106	34.964	11.784	0.053	1.092
LU	%	57.514	18.463	22.187	0.023	1.813
MR	%	91.964	6.133	1.755	0.011	0.136
FR	%	24.857	68.991	5.371	0.012	0.769
WC	%	32.052	44.515	16.732	5.427	1.273

Table S3 – Raw data concerning the relative midpoint impacts associated with the production of 1 kg of NC2.

Impact Cat.	*Unit*	*TiO_2 (TTBO)*	*$FeCl_3$*	*Urea*	*Ethanol*	*CDs - NC2*	*Water*	*Electricity*
GW	%	71.979	0.263	0.271	13.867	4.179	0.015	9.427
SO	%	60.745	0.705	0.145	2.774	22.699	0.043	12.888
IR	%	65.057	0.499	0.232	4.997	5.239	0.030	23.944
OF - HH	%	73.099	0.331	0.197	13.022	4.356	0.013	8.982
FPM	%	77.549	0.422	0.149	7.979	5.230	0.028	8.642
OF - TE	%	72.440	0.315	0.204	14.120	4.187	0.013	8.721
TA	%	73.464	0.338	0.198	9.391	6.004	0.031	10.575
FE	%	76.510	0.364	0.106	13.658	3.699	0.014	5.649
ME	%	45.554	0.280	0.275	2.556	46.546	0.014	4.775
TET	%	63.596	1.435	0.553	16.686	10.487	0.045	7.198

FET	%	81.707	0.721	0.235	7.891	4.546	0.019	4.881
MET	%	82.676	0.683	0.225	7.527	4.285	0.018	4.585
HC	%	93.514	0.194	0.081	2.761	1.261	0.009	2.180
HNC	%	75.227	0.891	0.278	9.793	6.701	0.029	7.080
LU	%	67.504	0.362	0.148	5.520	15.643	0.012	10.810
MR	%	95.507	0.189	0.082	2.133	1.118	0.007	0.964
FR	%	67.508	0.141	0.290	23.667	2.328	0.008	6.059
WC	%	79.266	0.308	0.991	6.437	5.805	1.979	5.214

Table S4 – Raw data concerning the relative midpoint impacts associated with the production of 1 kg of NC3.

Impact Cat.	*Unit*	*TiO_2 - Commercial*	*Ethylene Glycol*	*$AgNO_3$*	*Electricity*
GW	%	6.207	72.693	18.632	2.468
SO	%	5.656	41.681	49.200	3.464
IR	%	9.117	57.769	28.581	4.533
OF - HH	%	4.270	46.735	47.365	1.629
FPM	%	17.213	51.375	29.685	1.727
OF - TE	%	4.276	47.570	46.516	1.638
TA	%	23.514	45.776	28.544	2.165
FE	%	4.086	26.109	69.038	0.767
ME	%	16.899	43.358	38.156	1.587
TET	%	5.200	45.546	48.374	0.880
FET	%	0.977	7.413	91.433	0.177
MET	%	0.838	6.191	92.826	0.145
HC	%	5.669	54.201	38.546	1.584
HNC	%	1.424	8.795	89.573	0.209
LU	%	9.929	32.606	54.738	2.727
MR	%	24.155	4.392	71.370	0.084
FR	%	3.308	84.374	10.728	1.590
WC	%	14.300	71.458	12.539	1.703

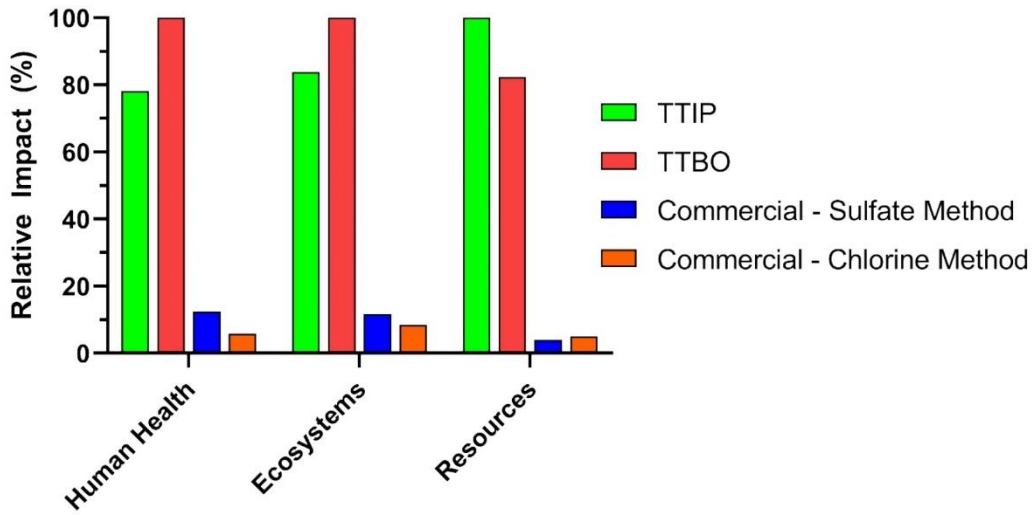


Figure S1 – Endpoint impact profiles of 4 different methods for the preparation of TiO_2.

2.3.3. Conclusion

This work studies the environmental profiles of three different photocatalytic TiO_2/CDs nanocomposites prepared for the visible-light-driven photodegradation of MB, which were prepared using different synthetic strategies, CDs, and sources of TiO_2, and presented different catalytic efficiencies. This study highlights that the environmental sustainability of TiO_2/CDs nanocomposites can be significantly improved through the careful selection of raw materials, particularly the sources of TiO_2 and the carbon precursors for CDs, while other factors, such as the electricity used, have a very low impact on the outcome.

During the LCA studies, using either weight-based or function-based FUs led to the same outcome. Namely, we observed that synthesizing TiO_2 from precursors such as TTIP and TTBO led to large environmental impacts, whereas using commercially available TiO_2 markedly reduced those burdens, given that the synthesis process via the chloride and sulphate methods is already optimized for yield and requires the least possible amount of raw materials. Secondly, although the CDs account for a smaller fraction of the total environmental impact, their contribution becomes more significant when synthesized from precursors like ethylene glycol and silver nitrate, leading to a larger environmental footprint. Substituting these commercial reagents with biomass-derived alternatives, such as corn stover, can further reduce environmental impacts, given that they replace artificial chemicals and that their environmental burdens are already accounted for in the life cycle of other products. This way, we reduce the environmental impacts associated with the materials used while promoting a circular economy that creates added value from otherwise discarded waste.

In summary, considering the good photocatalytic efficiency described in sections 2.1.2. and 2.2.1. and the LCA studies reported in section 2.3.1., the incorporation of biomass such as corn stover, if done properly, offers a promising path toward the development of high-performance, low-impact photocatalysts for sustainable wastewater treatment applications.

3. Conclusion and future perspectives

3.1. Development of visible-light-active photocatalytic nanocomposites

The main objective of this doctoral project was to develop an efficient sunlight-driven photocatalyst for the photodegradation of antibiotics in aqueous media. Water is essential for humanity, and thus, its contamination by organic pollutants is troublesome and must be addressed. However, conventional treatment methods are inefficient of removing these classes of pollutants, and alternatives must be developed. Even though photocatalysis using semiconductors such as TiO_2 is a very promising alternative, it poses several challenges that prevent its effective use under solar irradiation. Namely, TiO_2 requires high-energy UV radiation (only around 5% of the solar spectrum), has a poor photonic efficiency, and a low affinity toward organic compounds.

Given this, my work consisted of employing CDs to bridge the limitations posed by TiO_2 by preparing visible-light-active photocatalytic nanocomposites. CDs, because of their unique structure and properties, can extend the nanocomposites' absorption into the visible range, improve the separation of photogenerated charge carriers, and provide a suitable surface for interaction with organic compounds.

In the first stage of the project, we developed NC_{100}, made from TiO_2 nanoparticles and CDs from CA and EDA prepared via hydrothermal treatment. The resulting NC_{100} has a considerably higher photocatalytic efficiency over bare TiO_2. Namely, an enhancement of 367% was observed regarding the visible-light-driven photodegradation of MB (used as a model pollutant). Characterization via UV-Vis DRS and fluorescence spectroscopy suggests that this may be attributed to a higher uptake of light in the visible range and an improved separation of the photogenerated charge carriers. Furthermore, mechanistic studies revealed that, upon adding the CDs, there is a shift in the dominant reactive species behind the photodegradation, suggesting that carbon nanoparticles influence not only the resulting properties of NC_{100} but also the photocatalytic mechanism. Finally, LCA studies demonstrated that NC_{100} is a better alternative than TiO_2 when considering a function-based functional unit, as its environmental impacts are offset by a higher photocatalytic performance.

NC_{100} was followed by the development of $NC_{50:50}$, a similarly prepared nanocomposite in which the CDs synthesis was altered to incorporate corn stover, an organic residue of the corn industry, as a co-carbon precursor. Even though we now substituted some of the chemical grade commercial reagents with biomass, $NC_{50:50}$ still displayed, when compared to NC_{100}, a slightly better absorption in the visible range,

better photonic efficiency, and a slightly larger enhancement of the catalytic performance over TiO_2 (374% versus 367% for NC_{100}). Therefore, by incorporating corn stover, we not only create something of value from an otherwise discarded product and promote a circular economy, but we also achieve this while maintaining, and even slightly increasing, the photocatalytic performance of our nanocomposites. Moreover, LCA studies confirmed that $NC_{50:50}$ had lower environmental impacts, both when considering weight or function-based FUs. The smaller impact when using a weight-based FU is a result of avoiding the impacts associated with the production of the CA that would otherwise be required as the solar carbon source, whereas the higher performance of $NC_{50:50}$ further reduce its relative impacts when compared to NC_{100} and TiO_2, showcasing the potential of this being a viable strategy to upcycle organic waste into high-performance, sustainable photocatalysts.

Overall, these findings confirm that the conjugation of TiO_2 with biomass-derived CDs may be an effective approach to improve the visible-light responsiveness, and consequently the solar-light activity, of TiO_2. This strategy provides a basis for the development of environmentally sustainable nanocomposites for the efficient removal of organic pollutants in wastewater treatment applications.

3.2. Sunlight-driven photodegradation of ciprofloxacin

The widespread presence of antibiotics in wastewater is a result of human activity and, if left unchecked, may be hazardous both to human health and the environment. CIP is specifically relevant, as it is a representative of the fluoroquinolone family, a group of broad-spectrum antibiotics that contributes to the development of multidrug-resistant strains of both Gram-positive and Gram-negative bacteria. Given that quinolones were, in the recent past, the class of antibiotics most frequently prescribed to adults, they can be found in high concentrations in wastewater and have already been detected in wastewater treatment plants. Because of this widespread use, treatment guidelines frequently recommend the use of this type of antibiotic for less severe infections to delay the development of drug-resistant bacteria.

Because of the importance of CIP, developing a method that allows its efficient removal from wastewater is highly relevant, as common treatment methods are ineffective. To pursue this, the main objective of the doctoral project was to develop a highly efficient sunlight-driven photocatalyst for the photodegradation of CIP. After testing $NC_{50:50}$ toward the visible-light-driven photodegradation of organic dyes, we

tested it regarding the photodegradation of CIP under solar irradiation. Under simulated solar irradiation, $NC_{50:50}$ achieved a virtually complete removal of 20 ppm of CP within 20 minutes of irradiation and a rate constant (0.2372 min^{-1}), corresponding to a 217% increase of the photocatalytic efficiency over TiO_2. Although some intermediate by-products were initially detected, they were fully degraded over the course of the reaction. Furthermore, when tested under natural sunlight, $NC_{50:50}$ remained highly effective, achieving a full removal of CIP within 30 minutes of direct sunlight Irradiation, regardless of temperature and sky conditions, with only UV intensity influencing the degradation rate.

It is our opinion that this research validates the conjugation of TiO_2 with biomass-derived CDs as an effective strategy for achieving sustainable and efficient photodegradation of key contaminants like CIP under solar irradiation. The use of corn stover as a co-carbon precursor for CD synthesis not only upcycles an agricultural residue but also allows for a high catalytic efficiency. This confirms the potential of biomass-derived CDs to overcome the inherent limitations of TiO_2, offering an environmentally conscious approach to the development of sustainable nanocomposites for solar-driven wastewater treatment.

3.3. Life Cycle Assessment studies of photocatalytic TiO_2/CDs nanocomposites

The final experimental section of the thesis consists of a comprehensive LCA study of the impacts associated with three different TiO_2/CDs nanocomposites prepared for the visible-light-driven degradation of MB. The aim of this research was to fill the void of verified data regarding the environmental impacts associated with the development and fabrication of this type of early-stage nanomaterials.

The data obtained from the LCA studies revealed that, as expected, nanocomposites exhibiting the highest photocatalytic activity also presented the lowest environmental impacts when using a function-based functional unit. Among the various parameters analysed, the most influential factors contributing to the overall environmental footprint of the nanocomposites were the origin of the TiO_2 used and the nature of the CDs precursors. Namely, substituting the TiO_2 source with commercially available TiO_2 (for which the production processes were already optimized) and the CDs' conventional chemical precursors with biomass-derived sources, such as corn stover,

led to a marked reduction in environmental impacts associated with the synthesis of the CDs and, consequently, the nanocomposites. This finding highlights the importance of material sourcing in the sustainable design of nanocomposites and highlights the potential of integrating organic waste residues to produce high-performance photocatalysts with a lower ecological burden.

3.4. Future works

The work developed within this thesis highlights the potential of employing biomass-incorporating CDs to bridge TiO_2's limitations and improve the photocatalytic efficiency of the resulting nanocomposites. However, some work remains that could further add value to this research.

First, we still need to evaluate the performance of $NC_{50:50}$ using real wastewater samples, as opposed to model solutions. While initial results using MB and CIP have demonstrated high photocatalytic efficiency under both visible and solar irradiation, real wastewater samples contain a complex mixture of organic and inorganic contaminants, competing ions, and varying pH and turbidity levels that could affect the catalytic efficiency.

Additionally, efforts will be directed toward improving the recovery and reusability of the nanocomposite after treatment. This is crucial to advance the material development toward scalable, cost-effective, and environmentally responsible implementation in real-world wastewater treatment systems. A possible approach may be to embed the active materials onto solid supports such as cork. Namely, we expect that fixing the nanocomposite onto a cork foundation would provide an easier way of recovering the catalyst after use. Cork, given its porosity and buoyancy, is an ideal substrate as its properties ensure that the catalyst is fixed to a support that will always be near the top of the wastewater sample, ensuring that $NC_{50:50}$ would receive the maximum possible amount of irradiation, and thus, be more efficient.

Finally, concerning CDs, their unique properties and structure, low toxicity, and tunability will always provide a way to develop them into new applications. As an example, regarding water treatment, CDs can be used to sense pollutants, adsorb contaminants, act as antimicrobial agents, or directly remove pollutants via catalysis. Future research may explore the integration of CDs into hybrid filtration membranes, smart sensors for real-time water quality monitoring, or multifunctional materials capable of simultaneous detection and degradation of contaminants.